Spacecraft Uncooperative Rendezvous & Docking Control

A Model Predictive Control Design for Spacecraft Rendezvous and Docking to an uncooperative target

Tommaso Fricano

Master of Science Thesis

TU Delft Delft University of Technology

Delft Center for Systems and Control

Spacecraft Uncooperative Rendezvous & Docking Control

A Model Predictive Control Design for Spacecraft Rendezvous and Docking to an uncooperative target

Master of Science Thesis

For the degree of Master of Science in Systems and Control at Delft University of Technology

Tommaso Fricano

February 12, 2023

Faculty of Mechanical, Maritime and Materials Engineering (3mE) · Delft University of Technology

AAC HYPERION

The work in this thesis was supported by AAC Hyperion . Their cooperation is hereby gratefully acknowledged.

Abstract

The Model Predictive Control (MPC) method provides a control strategy providing inherent robustness and improved capabilities in handling constraints while guaranteeing the satisfaction of the control objective. In recent years, Model Predictive Control (MPC) has started to see more application for the purpose of Rendezvous and Docking (RVD) with an uncooperative target. This is both due to the increased capability of online solver algorithms and the increased interest and need for autonomous RVD to an uncooperative target for Active Debris Removal (ADR) and in orbit servicing. Acknowledging the potential applications of these developments, this thesis seeks to close the gap between research and real-time application of an MPC aimed at minimizing propellant consumption for such a RVD mission. In this thesis, an MPC strategy with the aim of decreasing propellant consumption is developed for an RVD mission. First, an overview will be given of some related orbital theory and the three relative orbital dynamics models, which will be used as prediction models for the MPC strategies. These models are the Clohessy Wiltshire (HCW) model, Xu-Wang model in Cartesian coordinates, model and STM developed by Yamanaka and Ankersen in ROE. An overview will be provided on the available MPC strategies developed until now. Second, the various MPC formulations that will be evaluated, for each mission phase, and their related constraints and cost function are presented. Next, the results of the all the MPC formulations for the different mission phases are presented. Finally, it is shown that the use of more accurate prediction models does not add any significant benefit in terms of propellant consumption and error for all mission phases. However, the use of robust techniques and the inclusion of disturbances in the prediction models is shown to have a clear benefit for all prediction models in terms of propellant consumption and error. The use of incremental input cost function is not shown to consistently improve the propellant use and error. It is determined that a robust MPC formulation using the HCW model with a disturbance estimator provides the best performance in terms of propellant use and error from far range to proximity operations.

Table of Contents

List of Figures

List of Tables

Acknowledgements

This report represent my graduation thesis for the master Systems and Control at the Delft University of Technology.

I would like to thank my supervisor for his guidance throughout the thesis, as well as support and understanding. Furthermore, I would like to thank my company supervisor or his continued support in the last two years, not only for the thesis but in my professional development as an engineer. Finally, a special thanks to Sasha Borovitskaya for all the help in reviewing my grammar and to my family for supporting me throughout.

Delft, University of Technology
February 12, 2023

Tommaso Fricano

Chapter 1

Introduction

In this research, the most suitable Model Predictive Control (MPC) strategy to control the Rendezvous and Docking (RVD) of a chaser spacecraft to an uncooperative target spacecraft will be determined from various proven strategies. The objective of Rendezvous and Docking (RVD) is to allow two spacecraft orbiting a central body to reach a desired relative configuration when in proximity. It has been an area of research since the early 1960s. The space industry has greatly expanded in the last decade thanks to many private entities entering the market and satellites becoming considerably cheaper due to standardization. With plans for constellations, planetary exploration, Active Debris Removal (ADR), and in-orbit servicing being mission architectures of the future, autonomous rendezvous and docking remains a key field of interest, specially regarding RVD with an uncooperative target (dead satellites, debris).

A typical rendezvous mission consist of several phases, each phase with different objectives and constraints. This research focuses on a 3 phase mission representative of a possible ADR mission, starting from orbit insertion at long range up to RVD. The guidance laws for a rendezvous mission are complex due to the relative orbital dynamics, different hard constraints for the different mission phases and fine margins for error during the docking phase. The main component of the guidance laws is thus the choice of which, relative dynamics, model to use. Historically and still to this day, the majority of guidance laws are based on the Clohessy Wiltshire (HCW) equations. The HCW equations are an early Linear Time Invariant (LTI) relative orbital dynamics model based on the assumptions of the satellites being in an unperturbed circular orbit and the distance between the two satellites being small compared to the orbit radius. In the context of a RVD, satellites and debris will not be under these assumptions, meaning a modelling error will be involved in the guidance laws. Small eccentricities are enough to induce significant positions errors, but the rich history of successful RVD missions as well as a wide variety of research has shown that these errors are not limiting to the completion of a RVD mission.

More complete models have since been developed and proven to be suitable in research but have not seen much flight heritage due to the good performance of HCW based guidance laws and heavier computational load. Thanks to improvements in technology, modern and

recent satellites can handle greater computational loads, creating an opportunity for more accurate models and more complex control algorithms to be applied. Traditionally, RVD missions were, carried out with pre-computed burns and small adjustments carried out by the astronauts. With more automation, classical control schemes such as bang-bang and Proportional Integral Derivative (PID) were applied. These control schemes are still not optimal for RVD missions as they are not able to handle complex constraints, but were still successful. Traditional feedback gains are not able to handle constraints which are an integral part of the RVD problem. MPC is proposed as it is able to take constraints into account in its formulation and compute an input that allow for them to be satisfied while optimizing the control objective. Thanks to modern computing power and the current speed of real-time solvers MPC is thus also a viable strategy for spacecraft applications such as RVD missions, which require slow to fast dynamics depending on the mission phase. Even though real-life application is still limited, various research MPC applications for RVD exist, but there has not been a comparative overview on what the best MPC strategy is for RVD with respect to propellant consumption for real-time application. In this thesis, a comparative overview of the performance of multiple MPC formulations using 3 different relevant prediction models will be presented.

1-1 Problem Statement

With the future looking to have a high demand for ADR, these missions could benefit from a proven general MPC strategy aimed at diminishing propellant use without sacrificing accuracy. ADR missions will mostly have to deal with uncooperative targets, not designed to be captured, increasing the complexity and required accuracy of the control strategy. Furthermore, ADR missions often include strict constraints such as approach trajectories, Line-of-Sight (LOS), holding points and soft-docking constraints. Due to limited knowledge of the exact state of the target, it is highly likely that parameters and constraint swill change during the mission itself requiring an adaptable closed loop strategy that MPC provides. A representative mission profile for ADR mission is the European Space Agency (ESA) On-line Reconfiguration Control System and Avionics Techniques (ORCSAT) mission presented in [22], but adapted to an uncooperative tumbling Earth orbiting satellite. This was deemed the most appropriate choice as there is detailed information on all the safety and reliability constraints as designed and deemed fit by an established space agency. The constraints involved in the terminal to capture phase will be adapted to include Line-of-Sight (LOS) constraints as the research is focused towards the capture of an uncooperative rotating or tumbling target. Thus, various MPC strategies for RVD proven for research applications will all be brought under the same baseline simulation and compared to determine which is best suited for such an ADR mission.

1-2 Report Outline

The structure of this report aims to provide more insight on the problem mentioned above. First, the heritage and relevance of the problem is presented by reviewing the history, current and future of RVD in Chapter 2. Next, the theoretical background and existing literature of

the relative orbital dynamic models as well as MPC is outlined in Chapter 3. In Chapter 4, the main research objectives and questions are presented. Next, in Chapter 5, the methodological approach to complete the research objectives is introduced by developing all the MPC formulations that will be evaluated for each mission. Chapter 6 will present all the results produced by this research. Finally, in Chapter 7, the conclusions drawn from the results, discussion, and recommendations for future research are presented.

Chapter 2

Historical Context and Rendezvous and Docking Heritage

This chapter will provide the historical context for defining this research problem, by presentin an overview of the RVD heritage. Next, a small overview of relevant past, current and future missions is given. The space debris problem is presented, introducing the problems involved with ADR missions and the need for a general automated solution. Finally, a mission profile is presented under which all the MPC strategies performance will be evaluated.

2-1 Background Information-Rendezvous and Docking

The objective of RVD is to allow two spacecraft orbiting a central body to reach a desired relative configuration when in proximity. It has been an area of research since the early 1960s. The former Soviet Union first attempted automated RVD with the Vostok program, but ultimately the United States would be successful first with manual RVD with the Gemini program. Both these programs were geared towards preparing the respective institutions for the moon landing, and so were the technology demonstration programs. The National Aeronautics and Space Administration (NASA) opted to go for a manual RVD approach as it deemed a manual approach would allow greater flexibility and would require less redundancy and complexity [59]. The success of the Gemini mission can be attributed to Clohessy and Wiltshire, who used Hill's equations describing the motion of the moon with respect to Earth, to describe the motion of a satellite relative to another in orbit. Furthermore, the Gemini missions reaffirmed NASA's worries about an automated approach, but soon enough the Russians achieved an automated approach in 1967 with the Soyuz program. This automated approach achieved the first ever automated RVD between two unmanned spacecraft, Kosmos 186 and 188. Since then autonomous RVD has been carried out in countless missions with notable names being the Apollo program, Skylab mission, Russian Salyut & Mir Space Station program, the Space Shuttle program and International Space Station (ISS) program and servicing missions carried out by the various servicing vehicles [15]. It is to be noted that

the majority of these RVD missions have been with a cooperative or collaborative target, meaning the target is either actively controlled or designed in a manner as to assist the RVD procedure.

The space industry has greatly expanded in the last decade thanks to a lot of private entities entering the market and satellites becoming considerably cheaper due to standardization. With plans for constellations, planetary exploration, active space debris removal, and in-orbit servicing being the expected mission architectures of the future, autonomous rendezvous and docking remains a key field of interest especially regarding RVD with an uncooperative target (dead satellites, debris). The recent SpaceX Dragon 2 ISS servicing mission and the planned European Space Agency (ESA) Clear Space mission being a current example of the continuing research in automated RVD missions [15].

2-2 Past, Recent, and Future missions

As mentioned earlier, most of the missions and research in RVD has been carried out by the Soviet and American programs, with only recently more private entities coming into play. The chosen approaches have been different from each other, and the technology has developed from human controlled to fully automated. In this section various examples will be discussed in details as to present the growth and evolution of the RVD approach. First, the manual approach used by the Gemini program will be presented. Second, the semi automated RVD approach carried out by the Space Shuttle will be presented, and finally the automated approach planned for the Deutsche Orbitale Servicing (DEOS) mission will be discussed.

Table 2-1: Attitude Determination Subsystem Components

Mission	Target Orbit	Target Characteristics	Autonomy	Guidance Algorithm
Gemini [20]	Circular	Cooperative and semi-active	Manned-CL, ground support	Based on HCW eqns. for close range, Hohmann type transfers for far range
Apollo [20]	Circular	Cooperative and active	Manned-CL, ground support	Based on Lambert targeting
Soyuz/Progress [15] [34]	Circular	Cooperative and semi-active	Automated, crew and ground support if required	Based on HCW eqns. for close range, Hohmann type transfers for far range
Space Shuttle Program [20]	Circular	Cooperative and passive Manned-Cl for close range, ground support	Automated far range,	Based on Lambert targeting
ETS-VII [40]	Near Circular	Cooperative and active	Autonomous	Based on HCW eqns. for close range, Hohmann type transfers for far range
ATV [29]	Near Circular	Cooperative and active	Highly automated, occasional ground support	Based on HCW eqns. for close range, Hohmann type transfers for far range
XSS [9]	Near Circular	Cooperative and passive	Semi-Autonomous	Partly based on HCW eqns.
DART [38]	Near Circular	Cooperative and passive	Autonomous	N/A
Orbital Express [8]	Circular	Cooperative and passive	Autonomous	N/A
DEOS [3]	Circular	Uncooperative	Autonomous	Based on HCW eqns. for close range, Hohmann type transfers for far range
Orion Program [46]	Near Circular	Cooperative and active	Semi-autonomous	N/A
ELSA-D [5]	Near Circular	Semi-uncooperative and semi-active	Autonomous	N/A
ClearSpace-1 [12]	Near Circular	Uncooperative and passive target	Autonomous	N/A

-

2-2-1 The Gemini Program

By 1961 the Americans had determined that rendezvous was feasible considering the existing technology. During the Mercury program experiments were carried out allowing astronauts to estimate the state of targets based on eyesight, the related results were then used for the organization of the Gemini program. One of the main objectives of the Gemini program was to carry out RVD.

The first rendezvous was completed by Gemini 5 and 6 in 1965, where they were manoeuvred within 30 cm of each other. Then in 1966, Gemini 8 successfully docked with the unmanned Agena target spacecraft. The Gemini program is of great relevance as it was the first to demonstrate RVD, closed loop manned piloting, nominal and off nominal scenario planning, reduced out-of-plane insertion error through launch window selection and the development of contingency procedures. The program was used as a technology demonstrator and the results and experiences would be used for the development of the Apollo program.

The computation of the chaser orbital adjustments was carried out by using ground based orbit determination for the target and chaser spacecrafts. To account for the accuracy limitations of the ground tracking, it was chosen to make use of closed-loop manned piloting techniques for the terminal mission phase. The chaser was fitted with a rendezvous radar and the target with the corresponding transponder as to determine the range, relative velocity and Line-of-Sight (LOS) angles. The required manoeuvres were computed using the Clohessy Wiltshire (HCW) equations through the on-board computer once the chaser was within radar range. The docking port on the target consisted of a cone with latches as to capture 3 fittings on the nose of the chaser spacecraft. This method was chosen due to its relative simplicity and reliability, allowing for a quick development time. Looking at Gemini 6, 3 possible mission profiles were studied, which are also visualized in Figure 2-1 [20] [32].

1. Tangetial Orbit: The Gemini spacecraft was inserted into an elliptical orbit, tangential to the target spacecraft. This would ensure a rendezvous near the apogee of the fourth orbit. This profile did not guarantee proper lighting conditions or consistent relative dynamics during the terminal phase. This profile is illustrated in Subfigure 1 of Figure 2-1.

2. Coelliptic Orbit: This method relied on placing the Gemini spacecraft in a co-elliptic orbit with respect to the target orbit. The intercept is then carried out once a certain criterion, like sufficient lighting, is met. This profile is illustrated in Subfigure 2 of Figure 2-1.

3. Direct Rendezvous: As the name states, the Gemini spacecraft would be placed on an intercept trajectory by its launch vehicle, Titan II. This in turn restricted the possible launch window and a final state which, is highly sensitive to ascent trajectory deviations. Another draw back is that the rendezvous occurs within the first orbit around Earth, giving less time for in-orbit system checks and the rendezvous procedure. This profile is illustrated in Subfigure 3 of Figure 2-1.

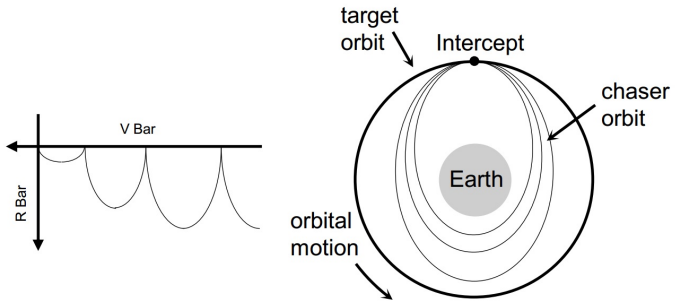

(a) Phase 1: Tangential orbit

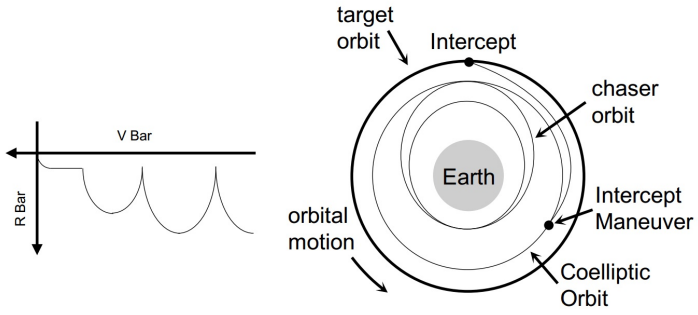

(b) Phase 2: Co-elliptical orbit

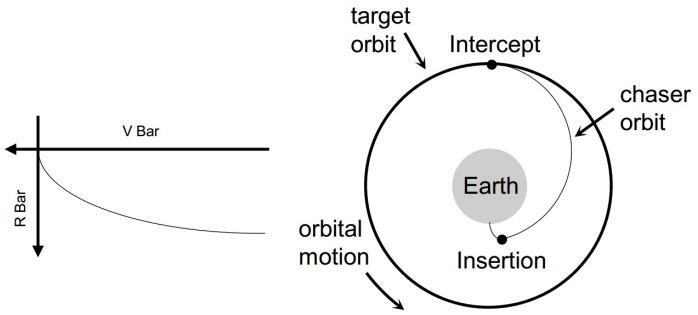

(c) Phase 3: Direct Rendezvous

Figure 2-1: Gemini 6 Mission phases [32] [20] [4]

The Coelliptic Orbit profile was chosen as the most adequate for the Gemini 6 mission as it provided plenty of time and control over the rendezvous procedure. These 3 mission profiles would go on to serve as the basis for future missions. The mission planning and piloting techniques developed during the Gemini program would then be used for the Apollo program. The Apollo program was the first program to require RVD for the completion of its mission objective, the Lunar Module (LM) required docking with the Command Service Module (CSM) after ascent from the moon. However, new rendezvous profile concepts before terminal phase initiation were required for Apollo. It is to be noted that if the LM was not able to carry out the rendezvous, the CSM would become the active spacecraft, thus both vehicles were fitted with the necessary sensors and equipment. The Apollo program would also make use of the co-elliptic profile and a short rendezvous profile capable of saving two hours [62]

[20].

2-2-2 Space Shuttle

The Space Shuttle was in service from 1983 to 2011, during this period it carried out 78 missions for, which RVD was part of the mission objective. The RVD technology was proven by the Gemini and Apollo program, so the RVD was no longer the primary objective as the Space Shuttle's main service was related to its payload. The Space Shuttle however, represents the first program to carry out RVD with passive targets. The majority of rendezvous targets of Space Shuttle were not designed for rendezvous, docking (retrieval) or in-orbit servicing. Besides not being designed for RVD the rendezvous targets were often smaller than the Space Shuttle (barring the Mir and ISS), compared to the Gemini and Apollo program where chaser and target were roughly the same size. Furthermore, due to the tighter tolerances on docking time and contact velocity for the Mir and ISS the docking velocity was an order of magnitude smaller compared to the 0.3 m/s used for the Gemini and Apollo missions. Lastly, the Space Shuttle made use of cameras compared to the LOS approach used by the Gemini and Apollo mission, it becomes clear that the Space Shuttle represented a significant increase in RVD capabilities and complexity [19] [20].

The challenges posed by this increased complexity were unfortunately only gradually recognized during the 1970s as the majority of the Space Shuttle design was finished. This resulted in the Space Shuttle missions requiring extensive mission specific procedures and trajectories, regardless of the advanced flexibility and capability provided by the Space Shuttle. This prevented routine or general practices being developed, as well as hardware or software development, due to cost and time constraints. The mission profiles of the Space Shuttle missions thus varied from mission to mission, but certain common practices were developed. The mission profile for ISS rendezvous is one of those examples, the Space Shuttle took up to 3 days from insertion to docking with the aid of 4 astronauts. The RVD was split into three phases: far-field, mid-field and proximity operations. During the far-field phase, the position of the Space Shuttle was computed using IMUs and star trackers together with ground based radar updates. The burn manoeuvres were then computed by the ground crew and uploaded to the Shuttle, which would then execute it automatically. During the mid-field phase, the crew was responsible for initiating targeting routines. Navigation was thus carried out from on-board the shuttle through built-in sensors and co-coordinated through a predefined timeline. During the final phase, the translation dynamics of the Shuttle were controlled manually, while the attitude control was automated. The relative position and velocities used by the crew were determined through the use of cameras and laser rangefinders. The docking was carried out by 4 astronauts, who had trained together for months. The Lambert targeting approach was used, just as for the Apollo program. A typical mission profile for Mir and ISS RVD is presented in Figure 2-2. It is to be noted that the Automated Transfer Vehicle (ATV) would later on carry out a fully automated approach to the ISS, thereby significantly decreasing the complexity and costs involved in ISS and Mir missions.

2-2-3 ClearSpace One Mission

Having taken a look at two historic programs, the mission representing the future of automated RVD with an uncooperative target will be discussed. This mission in question being ESA's

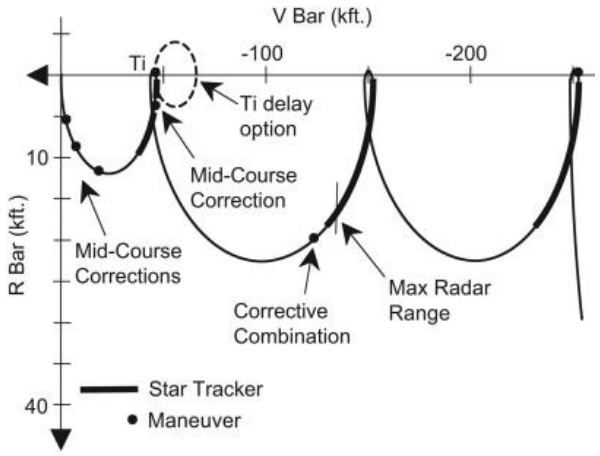

Figure 2-2: space Shuttle mission profile for Mir or ISS RVD [19]

ClearSpace-1 mission as it represents an application, which will be used more in the future, this will be discussed with more detail in the next section. The ClearSpace-1 mission's objective is to test technologies for the rendezvous, capture and de-orbit for End-of-Life (EOL) satellites, by rendezvousing and capturing a derelict Vega Secondary Payload Adapter (VESPA) and finally destructively de-orbit itself and the captured satellite.

Being an unmanned mission, it will carry out a fully automated RVD with an uncooperative target. The Orbital Express mission was able to demonstrate robotic autonomous RVD as well as in-orbit refuelling and servicing but still with a passive target [8]. As the majority of space "junk" are uncooperative targets the ClearSpace-1 mission will be of great importance for the future for the accessibility. ClearSpace-1 will make use of cameras to visually recognize the target and 4 robotic arms to capture it.The VESPA was chosen as a target due to being similar to a small satellite in size and having a simple shape, making the capture relatively simple for a first mission. The exact mission profile is not available, but it is likely that the autonomous RVD will be split into various mission phase, with flags that can be activated from the ground station so as to allow the satellite to proceed with the next mission phase. After this mission the intention is to develop the ClearSpace spacecraft towards multi object capture [12].

2-3 Space Servicing-Debris

Society have continuously become more reliant on space technology for everyday life operations such as telecommunications, navigation and national security. With the privatisation of the space market, technological developments and the increasing possibilities of space application, it is inevitable that the space industry will continue to grow. Examples of this are the 5G constellations and the interplanetary missions being developed. The amount of satellite launches per year are increasing exponentially from an average of around 100-200 launches per year until 2010 to an average of around 400-500 launches in the last 3 years and this is expected to keep increasing [14]. Many of these satellites are still functional (≈ 2700) however there is a large and growing amount of defunct satellites (≈ 2850), discarded rocket stages (≈ 1950) and debris objects (≈ 21000), which continue to orbit around Earth. It is to be

noted these are only the tracked objects and statistical models estimate millions more to be present [13]. Due to the Kessler effect and current functional satellites becoming defunct this number will only continue to grow and thus there is a need for solutions to ensure Low Earth Orbit (LEO) and Geosynchronous Earth Orbit (GEO) remain safe and operational. Furthermore, with the growing number of constellations that will be in orbit the same technology can be used for the inspection and servicing of faulty spacecraft.

If all future launches were to be cancelled the Kessler effect dictates that the amount of space debris shall continue due to collisions creating more debris and thus increasing the probability of another collision. This was verified through estimation in [31]. An example of this was the accidental collision between the operational satellite **Iridium 33** and the defunct satellite **Kosmos 2251** in 2009. Due to the collision both satellites were destroyed and over 1300 pieces of debris larger than 10 cm were created [52]. If launches are to continue without any mitigation solutions then the number of space debris will rise at an exponential rate, as shown in Figure 2-3.

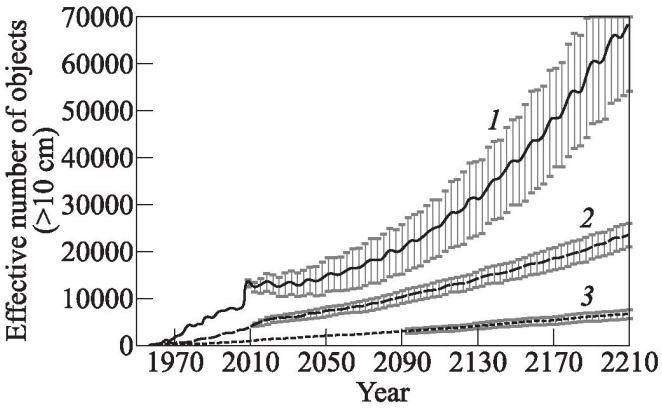

Figure 2-3: Projected growth of the $\geq$ 10 cm object population in LEO,MEO and GEO for the next 200 years. 1-LEO (200-2000 km altitude); 2-MEO (2000-35,586 km altitude); and 3-GEO (35,586-35,986 km altitude) [30]

To mitigate this issue the Inter-Agency Space Debris Coordination Committee (IADC) determined and imposed the Post Mission Disposal (PMD) rule as way to limit the orbital longevity of spacecraft. The PMD rule dictates that a spacecraft in the LEO should de-orbit itself within 25 years of mission completion and that a spacecraft in GEO is raised to a graveyard orbit after mission completion [23]. This mitigation will help slow down the growth of space debris objects but unfortunately it will not be enough to solve the problem, due to older satellites not having this capability. There is thus dire a need for Active Debris Removal (ADR) to ensure that LEO and GEO remain safe for use. It is estimated that through actively removing five space debris objects per year from orbit, it becomes possible to stabilize the growth of space debris [31]. ADR involves the use of spacecraft specifically designed to find and de-orbit debris or defunct spacecraft, such as the ClearSpace 1 satellite mentioned in the previous section. ADR will be especially use-full for clearing defunct satellites from already clustered orbits in high demand, which are mostly LEO such as the ISS orbit. This is because satellites represent objects with the potential of creating large amounts of smaller debris, which is much harder to capture, in case of a collision. Various concepts of de-orbiting

spacecraft have been developed as the capture mechanism, de-orbiting method and the mission profile, can vary. For example, the ClearSpace 1 satellite was designed with a net to capture the target satellite instead of a robotic arm as it was deemed to simplify and reduce the risk of the capture manoeuvre.

In the previous section it was discussed that even though there is plenty of heritage with RVD missions, they are limited to rendezvous and docking with a co-operative or passive target, not for an uncooperative target. This means that the target spacecraft is not designed for RVD, since it does not possess sensors for relative navigation (maybe even absolute navigation sensors) and mechanisms or systems to facilitate the capture. Furthermore, the target satellite will have attitude control and may be rotating or tumbling, which considering the likely presence of solar array and antennas, increases the risk of a collision. The danger of a collision or damage to the target satellite is further aggravated due to the possible presence of unused volatile energy sources such as propellant. The lack of accurate knowledge on the state of the target spacecraft due it being defunct will often require an inspection to be carried out of the target. This is done in order to evaluate if the capture can be carried out as planned or if it must be adjusted. The requirement of communication, illumination, holding points, inspection manoeuvres, safety zones, approach trajectories and relative state constraints are a result of these challenges. Strict requirements on the precision and reliability of the chaser satellite are also required as otherwise the risk of a collision will negate the possible benefits.

It is also important that the de-orbiting satellites are designed to have flexibility as to allow the capture and de-orbit of different target spacecrafts, target orbits and time frames. If this is not done each mission will require elaborate mission specific planning just as the Space Shuttle needed, which would considerably increase the costs and manpower required for each mission. It is pretty clear that it would be unlikely and unreliable that a manually controlled spacecraft could comply with all these requirements. Therefore, there is a need for autonomous RVD for ADR missions [4] [42] [63] [59] [39].

2-4 Mission Design

The scope of this research is to evaluate the most appropriate MPC strategy for RVD with respect to propellant consumption and completion time in general and not for a specific mission. It is therefore necessary that the chosen mission profile will be representative of the future ADR missions. In the last decade, the nano (1-10 kg) and micro (10-100 kg) satellite market has seen the largest growth. A major contributor to this is the growth of private companies producing standardized components for these satellites such that it is not necessary to design mission specific hardware and so significantly reducing the cost involved. This market is bound to continue growing with launch and component costs continuing to decrease with an estimated 2000 launches in the next 5 years. The small satellite (100-1000 kg) industry is also expected to grow thanks to constellations such as OneWeb and Starlink [48]. Many of these nano to small satellites that have been and will be launched are designed to comply with the PMD regulations, but do not possess active de-orbiting components. As mentioned in the previous section, this will not be enough to stabilize the Kessler effect. It was so decided to simulate the capture of a (rotating and tumbling) uncooperative nano-satellite in LEO orbit, as the LEO region is currently heavily clustered and remains the region with most demand. This likely means it will also be the region were ADR will be of higher demand.

The exact orbit is not of importance. This is because there is a need for a general approach and not a mission specific approach as highlighted in the previous section. Because of this, one of the areas of evaluation will be the performance of certain prediction models under eccentric orbits, it will be fruit full to carry out the evaluation of the control schemes for different eccentricities. It was chosen to use the mission profile of the ESA On-line Reconfiguration Control System and Avionics Techniques (ORCSAT) mission presented in [22], but adapted to an uncooperative tumbling Earth orbiting satellite. This was deemed the most appropriate choice as there is detailed information on all the safety and reliability constraints as designed and deemed fit by an established space agency. The mission profile is divided in three phases: intermediate range, short range and terminal to capture phase. They will be explained in detail in Chapter 5 respectively. The constraints involved in the terminal to capture phase will be adapted for to include Line-of-Sight (LOS) constraints as the research is focused towards the capture of an uncooperative rotating or tumbling target.

2-5 Conlcusion

In this Chapter, the heritage and required background information for RVD missions has been reviewed. Through this review, conclusions are drawn.

RVD has been an important field of research since the beginning days of the space missions. Being a critical component of being able to land on the moon, extensive research and methodology was developed during the Gemini program, with RVD being one of the main mission objectives. The Gemini program served as the baseline for the RVD strategies of the Apollo program. The RVD manoeuvres were, however, carried out manually by the pilots from the computations done by the onboard computer and relied on the then newly developed HCW equations. With the Space Shuttle, the RVD techniques became more automated but were still not fully automated and approached were still developed for specific missions. The ATV would be the firs to carry out fully automated RVD with the ISS greatly reducing the development costs and complexity of ISS and Mir missions.

With the continued growth of the space industry, more applications for RVD have appeared. Due to the shear amount of satellites that have been and are being launched, the space debris problem has created a dire need for satellites with RVD capabilities. If the Kessler effect is to be combatted, satellites able to de-orbit defunct satellites or debris are needed due to the lack of authority there is over space. Furthermore, with the increasing amount of constellations, there will also be a need for in orbit servicing in order to troubleshoot malfunctioning satellites or to examine causes of failure. There is a vast amount of research and development being carried out to develop general RVD techniques that can be applied to various scenarios.

Due to the majority of space debris being located in, LEO it is chosen to compare MPC formulations for the RVD with an uncooperative tumbling target satellite in LEO. In the following chapter, an overview will be given of the necessary scientific theory for this research.

Chapter 3

Theoretical background and literature review

The previous chapter presented an overview of Rendezvous and Docking (RVD) missions, from beginning to current technology, concluding with a valid mission profile to use as a comparison baseline. This chapter will present the necessary theoretical background relevant to the disciplines and topics that are covered in this field of research.

3-1 Modelling

An important aspect of the problem at hand is the choice of model for relative dynamics, which will be the basis of the guidance law used. The choice of model will determine the way the MPC will predict state evolution, and so directly affects the solution to the optimization problem. First, the reference frames relevant to this problem will be introduced. Next, an overview will be given of the possible choice of as relative dynamics model. Finally, the chosen models will be presented.

3-1-1 Reference Frames

There are two main reference frames that are relevant when dealing with relative dynamics of chaser and target.

The first reference frame is the Earth-centred Inertial. The ECI frame has its origin at the centre of mass of the Earth. As indicated by the name, the frame is inertial, meaning that it is not undergoing any rotation or acceleration. Due to the fact that the Earth is rotating, the coordinated system of the ECI frame is defined through an epoch and thus there are many possibilities. The most common is the Earth Mean Equator and Equinox frame, also named the J2000/EME2000 frame. The right-handed coordinate system of the frame is defined with the $\mathcal{X}$-axis directed towards the J2000 vernal equinox, the $\mathcal{Z}$-axis pointing towards the

celestial North Pole and the $\mathcal{Y}$-axis completes the right-handed coordinate system as shown in Figure 3-1 [55].

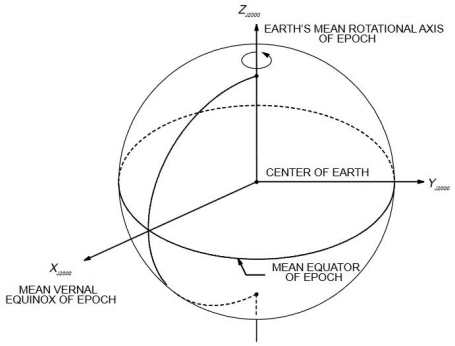

Figure 3-1: Earth-centred Inertial frame, $\mathcal{F}_{\mathcal{I}}$ [49]

The second reference frame and the most important, due to relative dynamics often being expressed in this frame, is the Local-Vertical, Local-Horizontal (LVLH). Being a body-fixed frame, its origin is located at the centre of mass of the spacecraft. The coordinate system of the frame is defined with the $\mathcal{X}$-axis is in the orbit radius direction, also known as the R-bar, and the $\mathcal{Z}$-axis pointing parallel to the orbit momentum vector in the orbit normal direction, also known as the H-bar, and the $\mathcal{Y}$-axis completes the right-handed coordinate system, also known as the V-bar. It is to be noted that the R-bar and V-bar together define the orbital plane, as can be seen in Figure 3-2.

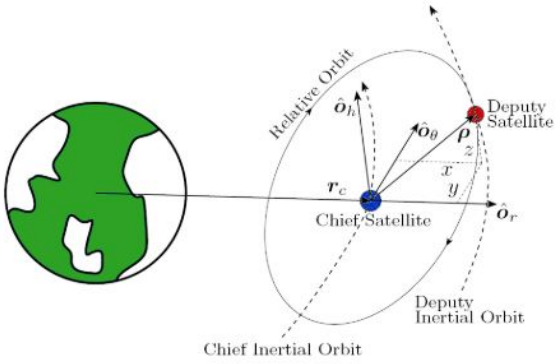

Figure 3-2: Local-Vertical, Local-Horizontal (LVLH) frame, $\mathcal{F}_{\mathcal{O}}$ [56]

3-1-2 Perturbations

There is a vast list of perturbations that occur in orbit around Earth. The magnitude of these perturbations is often small enough that they can be neglected as can be seen in Figure 3-3. From Figure 3-3 it also becomes clear that for Low Earth Orbit (LEO) the two most significant perturbations are the J_2 effect and atmospheric drag.

The J_2 perturbation is caused due to the Earth not actually being a perfect sphere, but an irregular shaped ellipsoid. This results in the Earth's mass not being evenly distributed and

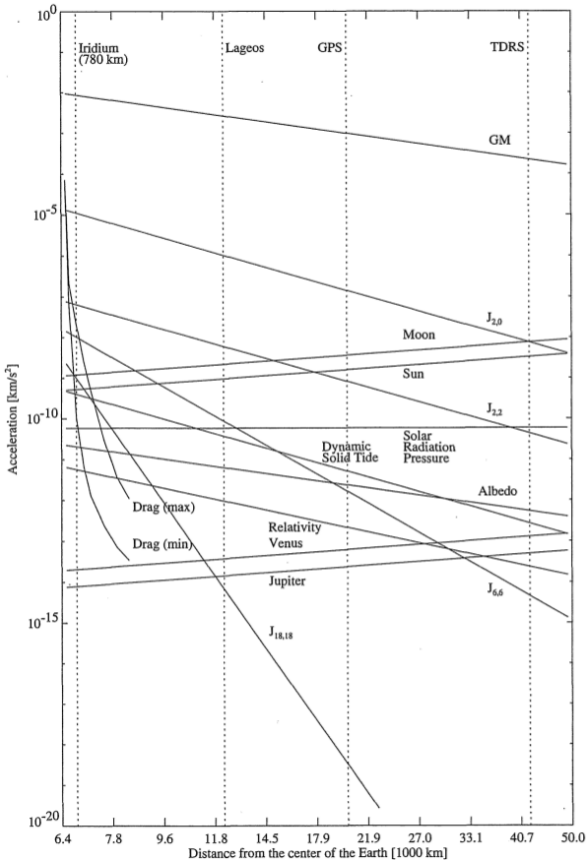

Figure 3-3: Magnitude of accelerations due to perturbations on Earth orbiting Satellites [36]

so causing the gravitational potential to be varying with latitude. The J_2 is just one of the perturbations caused by the irregularities in the gravity potential, the higher order terms are neglected due to being various orders of magnitudes smaller. The gravitational potential including the J_2 perturbation is given by (3-1), where $k_{J_2} = 3J_2\mu R_e^2/2$, R_e is earth's radius, J_2 is the second zonal harmonic coefficient of the Earth and γ is the geocentric latitude.

$$\mathbf{P}_{\text{grav},J_2} = -\frac{\mu}{r} - \frac{k_{J_2}}{r^3}(\frac{1}{3} - \sin\gamma^2) \tag{3-1}$$

The magnitude of the atmospheric drag on a satellite will depend on the altitude and the cross-sectional area of the satellite. The exact atmospheric density is not easy to find, as there are many models available that yield different results. Furthermore, the cross-sectional area of a satellite will be changing with the orientation of the satellite, making it quite complex to model the drag. An estimate of the drag and other J_2 terms will be added to the simulation according to 3-3. The drag will be added as a constant disturbance in the direction of motion and a further randomly distributed disturbance will be added on all three axes will be added.

These perturbations can thus be included in the dynamics model of the controller or chosen to be ignored. These perturbations can be included in the three models discussed in this section resulting in more complex models. The benefits of including them should be a lower

model error, but that will depend on the other assumptions the model is based on. Their inclusion on the controlled prediction model will further be discussed in the next section.

3-1-3 Relative Orbital Dynamics Models

An important part of the problem is the choice of model for relative dynamics. The choice of model will determine the way the MPC will predict state evolution and so directly affect the solution to the optimization problem. A vast amount of research involving relative dynamics in space has made use of the classical Clohessy Wiltshire (HCW) equations due to their simplicity and good accuracy considering the assumption of a circular reference orbit, small separations distances between the satellites and short time intervals. However, in reality many satellites, asteroids, and debris do not act under these assumptions so more complete models should be considered regardless of the flight heritage and success of the HCW equations.

For relative control with large separations and time intervals more exact models are required as to decrease modelling error which, causes excessive propellant consumption. There are various potential candidates. First, the Yamanaka-Ankersen (YA) model [61] which is numerically identical to the HCW equations but provides a State Transition Matrix that is also valid for elliptical orbits [61]. Next, Breger and How provide a State Transition Matrix based on Gauss' Variational Equalities (GVEs) expanded to include the J2 effects [6], but this model is computationally expensive. Finally, the nonlinear Xu-Wang model [60] which, is very accurate but hasn't been compared directly to the simpler HCW and YA model compared to the Koenig and D'Amico STM [28] which has been compared to the other models and provides increased accuracy for relative simplicity. The Koenig STM, YA model and the Breger and How GVE's are described in Relative Orbital Elements (ROE) which, is favourable for orbit design but requires transformation to the local frame for MPC implementation. The YA model further makes use of the true anomaly as an independent variable instead of time, requiring an extra computation, nonetheless it has been proven in application [22]. The Xu-Wang model on the other hand describes the relative motion directly in the local coordinate frame making it suitable for controller design, although it has only been applied for swarm-keeping strategies [37] it is very promising for the RVD application.

Based on the fact that Tillerson and How provided proof that the use of HCW will provide significant prediction errors and so increased fuel consumption [24]. The increased performance versus the increased complexity of these models must be evaluated. It is however to be noted that due to the potential performance improvement in propellant consumption is diminished for the terminal to capture phase due to the small relative separation. The potential benefit in the terminal to capture phase will be in terms of docking accuracy. The models that are compared are the HCW, YA and Xu-Wang model with disturbances for all three mission phases. These provide a good range of complexity as well as practical and research implementation, without being too computationally expensive or requiring any transformation matrices.

Clohessy-Wiltshire Equations (HCW)

The HCW equations have been the most frequently used in practice and in theoretical studies for RVD as well as formation flying [18] [50] [41] [7]. This is due to their simplicity and computational efficiency for control strategies. Regardless of its simplicity flight heritage and

theoretical studies have shown that it provides more than suitable accuracy to carry out a RVD mission.

The HCW equations are composed of three linearized differential equations developed in the LVLH frame. The differential equations are presented in (3-2).

$$\begin{aligned} \ddot{x} - 3n^2 x - 2n\dot{y} &= a_x \\ \ddot{y} + 2n\dot{x} &= a_y \\ \ddot{z} + n^2 z &= a_z \end{aligned} \tag{3-2}$$

where n is the mean motion of the orbit. The Centripetal acceleration is represented by the terms including the squared mean motion, while the Coriolis acceleration is represented by the terms including $2n$ [57]. As was discussed already in Subsection **??** the HCW model does not include perturbations or eccentricity. Furthermore, as the nonlinear equations are linearized with respect to the distance between target and chaser spacecraft, the model is only valid for separation of a few hundred meters between the two spacecraft [57]. Furthermore, clear from the differential equations that the $x - y$ plane motion is coupled, which makes sense considering that it is the orbital plane.

An analytical solution to eq::hcw exists and can be formulated in an STM, as presented in [56]. Through the STM it is thus possible to propagate the relative motion of the spacecraft over time. The HCW model then takes the following form:

$$\dot{Q}(t) = \Psi(\Delta t) Q(t_0) \tag{3-3}$$

where $Q = [x, y, z, \dot{x}, \dot{y}, \dot{z}]$ is the state vector, Δt is the elapsed time and t_0 the initial time. Finally, Ψ denotes the STM, which is given by:

$$\Psi(\Delta t) = \begin{bmatrix} 4 - 3\cos n\Delta t & 0 & 0 & \sin n\Delta t/n & \frac{2(1-\cos n\Delta t)}{n} & 0 \\ 6(\sin n\Delta t - n\Delta t) & 1 & 0 & \frac{2(\cos n\Delta t - 1)}{n} & \frac{4\sin n\Delta t}{n} - 3\Delta t & 0 \\ 0 & 0 & \cos n\Delta t & 0 & 0 & \frac{\sin n\Delta t}{n} \\ 3n\sin n\Delta t & 0 & 0 & \cos n\Delta t & 2\sin n\Delta t & 0 \\ 6n(\cos n\Delta t - 1) & 0 & 0 & -2\sin n\Delta t & 4\cos n\Delta t - 3 & 0 \\ 0 & 0 & -n\sin n\Delta t & 0 & 0 & \cos n\Delta t \end{bmatrix} \tag{3-4}$$

It should be noted that if $\dot{y}_0 = -2nx_0$ all secular terms will go to zero on so the resulting trajectory is periodic. The discrete time state space form of the HCW equations is presented in (3-5) [18].

$$x(k+1) = \underbrace{\begin{bmatrix} 4-3C & 0 & 0 & S/n & \frac{2(1-C)}{n} & 0 \\ 6(S-nT_s) & 1 & 0 & \frac{2(C-1)}{n} & \frac{4S-3nT_s}{n} & 0 \\ 0 & 0 & C & 0 & 0 & \frac{S}{n} \\ 3nS & 0 & 0 & C & 2S & 0 \\ 6n(C-1) & 0 & 0 & -2S & 4C-3 & 0 \\ 0 & 0 & -nS & 0 & 0 & C \end{bmatrix}}_{A} x(k) + \underbrace{\begin{bmatrix} \frac{1-C}{n^2} & \frac{2nT_s-2S}{n^2} & 0 \\ \frac{2(S-nT_s)}{n^2} & -\frac{3T_s^2}{2} + 4\frac{1-C}{n^2} & 0 \\ 0 & 0 & \frac{1-C}{n^2} \\ \frac{S}{n} & 2\frac{1-C}{n} & 0 \\ 2\frac{C-1}{n} & -3T_s + 4\frac{S}{n} & 0 \\ 0 & 0 & \frac{S}{n} \end{bmatrix}}_{B} u(k) \tag{3-5}$$

where, $C = \cos nT_s$ and $S = \sin nT_s$.

Yamanaka and Ankersen Model

The direct relative dynamics model developed by YAhas been used for theoretical design of MPC controllers for RVD [22] and will soon have flight heritage aboard the ESA PROBA-3 mission [2]. The model is a further development of the HCW to include eccentricity. The derivation is similar but for the fact that while HCW started from the EOM for a circular unperturbed orbit, YAused the EOM for a unperturbed eccentric orbit. The derivation relies on the assumption that the relative distance of the two satellites is negligible compared tot he orbital radius, just like the HCW model. The resulting equation of the relative in the target's satellite reference frame are the following:

$$\begin{bmatrix} \ddot{x} \\ \ddot{y} \\ \ddot{z} \end{bmatrix} = \begin{bmatrix} -k\omega^{\frac{3}{2}}x + 2\omega\dot{z} + \dot{\omega} + \omega^2 x \\ -k\omega^{\frac{3}{2}}y \\ 2k\omega^{\frac{3}{2}}z - 2\omega\dot{x} - \dot{\omega}x + \omega^2 z \end{bmatrix} + a_f + a_{cd} - a_{td} \tag{3-6}$$

The solution to these equations is found depending on the assumption that the chaser satellite is flying in free motion, $a_\mathrm{f} = 0$, and that the external forces on chaser and target satellite are identical, $a_\mathrm{cd} = a_\mathrm{td}$. Before determining the solution to the EOM, YAsimplified (3-6) to obtain the simplest final form. This is done by adopting the true anomaly of the target spacecraft, θ, as an independent variable instead of time, t and adopting the following transformation:

$$\begin{bmatrix} \tilde{x} \\ \tilde{y} \\ \tilde{z} \end{bmatrix} = (1 + e\cos\theta) \begin{bmatrix} x \\ y \\ z \end{bmatrix} = \rho \begin{bmatrix} x \\ y \\ z \end{bmatrix} \tag{3-7}$$

The resulting simplified EOM for relative motion becomes:

$$\begin{aligned} \tilde{x}'' &= 2\tilde{z}' \\ \tilde{y}'' &= -\tilde{y} \\ \tilde{z}'' &= 3\tilde{z}/\rho - 2\tilde{x}' \end{aligned} \tag{3-8}$$

In this form YA developed a solution by integrating the equation for, $\tilde{X}$, and the equation for $\tilde{y}$ as it is that of a harmonic oscillator. The problem is then reduced to solving a preceding

differential equation for $\tilde{z}$. YAdid this by proposing their own integral term in order to avoid singularities and achieve a STM simple for engineering use [61]. The solution so allows the propagation of the relative motion of a chaser and target spacecraft with true anomaly. The STM form of the solution is given by:

$$\tilde{Q}(\theta) = \Phi_{\theta_0}^{\theta}\tilde{Q}(\theta_0) = \Phi_{\theta}\Phi_{\theta_0}^{-1}\tilde{Q}(\theta_0) \tag{3-9}$$

where $\tilde{Q}$ is the transformed state vector excluding the out of plane components, Φ is the STM given by the multiplication of two matrices and θ and θ_0 are the initial and final true anomaly. The matrices compromising the STM are given below in (3-10) and (3-11).

$$\Phi_{\theta} = \begin{bmatrix} 1 & -\cos\theta(\rho+1) & \sin\theta(\rho+1) & 3\rho^2 J \\ 0 & \rho\sin\theta & \rho\cos\theta & (2-3e\rho\sin\theta J) \\ 0 & 2\rho\sin\theta & 2\rho\cos\theta - e & 3(1-2e\rho\sin\theta J) \\ 0 & \cos\theta + e\cos 2\theta & -(\sin\theta + e\sin 2\theta) & -3e(J(\cos\theta + e\cos 2\theta) + \sin\theta/\rho) \end{bmatrix} \tag{3-10}$$

$$\Phi_{\theta_0}^{-1} = \frac{1}{1-e^2}\begin{bmatrix} 1-e^2 & 3e\sin\theta_0(1+1/\rho) & -e\sin\theta_0(\rho+1) & 2-e\rho\cos\theta_0 \\ 0 & -3\sin\theta_0(1+e^2/\rho) & \sin\theta_0(\rho+1) & \rho\cos\theta_0 - 2e \\ 0 & -3(\cos\theta_0 + e) & \cos\theta_0(\rho+1)+e & -\rho\sin\theta_0 \\ 0 & 3\rho + e^2 - 1 & -\rho^2 & e\rho\sin\theta_0 \end{bmatrix} \tag{3-11}$$

where $J = h(t-t_0)/\rho^2$. The out of plane relative state is then computed through:

$$\begin{bmatrix} \tilde{y}_t \\ \tilde{v}_{y_t} \end{bmatrix} = \frac{1}{\rho_{\Delta\theta}}\begin{bmatrix} \cos\Delta\theta & \sin\Delta\theta \\ -\sin\Delta\theta & cos\Delta\theta \end{bmatrix}\begin{bmatrix} \tilde{y}_0 \\ \tilde{v}_{y_0} \end{bmatrix} \tag{3-12}$$

where $\Delta\theta = \theta - \theta_0$. The YASTM was shown to obtain a lower model error compared to the HCW model [51] at the cost of computational power. For control and simulation purposes one wishes to have the states propagated with time, but due to the true anomaly being used as independent variable the use of this model requires an extra computation. It is thus necessary to solve Kepler's equation at every time step to obtain the time, nonetheless this model has been implemented in real time MPC controllers, so this is not a limiting factor [22]. The resulting Linear Time Variant (LTV) discrete time state space model is presented in (3-13) as in [22].

$$x(k+1) = \underbrace{\Phi_{\theta_0}^{\theta}}_{A(t)}x(k) + \underbrace{\Phi_{\theta_0}^{\theta}\begin{bmatrix} 0_{3x3} \\ I_{3x3} \end{bmatrix}}_{B(t)}u(k) \tag{3-13}$$

however, here the inputs are impulsive ΔV. It is to be noted that the LVLH frame in which these equations are defined varies from the definition given in Subsection 3-1-1. The relation between the LVLH frame shown in Figure 3-2 and the one used by the 'equations is:

$$\begin{bmatrix} x_{\mathrm{YA}} \\ y_{\mathrm{YA}} \\ z_{\mathrm{YA}} \end{bmatrix} = \begin{bmatrix} y_{\mathrm{LVLH}} \\ -z_{\mathrm{LVLH}} \\ -x_{\mathrm{LVLH}} \end{bmatrix} \tag{3-14}$$

Xu-Wang Model

The Xu-Wang model was found not to have been used for theoretical or implementation studies for RVD, but it has been used for theoretical research of formation flight [10] [33] [7]. The model was futher expanded to include atmospheric drag by Morgan as explained in the previous subsection [37]. Before we expand on the model the Reference Satellite Variables (RSV) must be explained. This model developed by Xu and Wang proposed a set of variables named the Reference Satellite Variables (RSV) [60]. These variables could also be used to represent the motion of a target satellite, although they were not initially designed for that use. They are presented in this subsection due top their possible benefits for our scope. The full relative dynamic model will be presented with the other relative dynamic model later on.

The model is compromised of six differential equations describing the motion of the satellite using the RSV. The Reference Satellite Variables are the following:

- r: Orbital radius
- v_x: Radial velocity
- h: Angular momentum
- θ: True Anomaly
- i: Orbit inclination
- Ω: Right Ascension of the Ascending Node

It is to be noted that the first five variables are independent of the Ω and thus the first five variables are named the compact RSV. The six differential equations describing the variables are given in (3-15).

$$\begin{aligned}
\dot{r} &= v_x \\
\dot{v}_x &= -\frac{\mu}{r^2} + \frac{h^2}{r^3} - \frac{k_{J_2}}{r^4}(1 - 3\sin i^2 \sin\theta^2) \\
\dot{h} &= -\frac{k_{J_2} \sin i^2 \sin 2\theta^2}{r^3} \\
\dot{\theta} &= \frac{h}{r^2} - \frac{2k_{J_2} \cos i^2 \sin\theta^2}{hr^3} \\
\dot{i} &= -\frac{k_{J_2} \sin 2i \sin 2\theta}{2hr^3} \\
\dot{\Omega} &= -\frac{2k_{J_2} \cos i \sin\theta^2}{hr^3}
\end{aligned} \tag{3-15}$$

The model was developed based on the Lagrange Equation presented in (3-16).

$$\frac{\mathrm{d}}{\mathrm{dt}}\left(\frac{\partial \mathcal{L}}{\partial \mathbf{r}}\right) - \frac{\partial \mathcal{L}}{\partial \mathbf{r}} = \mathbf{F}_{\text{gen}} \tag{3-16}$$

where $\mathcal{L} = \mathbf{K} - \mathbf{P}$ is the Lagrangian, representing the difference between the kinetic and potential energy, and $\mathbf{F}_{\text{gen}}$ is the generalized force in each direction. The kinetic energy of the chaser spacecraft can be determined through $\mathbf{K}_{\text{chs}} = \frac{1}{2}\dot{\mathbf{r}}_{\text{chs}}^{\mathsf{T}}\dot{\mathbf{r}}_{\text{chs}}$, with the velocity of the chaser spacecraft $\dot{\mathbf{r}}_{\text{chs}}$, being in the ECI frame. The J_2 perturbed gravity potential is given by (3-1) and thus combining these together resulted in the relative dynamics model given in (3-17). The chaser spacecraft variables are denoted with the chs subscript, while for simplicity the target spacecraft variables have no subscript. It is to be noted that the variables of this model are the RSVs given by (3-15).

$$\begin{aligned}
\ddot{x}_{\text{chs}} &= 2\dot{y}_{\text{chs}}\omega_z - x_{\text{chs}}(\eta^2 - \omega_z^2) + y_{\text{chs}}a_z - z_{\text{chs}}\omega_x\omega_z - (\zeta_{\text{chs}} - \zeta)\sin i \sin\theta - r(\eta_{\text{chs}}^2 - \eta^2) + F_{\text{chs},x} \\
\ddot{y}_{\text{chs}} &= -2\dot{x}_{\text{chs}}\omega_z + 2\dot{z}_{\text{chs}}\omega_x - x_{\text{chs}}a_z - y_{\text{chs}}(\eta_{\text{chs}}^2 - \omega_z^2 - \omega_x^2) + z_{\text{chs}}a_x - (\zeta_{\text{chs}} - \zeta)\sin i \cos\theta + F_{\text{chs},y} \\
\ddot{z}_{\text{chs}} &= -2\dot{y}_{\text{chs}}\omega_x - x_{\text{chs}}\omega_x\omega_z - y_{\text{chs}}a_x - z_{\text{chs}}(\eta_{\text{chs}}^2 - \omega_x^2) - (\zeta_{\text{chs}} - \zeta)\cos i + F_{\text{chs},z}
\end{aligned} \tag{3-17}$$

where ω_x and ω_z are the orbital and steering rates, a_x and a_z are the orbital and steering accelerations and $F_{\text{chs},..}$ are the control forces of the chaser spacecraft. Furthermore, the accelerations ζ_{chs} and ζ are given by:

$$\begin{aligned}
\zeta_{\text{chs}} &= \frac{2k_{J_2}r_{\text{chs}}}{r_{\text{chs}}^5} \\
\zeta &= \frac{2k_{J_2}\sin i \sin\theta}{r^4}
\end{aligned} \tag{3-18}$$

The angular velocities η_{chs} and η are on the other hand given by:

$$\begin{aligned}
\eta_{\text{chs}}^2 &= \frac{\mu}{r_{\text{chs}}^3} + \frac{k_{J_2}}{r_{\text{chs}}^5} - \frac{5k_{J_2}r_{\text{chs}}^2}{r_{\text{chs}}^7} \\
\eta^2 &= \frac{\mu}{r^3} + \frac{k_{J_2}}{r^5} - \frac{5k_{J_2}\sin i^2 \sin\theta^2}{r^5}
\end{aligned} \tag{3-19}$$

where $r_{\text{chs},z}$ is the distance from the chaser satellite to the equatorial plane. With the EOM being a second order differential equation, combining these with (3-15) results in the entire model. The model can then be described through 11 first order differential equations, 6 first order equations derived from (3-17) and the 5 first order equations for the RSV presented in (3-15). This model was shown to achieve higher accuracy than the HCW, Tschauner-Hempel [54], Schweighart-Sedwick [47] and a non-linear unperturbed model developed by Gurfill [21] by the comparison carried out in [58]. This result is not surprising, as the Xu-Wang model is an exact perturbed nonlinear model, making it the most complete out of the models considered. The performance of the Xu-Wang model is however, not known compared to other exact nonlinear perturbed models high fidelity models.

As mentioned before, Morgan expanded this model in order to include atmospheric drag. This was done by replacing the control force vector $\mathbf{F}$ with a generalized force vector, $\mathbf{F}_{\text{gen}}$ as atmospheric drag is a non-conservative force. The expression for the generalized force vector is found in Apendix B of Morgan's paper, where it is named as Q_n [37].

A linearized version of the Xu-Wang model is presented in [58]. Wang notes that the only nonlinear terms are η_{chs}^2 and ζ_{chs} and thus by applying the Gegenbauer polynomial technique a linearized model of the Xu-Wang is obtained. The linearized model is presented in (3-20). For simplicity $s_x = \sin x$ and $c_x = \cos x$.

$$
\begin{aligned}
\ddot{x}_{\text{chs}} &= 2\dot{y}_{\text{chs}}\omega_z + x_{\text{chs}}\,(2\eta^2 + \omega_z^2 + \frac{2k_{J_2}}{r^5}(1 - s_i^2 s_\theta^2)) + y_{\text{chs}}\,(a_z + \frac{4k_{J_2}s_i^2 s_{2\theta}}{r^5}) - 5z_{\text{chs}}\omega_x\omega_z + a_{\text{chs},x} \\
\ddot{y}_{\text{chs}} &= -2\dot{x}_{\text{chs}}\omega_z + 2\dot{z}_{\text{chs}}\omega_x + x_{\text{chs}}\,(\frac{4k_{J_2}s_i^2 s_{2\theta}}{r^5} - a_z) - y_{\text{chs}}\,(\frac{2k_{J_2}s_i^2 c_\theta^2}{r^5} + \eta^2 - \omega_z^2 - \omega_x^2) + \\
&\quad z_{\text{chs}}\,(a_x - \frac{k_{J_2}s_{2i}c_\theta}{r^5}) + a_{\text{chs},y} \\
\ddot{z}_{\text{chs}} &= -2\dot{y}_{\text{chs}}\omega_x - 5x_{\text{chs}}\omega_x\omega_z - y_{\text{chs}}\,(\frac{k_{J_2}s_{2i}c_\theta}{r^5} + a_x) - z_{\text{chs}}\,(\frac{2k_{J_2}c_i^2}{r^5} + \eta^2 - \omega_x^2) + a_{\text{chs},z}
\end{aligned}
\tag{3-20}
$$

For the simulation the non-linear equations will be used, but for the MPC formulations a discrete time LTV state space form will be needed. So (3-20) will be discretized and put into matrix form for the controllers.

3-2 Controlling the Satellite

Controlling the RVD operation means computing the optimal accelerations required by the thrusters to achieve the various mission phase objectives and eventually dock to the target. This research is based on evaluating different MPC strategies, so an overview will be given of MPC theory. Traditional feedback gains aren't able to handle constraints which are an integral part of the RVD problem. MPC is proposed as it is able to take constraints into account in its formulation and compute an input that allows for them to be satisfied while optimizing the control objective. The advantage of an online MPC compared to a library of offline computed manoeuvres is that less memory is required and MPC is able to determine the optimum solution for the specific situation at that time interval as well as account for disturbances

3-2-1 Model Predictive Control

Model Predictive Control (MPC) is a class of computer-controlled algorithms, which make use of an explicit model to determine the most adequate control action based on the plant's predicted future response. The main concept of the MPC strategy is shown in Figure 3-4. A discrete time setting is used, and the figure shows the desired set point trajectory r_j (green), past state evolution (purple), the predicted state evolution (red) and control input (blue). The event (x_j, u_j) represents, the plant's state x_j, the control input u_j at the current time step j. The MPC makes use of the internal discrete time model of the plant to predict the plant's behaviours, from the current time step over the prediction horizon m_{p} (often N_{p}) . Subsequently, through an optimization problem the MPC computes (online) the optimal control sequence based on the chosen cost function, from the current time step over the

control horizon m_c (often N_c), which will result in predicted state evolution (red line). From the computed input sequence, the first one is the only one to be sent to the plan, the entire process is then carried out again for the following time step [45].

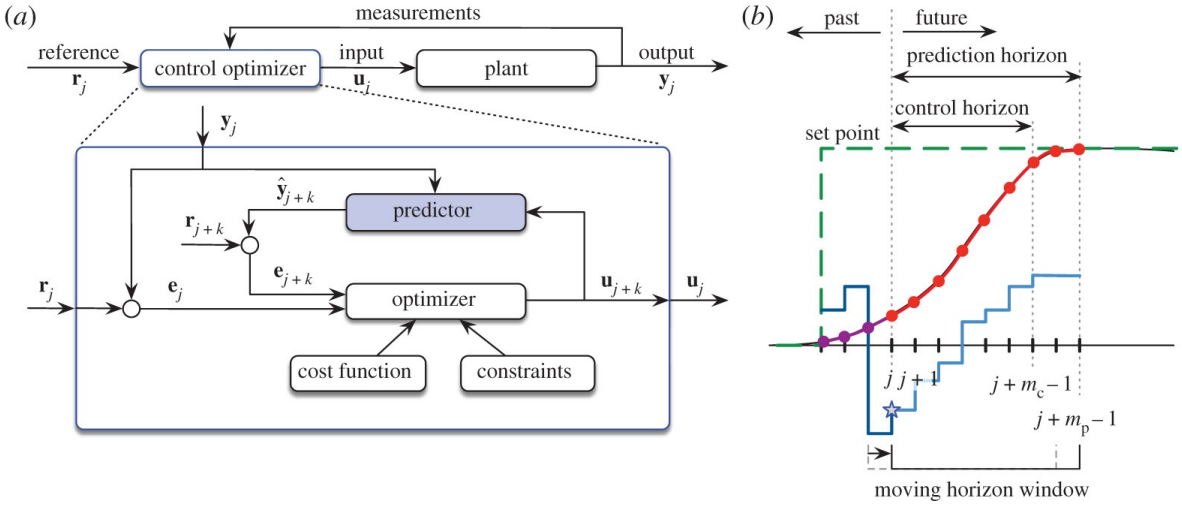

Figure 3-4: MPC formulation: (a) schematics (b) receding horizon control strategy [25]

MPC provides an advantage compared to traditional offline computation of a state feedback control law $u = \kappa(x)$, such as an Proportional Integral Derivative (PID) controller, in that it is able to control moving processes with hard (dynamic) constraints [35]. Something that traditional offline computed controllers are not able take into account. Furthermore, MPC allows one to implement a Dynamic Programming (DP) solution even though the plant is nonlinear and constrained or the state dimension is high [45].

The constrained MPC formulation is the simplest formulation besides the unconstrained MPC formulation. The unconstrained formulation will not be discussed separately as it is not of use to the rendezvous and docking problem. If a discrete time deterministic model of a system is cons“idered as in (3-21).

$$\begin{aligned} x(k+1) &= f(x(k), u(k)) \\ y(k) &= h(x(k), u(k)) \end{aligned} \tag{3-21}$$

where k denotes the time step, $x \in \mathbb{R}^{n_x}$ are the states of the system, $u \in \mathbb{R}^{n_u}$ are the control inputs and $y \in \mathbb{R}^{n_y}$ are the outputs of the system. Furthermore, $f(\bullet)$ and $h(\bullet)$ are continuous functions with the desired equilibrium of $f(0,0) = 0$ and it is assumed that the states are measurable. This model is necessary to the MPC formulation as the computation of the optimal control sequence is based on a prediction of the system outputs through an explicit model as explained in the previous subsection. A problem is that in reality systems and processes are described through Continuous-Time (CT) differential equations. In order to implement a MPC formulation, which functions in discrete time due to the nature of computer controlled processes, an adequate sampling time must be chosen for the CT system. Sampling is a result of computers storing CT signals by sequence of data points for each sampling instance. In the majority of applications the sampling instant is constant, in which case

the sampling period is often denoted by h or T_s. The choice of sampling period can have significant effects on the digital reconstruction of the CT signals, thus it will have to be taken into consideration in the MPC formulation [16]. The predicted outputs, future states and future control inputs of the MPC formulation can be denoted as:

$$\begin{aligned}\vec{x} &= \begin{bmatrix} x(k|k) & x(k+1|k) & \dots & x(k+N_p-1|k) \end{bmatrix}^\intercal \\ \vec{y} &= \begin{bmatrix} y(k|k) & y(k+1|k) & \dots & y(k+N_p-1|k) \end{bmatrix}^\intercal \\ \vec{u} &= \begin{bmatrix} u(k|k) & u(k+1|k) & \dots & u(k+N_c|k) \end{bmatrix}^\intercal \end{aligned} \tag{3-22}$$

where $y(k+i|k)$ is the predicted output at time instant $k+i$ based on the system information at time step $y(k)$, N_p is the prediction horizon and N_c is the control horizon. The prediction horizon determines the amount of time intervals taken into account in the optimization, while the control horizon determines the amount of control variables to be included in the optimization. The prediction horizon is thus always larger or equal to the control horizon, $N_c \leq N_p$. As the optimization variables are the control inputs, it is useful to express the predicted state evolution in terms of the input sequence. This will often be dependent on the model of the system. If the system can be expressed as a state space model, the state evolution is determined sequentially using the control inputs. Considering the simplest case of a discrete Linear Time Invariant (LTI) system shown in (3-23).

$$\begin{aligned} x(k+1) &= Ax(k) + Bu(k) \\ y(k) &= Cx(k) + Du(k) \end{aligned} \tag{3-23}$$

Through the state space matrices future state variables can thus be expressed in terms of the future control inputs as shown below:

$$\begin{aligned} x(k+1|k) &= Ax(k) + Bu(k) \\ x(k+2|k) &= Ax(k+1) + Bu(k+1) \\ &= A^2x(k) + ABu(k) + Bu(k+1) \\ &\vdots \\ x(k+N_p|k) &= A^{N_p}x(k) + \sum_{i=1}^{N_c} A^{i-1}Bu(k+N_c-i) \end{aligned} \tag{3-24}$$

Using the relations presented in (3-24) and the fact that $y = Cx$, it is possible to express the predicted output variables in terms of the control inputs. If the relations for the future output variables are stacked, the prediction model will be in the matrix form presented below:

$$\vec{y} = Tx(0) + S\vec{u} \tag{3-25}$$

where matrices T and S are defined as:

$$T = \begin{bmatrix} C \\ CA \\ CA^2 \\ \vdots \\ CA^{N_\mathrm{p}-1} \end{bmatrix}, \quad S = \begin{bmatrix} D & 0 & 0 & \cdots & 0 \\ CB & D & 0 & \cdots & 0 \\ CAB & CB & D & \cdots & 0 \\ \vdots & \vdots & \vdots & \vdots & \vdots \\ CA^{N_\mathrm{p}-1}B & CA^{N_\mathrm{p}-2}B & \cdots & CA^{N_\mathrm{p}-N_\mathrm{c}}B & D \end{bmatrix} \tag{3-26}$$

This matrix form of the prediction model will be of use for the cost function. The MPC formulation is dependent on a minimization problem for which the resulting computed control inputs result in the minimum value of the cost function. Typically, the cost function for the optimal control problem is the sum of the cost of the future responses over the prediction interval $[k, k+N_\mathrm{p}]$. This type of cost of function is expressed as:

$$J(x(k), u(k)) = \sum_{j=0}^{N_\mathrm{p}-1} l(x(k+j|k), u(k+j|k)) \tag{3-27}$$

where $l(x, u)$ represents the stage cost, which is often a quadratic cost function of the form:

$$l(x(k), u(k)) = ||x(k)||_Q^2 + ||u(k)||_R^2 = x^\intercal(k)Qx(k) + u^\intercal(k)Ru(k) \tag{3-28}$$

where Q and R are respectively positive semi-definite and positive definitive weighting matrices. The use of weighting matrices allows for many tuning options and trade-offs [17]. Another variation of cost function (3-27) is often used, which includes the terminal stage cost together with a terminal constraint in order to achieve nominal stability [45]. This terminal stage cost is a separate stage cost for the terminal state $x(k+N_\mathrm{p})$ and has the form:

$$l_N(x(k+N_\mathrm{p})) = x(k+N_\mathrm{p})^\intercal P x(k+N_\mathrm{p}) \tag{3-29}$$

where P is a positive definite matrix, and is often chosen as the solution to the Ricati equation for matrices (A, B, Q, R). Next to the terminal stage cost a constraint will be imposed on the terminal state $x(k+N_\mathrm{p}) \in \mathbb{X}_\mathrm{f}$, where $\mathbb{X}_\mathrm{f}$ is a positive invariant set [45].

The majority of systems in real life have physical and control limitations. These limitations are taken into consideration through constraints in the MPC formulation. These limitations can be formulated into three main types of constraints: hard, soft and set-point approximation, as is presented in Figure 3-5. Hard constraints are constraints which can not be violated. They are defined by closed and compact sets for the state and input, and are formulated as inequalities as presented in (3-30).

$$\begin{aligned} x \in \mathbb{X} \subset \mathbb{R}^{n_x}, \quad & x_{\min} \leq x(k) \leq x_{\max} \\ u \in \mathbb{U} \subset \mathbb{R}^{n_u}, \quad & u_{\min} \leq u(k) \leq u_{\max} \end{aligned} \tag{3-30}$$

On the other hand, soft constraints, as the name suggests, allow some violation of the constraint boundary at the expense of an added penalty to the cost function. This way the optimization problem will favour the constraints not being violated but violations can occur

if necessary. These type of constraints can be included into the MPC formulation through the implementation of slack variables or a penalty functions in the cost function [26]. Slack variables are implemented in the hard constraints inequalities resulting in inequalities (3-31).

$$\begin{aligned} x_{\min} - \epsilon \leq x(k) \leq x_{\max} + \epsilon \\ u_{\min} - \epsilon \leq u(k) \leq u_{\max} + \epsilon \end{aligned} \tag{3-31}$$

where, ϵ are the slack variables. The penalty related to the use of slack variables is then added to the original cost function, resulting in the following:

$$J_{\text{slack}} = J(x(k), u(k)) + \rho||e|| \tag{3-32}$$

where ρ is the constraint violation penalty weight. It is to be noted that the slack variables will increase the dimension of the optimization problem. Exact penalty functions can be implemented into the MPC formulation in a similar manner, by explicitly adding the functions to the cost function without the definition of extra variables. Considering the function $c(\cdot)$ represents the magnitude of the constraint violation then the cost function becomes:

$$J_{\text{pen},f} = J(x(k), u(k)) + \rho||c(x(k), u(k))|| \tag{3-33}$$

Finally, the set-point approximation is another soft constraint type. A set point is defined for each soft constraints and so a penalty function for both sides to the constraint is added to the cost function.

The use of the stage cost function is aimed at minimizing the (squared) error of the state with respect to the origin of the system. This is functional for a standard regulator problem, but in practical applications reference tracking problem is very common. The cost will then be aimed at minimizing the (squared) error between the reference and state trajectory. Just as for the constraints there are various methods in which a reference trajectory can be defined and they are presented in Figure 3-6. The four methods are the set-point, zone, reference trajectory and funnel method, the shaded area in the figures represents the tracking error. The set-point reference trajectory corresponds to a constant reference trajectory i.e. $r(k) = r$, $\forall k$, penalty is awarded for above or below the reference. The second method is zone control tracking, which is aimed at keeping the state within certain bounds i.e. $r_{\min} \leq r(k) \leq r_{\max}$. They are ultimately state constraints and is implemented as such. The third method is the reference trajectory, which is ultimately a time varying set-point reference where all deviations from the trajectory are penalized. Lastly, the funnel method is the combination of the zone and reference trajectory method. The bounds of the reference zone are thus defined by two separate reference trajectories. The slope of the funnel is a tuning parameter that will affect the controller performance.

The cost function for the reference tracking problem is constructed in a similar manner as the regulator problem. Besides the vectors presented in (3-22), if we also consider the reference trajectory vector below:

$$\vec{r} = \begin{bmatrix} r(k|k) & r(k+1|k) & r(k+2|k) & \cdots & r(k+N_{\text{p}}-1|k) \end{bmatrix}^{\mathsf{T}} \tag{3-34}$$

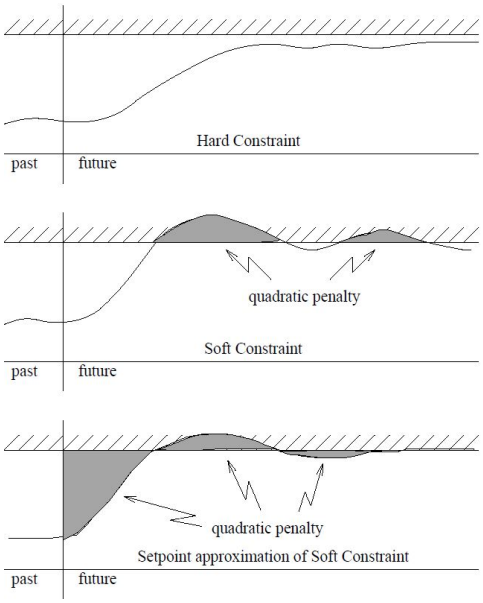

Figure 3-5: Hard, Soft and Set-point approximation constraints [43]

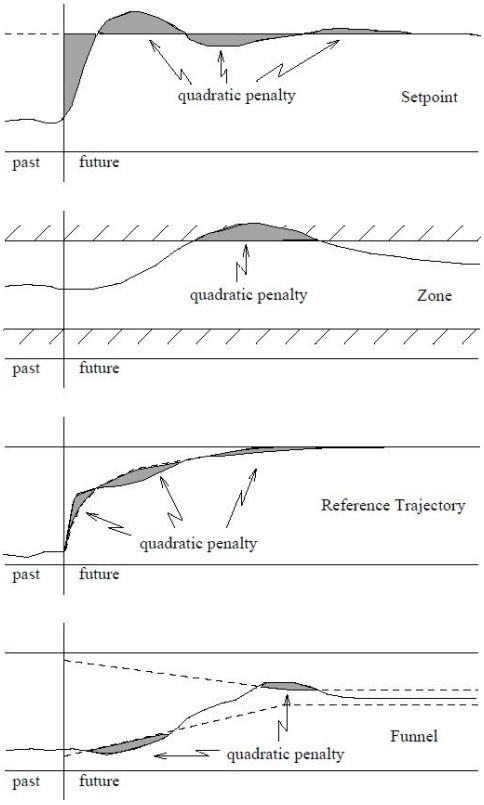

Figure 3-6: Set-point, zone, reference and funnel reference trajectories [43]

Defining the tracking error as, $e(k) = r(k) - x(k)$, the stage cost function (3-28) then becomes:

$$l(e(k), u(k)) = ||e(k)||_Q^2 + ||u(k)||_R^2 = e^\intercal(k)Qe(k) + u^\intercal(k)Ru(k) \tag{3-35}$$

All the elements necessary for the constrained optimal control problem have been defined, and Can consequently be formulated. Considering the defined sequences, constraints, and cost function, the constrained optimal control problem is then defined as:

$$\begin{aligned}
&\min_u J(x(k|k), u(k|k)) \\
&\text{subject to:} \\
&x(k+1) = Ax(k) + Bu(k) \\
&y(k) = Cx(k) + Du(k) \\
&x_{\min} \leq x(k) \leq x_{\max} \quad \text{or other} \\
&u_{\min} \leq u(k) \leq u_{\max} \quad \text{or other}
\end{aligned} \tag{3-36}$$

3-3 Conclusion

In this Chapter, all the required existing theory was reviewed in order to provide a basis of understanding of the current knowledge and approaches. From this review, conclusions were drawn.

Relative Dynamic models are mostly described in the LVLH frame centred around the target satellite. The most significant disturbances to affect LEO satellites are the J_2 effect and atmospheric drag. These will be added to the simulation as to improve the accuracy of the investigation. Extensive research has been carried out in the development of relative dynamic models, but there are too many to compare in this thesis. Three models are chosen of increased complexity to compare. The HCW model is chosen as the baseline due to its flight heritage and representing the industry standard. Next, the YA model will be the second step, as it presents a further development of the HCW model to include eccentricity and has been applied for this purpose in research. Finally, the Xu-Wang model will be the final step. It is an exact model including eccentricity and the J_2 effect, but its propagation performance has not been compared to the other two models before and has not been applied for control applications yet. All three models rely on expressing the relative position and velocity in the LVLH frame. The HCW is a LTI model while the YA model is LTV. The Xu-Wang model is also LTV, but also requires the propagation of 6 RSV and is the most computationally expensive but deemed to be able to be real time applicable within the constraints of the mission.

Control of the chaser spacecraft is dependent on the mission phase objectives. The measurement and estimation of all the required variables for the control of the chaser spacecraft will not include in this research, as it is not relevant to the comparison of different MPC formulations. MPC provides a useful control strategy that is able to handle constraints and assures that they will be satisfied while optimizing the control objective. As an online optimization control scheme it provides the ability to compute the optimum solution for the specific instance compared to offline control schemes. Considering that RVD missions include a wide range of hard constraints that must be satisfied for mission success, MPC is well suited for this problem. Besides the choice of prediction model, the type of MPC formulation is dependent on the cost function and constraints that are used. The choice of prediction model to be evaluated has been made, but the choices regarding constraints, cost functions and robust or non-linear formulations will be presented further on.

To conclude, with an overview of all the required knowledge regarding RVD heritage, relative dynamic models and MPC the problem will be formulated in the coming chapter. Before developing the methodology.

Chapter 4

Problem Formulation

The historical context, as well as the existing and future challenges of RVD were explained in Chapter 2. Next, the research context and theoretical background were presented in Chapter 3. From this, it became evident that even though there have been theoretical and research applications for Model Predictive Control (MPC) in RVD missions, there is a gap of knowledge present about combining aspects from these applications and comparing them under the same baseline. In the last two decades various researchers have developed MPC controllers for rendezvous and docking due to the growing interest and feasibility of autonomous rendezvous and docking as mentioned in Chapter 1. The goal of this research is to fill this knowledge gap by integrating this knowledge and comparing it under the same baseline to determine the most appropriate Model Predictive Control (MPC) strategy for Rendezvous and Docking (RVD) to an uncooperative target with respect to propellant consumption and completion time, while being real-time applicable. This research will specifically aim to combine all the produced knowledge in determining the optimal controller for propellant use and docking accuracy for real-time implementation.

4-1 Research Objectives

The primary objective of this research is to determine an optimal MPC formulation for propellant use and docking accuracy for real-time application. The control strategy must be able to of guiding the chaser spacecraft to the target spacecraft and dock with it. The control strategy must be able to satisfy each mission phase objective while minimizing fuel consumption. In order to realize the main objective, the following sub-objectives must be achieved:

- Develop and compare prediction models describing the relative dynamics between the chaser and target satellite. The models must capture all the necessary processes that affect the chaser and target. Then one can determine which prediction model describing the dynamics of the chaser and target satellite is best suited for minimizing propellant use while maintaining accuracy.

- Determine if the inclusion of processes that are not included in the in prediction models can improve the propellant consumption of the chaser target. Frameworks must be chosen on how to captivate these processes and how to introduce them in the prediction models.
- Develop various suitable MPC formulations for controlling the chaser satellite. The formulations must be able to generate an optimal control sequence to ensure the chaser satisfies its constraints and is able to dock with the target satellite.

4-2 Research Questions

From the objectives explained above, we are able to elaborate research questions that will function as the scope of this thesis.

4-2-1 Main Research Question

What type of model predictive control strategy is best suited for real-time application in the complete rendezvous and docking problem, to minimize propellant use while maintaining adequate completion time?

4-2-2 Sub Research Questions

1. *What type of relative orbital dynamics model allows for the best description of the target and chaser spacecraft in orbit as to minimize propellant consumption and completion time?*
    - *Does the use of a more accurate model compared to the Clohessy Wiltshire (HCW) model provide any significant propellant savings and docking accuracy improvement for each mission phase while retaining real-time applicability?*
    - *Does the modelling of disturbances provide any increase in propellant use throughout the mission and docking performance during the terminal phase?*
2. *How can (LP, Time-Varying, Non-Linear, Stochastic and Robust) an MPC algorithm be constructed to carry out rendezvous and docking mission with an uncooperative (still, rotating or tumbling) target?*
    - *What type of MPC strategy is best suited for the various mission phases for the designated MPC strategy?*
    - *What are the limitations imposed on the chaser spacecraft for the various rendezvous and docking mission phases, and how can we transform these to input and state constraints?*
    - *What type of cost function will guarantee the best compromise between propellant use and docking strategy for each mission phase?*

Chapter 5

Methodological approach

Having reviewed all the necessary heritage and theory as well as having presented the problem formulation. The exact methodological approach developed using the theory and heritage, to answer the research questions will be presented. In this Chapter the various mission phases and their Model Predictive Control (MPC) strategy for each mission phase will be presented.

5-1 Intermediate Range

The objective of the first phase of a rendezvous and docking mission will be to synchronise the orbit of the chaser with that of the target spacecraft. The objective must be completed in finite time while minimizing fuel consumption. The controller must so be able to bring the chaser to within 20 km. Launchers have an orbit-insertion accuracy of ±30 km, so similar as in [22] the chaser satellite will begin around 300 km behind the target with a 30 km deviation in semi major axis. The orbital initial conditions are presented in Table 5-1.

Table 5-1: Orbital Parameters for Target and Chaser

Orbital Parameters	Target	Chaser
Semi Major axis [km]	6918.6	6888.6
Eccentricity	0.013611	0.013611
Inclination [deg]	60	60
Argument of Perigee [deg]	103.89	103.89
Right Ascension of the Ascending Node [deg]	123.61	123.61
True Anomaly [deg]	5	2

5-1-1 State Constraints

This mission phase is the least complex in terms of the constraints involved. There are only 2 state constraints involved. The idea of including a free drift trajectory constraint, as done in

[22] was not done because on Mars there are no other satellites to take into account in Low Earth Orbit (LEO) ensuring the chaser satellite does not crash with the target in free drift, still allow the risk for a collision to remain. It would thus not impact the possible collateral damage caused due to loss of control, and that would be best solved through backup systems or other safety systems. The first constraint is a running constraint ensuring the chaser remains behind the target and is presented in (5-1).

$$\underbrace{\begin{bmatrix} 0 & 1 & 0 & 0 & 0 & 0 \end{bmatrix}}_{A_{\text{freedrift}}} x(k) \leq 0 \tag{5-1}$$

Finally, the second and last state constraint is a terminal constraint set on the along track distance between the chaser and target. As the objective of this mission phase is to get the chaser within 20 km of the target, the terminal constraint imposes that the chaser be within 30 km and 10 km as shown in (5-2).

$$\underbrace{\begin{bmatrix} 0 & -1 & 0 & 0 & 0 & 0 \\ 0 & 1 & 0 & 0 & 0 & 0 \end{bmatrix}}_{A_{\text{terminal}}} x(N_p) \leq \underbrace{\begin{bmatrix} 30 \times 10^3 \\ -10 \times 10^3 \end{bmatrix}}_{b_{\text{terminal}}} \tag{5-2}$$

it is to be noted that the constraints will differ for the Yamanaka-Ankersen (YA) prediction model due to the different definition of the LVLH reference frame as explained in Subsection 3-1-1.

5-1-2 Input Constraints

The input constraints are defined in the form of a maximum deliverable acceleration on each input vector element, as presented in (5-33).

$$\begin{aligned} -u_{\text{lim}} \leq u_i(j|t) \leq u_{\text{lim}}, \quad i \in \{1,2,3\} \\ u_{\text{lim}} = D_\tau \frac{F_c}{m} \\ u_{\text{lim YA}} = D_\tau \frac{F_c T_s}{m} \end{aligned} \tag{5-3}$$

where F_c N is the force capacity, m kg is the mass of the chaser craft and D_τ is the thruster duty cycle as the fraction of the sampling period. As the YA model requires ΔV as an input, its bound is represented by $u_{\text{lim YA}}$.

5-1-3 Disturbance Estimator

The three prediction models used are of different degrees of accuracy. The HCW model includes no disturbances and eccentricity, the YA model includes eccentricity but no disturbances, while the Xu-Wang model includes eccentricity and the J_2 effect. As was mentioned in Sub-Section 3-1-2 the most significant disturbances for LEO are atmospheric drag and the

J_2 effect meaning a constant disturbance of 10^{-4} m/s^2 will be added to the along track direction to represent drag as well as random normally distributed disturbances in all directions of 10^{-5} m/s^2 to represent other disturbances according to Figure 3-3.

Disturbance estimators will be added to the prediction models to evaluate if they can provide performance benefits in terms of propellant consumption. The inclusion of a disturbance in the prediction model will tighten state and input constraints. Most robust techniques make use of the worst possible disturbance at the cost of performance, but the current estimated disturbance will be used instead. Two types of disturbance estimators will be used. The first is the simplest form of the disturbance estimators and is presented in (5-4).

$$\begin{aligned} \hat{x}(k+1) &= A\hat{x}(k) + Bu(k) + \delta(k) \\ \delta(k) &= x(k) - \hat{x}(k) \end{aligned} \tag{5-4}$$

The second disturbance estimator used is one presented in [22] as it has been proven to work and will useful to compare its performance compared to a classical one. The disturbance estimator is presented in (5-4).

$$\begin{aligned} \hat{x}(k+1) &= A\hat{x}(k) + Bu(k) + \delta(k) \\ \delta(k) &= \delta(k-1) + W * (x(k) - \hat{x}(k)) \end{aligned} \tag{5-5}$$

5-1-4 Delay

The MPC formulation functions under the assumption that the optimal input is determined for the current time step and is then applied, however in real life it will take time to process sensor data, solve the optimization problem and apply the desired input. A delay will thus be present in the system, on SmallSats and CubeSats processing power is no longer limiting, but it will still be advantageous to see if the system can function with one-step delay. The delayed prediction model is presented in (5-36).

$$\begin{bmatrix} \hat{x}(k+1) \\ u(k) \end{bmatrix} = \begin{bmatrix} A & B \\ 0 & 0 \end{bmatrix} \begin{bmatrix} \hat{x}(k) \\ u(k-1) \end{bmatrix} + \begin{bmatrix} 0 \\ I \end{bmatrix} u(k) \tag{5-6}$$

As an incremental input cost function will also be evaluated, a delayed prediction model formulation including incremental input must also be used and is presented in (5-7):

$$\begin{bmatrix} \hat{x}(k+1) \\ u(k) \end{bmatrix} = \begin{bmatrix} A & B \\ 0 & I \end{bmatrix} \begin{bmatrix} \hat{x}(k) \\ u(k-1) \end{bmatrix} + \begin{bmatrix} 0 \\ I \end{bmatrix} \Delta u(k) \tag{5-7}$$

5-1-5 Cost Function

The two cost functions that will be evaluated are the standard quadratic cost function represented by (5-37) with a terminal stage cost. The second cost function that will be evaluated

will be a quadratic cost function with terminal stage cost but also including a penalty on the change in input, also referred to as incremental input cost function, shown in (5-38).

$$J(x(k),u(k))_u = \sum_{k=1}^{N_\mathrm{p}-1} ((x(k)-r(k))^\intercal Q(x(k)-r(k)) + u^\intercal(k)Ru(k)) + x(N_p)^\intercal P x(N_p) \quad (5\text{-}8)$$

$$J(x(k),u(k))_{\Delta u} = \sum_{k=1}^{N_\mathrm{p}-1} ((x(k)-r(k))^\intercal Q(x(k)-r(k)) + \Delta u^\intercal(k)R_{\Delta u}\Delta u(k) + u^\intercal(k)Ru(k)) + x(N_p)^\intercal P x(N_p) \quad (5\text{-}9)$$

5-1-6 MPC Formulations

With the three different prediction models, two robust models and two cost functions it will result in more than 10 MPC formulations to be compared. We will not explicitly state all of them due to redundancies but all their performance will be shown in the results. The non delayed formulations will have form (5-10), while the delayed formulations will have form (5-11).

$$\begin{aligned}
&\min_u J(x(k),u(k)) \quad or \quad J(x(k),u(k))_{\Delta u} \\
&\text{subject to:} \\
&x(0) = x_{\text{intial}} \\
&x(k+1) = Ax(k) + Bu(k) \quad \text{or} \quad x(k+1) = Ax(k) + Bu(k) + \delta(k), \quad k \in [0, N_p) \\
&A_{\text{freedrift}}x(k) \leq 0, \quad \forall k \\
&A_{\text{terminal}}x(k) \leq b_{\text{terminal}}, \quad k = N_p \\
&u_{\min} \leq u(k) \leq u_{\max}, \quad k \in [0, N_p)
\end{aligned} \quad (5\text{-}10)$$

$$\begin{aligned}
&\min_u J(x(k),u(k)) \quad or \quad J(x(k),u(k))_{\Delta u} \\
&\text{subject to:} \\
&x(0) = x_{\text{intial}} \quad \& \quad u(-1) = u_{\text{initial}} \\
&x(k+1) = Ax(k) + Bu(k-1) \quad \text{or} \quad x(k+1) = Ax(k) + Bu(k-1) + \delta(k), \quad k \in [0, N_p) \\
&A_{\text{freedrift}}x(k) \leq 0, \quad \forall k \\
&A_{\text{terminal}}x(k) \leq b_{\text{terminal}}, \quad k = N_p \\
&u_{\min} \leq u(k-1) \leq u_{\max}, \quad k \in [0, N_p)
\end{aligned} \quad (5\text{-}11)$$

5-2 Short Range

The objective of the short range phase is to reduce the along track separation between the chaser and target spacecraft from $10 - 30$ km to a few hundred meters. This objective must again be satisfied while minimizing fuel consumption. This will be done through controlling the satellite to a 100 m within the target while remaining in field of view of the target and then for it to stay at a holding point there until the next mission phase is activated, similar as was done for the Mars sample return mission [22].

5-2-1 State Constraints

This mission phase will thus have a terminal constraint related to the holding point at then end. The constraint requires the chaser spacecraft to be in a box, centred on the point x_{hp}, with an in-plane width of x_{hp} and out of plane width of x_{hp}. This as so to prevent large overshoot when switching to the capture controller. The constraint takes the form:

$$\begin{bmatrix} I & 0 \\ -I & 0 \end{bmatrix} x(j_N) \leq c_{\text{hp}}(j_N) \tag{5-12}$$

where $j_N = t + N_{\text{p}} T_{\text{s}}$. Similar constraints are formulated for the chaser position after 1/4, 1/2, 3/4 orbits in terms of true anomaly.

$$\begin{bmatrix} I & 0 \\ -I & 0 \end{bmatrix} A(j_N : j_N + \Delta T) x(j_N) \leq c_{\text{hp}}(j_N + \Delta T), \quad \forall \Delta T \in \{T_{1/4}, T_{1/2}, T_{3/4} T\} \tag{5-13}$$

The corresponding true anomaly for the 1/4, 1/2, 3/4 and 1 orbits can be easily computed as a full orbit is 2π. Using these values and through the mean anomaly (5-14), where Δt is the time since the last passing of the perigee and n_{tgt} is the mean anomaly rate [57], the corresponding time for the orbits is then determined through (5-15), where T_{orb} is the orbital period of the target.

$$M_{\text{tgt}}(t) = 2 \tan^{-1} \frac{\sqrt{1 - e_{\text{tgt}}} \tan \theta_{\text{tgt}}(t)/2}{e_{\text{tgt}} \sqrt{1 - e_{\text{tgt}}^2} - \frac{\sqrt{1+e_{\text{tgt}}} \sin \theta_{\text{tgt}}(t)}{(1+e_{\text{tgt}}) \cos \theta_{\text{tgt}}(t)}} = n_{\text{tgt}} \Delta t \tag{5-14}$$

$$\begin{aligned} T_{1/4} &= ((\Delta t(j_{N_{\text{p}}} + T_{1/4}) - \Delta t(j_{N_{\text{p}}}) \mod T_{\text{orb}}) \\ T_{1/2} &= ((\Delta t(j_{N_{\text{p}}} + T_{1/2}) - \Delta t(j_{N_{\text{p}}}) \mod T_{\text{orb}}) \\ T_{3/4} &= ((\Delta t(j_{N_{\text{p}}} + T_{3/4}) - \Delta t(j_{N_{\text{p}}}) \mod T_{\text{orb}}) \end{aligned} \tag{5-15}$$

Then $c_{\text{hp}}(t)$ is defined by (5-16).

$$c_{\text{hp}}(t) = \begin{bmatrix} -x_{\text{hp}}/2 + |\delta_{x_{\text{href}}}| \\ x_{\text{hp}}/2 \\ x_{\text{hp}}/2 + |\delta_{z_{\text{href}}}| \\ 3 * x_{\text{hp}}/2 + |\delta_{x_{\text{href}}}| \\ 0.3 x_{\text{hp}}/2 \\ x_{\text{hp}}/2 + |\delta_{z_{\text{href}}}| \end{bmatrix} \tag{5-16}$$

where $\delta_{x_{\text{href}}}$ and $\delta_{z_{\text{href}}}$ are tolerances representing the upper bound for the propagation of the worst-case sensor uncertainty through the prediction model, and thus further tighten the constraints of a robust MPC formulation. As shown in (5-17), where $w_{\max}$ is the victory containing the maximum absolute navigation errors and $A^{+}(t)$ is a matrix whose elements are the absolute values of the corresponding elements in $A(t)$.

$$\begin{bmatrix} \delta_{x_{\text{href}}} \\ \delta_{y_{\text{href}}} \\ \delta_{z_{\text{href}}} \end{bmatrix} = A^{+}(j : j + T_{\text{s}}) w_{\max} \tag{5-17}$$

it is to be noted that the constraints will differ for the YA prediction model compared to the HCW and Xu-Wang model due to the different definition of the LVLH reference frame as explained in Subsection 3-1-1.

5-2-2 Input Constraints

The input constraints are defined in the form of a maximum deliverable acceleration on each input vector element, as presented in (5-33).

$$\begin{aligned} -u_{\text{lim}} \leq u_i(j|t) \leq u_{\text{lim}}, \quad i \in \{1, 2, 3\} \\ u_{\text{lim}} = D_\tau \frac{F_c}{m} \\ u_{\text{lim YA}} = D_\tau \frac{F_c T_s}{m} \end{aligned} \tag{5-18}$$

where F_c N is the force capacity, m kg is the mass of the chaser craft and D_τ is the thruster duty cycle as the fraction of the sampling period. As the YA model requires ΔV as an input, its bound is represented by $u_{\text{lim YA}}$.

5-2-3 Disturbance Estimator

The three prediction models used are of different degrees of accuracy. The HCW model includes no disturbances and eccentricity, the YA model includes eccentricity but no disturbances, while the Xu-Wang model includes eccentricity and the J_2 effect. As was mentioned in Sub-Section 3-1-2 the most significant disturbances for LEO are atmospheric drag and the J_2 effect meaning a constant disturbance of 10^{-4} m/s^2 will be added to the along track direction to represent drag as well as random normally distributed disturbances in all directions of 10^{-5} m/s^2 to represent other disturbances according to Figure 3-3.

Disturbance estimators will be added to the prediction models to evaluate if they can provide performance benefits in terms of propellant consumption. The inclusion of a disturbance in the prediction model will tighten state and input constraints most robust techniques make use of the worst possible disturbance at the cost of performance, but the current estimated disturbance will be used instead. Two types of disturbance estimators will be used. The first is the simplest form of the disturbance estimators and is presented in (5-19).

$$\begin{aligned} \hat{x}(k+1) &= A\hat{x}(k) + Bu(k) + \delta(k) \\ \delta(k) &= x(k) - \hat{x}(k) \end{aligned} \tag{5-19}$$

The second disturbance estimator used is one presented in [22] as it has been proven to work and will useful to compare its performance compared to a classical one. The disturbance estimator is presented in (5-19).

$$\begin{aligned} \hat{x}(k+1) &= A\hat{x}(k) + Bu(k) + \delta(k) \\ \delta(k) &= \delta(k-1) + W * (x(k) - \hat{x}(k)) \end{aligned} \tag{5-20}$$

5-2-4 Delay

The MPC formulation functions under the assumption that the optimal input is determined for the current time step and is then applied, however in real life it will take time to process sensor data, solve the optimization problem and apply the desired input. A delay will thus be present in the system, on SmallSats and CubeSats processing power is no longer limiting, but it will still be advantageous to see if the system can function with one-step delay. The delayed prediction model is presented in (5-36).

$$\begin{bmatrix} \hat{x}(k+1) \\ u(k) \end{bmatrix} = \begin{bmatrix} A & B \\ 0 & 0 \end{bmatrix} \begin{bmatrix} \hat{x}(k) \\ u(k-1) \end{bmatrix} + \begin{bmatrix} 0 \\ I \end{bmatrix} u(k) \tag{5-21}$$

5-2-5 Cost Function

The two cost functions that will be evaluated are the standard quadratic cost function represented by (5-37) with a terminal stage cost. The second cost function that will be evaluated will be a quadratic cost function with terminal stage cost but also including a penalty on the change in input, also referred to as incremental input cost function, shown in (5-38).

$$J(x(k), u(k)) = \sum_{k=1}^{N_\mathrm{p}-1} ((x(k) - r(k))^\intercal Q(x(k) - r(k)) + u^\intercal(k) R u(k) + x(N_p)^\intercal P x(N_p) \tag{5-22}$$

$$\begin{aligned} J(x(k), u(k))_{\Delta u} = \sum_{k=1}^{N_\mathrm{p}-1} ((x(k) - r(k))^\intercal Q(x(k) - r(k)) + \Delta u^\intercal(k) R_{\Delta u} \Delta u(k) + u^\intercal(k)) R u(k) \\ + x(N_p)^\intercal P x(N_p) \end{aligned} \tag{5-23}$$

5-2-6 MPC Formulations

With the three different prediction models, two robust models and two cost functions it will result in more than 10 MPC formulations to be compared. We will not explicitly state all of them due to redundancies, but all their performance will be shown in the results. The non delayed formulations will have form (5-24), while the delayed formulations will have form (5-25).

$$\begin{aligned}
&\min_u J(x(k),u(k)) \quad or \quad J(x(k),u(k))_{\Delta u} \\
&\text{subject to:} \\
&x(0) = x_{\text{intial}} \\
&x(k+1) = Ax(k) + Bu(k) \quad \text{or} \quad x(k+1) = Ax(k) + Bu(k) + \delta(k), \quad k \in [0, N_p) \\
&A_{\text{hp}} x(k) \leq b_{\text{hp}}, \quad k = N_p \\
&u_{\min} \leq u(k) \leq u_{\max}, \quad k \in [0, N_p)
\end{aligned} \tag{5-24}$$

$$\begin{aligned}
&\min_u J(x(k),u(k)) \quad or \quad J(x(k),u(k))_{\Delta u} \\
&\text{subject to:} \\
&x(0) = x_{\text{intial}} \quad \& \quad u(-1) = u_{\text{initial}} \\
&x(k+1) = Ax(k) + Bu(k-1) \quad \text{or} \quad x(k+1) = Ax(k) + Bu(k-1) + \delta(k), \quad k \in [0, N_p) \\
&A_{\text{hp}} x(k) \leq b_{\text{hp}}, \quad k = N_p \\
&u_{\min} \leq u(k) \leq u_{\max}, \quad k \in [0, N_p)
\end{aligned} \tag{5-25}$$

5-3 Terminal to Capture

The objective of the terminal to capture phase is to reduce the along track separation to between chaser and target and dock to the target or remain at a safe distance. If the target is rotating, then the chaser is to dock to the target without any collisions, The chaser will start 100 m behind the target as that is where the previous mission phase will leave it and approach while remaining within a field of view cone. For this phase, it is assumed the orientation of the chaser is taken care of by the ADCS unit of the satellite as to point the chaser in the desired direction, thorough reaction wheels.

As the reference for the cost function will be the position of the docking port if the target is rotating, this will not be constant. The state space system is thus augmented to include the position of the docking port and the offset between chaser and docking port, as done in [11]. The discrete dynamics of the docking port are presented in (5-26).

$$\begin{bmatrix} r_x(k+1) \\ r_y(k+1) \\ r_z(k+1) \end{bmatrix} = A_{\text{rot}}(\theta(k)) \begin{bmatrix} r_x(k) \\ r_y(k) \\ r_z(k) \end{bmatrix} \tag{5-26}$$

where $R_{\text{rot}}(\theta(k))$ is an Euler Rotation matrix. For a target rotation about it z axis this is:

$$A_{\text{rot}}(\theta(k)) = \begin{bmatrix} \cos(\theta(k)) & -\sin(\theta(k)) & 0 \\ \sin(\theta(k)) & \cos(\theta(k)) & 0 \\ 0 & 0 & 1 \end{bmatrix} \tag{5-27}$$

The distance to the docking port is then defined as:

$$\begin{bmatrix} \sigma_x(k) \\ \sigma_y(k) \\ \sigma_z(k) \end{bmatrix} = \begin{bmatrix} x(k) \\ y(k) \\ z(k) \end{bmatrix} - \begin{bmatrix} r_x(k) \\ r_y(k) \\ r_z(k) \end{bmatrix} \tag{5-28}$$

Resulting in the state vector:

$$\vec{x}(k) = \begin{bmatrix} x(k) & y(k) & z(k) & v_x(k) & v_y(k) & v_z(k) & r_x(k) & r_y(k) & r_z(k) & \dots \\ \sigma_x(k) & \sigma_y(k) & \sigma_z(k) & & & & & & & \end{bmatrix}^{\mathsf{T}} \tag{5-29}$$

augmented state space system presented in (5-30).

$$\vec{x}(k+1) = \begin{bmatrix} A_{\text{RD}}(k) & 0_{3\times3} & 0_{3\times3} \\ 0_{3\times6} & A_{\text{rot}}(\theta(k)) & 0_{3\times3} \\ \text{I}_{3\times3} \quad 0_{3\times3} & -\text{I}_{3\times3} & 0_{3\times3} \end{bmatrix} \vec{x}(k) + \begin{bmatrix} B_{\text{RD}}(k) \\ 0_{6\times3} \end{bmatrix} \vec{u}(k) \tag{5-30}$$

where $A_{\text{RD}}(k)$ and $B_{\text{RD}}(k)$ represent the relative dynamics state space matrices.

5-3-1 State Constraints

This mission phase will include one main running constraint related to the docking port. They are modelled as a rectangular cone placed along the docking port. These are then expressed as tetrahedral forbidden zones described by a set of linear equations for each plan as shown in Figure 5-1 to retain simplicity.Through, Lossless convexification (LCvx) non-linear Line-of-Sight (LOS) constraints can be formulated as linear LOS constraints given by (5-31).

$$\underbrace{\begin{bmatrix} c_x & 1 & 0 \\ -c_x & 1 & 0 \\ 0 & 1 & c_z \\ 0 & 1 & -c_z \\ 0 & 1 & 0 \end{bmatrix}}_{A_{\text{los}}} \underbrace{\begin{bmatrix} x(k) \\ y(k) \\ z(k) \end{bmatrix}}_{\vec{x}_{\text{pos}}} \leq \underbrace{\begin{bmatrix} c_{x0} \\ c_{x0} \\ c_{z0} \\ c_{z0} \\ c_{y0} \end{bmatrix}}_{b_{\text{los}}} \tag{5-31}$$

If the target is rotating, these constraints must be transformed to take into account the new orientation of the target satellite in the LVLH frame. This is done by rotating the first three columns of, A_{los} as shown in (5-32), assuming knowledge of the rotation angle θ is known.

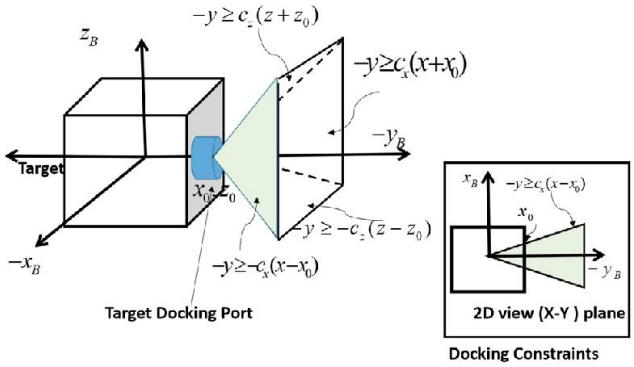

Figure 5-1: Line-of-Sight (LOS) constraint [44]

$$\underbrace{A_{\text{los}} R_{\text{rot}}(\theta(k))}_{A_{\text{los,rot}}} \vec{x}_{\text{pos}}(k) \leq b_{\text{los}} \tag{5-32}$$

It is thus assumed the angular rate of the target satellite is known in order to predict the location of the docking port. It is to be noted that the constraints will differ for the YA prediction model compared to the HCW and Xu-Wang model due to the different definition of the LVLH reference frame as explained in Subsection 3-1-1.

5-3-2 Input Constraints

The input constraints are defined in the form of a maximum deliverable acceleration on each input vector element, as presented in (5-33).

$$\begin{aligned} -u_{\text{lim}} \leq u_i(j|t) \leq u_{\text{lim}}, \quad i \in \{1,2,3\} \\ u_{\text{lim}} = D_\tau \frac{F_c}{m} \\ u_{\text{lim YA}} = D_\tau \frac{F_c T_s}{m} \end{aligned} \tag{5-33}$$

where F_c N is the force capacity, m kg is the mass of the chaser craft and D_τ is the thruster duty cycle as the fraction of the sampling period. As the YA model requires ΔV as an input, its bound is represented by $u_{\text{lim YA}}$.

5-3-3 Disturbance Estimator

The three prediction models used are of different degrees of accuracy. The HCW model includes no disturbances and eccentricity , the YA model includes eccentricity but no disturbances, while the Xu-Wang model includes eccentricity and the J_2 effect. As was mentioned in Sub-Section 3-1-2 the most significant disturbances for LEO are atmospheric drag and the

J_2 effect meaning a constant disturbance of 10^{-4} m/s^2 will be added to the along track direction to represent drag as well as random normally distributed disturbances in all directions of 10^{-5} m/s^2 to represent other disturbances according to Figure 3-3.

Disturbance estimators will be added to the prediction models to evaluate if they can provide performance benefits in terms of propellant consumption. The inclusion of a disturbance in the prediction model will tighten state and input constraints most robust techniques make use of the worst possible disturbance at the cost of performance, but the current estimated disturbance will be used instead. Two types of disturbance estimators will be used. The first is the simplest form of the disturbance estimators and is presented in (5-34).

$$\begin{aligned} \hat{x}(k+1) &= A\hat{x}(k) + Bu(k) + \delta(k) \\ \delta(k) &= x(k) - \hat{x}(k) \end{aligned} \tag{5-34}$$

The second disturbance estimator used is one presented in [22] as it has been proven to work and will useful to compare its performance compared to a classical one. The disturbance estimator is presented in (5-34).

$$\begin{aligned} \hat{x}(k+1) &= A\hat{x}(k) + Bu(k) + \delta(k) \\ \delta(k) &= \delta(k-1) + W * (x(k) - \hat{x}(k)) \end{aligned} \tag{5-35}$$

5-3-4 Delay

The MPC formulation functions under the assumption that the optimal input is determined for the current time step and is then applied, however in real life it will take time to process sensor data, solve the optimization problem and apply the desired input. A delay will thus be present in the system, on SmallSats and CubeSats processing power is no longer limiting, but it will still be advantageous to see if the system can function with one-step delay. The delayed prediction model is presented in (5-36).

$$\begin{bmatrix} \hat{x}(k+1) \\ u(k) \end{bmatrix} = \begin{bmatrix} A & B \\ 0 & 0 \end{bmatrix} \begin{bmatrix} \hat{x}(k) \\ u(k-1) \end{bmatrix} + \begin{bmatrix} 0 \\ I \end{bmatrix} u(k) \tag{5-36}$$

5-3-5 Cost Function

The two cost functions that will be evaluated are the standard quadratic cost function represented by (5-37) with a terminal stage cost. The second cost function that will be evaluated will be a quadratic cost function with terminal stage cost but also including a penalty on the change in input, also referred to as incremental input cost function, shown in (5-38).

$$J(x(k), u(k)) = \sum_{k=1}^{N_\mathrm{p}-1} ((x(k) - r(k))^\intercal Q(x(k) - r(k)) + u^\intercal(k) R u(k) + x(N_p)^\intercal P x(N_p) \tag{5-37}$$

$$J(x(k),u(k))_{\Delta u} = \sum_{k=1}^{N_\mathrm{p}-1} ((x(k)-r(k))^\intercal Q(x(k)-r(k)) + \Delta u^\intercal(k) R_{\Delta u} \Delta u(k)) + u^\intercal(k) R u(k) + x(N_p)^\intercal P x(N_p) \tag{5-38}$$

5-3-6 MPC Formulations

With the three different prediction models, two robust models and two cost functions, it will result in more than 10 MPC formulations to be compared. We will not explicitly state all of them due to redundancies, but all their performance will be shown in the results. The non delayed formulations will have form (5-39), while the delayed formulations will have form (5-40).

$$\begin{aligned}
&\min_u J(x(k),u(k)) \quad or \quad J(x(k),u(k))_{\Delta u} \\
&\text{subject to:} \\
&x(0) = x_\mathrm{intial} \\
&x(k+1) = Ax(k) + Bu(k) \quad \text{or} \quad x(k+1) = Ax(k) + Bu(k) + \delta(k), \quad k \in [0, N_p) \\
&A_{\mathrm{los,rot}}(k)\vec{x}_{\mathrm{pos}}(k) \leq b_{\mathrm{los}}, \quad \forall k \\
&u_{\min} \leq u(k) \leq u_{\max}, \quad k \in [0, N_p)
\end{aligned} \tag{5-39}$$

$$\begin{aligned}
&\min_u J(x(k),u(k)) \quad or \quad J(x(k),u(k))_{\Delta u} \\
&\text{subject to:} \\
&x(0) = x_\mathrm{intial} \quad \& \quad u(-1) = u_\mathrm{initial} \\
&x(k+1) = Ax(k) + Bu(k-1) \quad \text{or} \quad x(k+1) = Ax(k) + Bu(k-1) + \delta(k), \quad k \in [0, N_p) \\
&A_{\mathrm{los,rot}}(k)\vec{x}_{\mathrm{pos}}(k) \leq b_{\mathrm{los}}, \quad \forall k \\
&u_{\min} \leq u(k) \leq u_{\max}, \quad k \in [0, N_p)
\end{aligned} \tag{5-40}$$

5-4 Conclusion

In this Chapter, the methodological approach developed to answer the research questions was presented. The result is a compilation of MPC formulations that will be evaluated for each mission phase. The mission was divided into three mission-phases. Intermediate range, close range and terminal to capture phase.

The objective of the intermediate range is to bring the chaser satellite within 20 km of the target after orbit insertion. The constraints involved in this mission phase are relatively simple. The chaser is required to stay behind the target at all times, and the chaser must end up between 30 and 10 km behind the target. The inputs are constrained by the maximum

deliverable thrust and a chosen duty cycle. Besides the different prediction models, a delayed MPC formulation will be developed for each prediction model as it is not possible for the target spacecraft to apply the input at the same time it obtains its measurements. Furthmore, for each prediction model besides the delayed formulation two more formulations will be developed using two different disturbance estimators. Finally these formulations will be evaluated with the traditional quadratic cost function and an incremental input cost function. This will result in 7 different MPC formulation per prediction model.

The objective of the short range phase is to bring the chaser satellite to within a 100 m of the target satellite and place the chaser satellite in a holding point until the next mission phase is activated. The constraints in this mission phase are slightly more complex due to the holding point, which are formulated as a terminal constraint. The input constraints remain the same as for the intermediate range as well ass the delayed formulation, disturbance estimators and cost functions that will be used. Resulting again in 7 MPC formulations per prediction model.

Lastly, the objective of the terminal to capture phase is for the chaser to approach the target and dock while remaining in LOS of the target. In order to carry out docking, all three prediction models are augmented to include the position of the docking port and the relative distance between chaser and target port. This mission phase is the most demanding in terms of constraints. LOS constraints are formulated as running and terminal constraint. Input constraints are kept the same except for excluding the duty cycle due to the short sampling period involved in this mission phase. The delayed formulation, disturbance estimators and cost functions that will be used are kept the same, resulting in 7 MPC formulations per prediction model.

Chapter 6

Implementation and Results

This chapter contains the implementation and testing of the MPC algorithm for real problem instances, in order to obtain a valid assessment of the performance of the controller. The implementation of the MPC algorithm is done for two cases. Since there are also different parameters to be defined, multiple runs for each climate log is performed.

6-1 Simulation

As mentioned in Subsection 3-1-3 the nonlinear Xu-Wang model will be used as the environment simulation due to it being the most complete model. The Xu-Wang model includes J_2 accelerations and can include drag. It was chosen to however model drag as a constant disturbance in the direction of flight according to Figure 3-3, resulting in an acceleration of $\approx 6.67 \times 10^{-4}\ m/s^2$, and to account for other disturbances a randomly distributed disturbance with variance of $1 \times 10^{-5}\ m/s^2$ is added to all three axes.

Furthermore, the maximum allowable thrust in each direction is chosen to be 20 N as that is a realistic thrust value for possible thrusters that could fit on a RVD satellite such as the ELSA-d satellite [1] [27]. Although thrusters are not fully throttleable, with an 8 thruster configuration such as on the ELSA-d satellite wide ranges are producible through differential thrust. A limit is set at 1 N of differential thrust and that is used as a Minimum Impulse Bit (MIB). By setting the duty cycle in the input constraints, $D_\tau = 1/\sqrt{2}$ this imposed 1-norm constraint can be used to conservatively guarantee satisfaction of a 2-norm constraint on the maximum deliverable thrust in any direction. Lastly, the navigation uncertainties are presented in Table 6-1, where beyond visual range they are the uncertainties of GPS and within visual range an assumption based on performance on Light Detection and Ranging (LIDAR) and cameras.

6-2 Intermediate Range FITG

In this Section the results of the controllers for Intermediate range presented in Section 5-1 will be presented. For simplicity, the initial conditions are presented again in Table 6-2.

Table 6-1: Navigation Uncertainty σ

Direction	Beyond Visual Range ($> 100\ m$)	$< 100\ m$
x	4	0.1
y	4	0.1
x	4	0.1
v_x	0.001	0.001
v_y	0.001	0.001
v_z	0.001	0.001

Table 6-2: Orbital Parameters for Target and Chaser

Orbital Parameters	Target	Chaser
Semi Major axis [km]	6918.6	6948.6
Eccentricity	0.013611	0.013611
Inclination [deg]	60	60
Argument of Perigee [deg]	103.89	103.89
Right Ascension of the Ascending Node [deg]	123.61	123.61
True Anomaly [deg]	5	2

These initial conditions results in the following offsets in distance, m, and velocity, m/s in the LVLH frame;

$$x(0) = \begin{bmatrix} 29174.95 & -357344.63 & 0 & -5.41 & -49.57 & 0 \end{bmatrix}^{\mathsf{T}} \tag{6-1}$$

It was chosen to ensure that the combination of sampling time and prediction horizon result in a prediction of 1.5 orbits.

6-2-1 HCW LMPC controllers

In this subsection, the results of the Clohessy Wiltshire (HCW) based LMPC formulations will be presented. It is to be noted that with the use of the HCW prediction model, using a sampling time of 340 seconds and a prediction horizon of, $N_p = 25$ steps was not possible for the delayed controllers, thus a smaller sampling period was chosen of 200 seconds combined with a prediction horizon of $N_p = 43$ was used to still have a prediction horizon of 1.5 orbits. The cost matrices Q and R used for the simulations are presented below:

$$\begin{aligned} Q = &\quad \text{diag}\begin{pmatrix} 1\times10^{-6} & 1\times10^{-6} & 1\times10^{-6} & 1\times10^{-1} & 1\times10^{-1} & 1\times10^{-1} \end{pmatrix} \\ P = &\quad \text{diag}\begin{pmatrix} 15000 & 15000 & 15000 \end{pmatrix} \end{aligned} \tag{6-2}$$

Normal vs Delayed LMPC

Firstly, the trajectory and commanded input of the normal LMPC vs the delayed LMPC are presented in Figure 6-1. The trajectory in the orbital plane is presented in 6-2.

It can be seen from the figures that regardless of the smaller sampling period, the delayed controller is slower and has more of an overshoot. The out of plane oscillations in the Z axis can be damped at the cost of more propellant use but for the scope of the first mission phase it is not required or important. The total ΔV required by the controllers will be presented at the end, with the remainder of the controllers.

Delayed LMPC with disturbance estimators

Next, in Figure 6-3 the trajectory and commanded input of the delayed LMPC vs the delayed LMPC with the two disturbance estimators presented in Subsection 5-1-3 are presented. Their trajectory in the orbital plane is shown in Figure 6-4.

The W of the disturbance estimator presented in (5-5) was set to:

$$W = 1 \times 10^{-3} * \mathrm{I}_{nx} \tag{6-3}$$

From the figures, it is clear that the classical disturbance estimator presented in (5-4) is able to increase the speed of the delayed controller. The W matrix disturbance estimator does not seem to provide many benefits except a slight increase in response time. Completion time is not of importance for this mission phase, but is an important observation.

Incremental Input Delayed LMPC with disturbance estimators

Finally, in Figure 6-5 the trajectory and commanded input of the incremental input delayed LMPC vs incremental input delayed LMPC with the two disturbance estimators presented in Subsection 5-1-3 are presented. The same W matrix was used as for the delayed controllers. In Figure 6-6 the orbital plane trajectory of the controllers is presented. The disturbance estimators can be seen to have the same effect as for the normal delayed case.

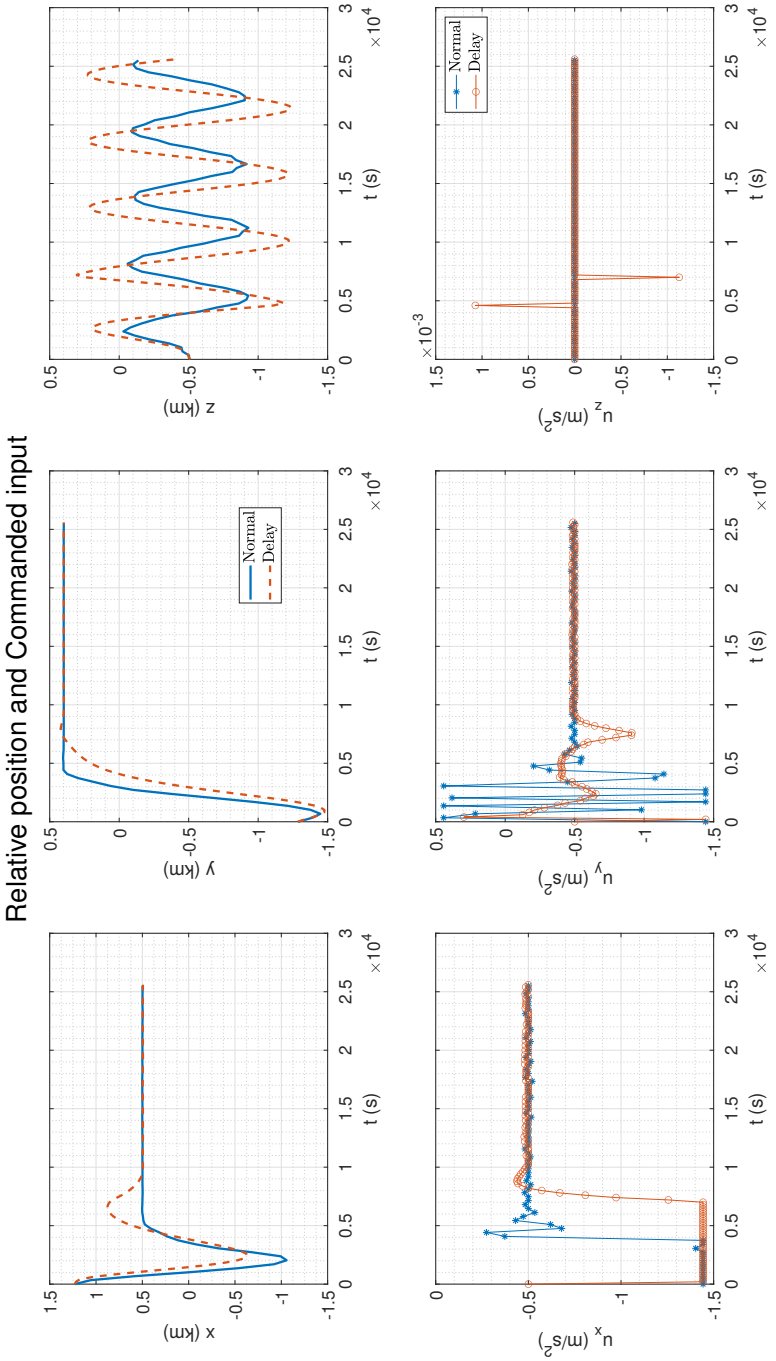

Figure 6-1: Response of HCW LMPC and delayed HCW LMPC for Intermediate range

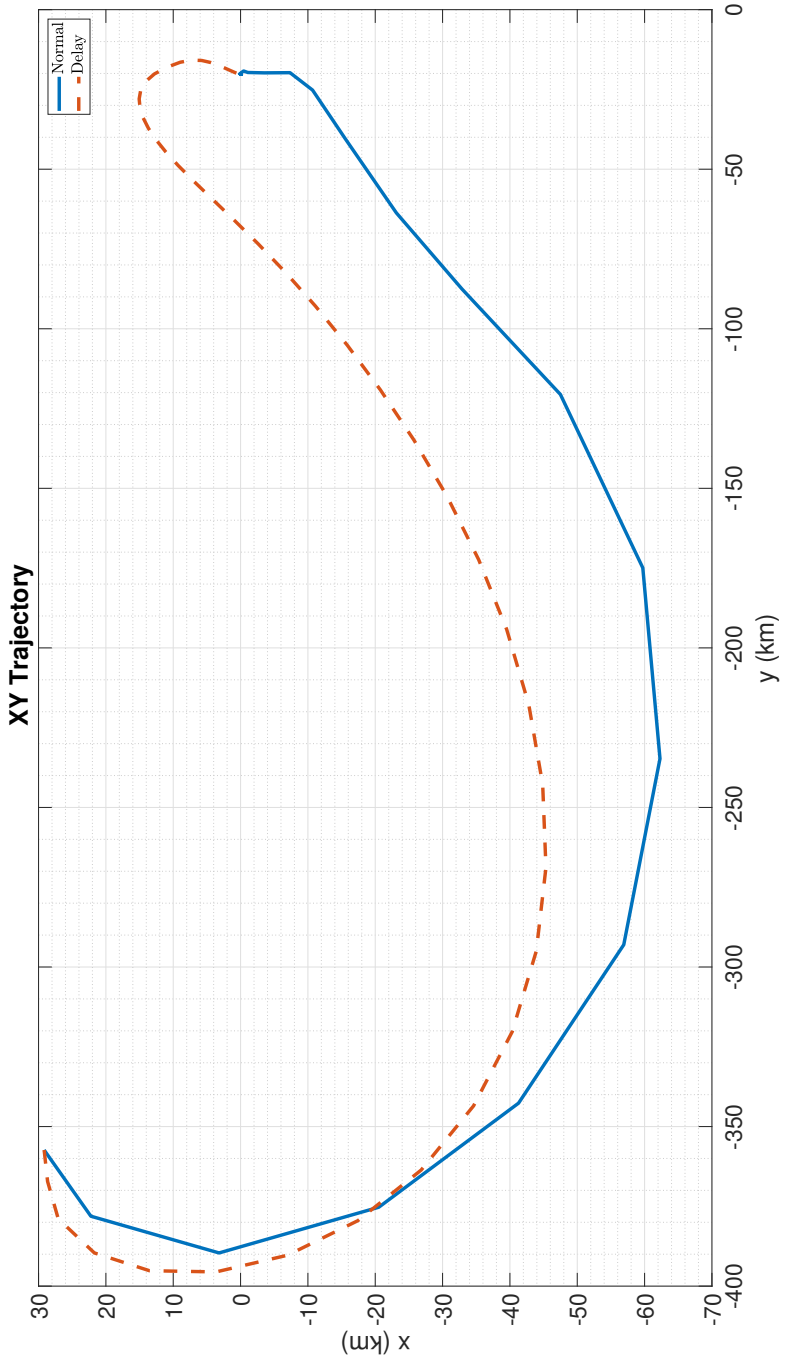

Figure 6-2: Orbital Plane trajectory of HCW LMPC and delayed HCW LMPC for Intermediate range

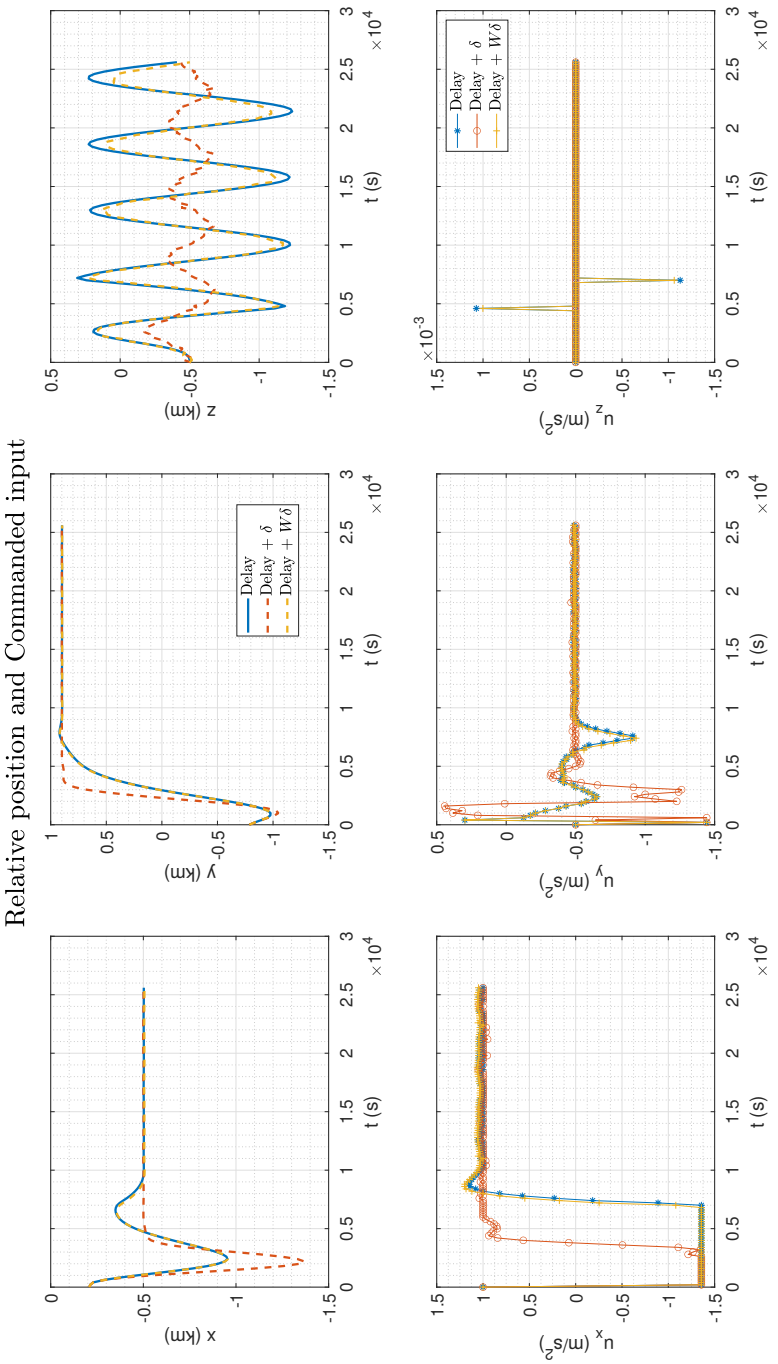

Figure 6-3: Response of delayed HCW LMPC vs delayed HCW LMPC with disturbance estimators for Intermediate range

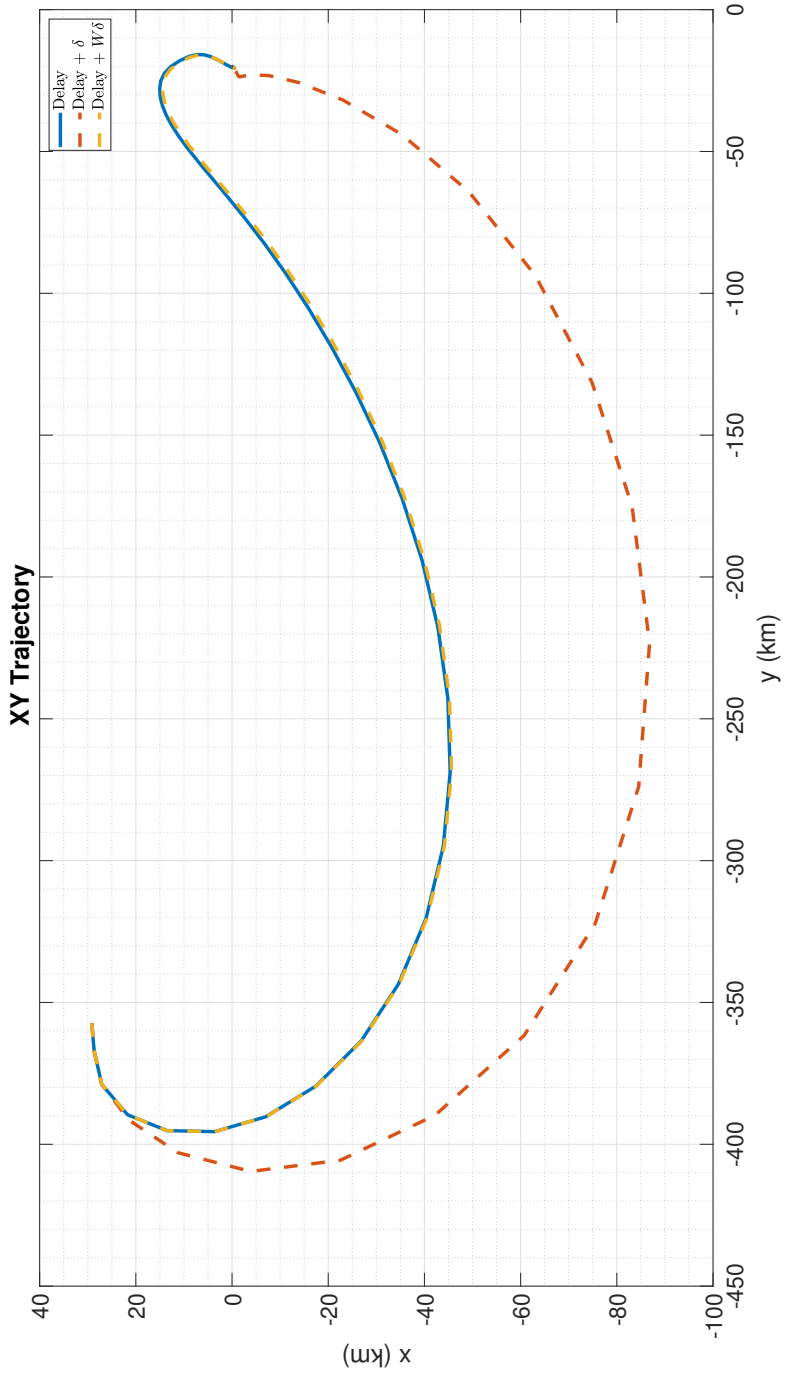

Figure 6-4: Orbital Plane trajectory of delayed HCW LMPC vs delayed HCW LMPC with disturbance estimators for Intermediate range

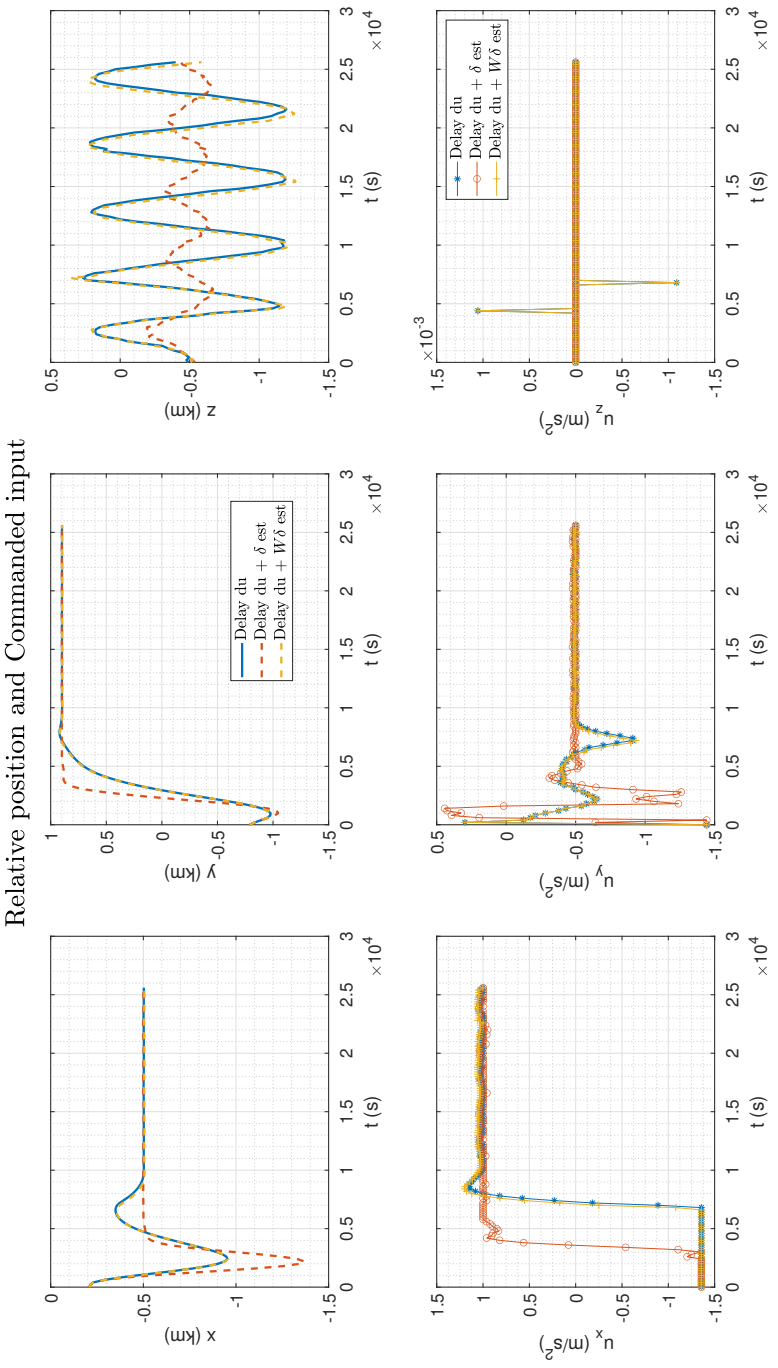

Figure 6-5: Orbital Plane trajectory of Δu delayed HCW LMPC vs Δu delayed HCW LMPC with disturbance estimators for Intermediate range

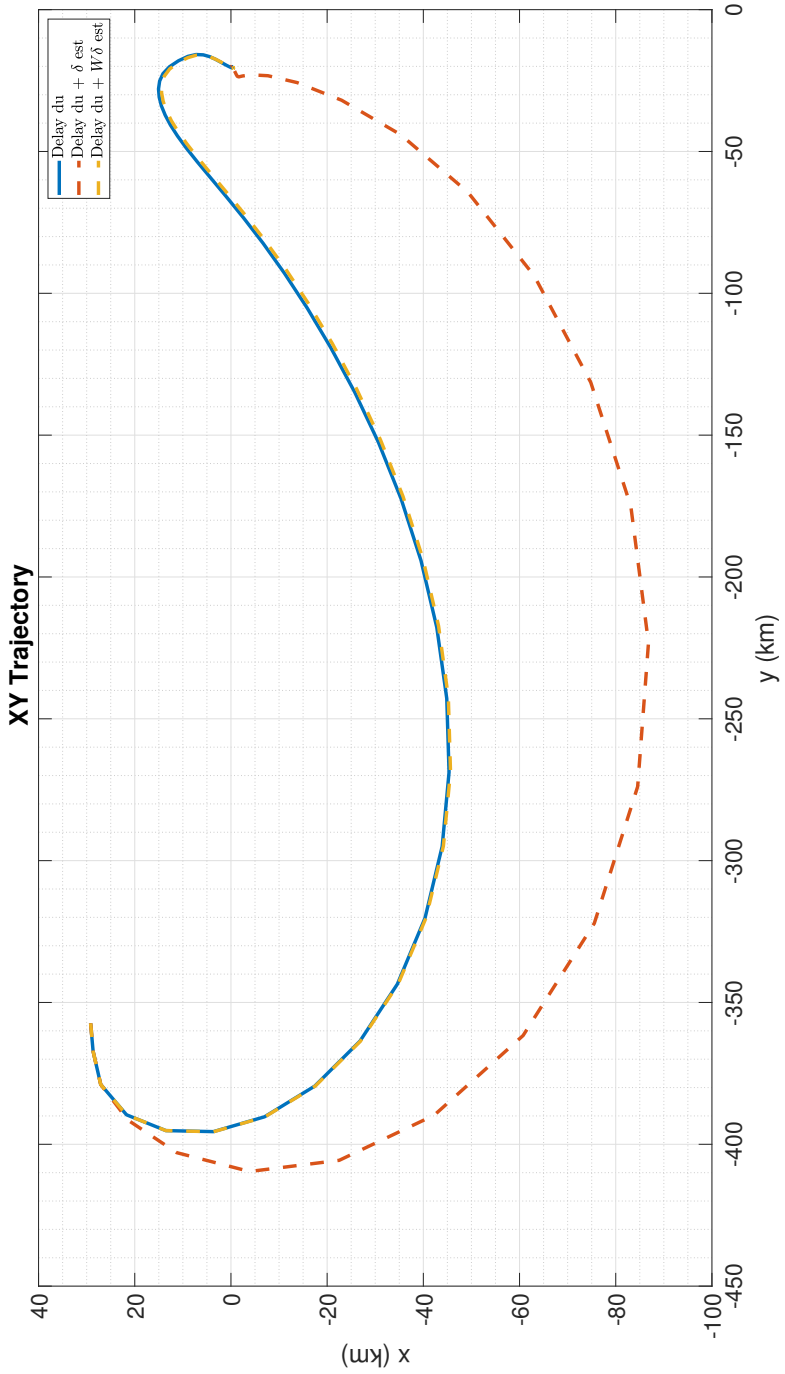

Figure 6-6: Orbital Plane trajectory of Δu HCW controllers for Intermediate range

ΔV and Steady state error

As the simulation did not include a time varying mass and modelled thrusters, it is best suited to compare required ΔV in order to not introduce more assumptions. The steady state error was computed as the Root Mean Squared (RMS) error from the 10000 to 25000 seconds in the simulation. From the figures, it is clear that by 10000 seconds the chaser has arrived at its first objective of 20 km behind the target. Measuring the RMS from that point gives an indication of the steady state error after the chaser has settled and awaits to begin the second mission phase.

The required ΔV and RMS errors for each controller are presented in Table 6-3. It is clear from the table that the delayed LMPC reduces performance in terms of ΔV required and error regardless of its smaller sampling time. Even though translation error is in itself not an issue for the first mission phase, LEO orbits can be quite full, and it is important that the chaser can be controlled with accuracy. Furthermore, it can be seen that the classical disturbance estimator provides a significance performance benefit both in terms of ΔV and steady state error while the W matrix disturbance estimator presented in [22] degrades performance for the delayed controller and only provides an δV improvement for the incremental input delayed controllers. Lastly, it is to be noted that while the incremental input cost function does not provide any significant improvement to the classical one. However, the combination of the incremental input cost function with the classical disturbance estimator is able to provide the best performance in terms of ΔV and error even with respect to the non-delayed quadratic cost function LMPC, almost halving the required ΔV.

Table 6-3: Results for HCW Intermediate Range controllers

Controller	ΔV $[m/s]$	RMS error x $[m]$	RMS error y $[m]$	RMS error z $[m]$
LMPC	610.55	64.73	183.76	13.79
delayed LMPC	728.24	220.91	307.53	90.53
delayed LMPC + δ est	539.66	84.66	59.91	18.03
delayed LMPC + W δ est	731.79	416.99	594.77	96.01
Δu delayed LMPC	728.13	218.66	307.75	72.88
Δu delayed LMPC + δ est	539.42	87.42	44.17	26.97
Δu delayed LMPC + W δ est	731.74	424.85	594.30	81.93

6-2-2 Yamanaka-Ankersen LMPC controllers

In this subsection, the results of the Yamanaka-Ankersen (YA) based LMPC formulations will be presented. It is to be noted that with the use of the YA prediction model, using a sampling time of 340 seconds and a prediction horizon of, N_p, 25 was possible for the delayed controllers, but to have a fair comparison a smaller sampling period of 200 seconds combined with a prediction horizon of $N_p = 43$ was used just as for the HCW intermediate range controllers. The cost matrices Q and R used for the simulations are presented below:

$$\begin{aligned} Q = &\quad \text{diag}\begin{pmatrix} 1\times10^{-3} & 1\times10^{-3} & 1\times10^{-3} & 1\times10^{3} & 1\times10^{3} & 1\times10^{3} \end{pmatrix} \\ P = &\quad \text{diag}\begin{pmatrix} 15000 & 15000 & 15000 \end{pmatrix} \end{aligned} \tag{6-4}$$

Normal vs Delayed LMPC

Firstly, the trajectory and commanded input of the normal LMPC vs the delayed LMPC are presented in Figure 6-7. The trajectory in the orbital plane is presented in 6-8.

It can be seen from the figures that regardless of the smaller sampling period, the delayed controller is slower, but unlike for the HCW there is no increase in overshoot. The out of plane oscillations in the Z axis can be damped at the cost of more propellant use, but for the scope of the first mission phase it is not required or important. Furthermore, unlike for the HCW controllers, the trajectory of the delayed controller does not change as radically, as the form and approach is still the same except for a larger deviation in the radial direction. The total ΔV required by the controllers will be presented at the end, with the remainder of the controllers.

Delayed LMPC with disturbance estimators

Next, in Figure 6-9 the trajectory and commanded input of the delayed LMPC vs the delayed LMPC with the two disturbance estimators presented in Subsection 5-1-3 are presented. Their trajectory in the orbital plane is shown in Figure 6-10.

The W of the disturbance estimator presented in (5-5) was set to:

$$W = 1 \times 10^{-3} * \mathrm{I}_{nx} \tag{6-5}$$

From the figures, it is clear that both estimators help improve the performance of the LMPC is able to increase the speed of the delayed controller. The W matrix disturbance estimator is, unlike for the HCW, able to provide an increase in performance and, as can be seen from Figure 6-10 its trajectory has less deviation than that the classical disturbance estimator. This provides insight on how the YA model is more sensitive to disturbances. Completion time is not of importance for this mission phase, but is an important observation.

Incremental Input Delayed LMPC with disturbance estimators

Finally, in Figure 6-11 the trajectory and commanded input of the incremental input delayed LMPC vs incremental input delayed LMPC with the two disturbance estimators presented in Subsection 5-1-3 are presented. The same W matrix was used as for the delayed controllers. In Figure 6-12 the orbital plane trajectory of the controllers is presented. The disturbance estimators can be seen to have the same effect as for the normal delayed case, but the incremental input is able to do decrease the deviation in the radial direction of the trajectory.

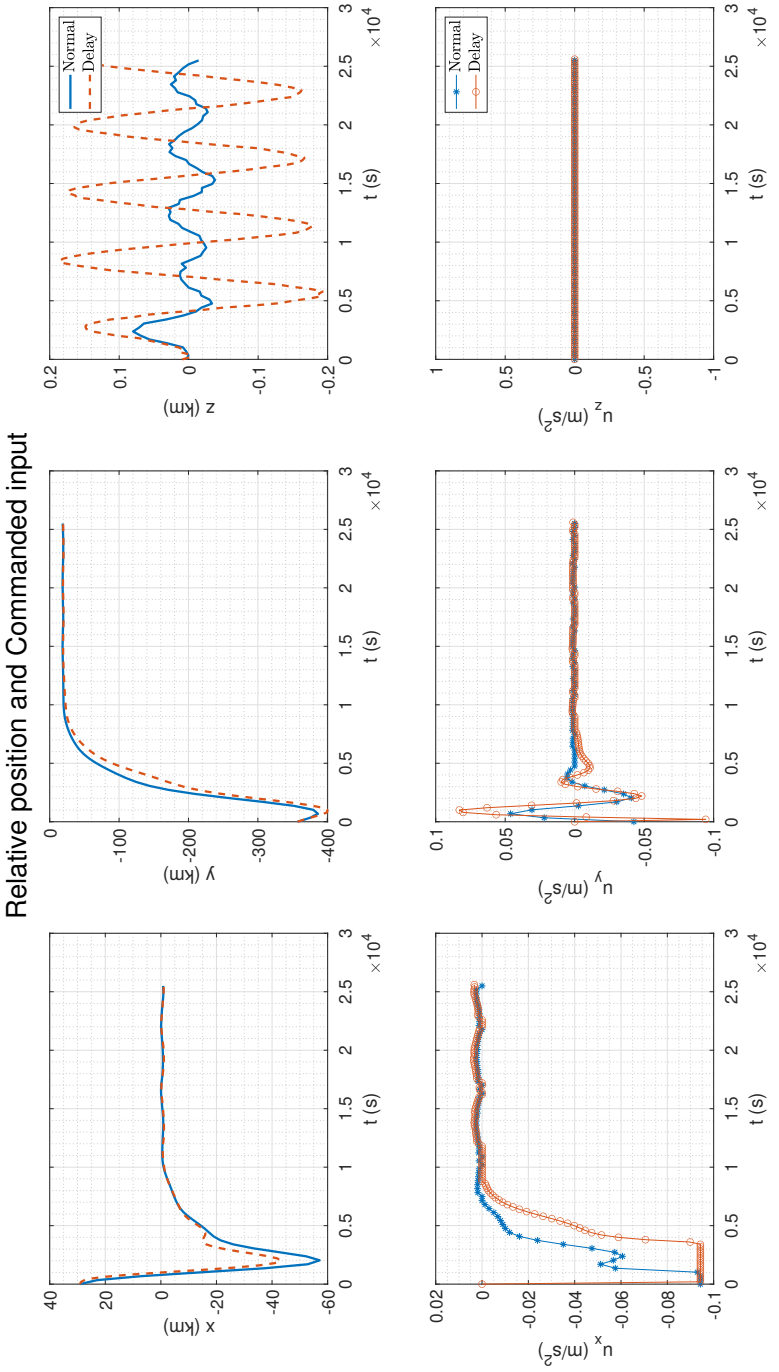

Figure 6-7: Response of YA LMPC and delayed YA LMPC for Intermediate range

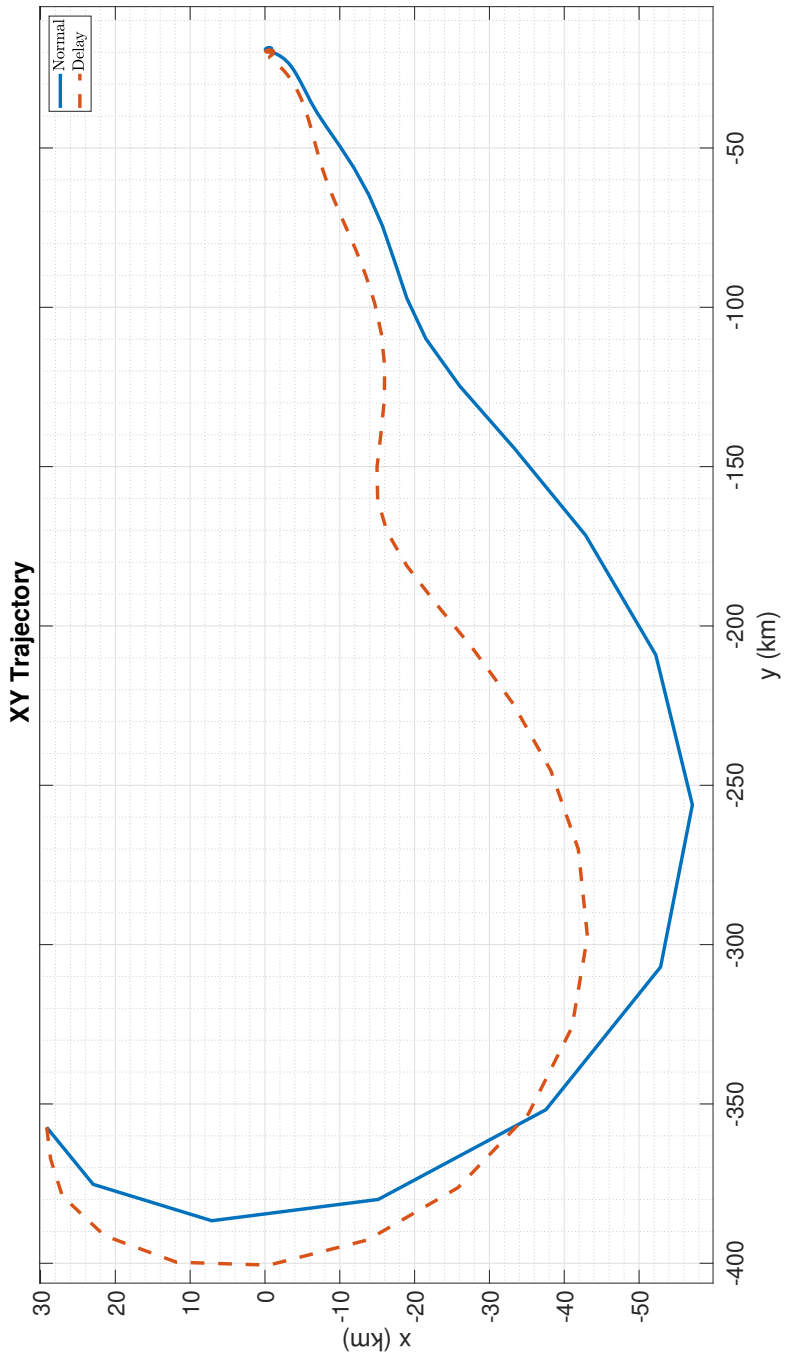

Figure 6-8: Orbital Plane trajectory of YA LMPC and delayed YA LMPC for Intermediate range

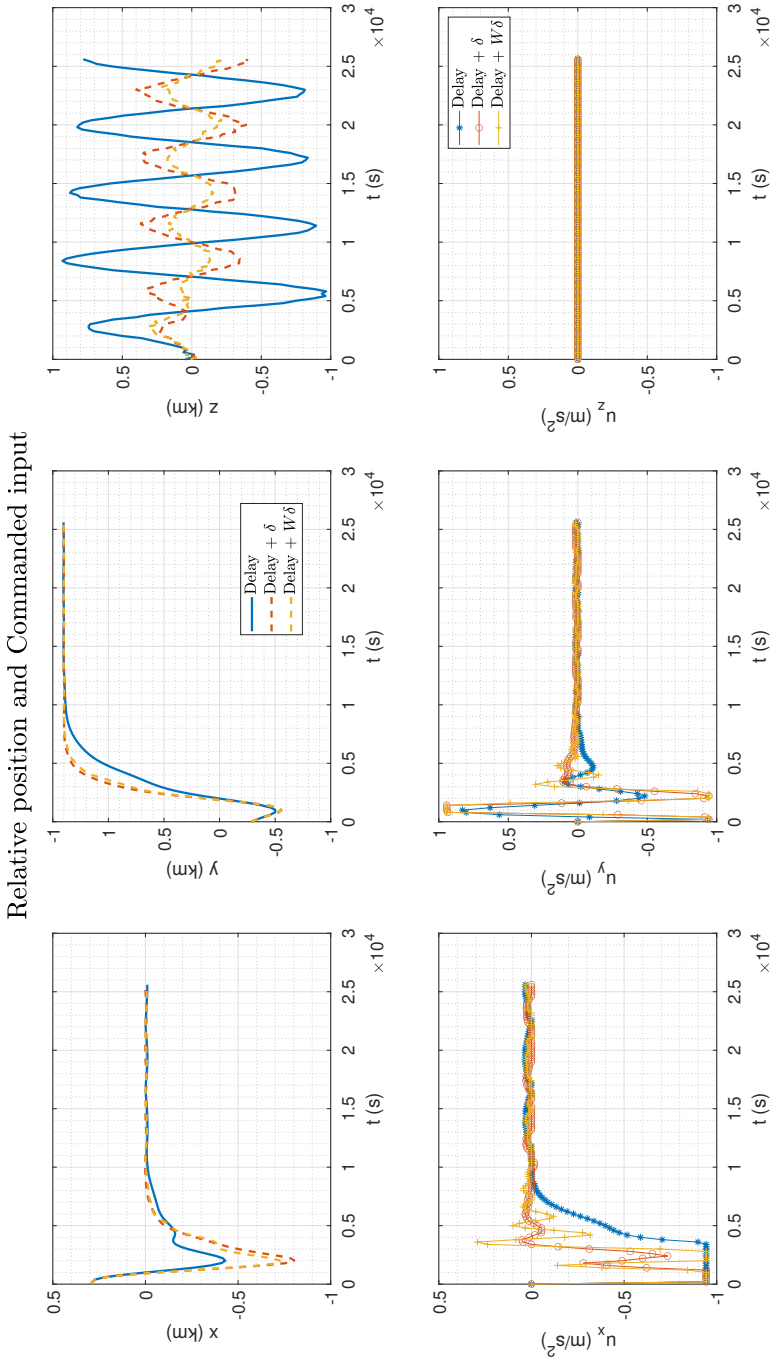

Figure 6-9: Response of delayed YA LMPC vs delayed YA LMPC with disturbance estimators for Intermediate range

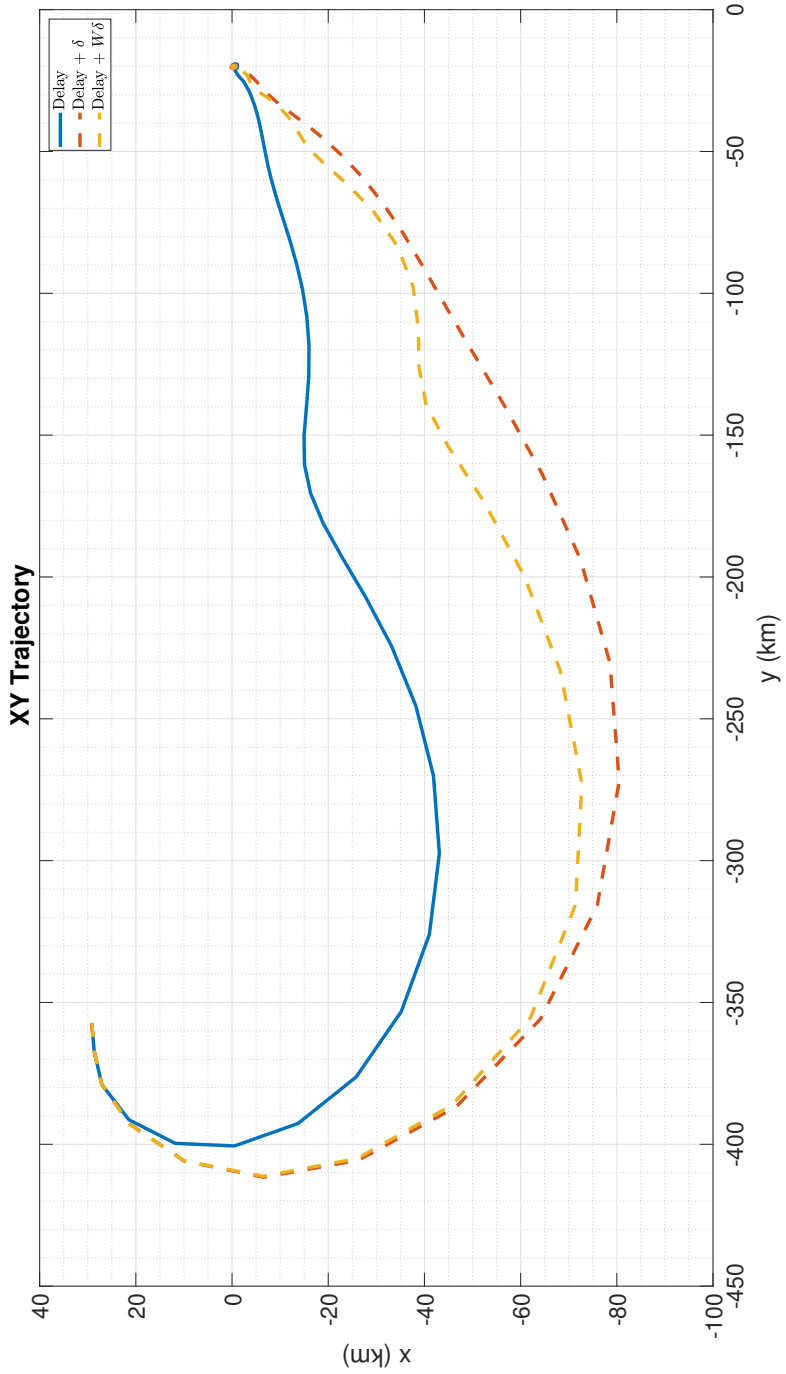

Figure 6-10: Orbital Plane trajectory of delayed YA LMPC vs delayed YA LMPC with disturbance estimators for Intermediate range

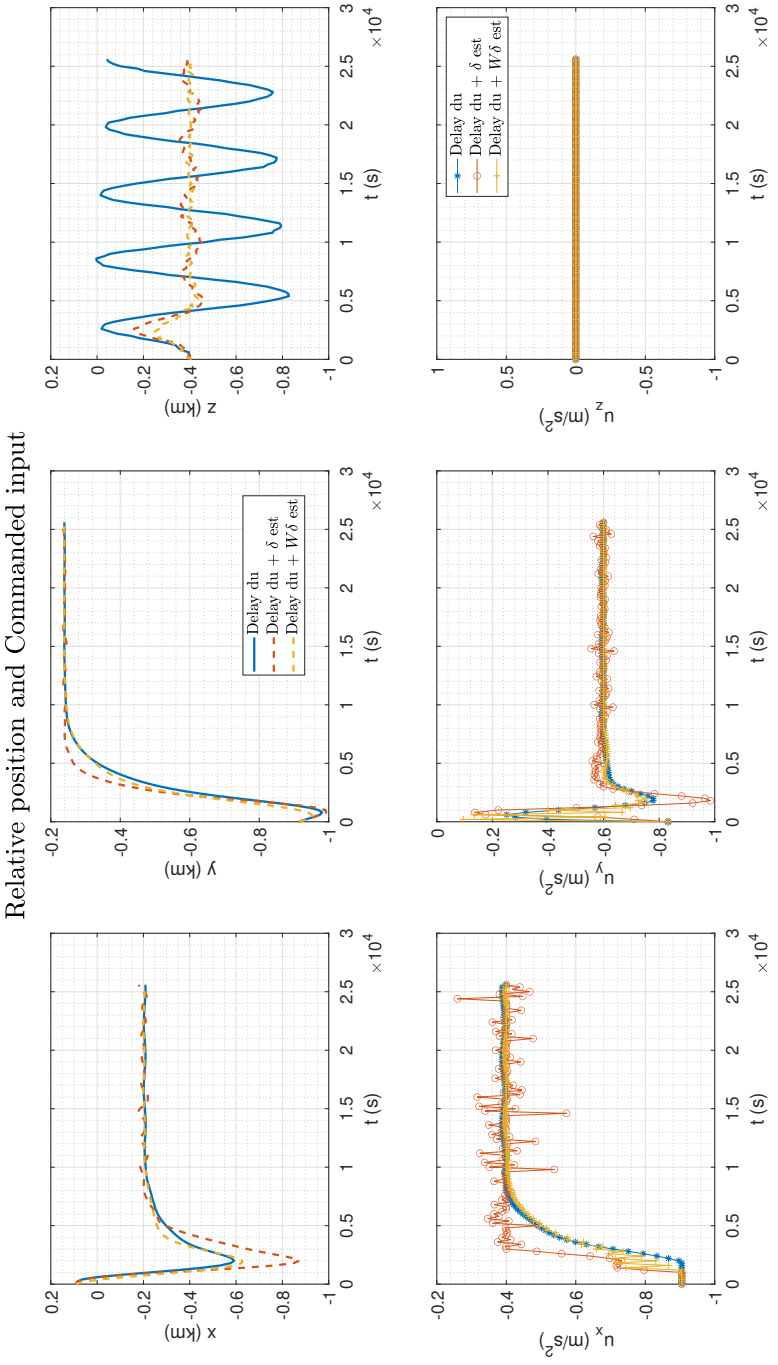

Figure 6-11: Orbital Plane trajectory of Δu delayed YA LMPC vs Δu delayed YA LMPC with disturbance estimators for Intermediate range

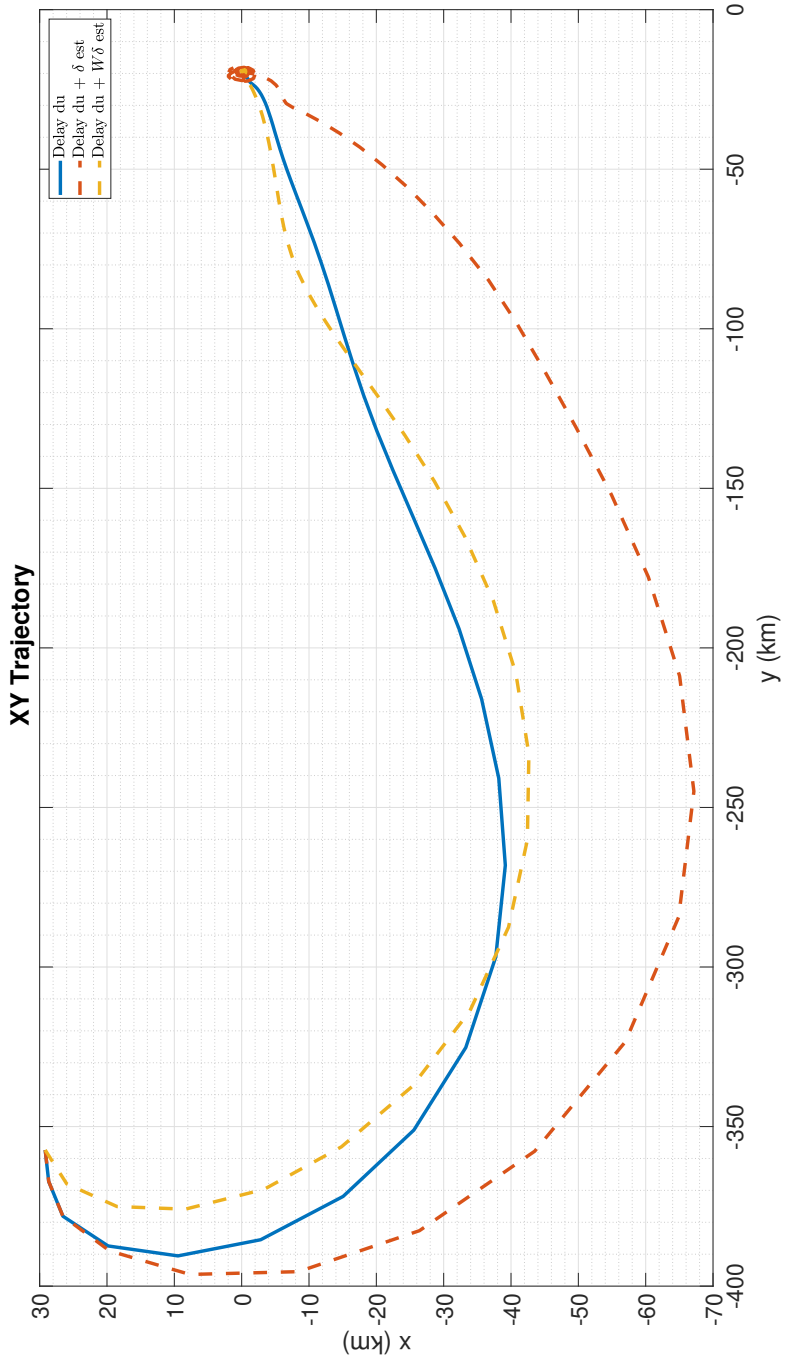

Figure 6-12: Orbital Plane trajectory of Δu YA controllers for Intermediate range

ΔV and Steady state error

As the simulation did not include a time varying mass and modelled thrusters, it is best suited to compare required ΔV in order to not introduce more assumptions. The steady state error was computed as the Root Mean Squared (RMS) error from the 10000 to 25000 seconds in the simulation, with the same reasoning that was done for the HCW controllers.

The required ΔV and RMS errors for each controller are presented in Table 6-4. The results are similar to those for the HCW controller. It is clear from the table that the delayed LMPC reduces performance in terms of ΔV required and error regardless of its smaller sampling time. Even though translation error is in itself not an issue for the first mission phase, LEO orbits can be quite full, and it is important that the chaser can be controlled with accuracy. Furthermore, it can be seen that the disturbance estimators provide a significance performance benefit both in terms of ΔV and steady state error, with the classical disturbance estimator providing better ΔV performance but the W disturbance estimator better performance in terms of RMS. Furthermore, unlike for the HCW controller, it is to be noted that the incremental input cost function and its combination with disturbance estimators does not provide any significant improvement to the classical one. Lastly, an important observation is that the RMS of the YA controllers is considerably larger than that of the HCW controllers, but with a better performance in terms of ΔV. Thus even though the YA model takes eccentricity into account and is a higher fidelity model for propagation, it does not seem to be suited for control.

Table 6-4: Results for YA Intermediate Range controllers

Controller	ΔV $[m/s]$	RMS error x $[m]$	RMS error y $[m]$	RMS error z $[m]$
LMPC	428.17	612.52	919.95	26.60
delayed LMPC	650.14	760.49	845.46	113.58
delayed LMPC + δ est	474.74	411.51	371.02	57.07
delayed LMPC + W δ est	572.14	493.04	261.41	41.47
Δu delayed LMPC	664.34	605.19	820.63	211.84
Δu delayed LMPC + δ est	586.54	615.01	616.89	27.87
Δu delayed LMPC + W δ est	599.24	380.28	965.96	4.65

6-2-3 Xu-Wang LMPC controllers

In this subsection, the results of the Xu-Wang based LMPC formulations will be presented. It is to be noted that with the use of the Xu-Wang prediction model, using a sampling time of 340 seconds and a prediction horizon of, N_p, 25 was possible for the delayed controllers, but to have a fair comparison a smaller sampling period of 200 seconds combined with a prediction horizon of $N_p = 43$ was used just as for the HCW intermediate range controllers. The cost matrices Q and R used for the simulations are presented below:

$$\begin{aligned} Q = &\quad \text{diag}\begin{pmatrix} 1\times10^{-6} & 1\times10^{-6} & 1\times10^{-6} & 1\times10^{-1} & 1\times10^{-1} & 1\times10^{-1} \end{pmatrix} \\ P = &\quad \text{diag}\begin{pmatrix} 15000 & 15000 & 15000 \end{pmatrix} \end{aligned} \tag{6-6}$$

Normal vs Delayed LMPC

Firstly, the trajectory and commanded input of the normal LMPC vs the delayed LMPC are presented in Figure 6-13. The trajectory in the orbital plane is presented in 6-14.

It can be seen from the figures that the delayed controller is only slightly slower, and out of the three prediction model it is the one where the delay has the least effect in term of response and trajectory.

Delayed LMPC with disturbance estimators

Next, in Figure 6-15 the trajectory and commanded input of the delayed LMPC vs the delayed LMPC with the two disturbance estimators presented in Subsection 5-1-3 are presented. Their trajectory in the orbital plane is shown in Figure 6-16.

The W of the disturbance estimator presented in (5-5) was set to:

$$W = 1 \times 10^{-3} * \mathrm{I}_{nx} \tag{6-7}$$

From the figures, it is clear that the classical disturbance estimator presented in (5-4) is able to increase the speed of the delayed controller at the expense of a larger deviation in the radial direction X. The W matrix disturbance estimator does not seem to provide many benefits.

Incremental Input Delayed LMPC with disturbance estimators

Finally, in Figure 6-15 the trajectory and commanded input of the incremental input delayed LMPC vs incremental input delayed LMPC with the two disturbance estimators presented in Subsection 5-1-3 are presented. The same W matrix was used as for the delayed controllers. In Figure 6-18 the orbital plane trajectory of the controllers is presented. The disturbance estimators can be seen to have the same effect as for the normal delayed case, and it can be seen that the combination of the incremental input cost function combined with the classical disturbance estimator is able to have the smallest steady state offset.

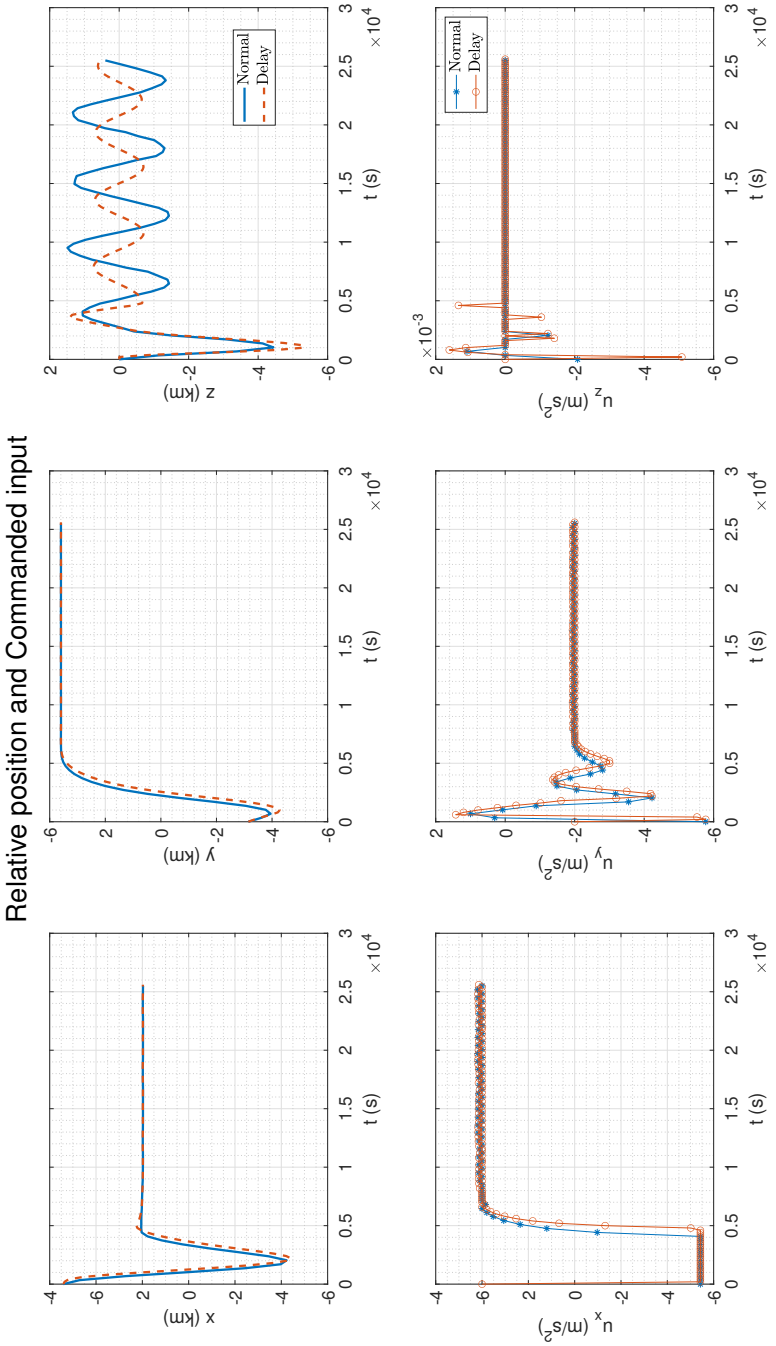

Figure 6-13: Response of Xu-Wang LMPC and delayed Xu-Wang LMPC for Intermediate range

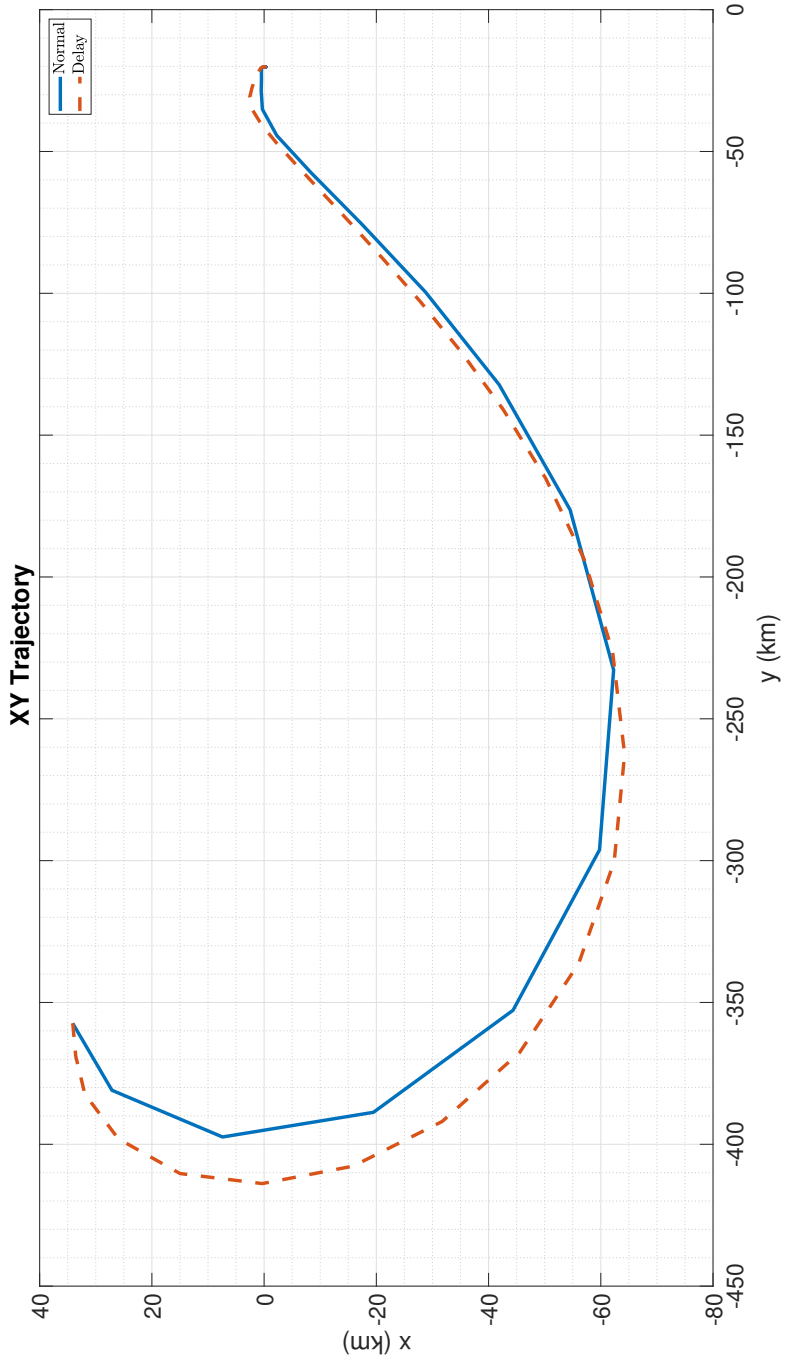

Figure 6-14: Orbital Plane trajectory of Xu-Wang LMPC and delayed LMPC for Intermediate range

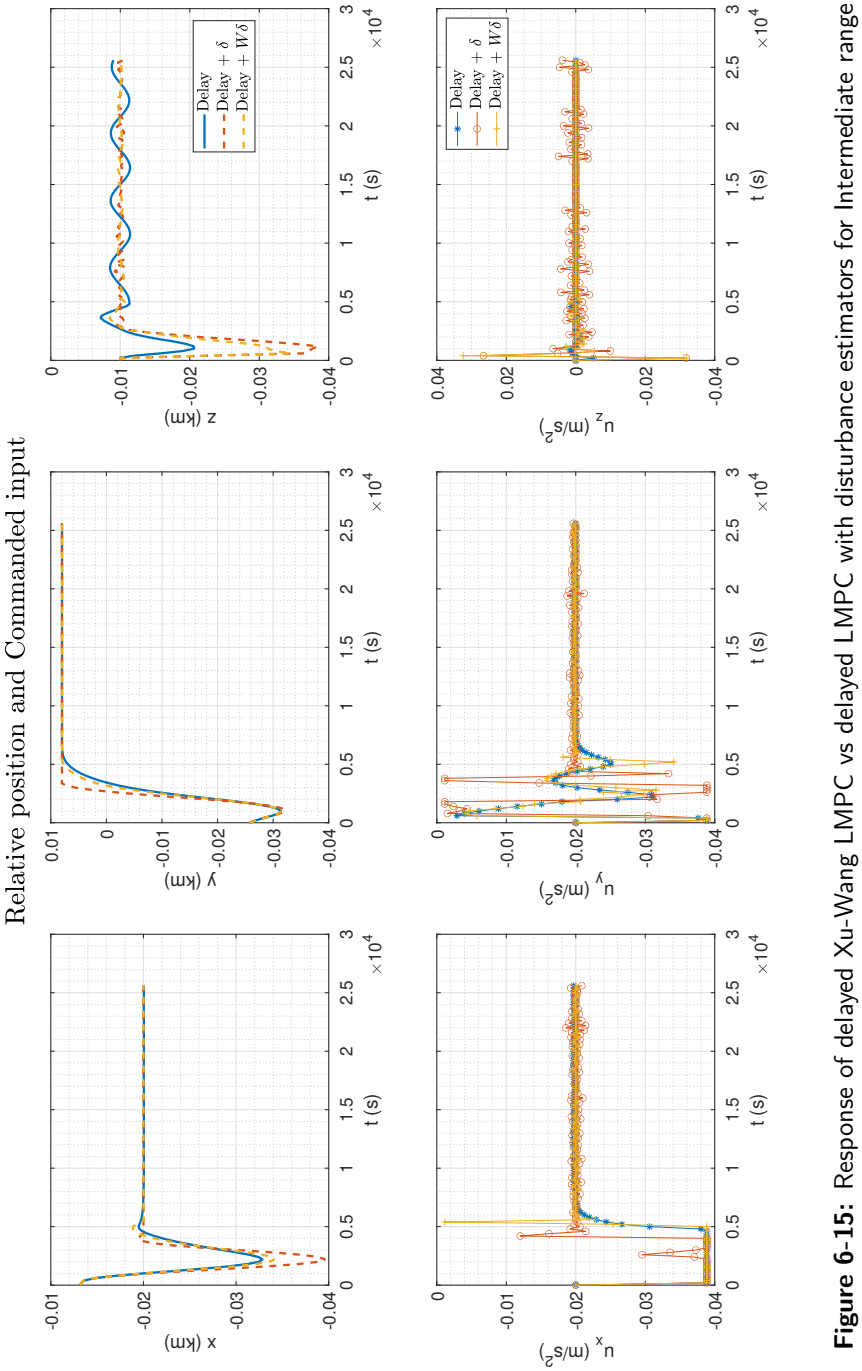

Figure 6-15: Response of delayed Xu-Wang LMPC vs delayed LMPC with disturbance estimators for Intermediate range

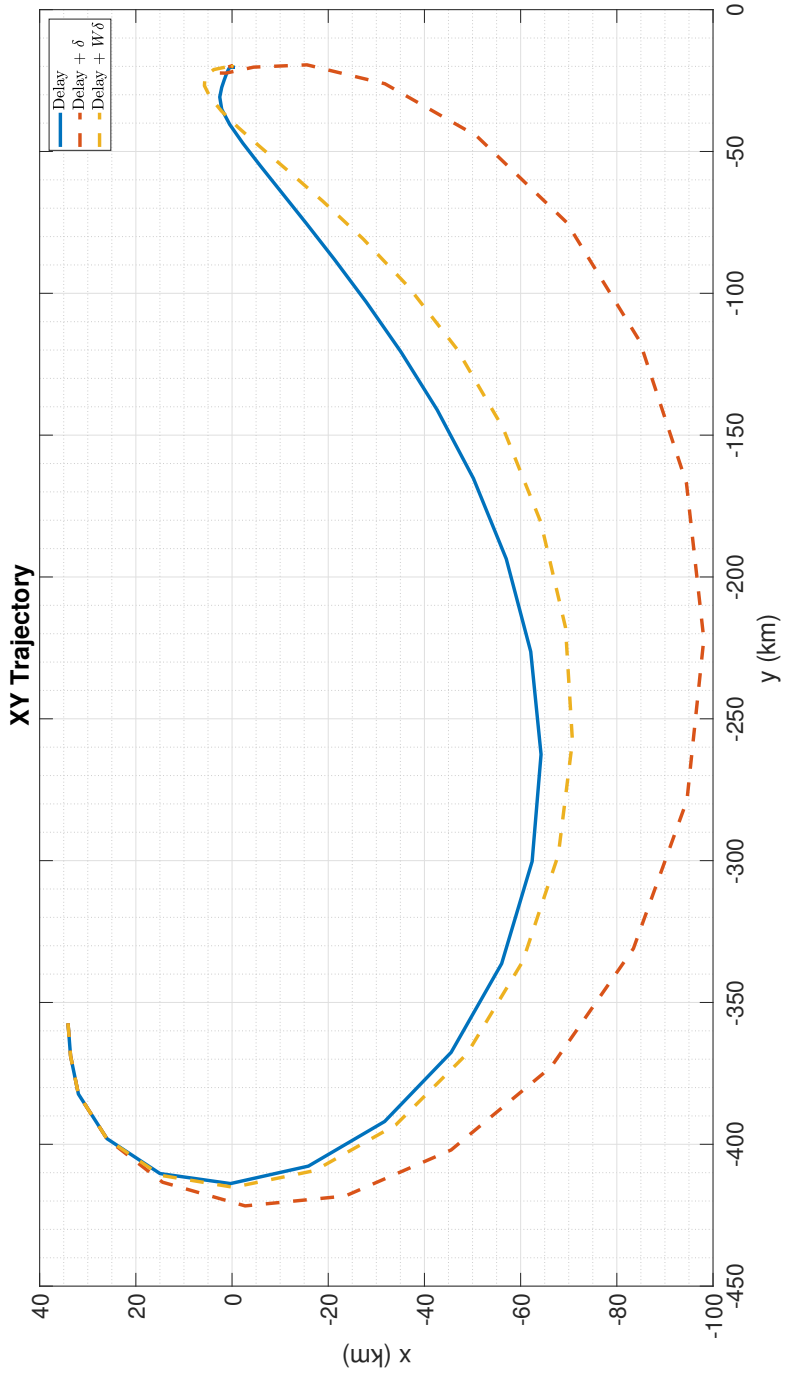

Figure 6-16: Orbital Plane trajectory of delayed Xu-Wang LMPC vs delayed LMPC with disturbance estimators for Intermediate range

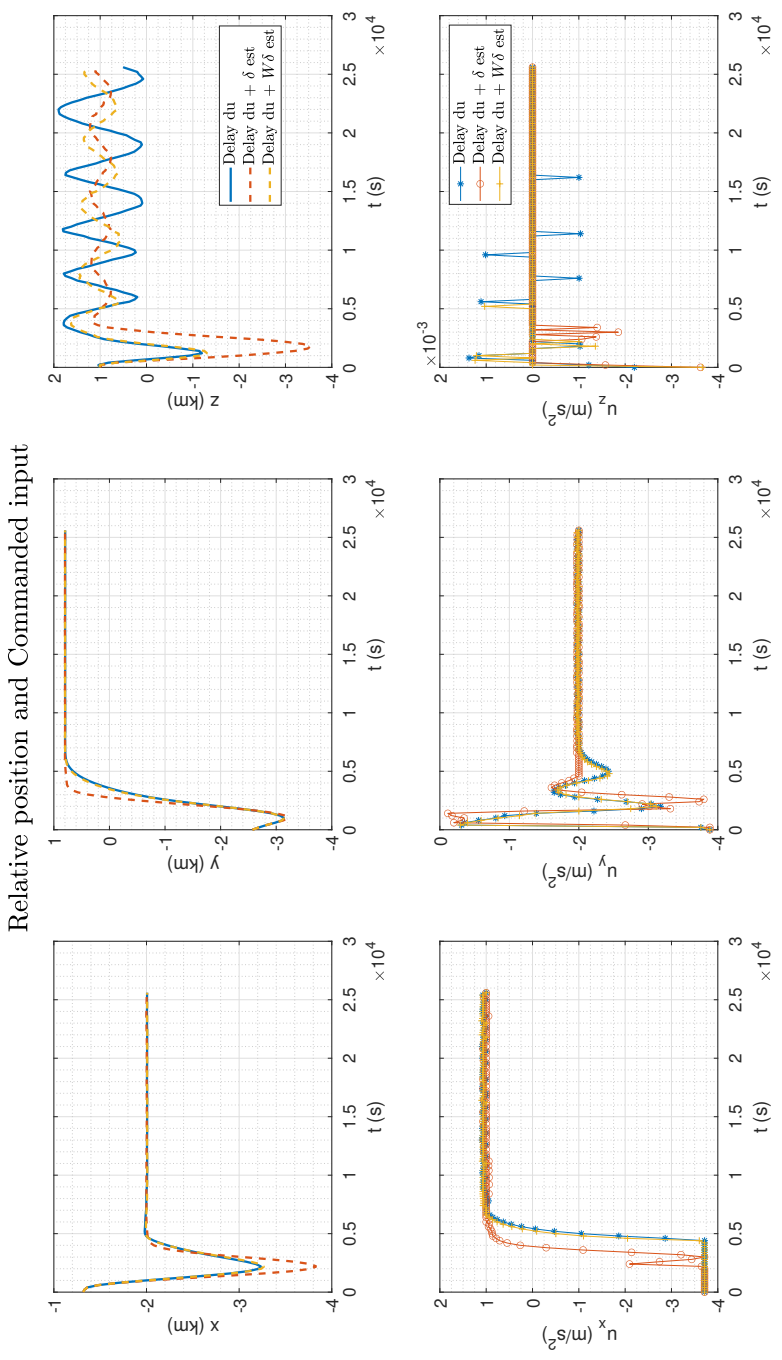

Figure 6-17: Response of delayed of Δu delayed Xu-Wang LMPC vs Δu delayed Xu-Wang LMPC with disturbance estimators for Intermediate range

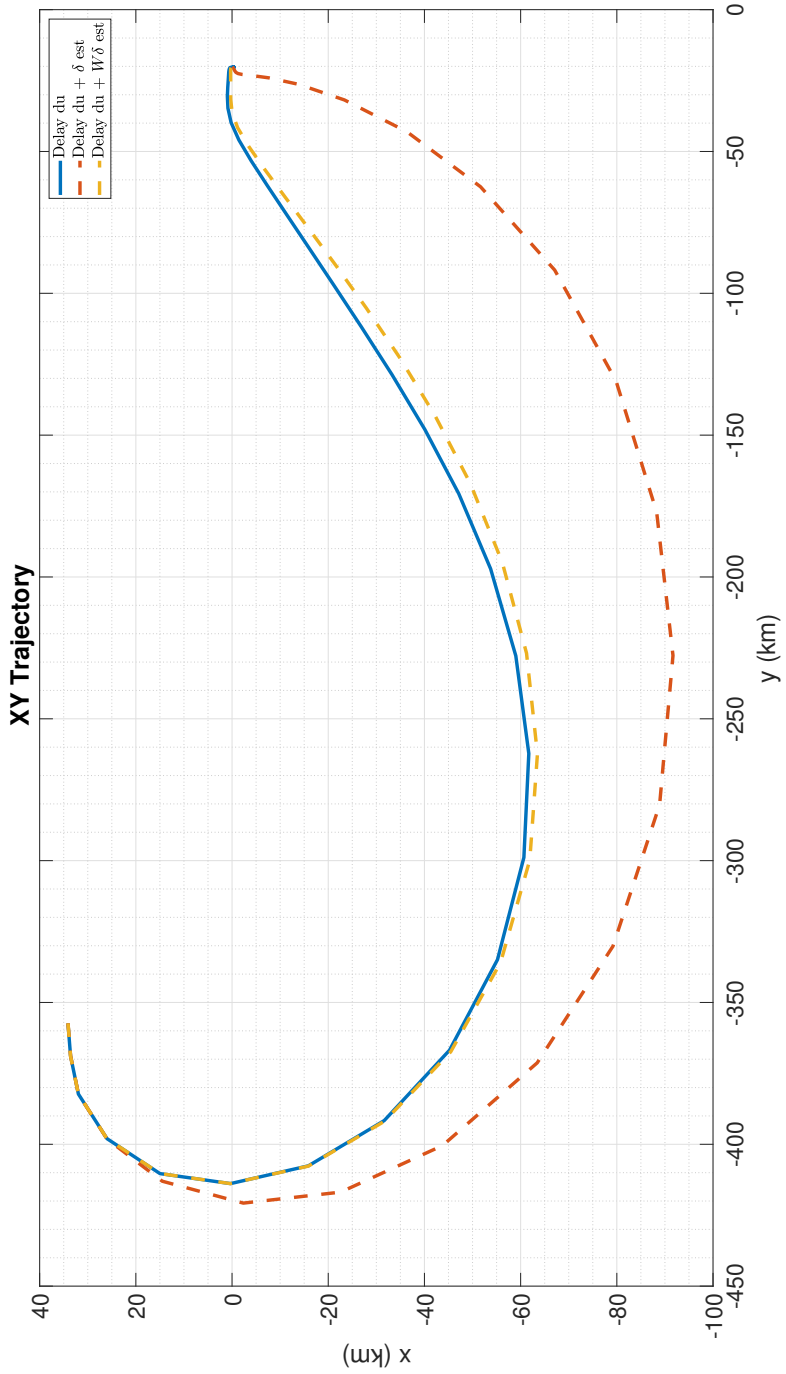

Figure 6-18: Orbital Plane trajectory of Δu XU LMPC and Δu delayed Xu-Wang LMPC for Intermediate range

ΔV and Steady state error

As the simulation did not include a time varying mass and modelled thrusters, it is best suited to compare required ΔV in order to not introduce more assumptions. The steady state error was computed as the Root Mean Squared (RMS) error from the 10000 to 25000 seconds in the simulation, with the same reasoning that was done for the HCW and YA controllers. From the figures, it is clear that by 10000 seconds the chaser has arrived at its first objective of 20 km behind the target. Measuring the RMS from that point gives an indication of the steady state error after the chaser has settled and awaits to begin the second mission phase.

The required ΔV and RMS errors for each controller are presented in Table 6-5. It is clear from the table that the delayed LMPC reduces performance in terms of ΔV required and error regardless of its smaller sampling time, although the reduction in performance is minimal compared to the other prediction models. Even though translation error is in itself not an issue for the first mission phase, LEO orbits can be quite full, and it is important that the chaser can be controlled with accuracy. Furthermore, it can be seen that the classical disturbance estimator provides a significance performance benefit both in terms of ΔV and steady state error while the W matrix disturbance estimator presented in [22] degrades performance for the delayed controller and only provides an δV improvement for the incremental input delayed controllers. Lastly, it is to be noted that while the incremental input cost function does not provide any improvement to the classical one. However, the combination of the incremental input cost function with the classical disturbance estimator is able to provide the best combined performance in terms of ΔV and error even with respect to the non-delayed quadratic cost function LMPC.

Table 6-5: Results for Xu-Wang Intermediate Range controllers

Controller	ΔV $[m/s]$	RMS error x $[m]$	RMS error y $[m]$	RMS error z $[m]$
LMPC	668.85	197.45	191.42	110.65
delayed LMPC	700.23	212.51	228.54	53.69
delayed LMPC + δ est	610.54	90.13	50.64	20.10
delayed LMPC + W δ est	704.17	323.93	144.44	51.22
Δu delayed LMPC	718.52	266.17	279.66	94.71
Δu delayed LMPC + δ est	608.56	129.63	65.62	82.80
Δu delayed LMPC + W δ est	703.73	324.54	138.23	38.23

6-2-4 Conclusion

In this section, we will compare the best controllers for each of the tree prediction models. The best performing controllers are presented in Table 6-6. It is clear from the table that the inclusion of a disturbance estimator has clear benefits in terms of ΔV and RMS for the intermediate range phase. The usage of a more accurate prediction model does also not guarantee a decrease in ΔV or steady state error. The YA controller provided the best performance in terms ΔV but at the expense of the worst steady state error even though it represents a more complete model than the HCW model. This is likely due to the YA STM being computed based on the assumption that the chaser satellite is flying in free motion, and that the external forces on chaser and target satellite are identical, which is not so under

control. The Xu-Wang model provided the best performance in terms of steady state error, which is to be expected as the simulation is based on its non-linear counterpart, however it did not provide better ΔV performance than the YA and HCW controllers. This is likely due to the controller compensating for disturbances included in the model to achieve this better steady state error. Overall, the HCW controllers provide the best compromise in performance between ΔV and steady state error. Considering that both the YA and Xu-Wang require the integration of the RSV's at every computation being LTV systems, the HCW model provides better performance for no computational expense. Furthermore, it is clear that the use of robust techniques improves performance for all models, as the inclusion of disturbance estimator proved a significant difference for all prediction models as expected.

Table 6-6: Results for the Intermediate Range controllers

Controller	ΔV $[m/s]$	RMS error x $[m]$	RMS error y $[m]$	RMS error z $[m]$
HCW Δu delayed LMPC + δ est	539.42	87.42	44.17	26.97
YA delayed LMPC + δ est	474.74	411.51	371.02	57.07
Xu-Wang delayed LMPC + δ est	610.54	90.13	50.64	20.10

The compared responses and trajectories of the three controllers are presented in Figures 6-19 and 6-20.

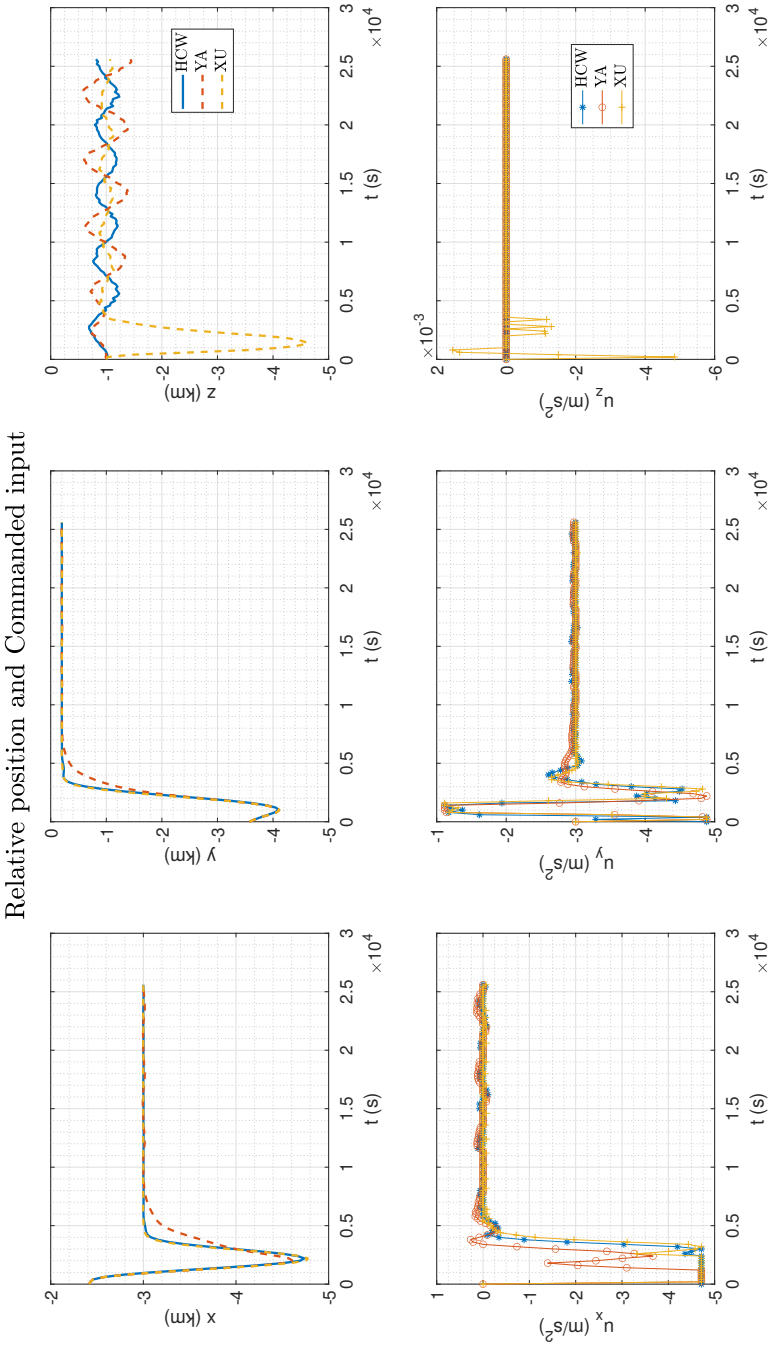

Figure 6-19: Response of best performing Intermediate Range HCW, YA and Xu-Wang controllers

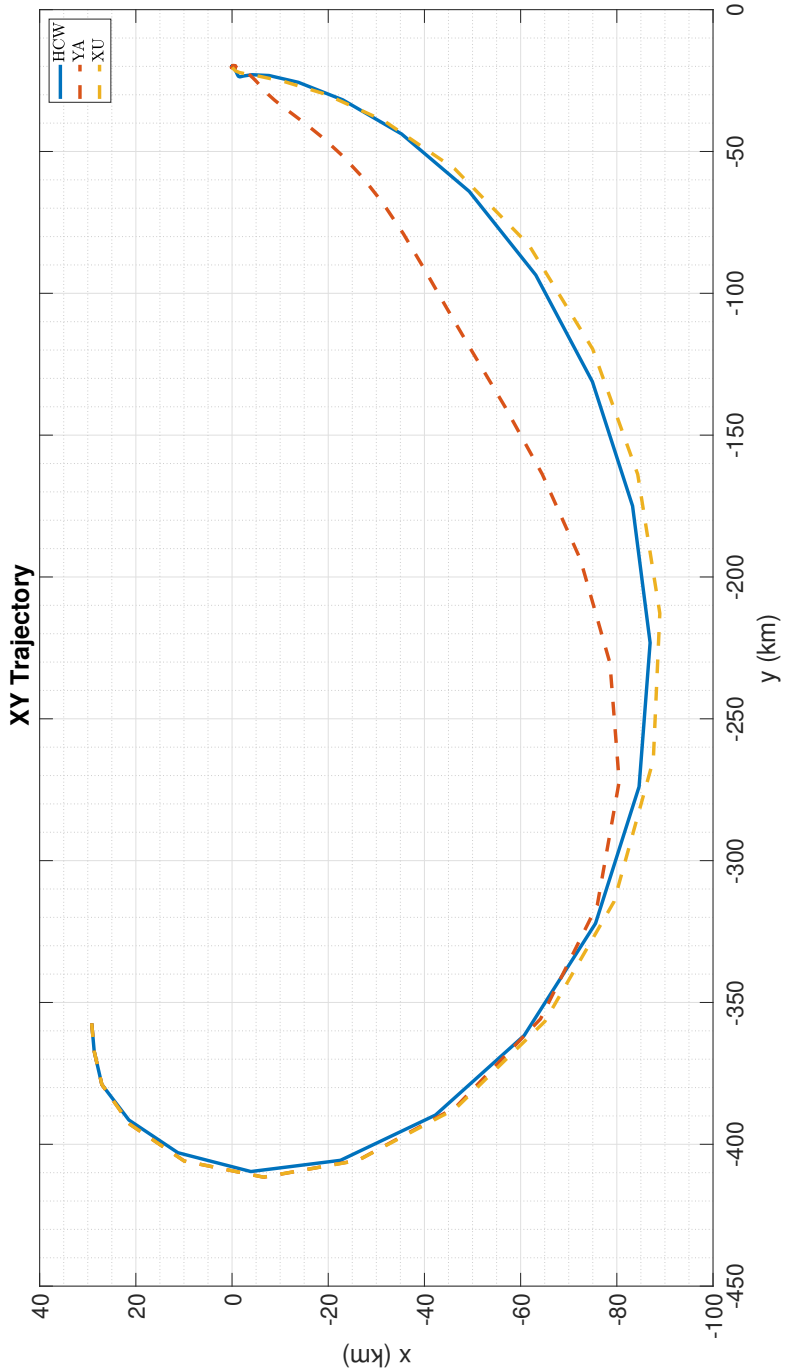

Figure 6-20: Orbital Plane trajectory best performing Intermediate Range HCW, YA and Xu-Wang controllers

6-3 Short Range INTG

In this Section the results of the controllers for the Short range phase presented in Section 5-2 will be presented. The initial conditions for this phase are presented below, with a slight offset in each axis to represent the RMS error of the controllers in the first phase.

$$x(0) = \begin{bmatrix} 100 & -20100 & 100 & 0 & 0 & 0 \end{bmatrix}^{\mathsf{T}} \tag{6-8}$$

Due to the shorter nature of this mission phase, sampling time and prediction horizon were chosen to account for one orbital period.

6-3-1 HCW LMPC controllers

In this subsection, the results of the HCW based LMPC formulations will be presented. It is to be noted that with the use of the HCW prediction model, using a sampling time of 200 seconds and a prediction horizon of, $N_p = 29$ steps was not possible for the delayed controllers, thus a smaller sampling period was chosen of 150 seconds combined with a prediction horizon of $N_p = 38$ was used to still have a prediction horizon of 1 orbit. The cost matrices Q and R used for the simulations are presented below:

Table 6-7: Cost matrices for HCW Short Range Controllers

Controller	Q_x	$Q_{\dot{x}}$	R_u or $R_{\Delta u}$
LMPC	1×10^{1}	1×10^{6}	1000
delayed LMPC	1×10^{-1}	1×10^{5}	1000
delayed LMPC + δ est	1×10^{0}	1×10^{5}	1000
delayed LMPC + W δ est	1×10^{-1}	1×10^{5}	1000
Δu delayed LMPC	1×10^{-1}	1×10^{5}	1000
Δu delayed LMPC + δ est	1×10^{-1}	1×10^{5}	1000
Δu delayed LMPC + W δ est	1×10^{-1}	1×10^{5}	1000

Normal vs Delayed LMPC

Firstly, the trajectory and commanded input of the normal LMPC vs the delayed LMPC are presented in Figure 6-21. The trajectory in the orbital plane is presented in 6-22 and 6-23.

It can be seen from the figures that regardless of the smaller sampling period, the delayed controller is slower and has more of an overshoot. The out of plane oscillations in the Z axis can be damped at the cost of more propellant use, but for the scope of this mission phase it is not required or important. Furthermore, it is clear that the delayed controller is not able to control and keep the chaser satellite within the rectangular holding point. The total ΔV required by the controllers will be presented at the end, with the remainder of the controllers.

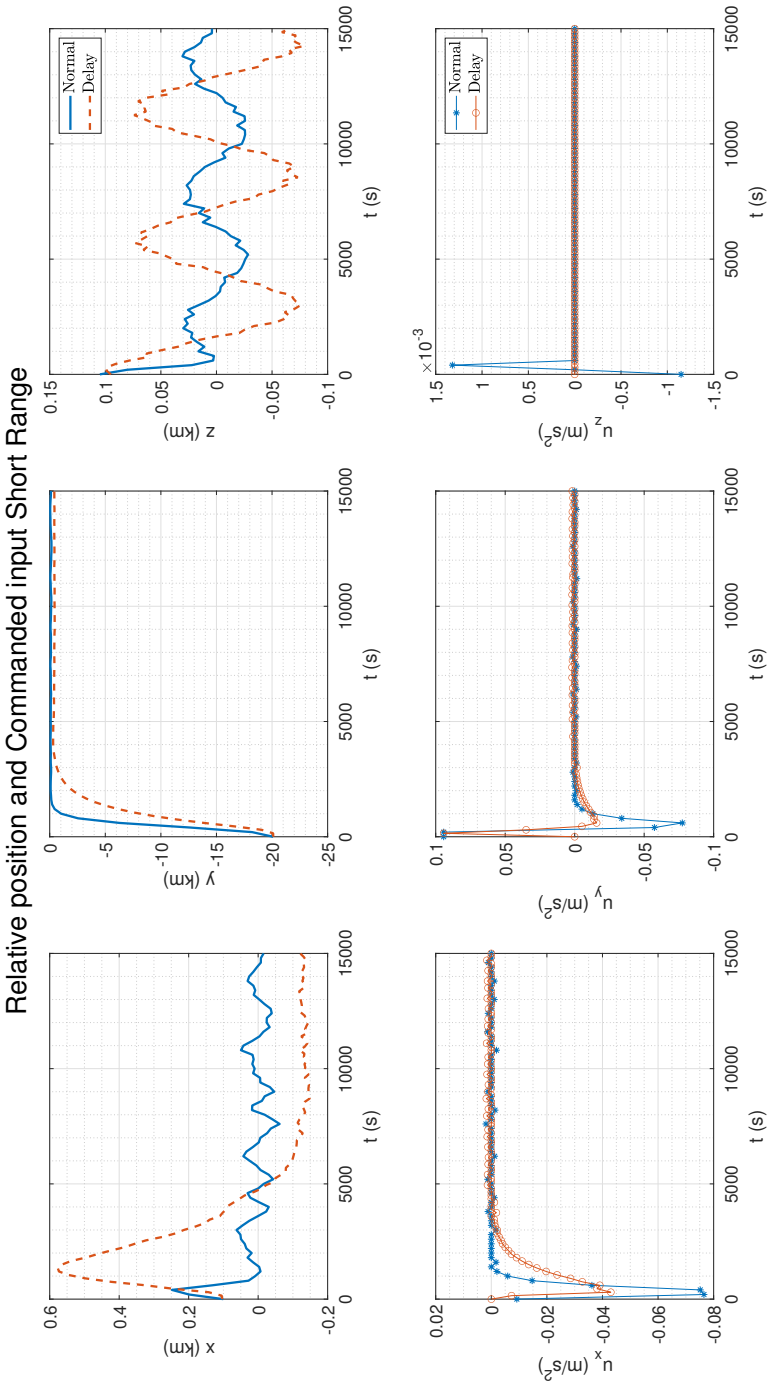

Figure 6-21: Response of HCW LMPC and delayed HCW LMPC for Short range

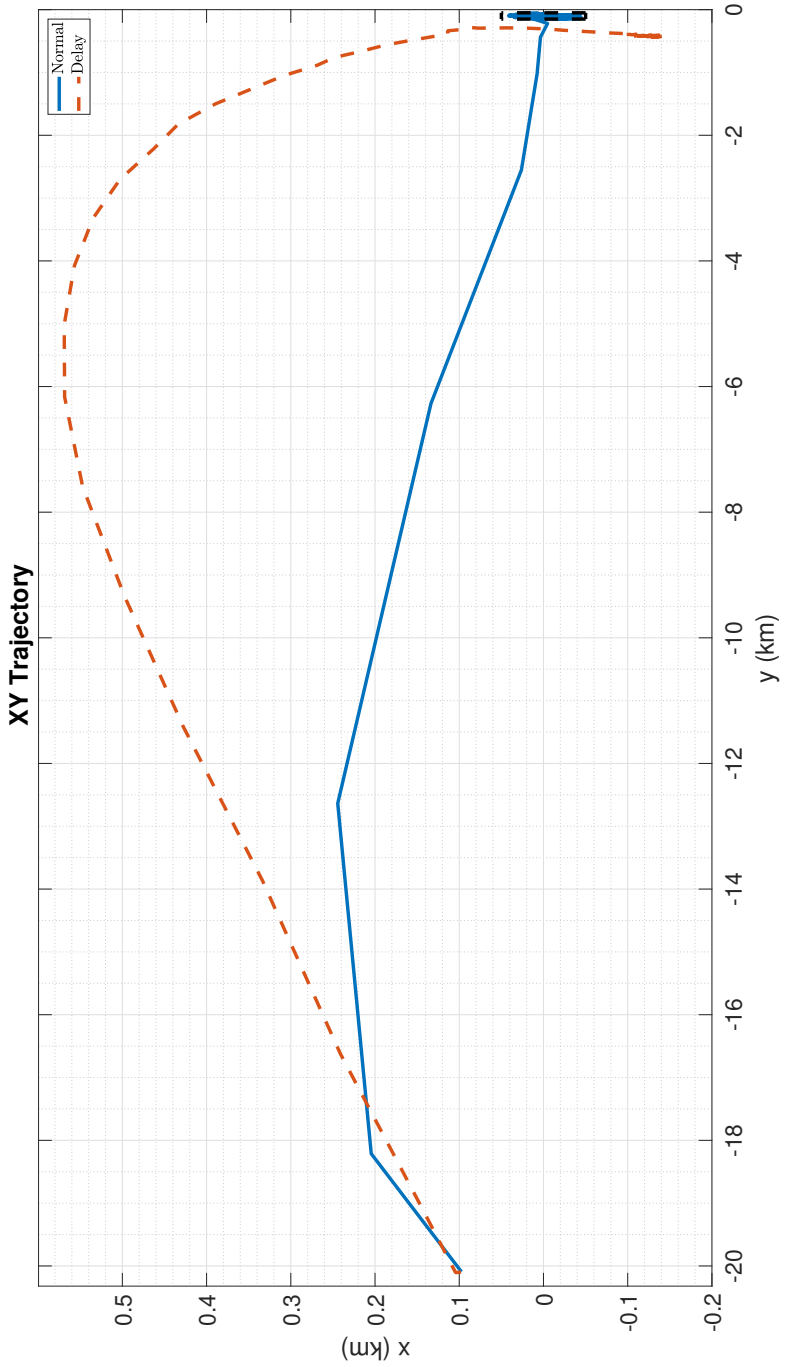

Figure 6-22: Orbital Plane trajectory of HCW LMPC and delayed HCW LMPC for Short range

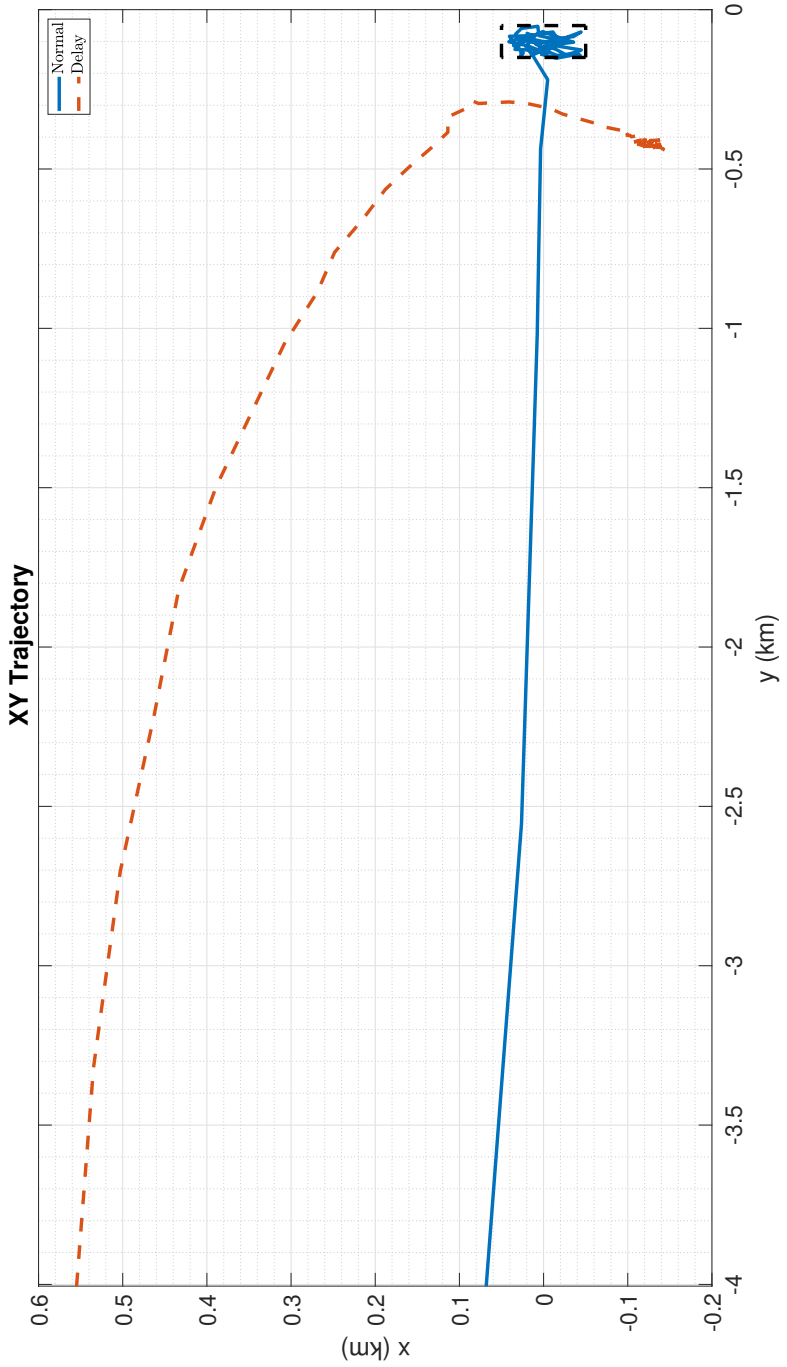

Figure 6-23: Magnified Orbital Plane trajectory of HCW LMPC and delayed HCW LMPC for Short range

Delayed LMPC with disturbance estimators

Next, in Figure 6-24 the trajectory and commanded input of the delayed LMPC vs the delayed LMPC with the two disturbance estimators presented in Subsection 5-1-3 are presented. Their trajectory in the orbital plane is shown in Figure 6-25 and 6-26.

The W of the disturbance estimator presented in (5-5) was set to:

$$W = 1 \times 10^{-3} * \mathrm{I}_{nx} \tag{6-9}$$

From the figures, it becomes evident that the classical disturbance estimator presented in (5-4) is able to increase the speed of the delayed controller, and is able to satisfy the terminal holding point constraint. The W matrix disturbance estimator does not seem to provide many benefits except a slight increase in response time. Completion time is not of importance for this mission phase, but is an important observation.

Incremental Input Delayed LMPC with disturbance estimators

Finally, in Figure 6-27 the trajectory and commanded input of the incremental input delayed LMPC vs incremental input delayed LMPC with the two disturbance estimators presented in Subsection 5-1-3 are presented. The same W matrix was used as for the delayed controllers. In Figure 6-28 and 6-29 the orbital plane trajectory of the controllers is presented. The disturbance estimators can be seen to have the same effect as for the normal delayed case, meaning the use of an incremental input model and cost function by itself does not help with satisfying the holding point constraint, but the use of the classical disturbance estimator does.

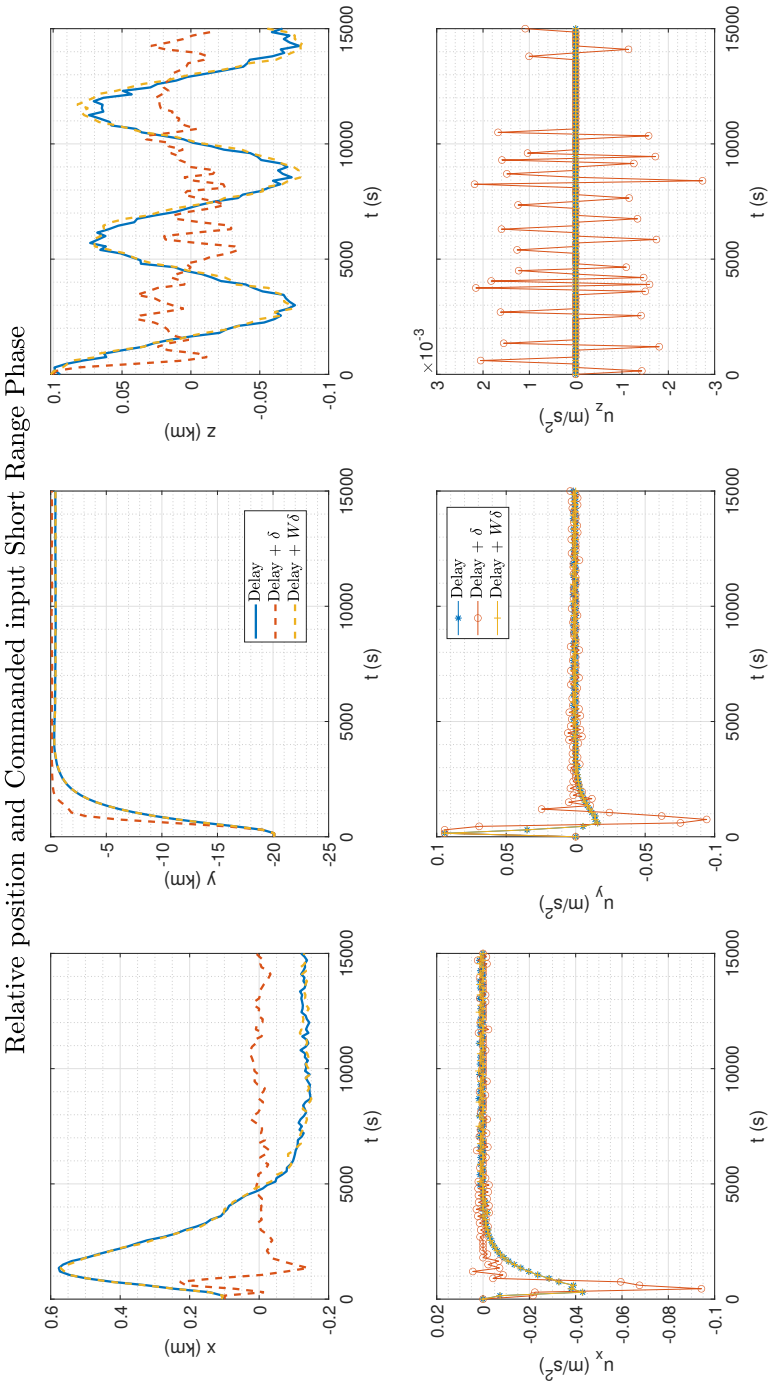

Figure 6-24: Response of delayed HCW LMPC vs delayed HCW LMPC with disturbance estimators for Short range

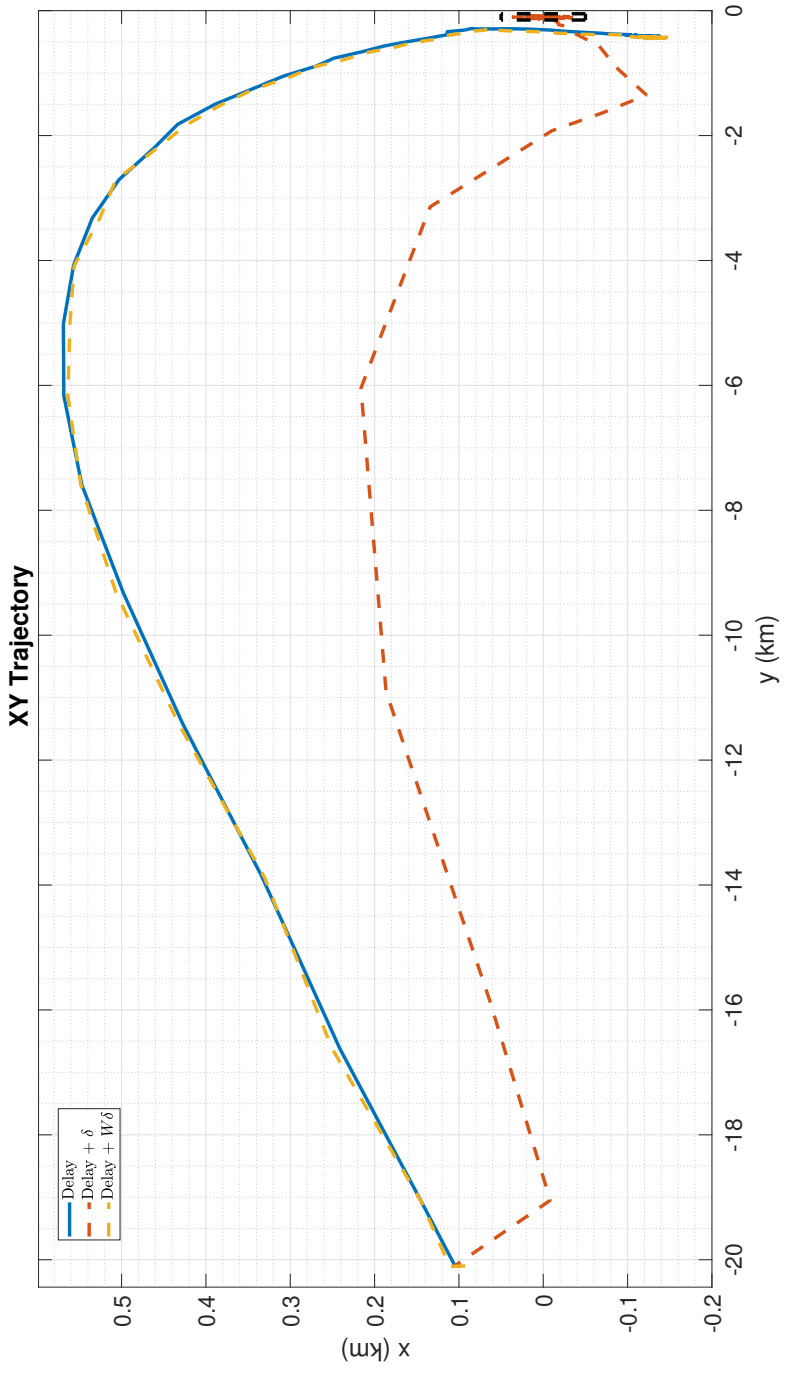

Figure 6-25: Orbital Plane trajectory of delayed HCW LMPC vs delayed HCW LMPC with disturbance estimators for Short range

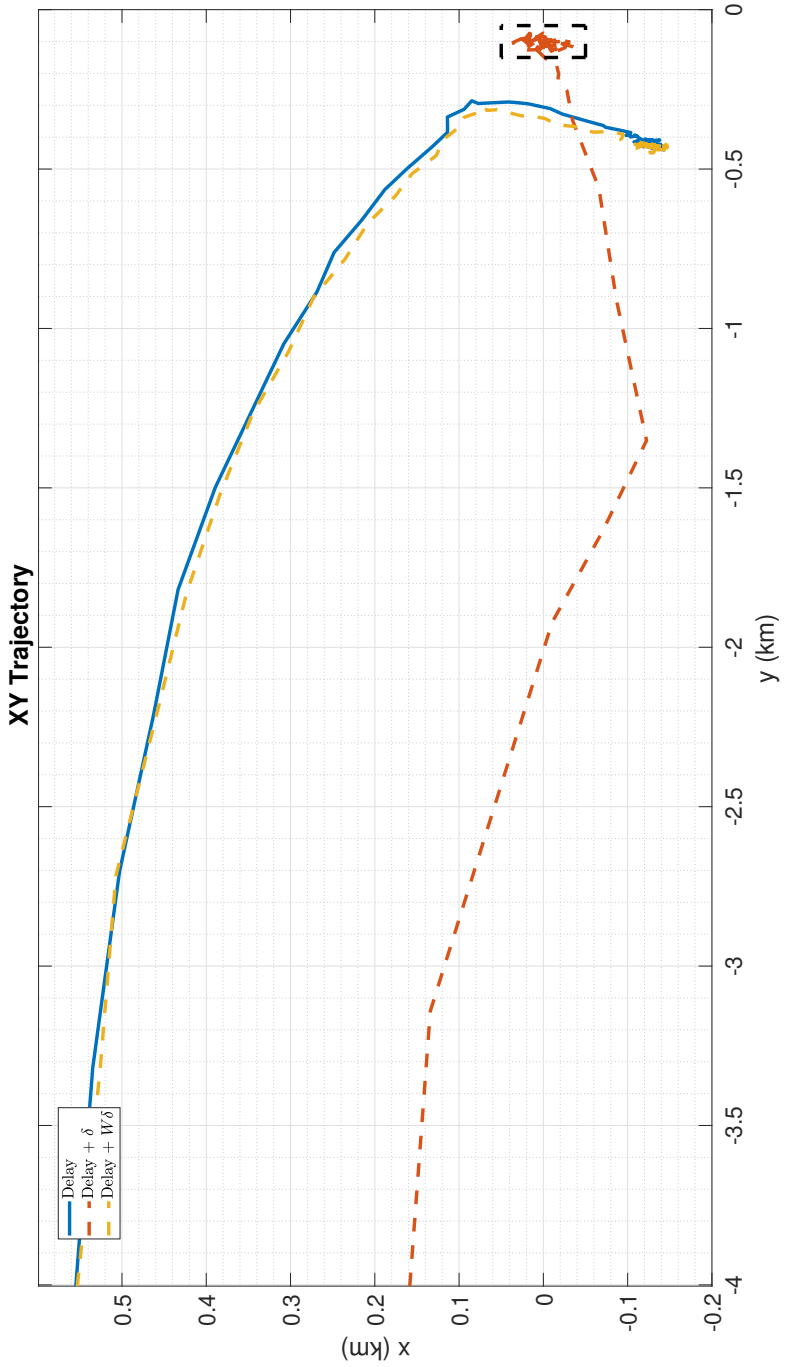

Figure 6-26: Magnified Orbital Plane trajectory of delayed HCW LMPC vs delayed HCW LMPC with disturbance estimators for Short range

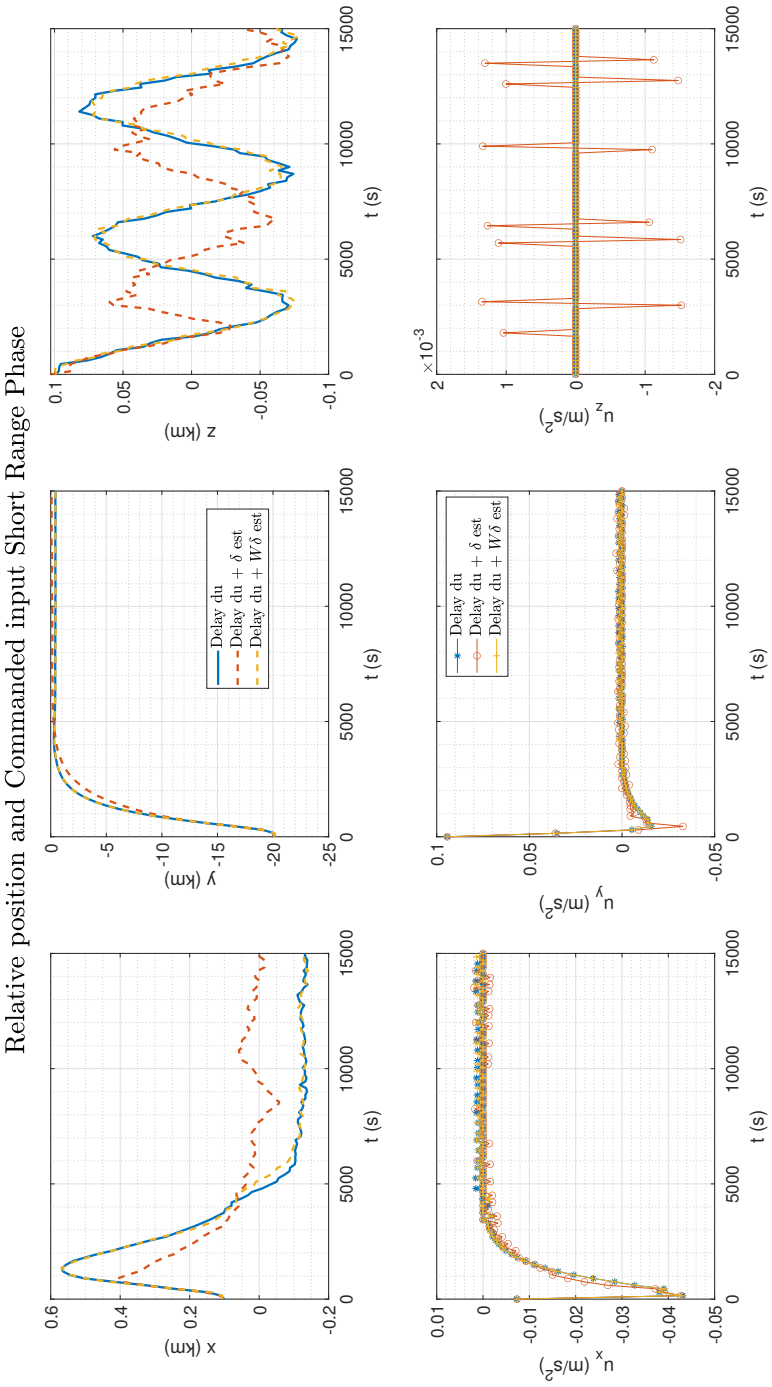

Figure 6-27: Orbital Plane trajectory of Δu delayed HCW LMPC vs Δu delayed HCW LMPC with disturbance estimators for Short range

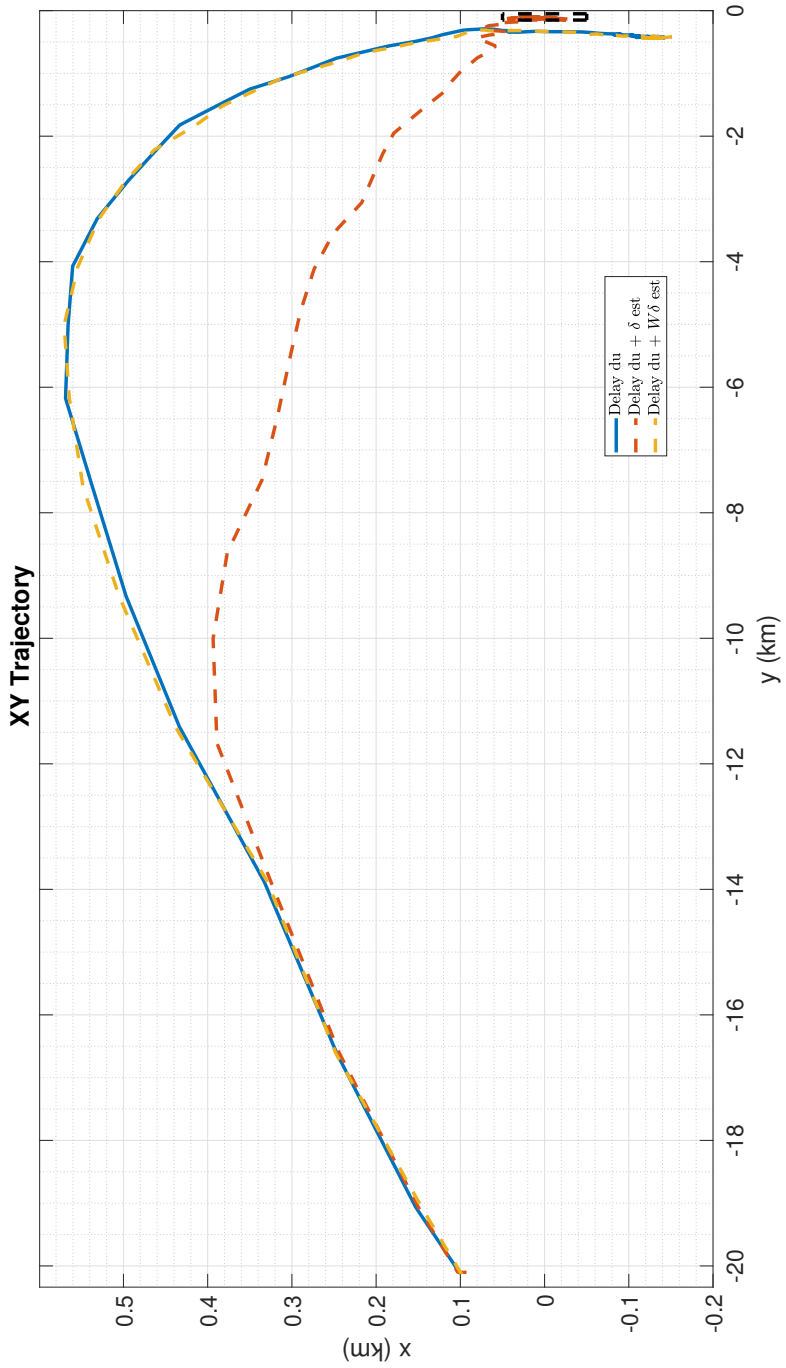

Figure 6-28: Orbital Plane trajectory of Δu HCW controllers, for Short range

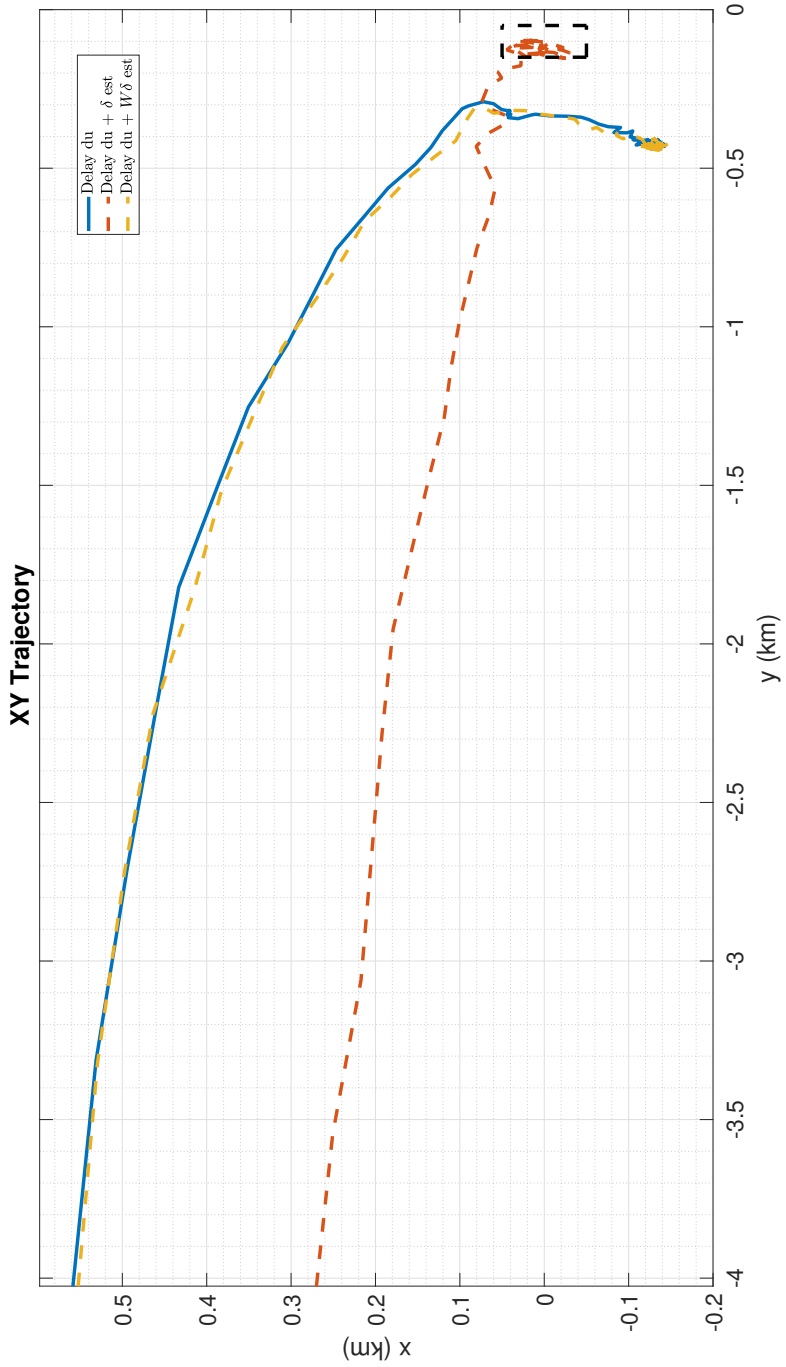

Figure 6-29: Magnified Orbital Plane trajectory of Δu HCW controllers, for Short range

ΔV and Steady state error

As the simulation did not include a time varying mass and modelled thrusters, it is best suited to compare required ΔV in order to not introduce more assumptions. The steady state error was computed as the Root Mean Squared (RMS) error from the 10000 to 15000 seconds in the simulation. From the figures, it is clear that by 10000 seconds the chaser has arrived at its first objective of 20 km behind the target. Measuring the RMS from that point gives an indication of the steady state error after the chaser has settled and awaits to begin the second mission phase.

The required ΔV and RMS errors for each controller are presented in Table 6-8. It is clear from the table that the delayed LMPC reduces performance in terms of ΔV required and error regardless of its smaller sampling time. The reduction in performance is such that it is not feasible for this mission phase as it is not able to keep the chaser within the desired holding point as was explained. This was the case for all delayed controllers except the two making use of a classical disturbance estimator. This can be seen in Table 6-8 significance performance benefit in terms of steady state error while the W matrix disturbance estimator presented in [22] doesn't offer any benefit compared to the delayed LMPC. The delayed LMPC with classical disturbance estimator is able to satisfy the holding point constraint, but at the cost of more ΔV usage compared to the normal LMPC. Lastly, it is to be noted that while the incremental input cost function does not provide any significant improvement to the classical one. However, the combination of the incremental input cost function with the classical disturbance estimator is able to provide the best performance in terms of ΔV and error even with respect to the non-delayed quadratic cost function LMPC, requiring less ΔV while also satisfying the holding point constraint.

Table 6-8: Results for HCW Intermediate Range controllers

Controller	ΔV $[m/s]$	RMS error x $[m]$	RMS error y $[m]$	RMS error z $[m]$
LMPC	125.58	17.32	22.30	7.11
delayed LMPC	95.95	91.60	229.78	36.26
delayed LMPC + δ est	174.45	10.96	11.13	14.99
delayed LMPC + W δ est	95.89	91.26	235.98	37.00
Δu delayed LMPC	95.46	92.27	232.03	38.06
Δu delayed LMPC + δ est	98.20	26.74	19.89	24.11
Δu delayed LMPC + W δ est	96.06	93.88	232.40	39.83

6-3-2 Yamanaka-Ankersen LMPC controllers

In this subsection, the results of the YA based LMPC formulations will be presented. It is to be noted that with the use of the YA prediction model, using a sampling time of 200 seconds and a prediction horizon of, $N_p = 28$ was possible for the delayed controllers, but to have a fair comparison a smaller sampling period of 150 seconds combined with a prediction horizon of $N_p = 31$ was used just as for the HCW short range controllers. The cost matrices Q and R used for the simulations are presented below:

Table 6-9: Cost matrices for YA Short Range Controllers

Controller	Q_x	$Q_{\dot{x}}$	R_u or $R_{\Delta u}$
LMPC	1×10^{1}	1×10^{6}	1000
delayed LMPC	1×10^{0}	1×10^{6}	1000
delayed LMPC + δ est	1×10^{-3}	1×10^{4}	1000
delayed LMPC + W δ est	1×10^{-1}	1×10^{5}	10000
Δu delayed LMPC	1×10^{-1}	1×10^{5}	1000
Δu delayed LMPC + W δ est	1×10^{-1}	1×10^{5}	1000

Normal vs Delayed LMPC

Firstly, the trajectory and commanded input of the normal LMPC vs the delayed LMPC are presented in Figure 6-30. The trajectory in the orbital plane is presented in 6-31 and 6-32.

It can be seen from the figures that regardless of the smaller sampling period, the delayed controller is slower, but unlike for the HCW there is no increase in overshoot. The out of plane oscillations in the Z axis can be damped at the cost of more propellant use, but for the scope of the first mission phase it is not required or important. Furthermore, unlike for the HCW controllers, the trajectory of the delayed controller does not change as radically, as the form and approach is still the same except for a larger deviation in the radial direction. It is to be noted that neither the normal nor delayed controller are able to satisfy the holding point constraint, meaning both controllers are not viable options for this mission phase.

Delayed LMPC with disturbance estimators

Next, in Figure 6-33 the trajectory and commanded input of the delayed LMPC vs the delayed LMPC with the two disturbance estimators presented in Subsection 5-2-3 are presented. Their trajectory in the orbital plane is shown in Figure 6-34 and 6-35. The W of the disturbance estimator presented in (5-5) was set to:

$$W = 1 \times 10^{-3} * \mathrm{I}_{nx} \tag{6-10}$$

From the figures, it becomes evident that both estimators do not help improve the performance of the delayed LMPC. None of the controllers again are able to keep the chaser inside the holding point accurately. This follows the trend that the YA model is more sensitive and results in more offset. It is also to be noted that the classical disturbance estimator hard to tune and make functioning due to the controller becoming even more sensitive.

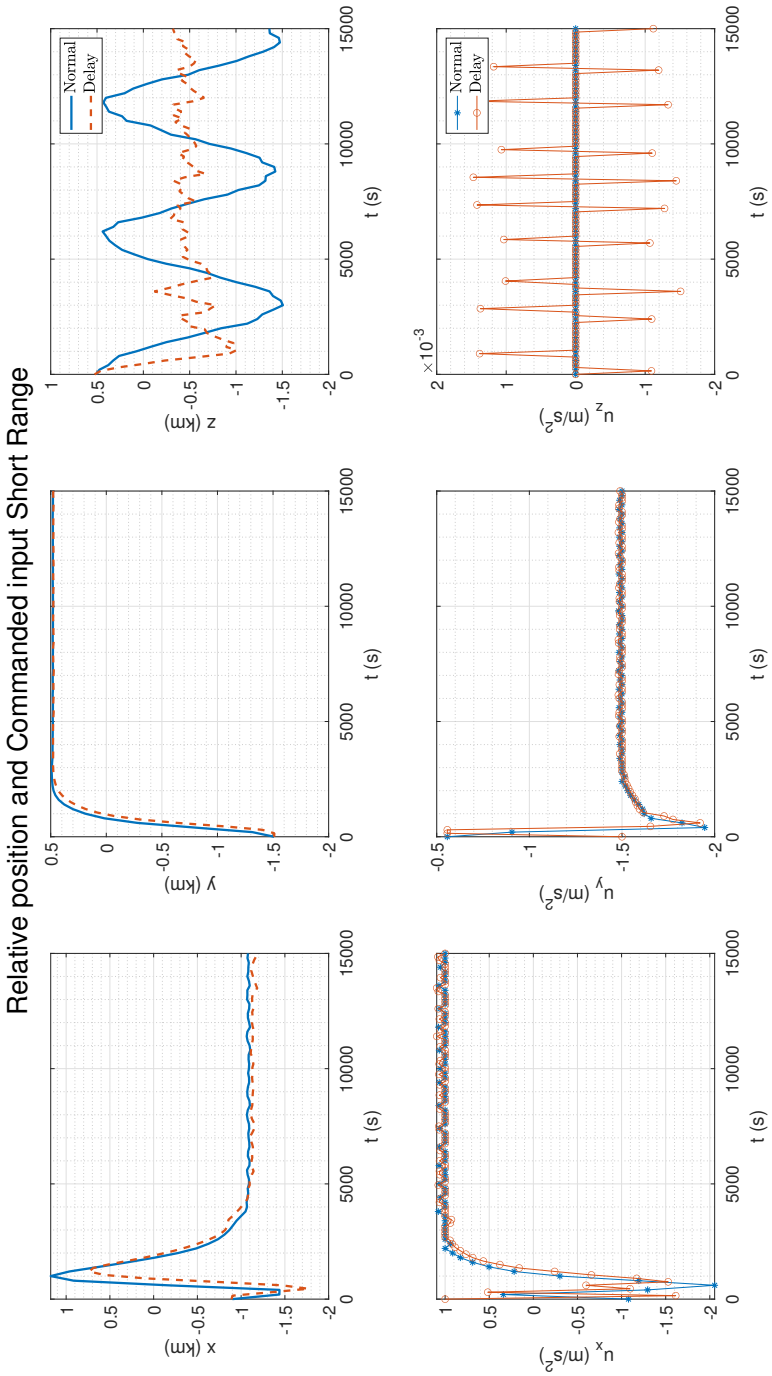

Figure 6-30: Response of YA LMPC and delayed LMPC for Short range

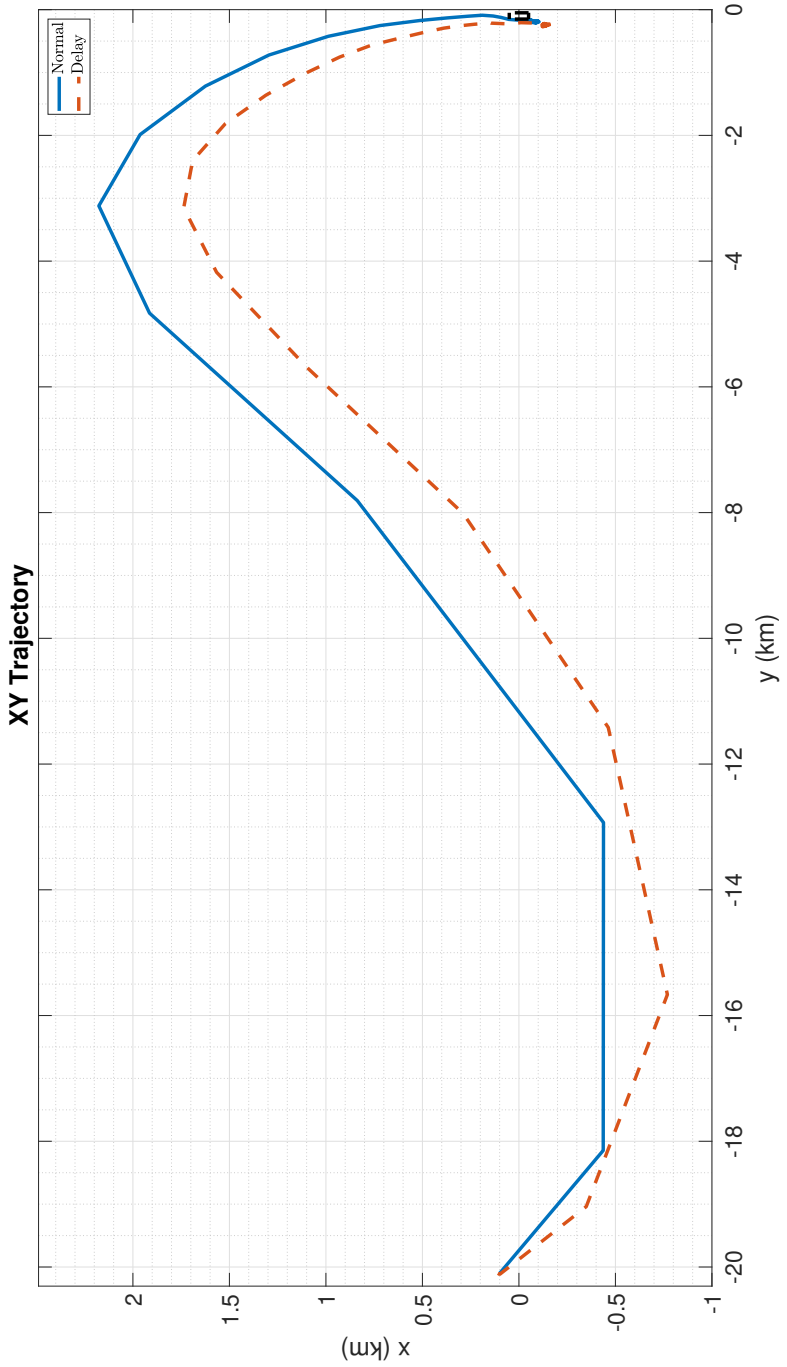

Figure 6-31: Orbital Plane trajectory of YA LMPC and delayed LMPC for Short range

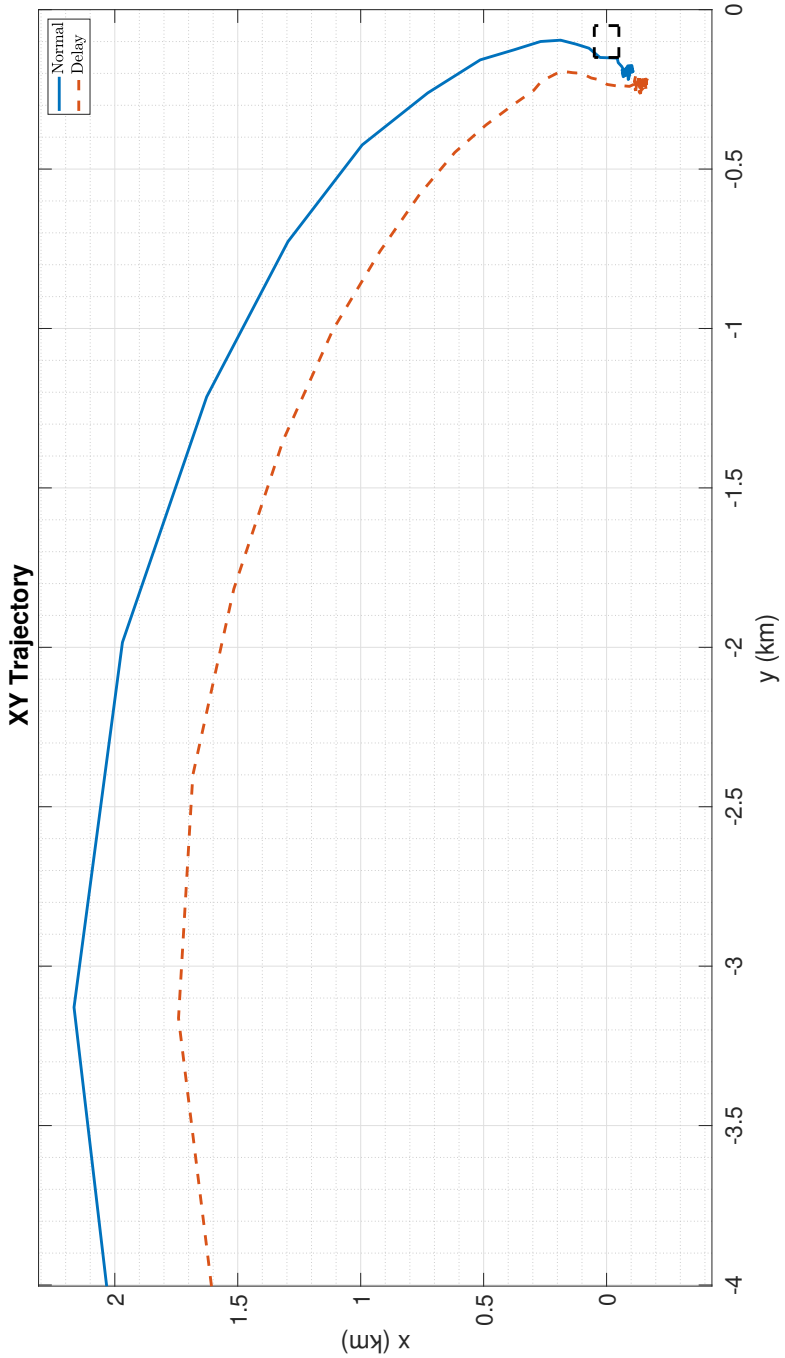

Figure 6-32: Magnified Orbital Plane trajectory of YA LMPC and delayed LMPC for Short range

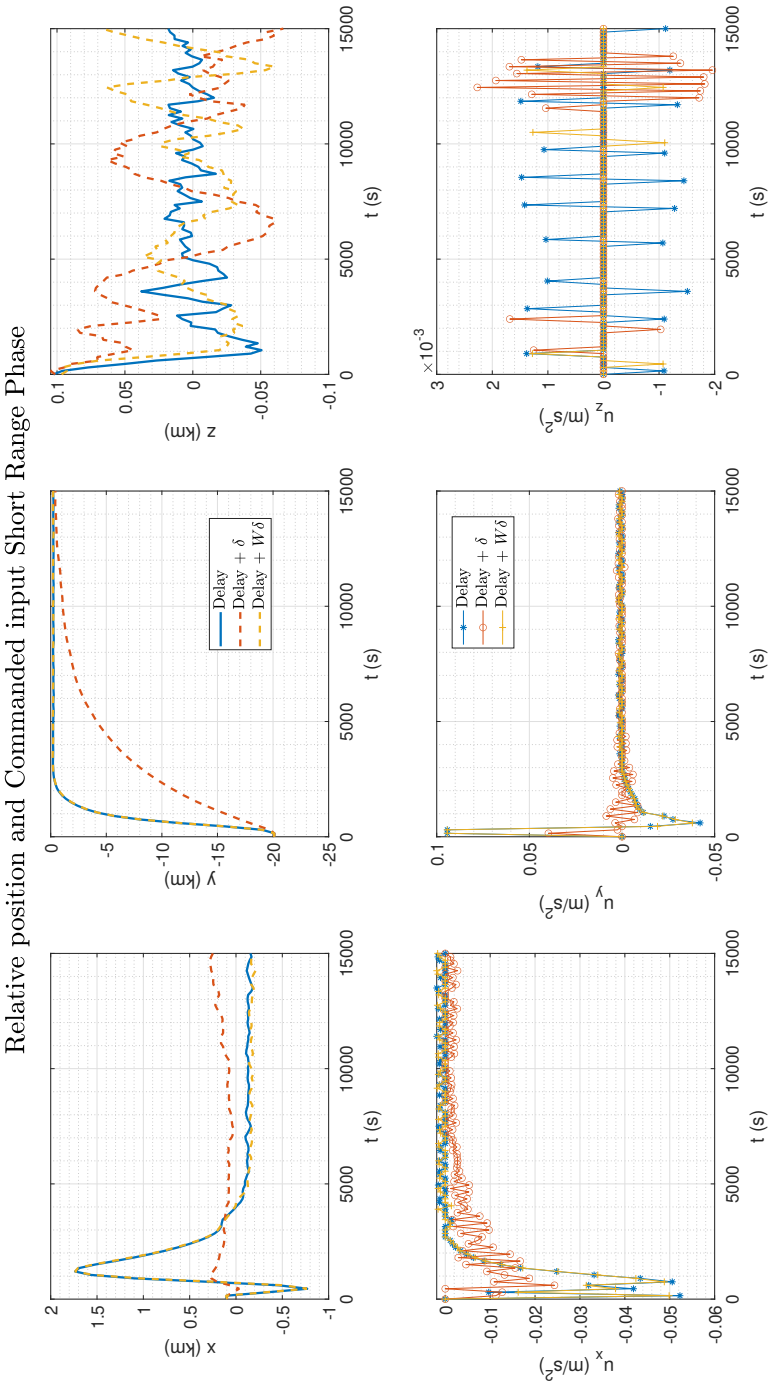

Figure 6-33: Response of delayed YA LMPC vs delayed YA LMPC with disturbance estimators for Short range

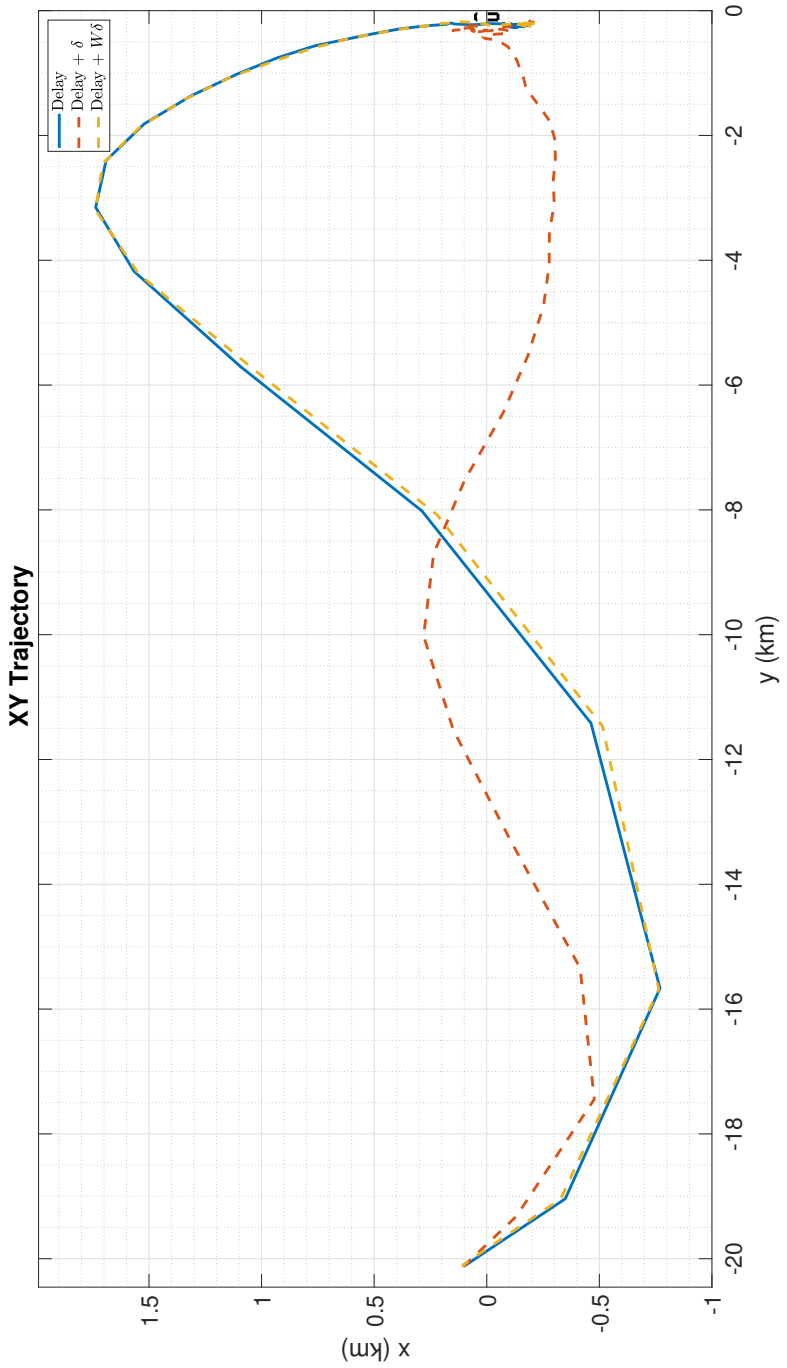

Figure 6-34: Orbital Plane trajectory of delayed YA LMPC vs delayed LMPC with disturbance estimators for Short range

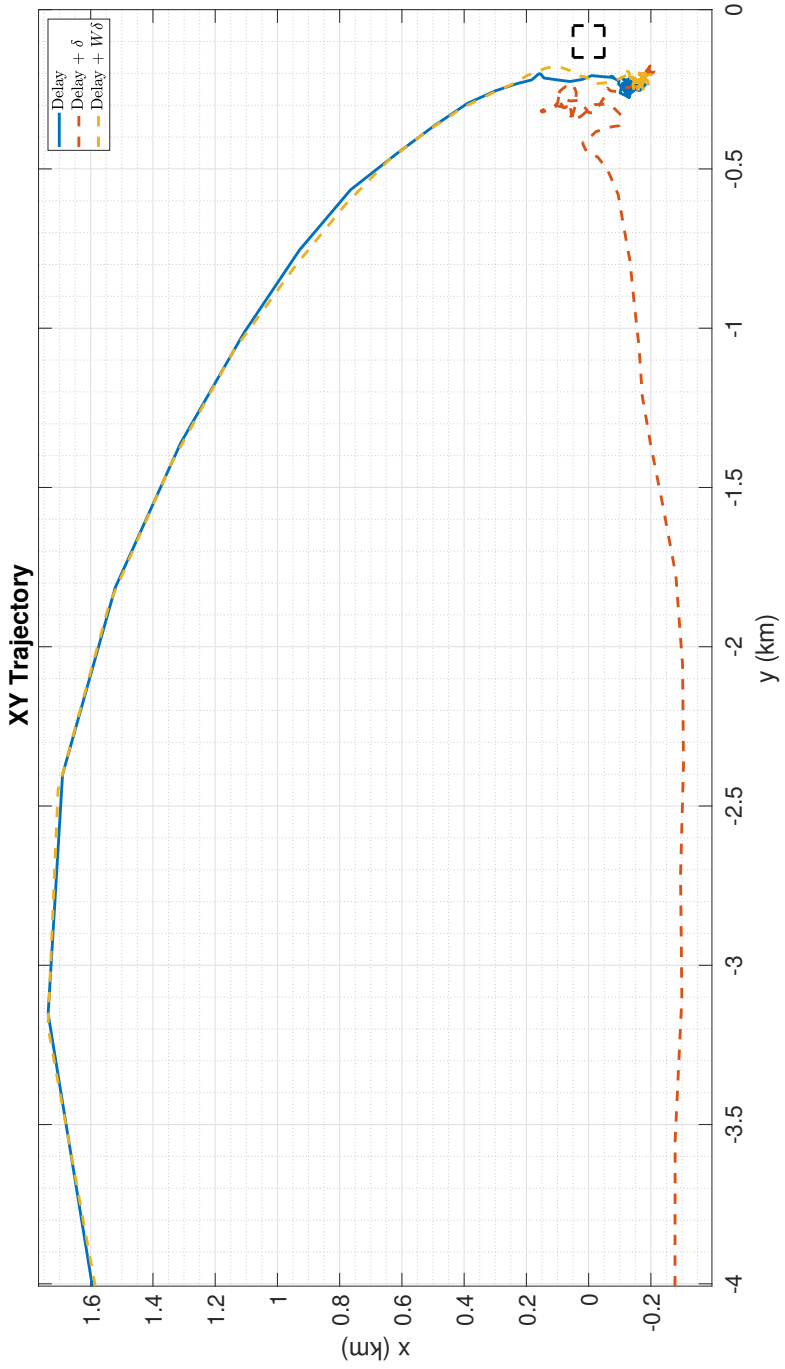

Figure 6-35: Magnified Orbital Plane trajectory of delayed YA LMPC vs delayed LMPC with disturbance estimators for Short range

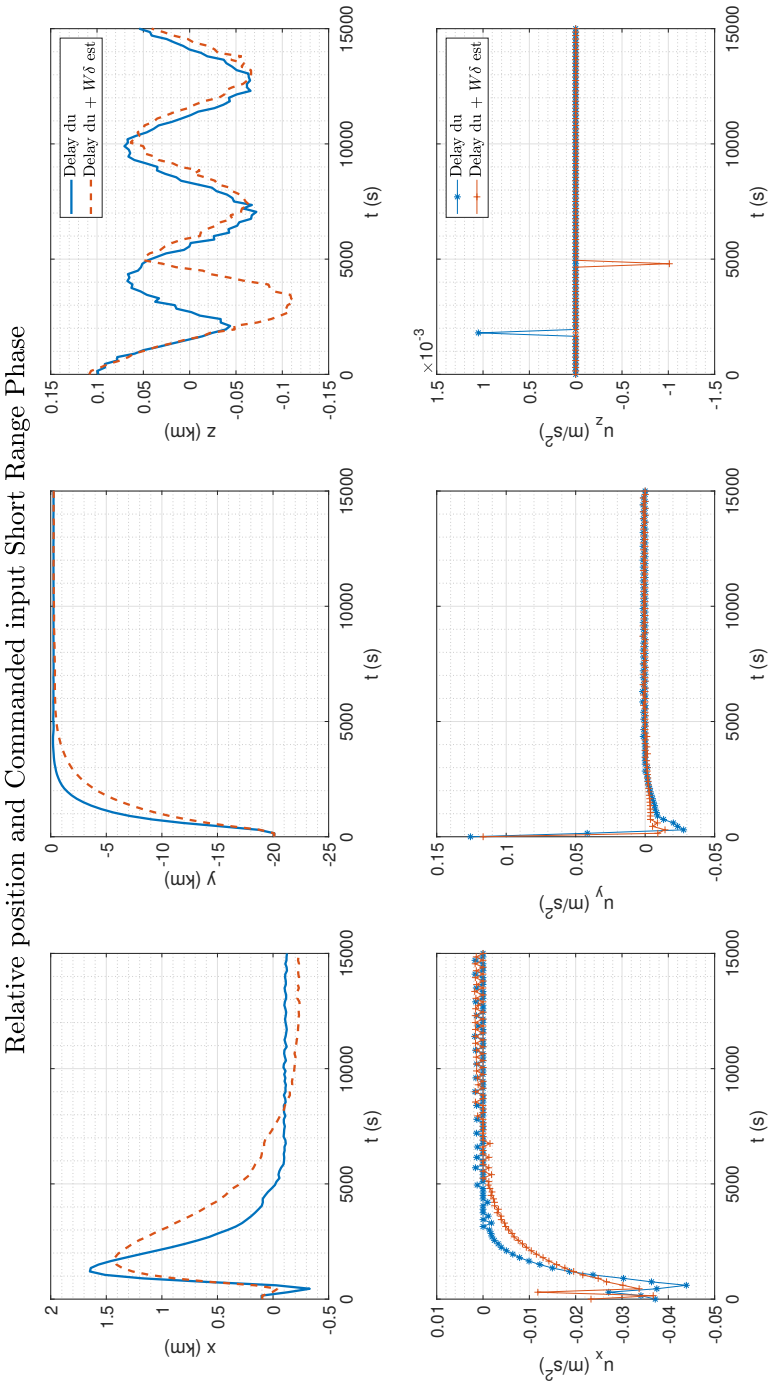

Figure 6-36: Orbital Plane trajectory of Δu delayed YA LMPC vs Δu delayed YA LMPC with disturbance estimators for Short range

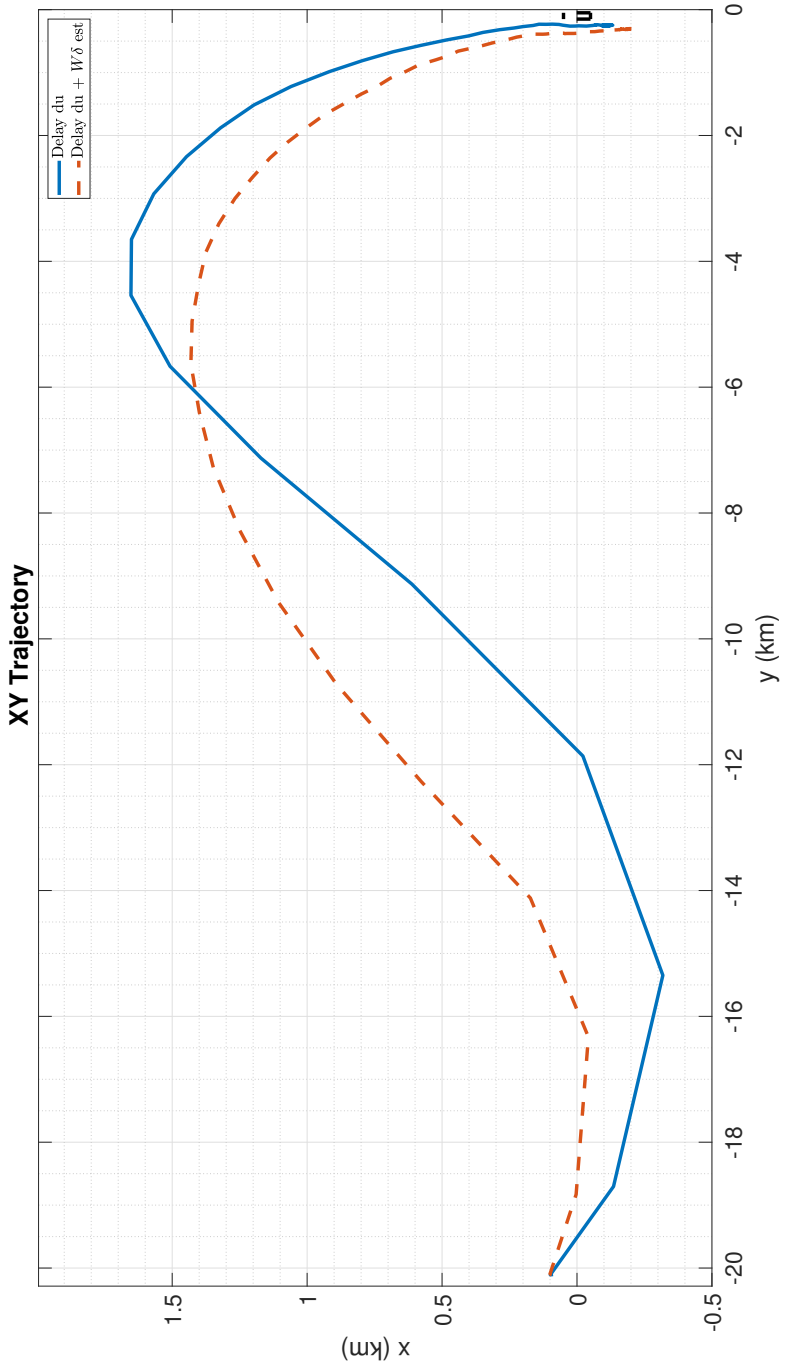

Figure 6-37: Orbital Plane trajectory of Δu YA controllers for Short range

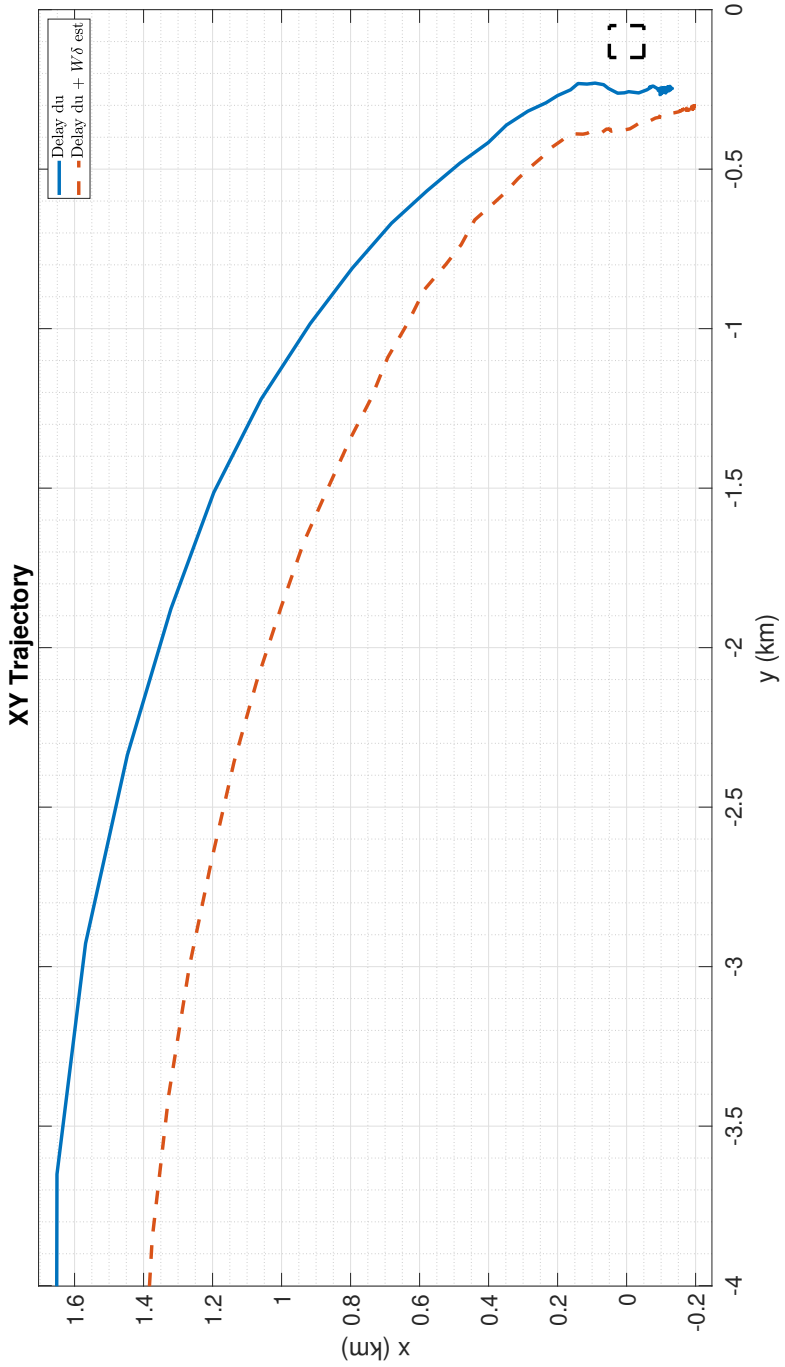

Figure 6-38: Magnified Orbital Plane trajectory of Δu YA controllers for Short range

Incremental Input Delayed LMPC with disturbance estimators

Finally, in Figure 6-36 the trajectory and commanded input of the incremental input delayed LMPC vs incremental input delayed LMPC with the W matrix disturbance estimator presented in Subsection 5-2-3 are presented. The same W matrix was used as for the delayed controllers. In Figures 6-37 and 6-38 the orbital plane trajectory of the controllers is presented. The classical disturbance estimator was not included as it was not able to control the satellite and keep it close to the holding point. The disturbance estimator can be seen to not improve performance and not satisfy the holding point constraint again. It can be concluded that the YA model is too sensitive for application in this mission phase.

ΔV and Steady state error

As the simulation did not include a time varying mass and modelled thrusters, it is best suited to compare required ΔV in order to not introduce more assumptions. The steady state error was computed as the Root Mean Squared (RMS) error from the 10000 to 15000 seconds in the simulation, with the same reasoning that was done for the HCW controllers.

The required ΔV and RMS errors for each controller are presented in Table 6-10. Even though none of the controllers using the YA model were able to satisfy the mission phase constraints, the results are still presented. The main conclusion that we can draw is not from the numbers, but that the YA prediction model

Table 6-10: Results for YA Short Range controllers

Controller	ΔV $[m/s]$	RMS error x $[m]$	RMS error y $[m]$	RMS error z $[m]$
LMPC	125.27	84.00	96.59	60.02
delayed LMPC	121.91	142.95	131.81	35.46
delayed LMPC + δ est	84.45	120.24	654.68	14.06
delayed LMPC + W δ est	122.13	166.81	121.99	47.92
Δu delayed LMPC	113.46	133.50	158.09	60.31
Δu delayed LMPC + W δ est	101.18	209.44	188.30	64.48

6-3-3 Xu-Wang LMPC controllers

In this subsection, the results of the Xu-Wang based LMPC formulations will be presented for the short range phase. It is to be noted that with the use of the Xu-Wang prediction model, using a sampling time of 200 seconds and a prediction horizon of, N_p, 29 was possible for the delayed controllers, but to have a fair comparison a smaller sampling period of 150 seconds combined with a prediction horizon of $N_p = 38$ was used just as for the HCW intermediate range controllers. The cost matrices Q and R used for the simulations are presented in Table 6-11.

Normal vs Delayed LMPC

Firstly, the trajectory and commanded input of the normal LMPC vs the delayed LMPC are presented in Figure 6-39. The trajectory in the orbital plane is presented in Figures 6-40 and

Table 6-11: Cost matrices for Xu-Wang Short Range Controllers

Controller	Q_x	$Q_{\dot{x}}$	R_u or $R_{\Delta u}$
LMPC	1×10^0	1×10^4	15000
delayed LMPC	1×10^0	1×10^5	15000
delayed LMPC + δ est	1×10^0	1×10^5	15000
delayed LMPC + W δ est	1×10^0	1×10^5	15000
Δu delayed LMPC	1×10^0	1×10^5	15000
Δu delayed LMPC + δ est	1×10^0	1×10^5	15000
Δu delayed LMPC + W δ est	1×10^0	1×10^5	15000

6-41.

It can be seen from the figures that the delayed controller is only slightly slower, and unlike the HCW model the delayed controller is still able to satisfy the holding point constraint. It is also to be noted though that the delayed controller takes a much more direct trajectory to the holding point.

Delayed LMPC with disturbance estimators

Next, in Figure 6-39 the trajectory and commanded input of the delayed LMPC vs the delayed LMPC with the two disturbance estimators presented in Subsection 5-1-3 are presented. Their trajectory in the orbital plane is shown in Figures 6-43 and 6-44. The W of the disturbance estimator presented in (5-5) was set to:

$$W = 1 \times 10^{-3} * \mathrm{I}_{nx} \tag{6-11}$$

From the figures, it becomes evident that the classical disturbance estimator presented in (5-4) is able to increase the speed of the delayed controller at the expense of a larger deviation in the radial direction X. The W matrix disturbance estimator does not seem to provide many benefits and prevents the controller from satisfying the holding point constraint. The classical disturbance estimator is however able to follow a more direct trajectory that does not overshoot the holding point and also satisfy the terminal constraint.

Incremental Input Delayed LMPC with disturbance estimators

Finally, in Figure 6-45 the trajectory and commanded input of the incremental input delayed LMPC vs incremental input delayed LMPC with the two disturbance estimators presented in Subsection 5-1-3 are presented. The same W matrix was used as for the delayed controllers. In Figures 6-46 and 6-47 the orbital plane trajectory of the controllers is presented. Firstly, it is clear from the figures that the incremental input cost function by itself prevents the controller from satisfying the holding point constraint. The disturbance estimators can then be seen to have the same effect as for the normal delayed case, and it can be seen that the combination of the incremental input cost function combined with the classical disturbance estimator is able to have the smallest steady state offset and satisfy the terminal constraint.

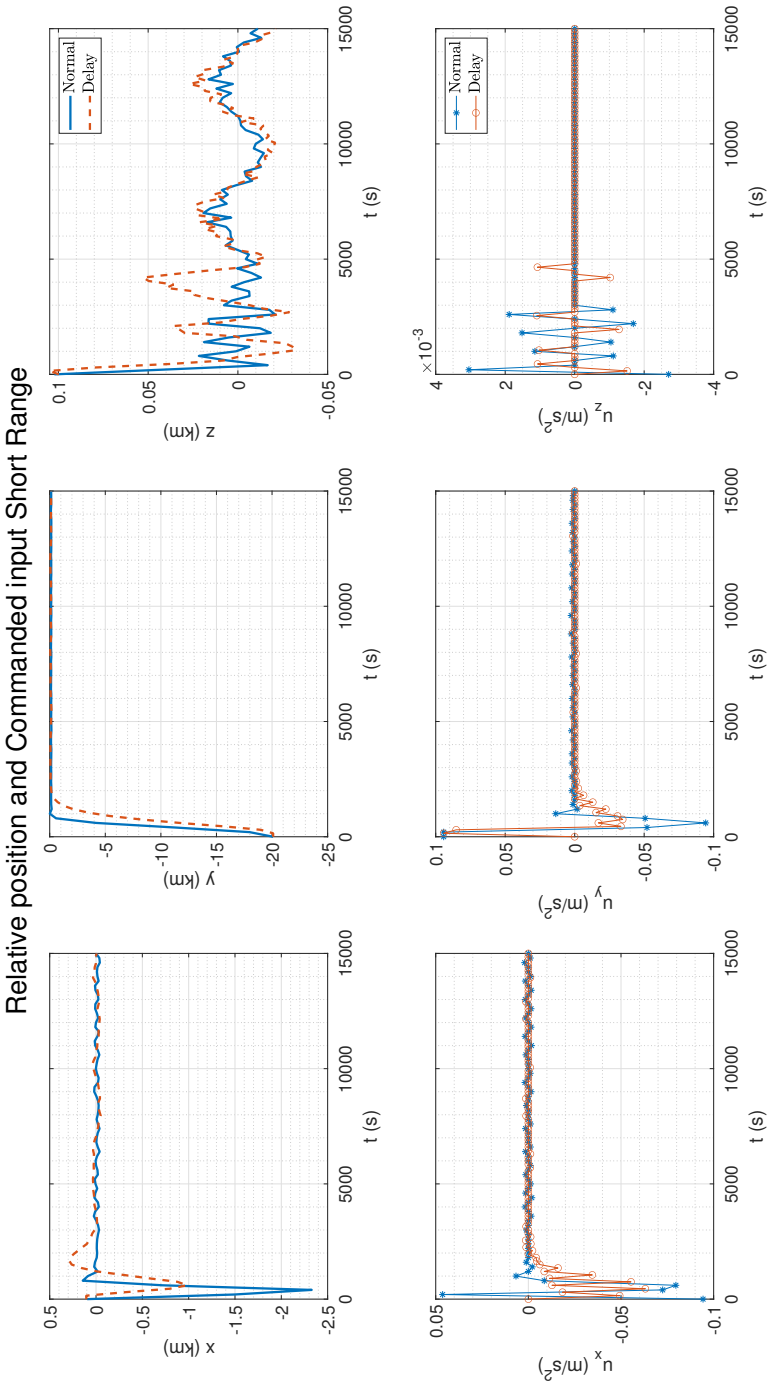

Figure 6-39: Response of Xu-Wang LMPC and delayed Xu-Wang LMPC for Short range

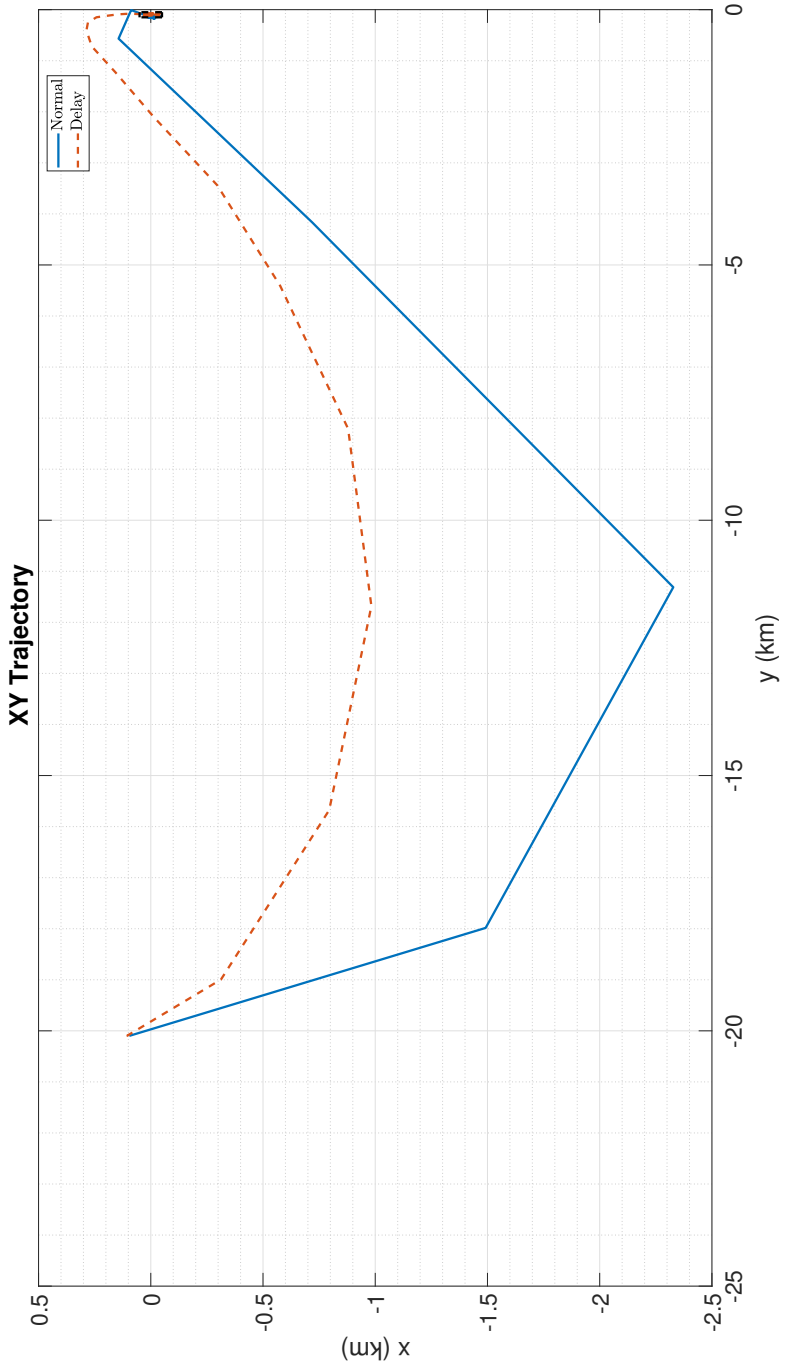

Figure 6-40: Orbital Plane trajectory of Xu-Wang LMPC and delayed LMPC for Short range

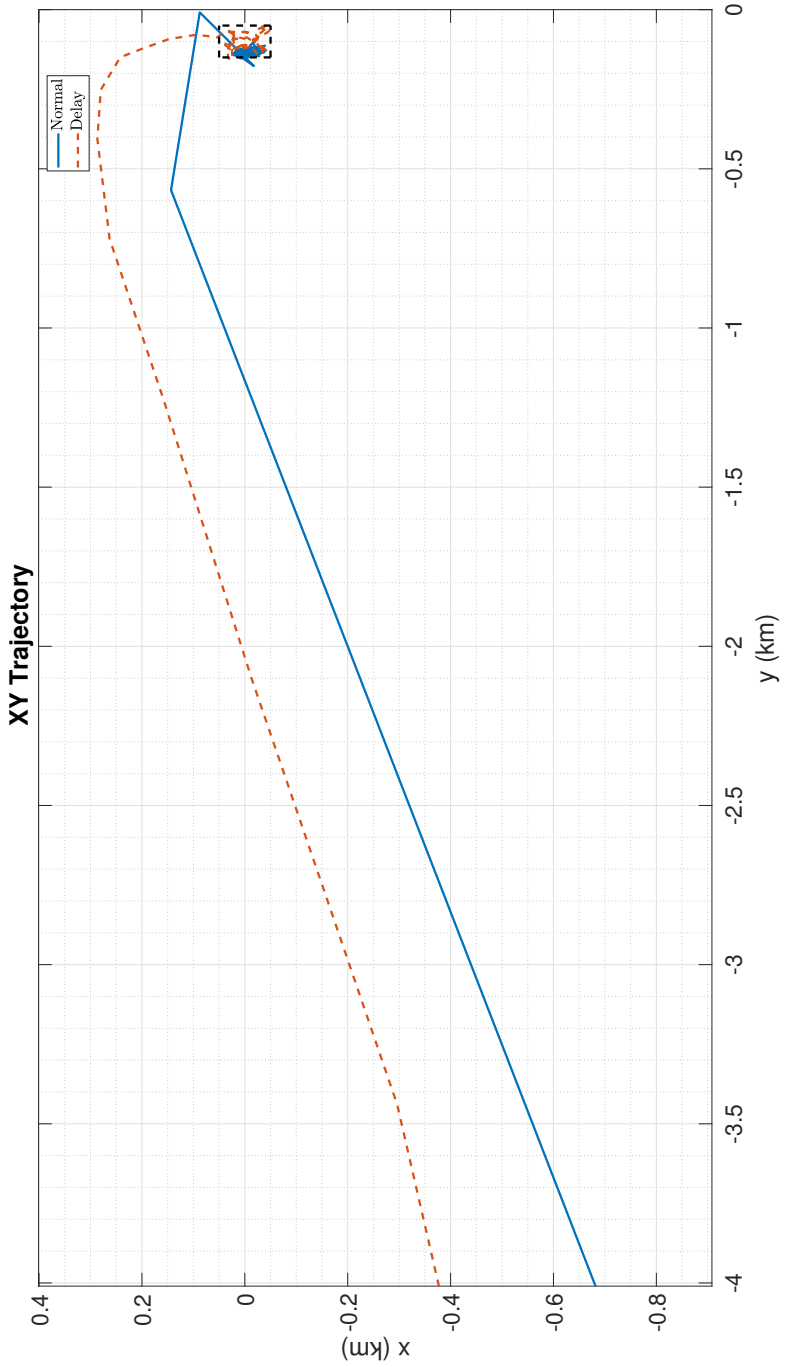

Figure 6-41: Magnified Orbital Plane trajectory of Xu-Wang LMPC and delayed LMPC for Short range

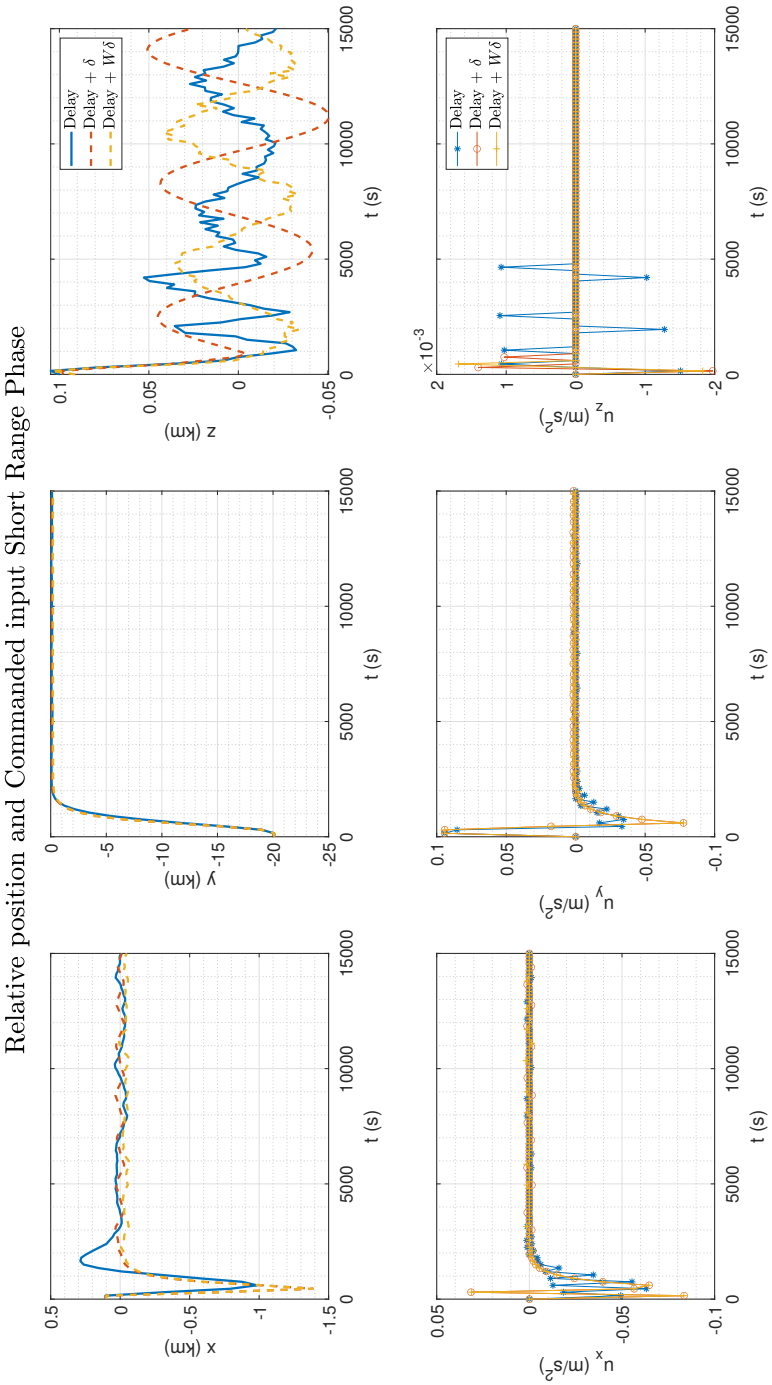

Figure 6-42: Response of delayed Xu-Wang LMPC vs delayed LMPC with disturbance estimators for Short range

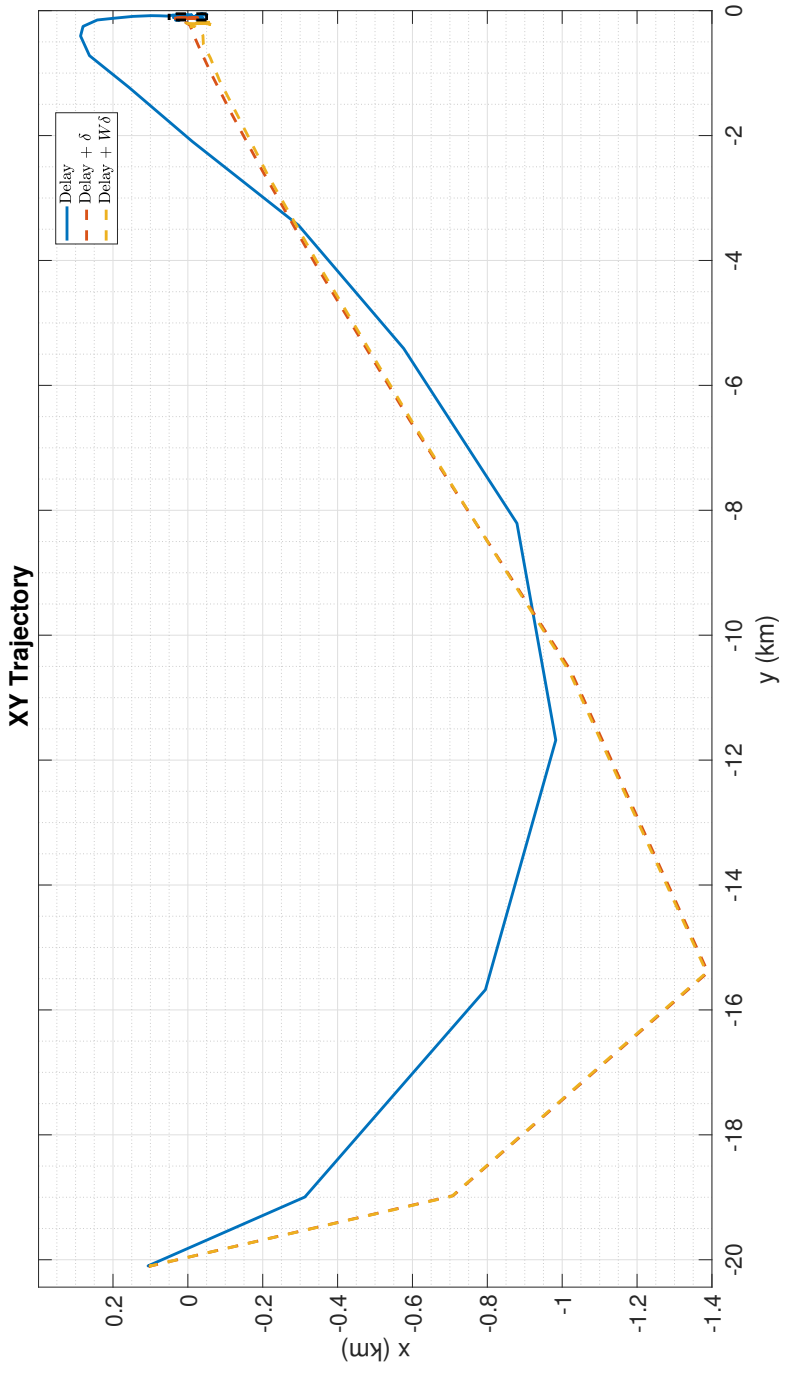

Figure 6-43: Orbital Plane trajectory of delayed Xu-Wang LMPC vs delayed LMPC with disturbance estimators for Short range

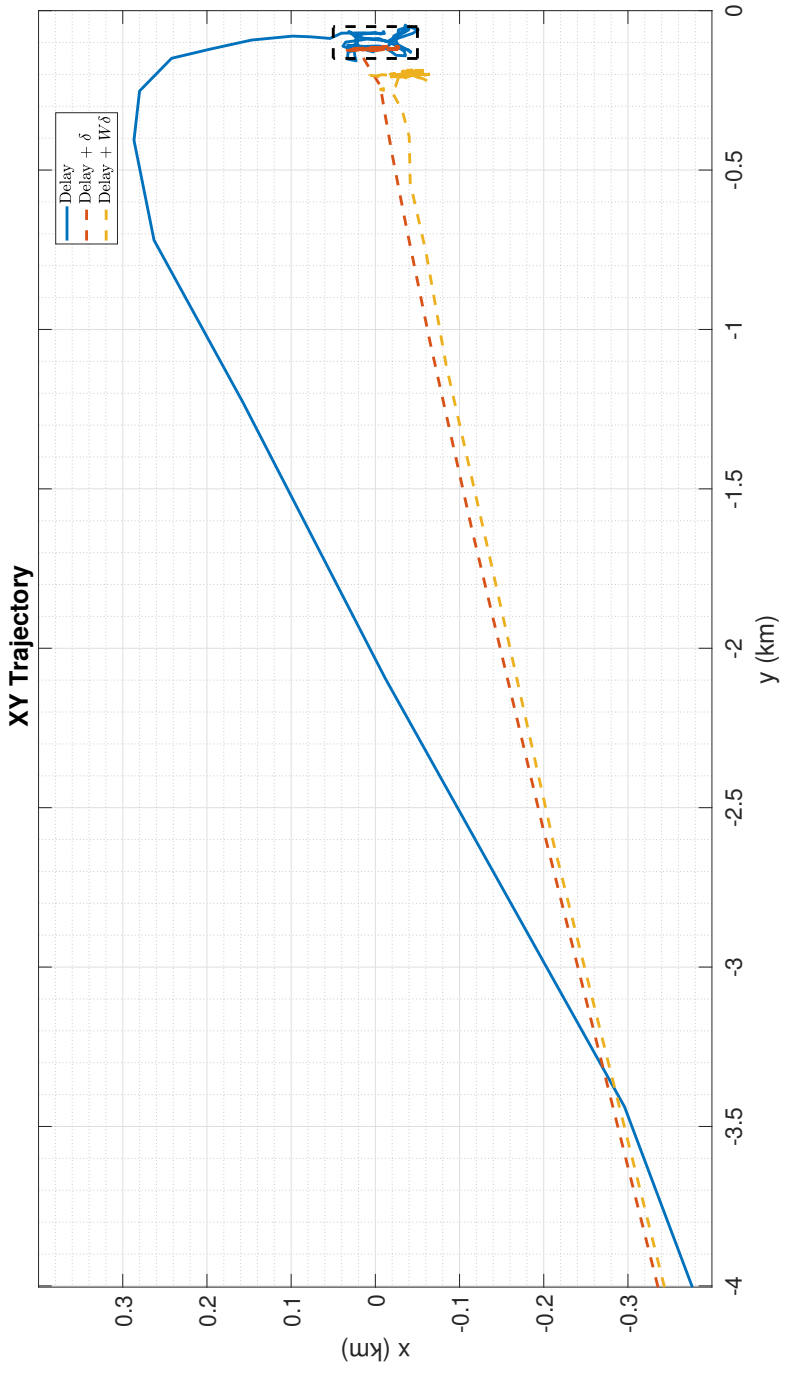

Figure 6-44: Magnified Orbital Plane trajectory of delayed Xu-Wang LMPC vs delayed LMPC with disturbance estimators for Short range

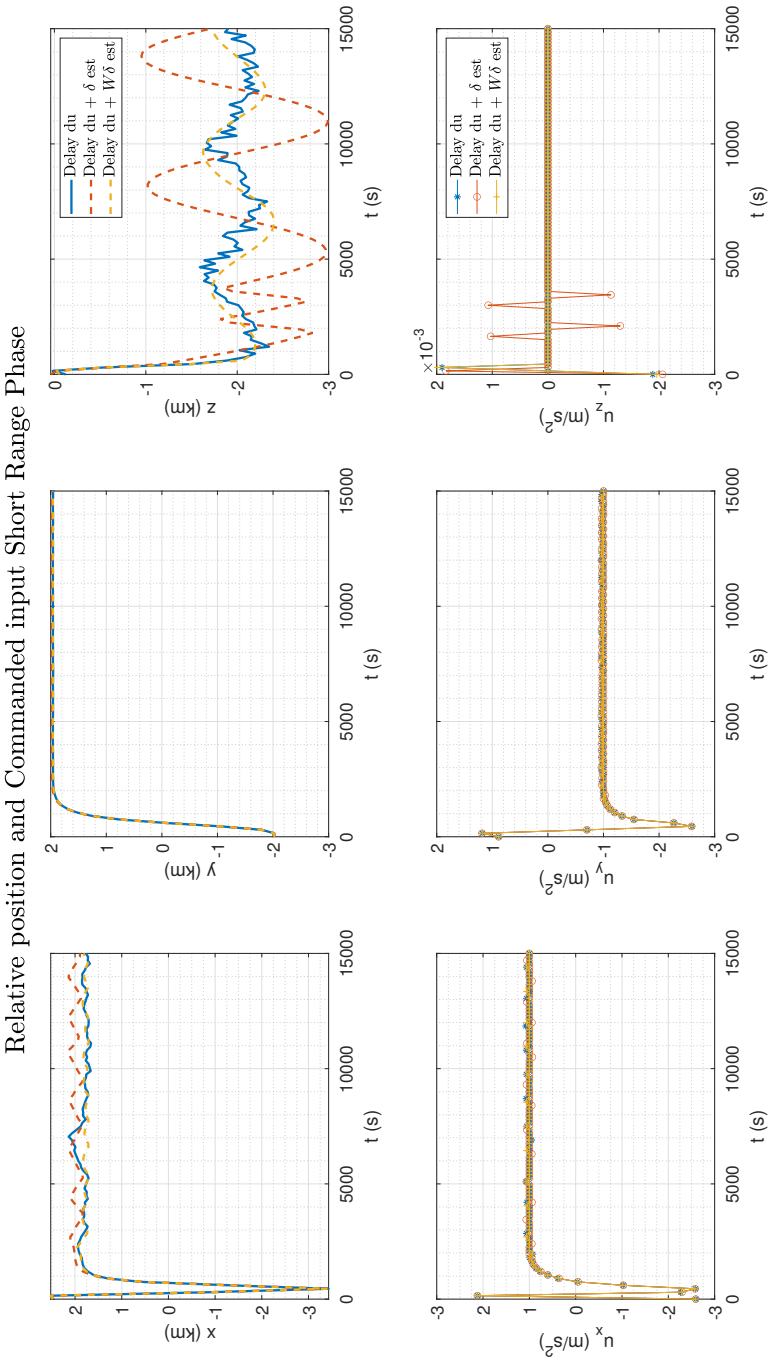

Figure 6-45: Response of delayed of Δu delayed Xu-Wang LMPC vs Δu delayed Xu-Wang LMPC with disturbance estimators for Short range

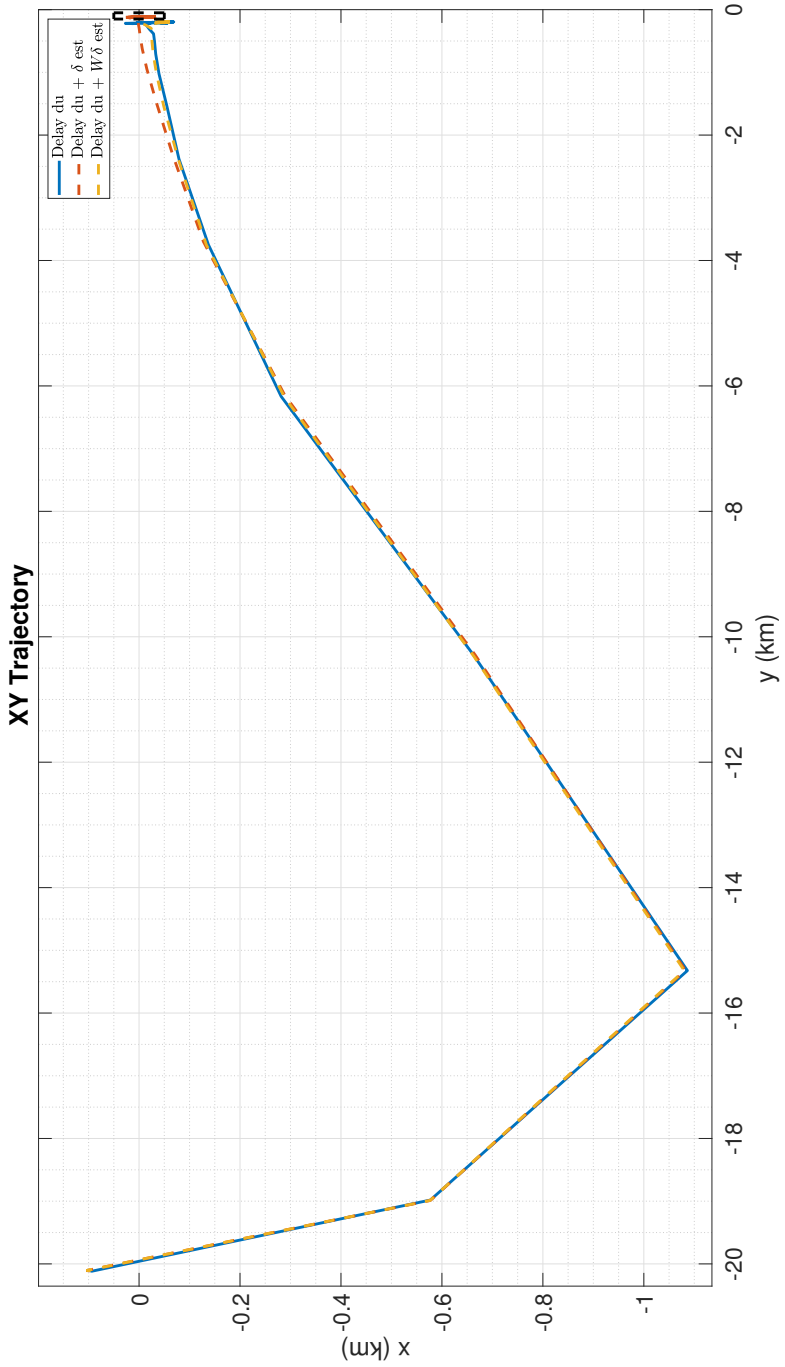

Figure 6-46: Orbital Plane trajectory of Δu XU LMPC and Δu delayed XU LMPC for Short range

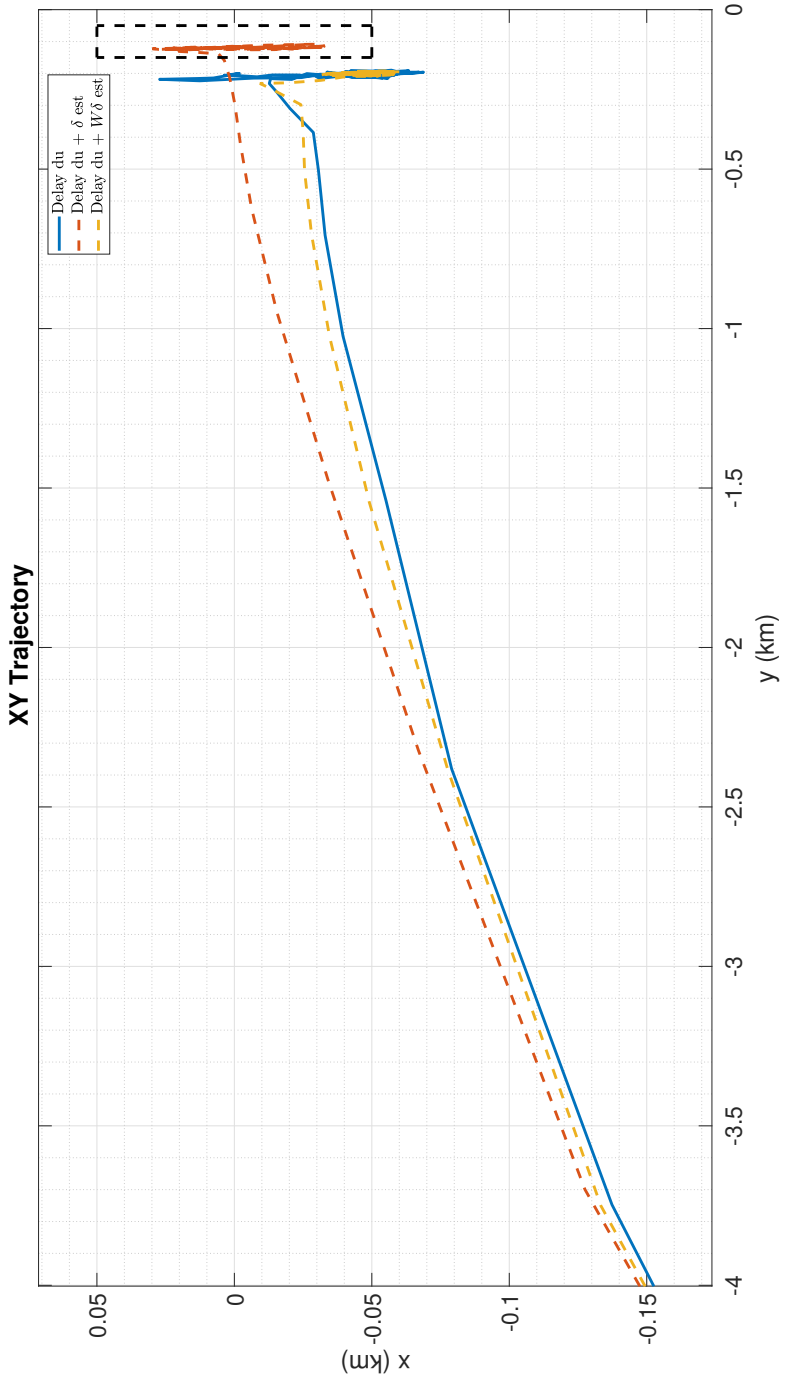

Figure 6-47: Magnified Orbital Plane trajectory of Δu XU LMPC and Δu delayed XU LMPC for Short range

ΔV and Steady state error

As the simulation did not include a time varying mass and modelled thrusters, it is best suited to compare required ΔV in order to not introduce more assumptions. The steady state error was computed as the Root Mean Squared (RMS) error from the 10000 two 15000 seconds in the simulation, with the same reasoning that was done for the HCW and YA controllers. From the figures, it becomes evident that by 10000 seconds the chaser has arrived at a stationary holding position. Measuring the RMS from that point gives an indication of the steady state error after the chaser has settled and awaits to begin the second mission phase.

The required ΔV and RMS errors for each controller are presented in Table 6-12. It is clear from the table that the delayed LMPC reduces performance in terms of error regardless of its smaller sampling time, although ΔV required by the delayed controller is significantly less. This is likely explained by the non-delayed controller having a lower cost on the relative velocity components. Furthermore, it can be seen that the classical disturbance estimator does not provide a significance performance benefit both in terms of ΔV and steady state error as for the first mission phase. The W matrix disturbance estimator presented in [22] degrades performance for the delayed controller and for the incremental input delayed controllers. Lastly, it is to be noted that while the incremental input cost function does not provide any improvement to the classical one. However, the combination of the incremental input cost function with the classical disturbance estimator is able to provide performance improvement in terms of steady state error even with respect to the non-delayed quadratic cost function LMPC.

Table 6-12: Results for Xu-Wang Intermediate Range controllers

Controller	ΔV $[m/s]$	RMS error x $[m]$	RMS error y $[m]$	RMS error z $[m]$
LMPC	162.62	14.50	26.30	6.94
delayed LMPC	101.72	21.39	19.56	10.40
delayed LMPC + δ est	122.63	11.53	14.67	25.25
delayed LMPC + W δ est	121.77	31.59	75.51	18.87
Δu delayed LMPC	123.86	37.45	79.98	5.89
Δu delayed LMPC + δ est	125.27	12.69	14.87	25.33
Δu delayed LMPC + W δ est	123.95	36.23	77.42	8.80

6-3-4 Conclusion

In this section, we will compare the best controllers for each of the tree prediction models. The best performing controllers are presented in Table 6-13. The YA controllers are left out, as by not being able to satisfy the holding point constraint, they are not feasible controllers. This is likely due to the YA STM being computed based on the assumption that the chaser satellite is flying in free motion, and that the external forces on chaser and target satellite are identical, which is not so under control. x It is clear from the table that the inclusion of a disturbance estimator has clear benefits in terms of ΔV and RMS for the short range phase too. The usage of a more accurate prediction model does also not guarantee a decrease in ΔV or steady state error. The HCW controller provided the best performance in terms ΔV but at the expense of steady state error compared to the Xu-Wang controller. The Xu-Wang

model provided the best performance in terms of steady state error, which is to be expected as the simulation is based on its non-linear counterpart, however it did not provide better ΔV performance than the HCW controllers. This is likely due to the controller compensating for disturbances included in the model to achieve this better steady state error, which can be seen in Figures 6-79 and 6-80 with the trajectory of the Xu-Wang controller being more direct. Overall, the HCW controllers provide the best compromise in performance between ΔV and steady state error. Considering that the Xu-Wang model requires the integration of the RSV's at every computation being LTV systems, the HCW model provides better performance for no computational expense. Furthermore, it is also evident that constraint tightening through robust methods by itself did not guarantee constraint satisfaction but through the modelling of the disturbance in the prediction model performance was improved and the holding point was satisfied.

Table 6-13: Results for the Intermediate Range controllers

Controller	ΔV $[m/s]$	RMS error x $[m]$	RMS error y $[m]$	RMS error z $[m]$
HCW Δu delayed LMPC + δ est	98.20	26.74	19.89	24.11
XU delayed LMPC + δ est	122.63	11.53	14.67	25.25

The compared responses and trajectories of the three controllers are presented in Figures 6-78, 6-79 and 6-80

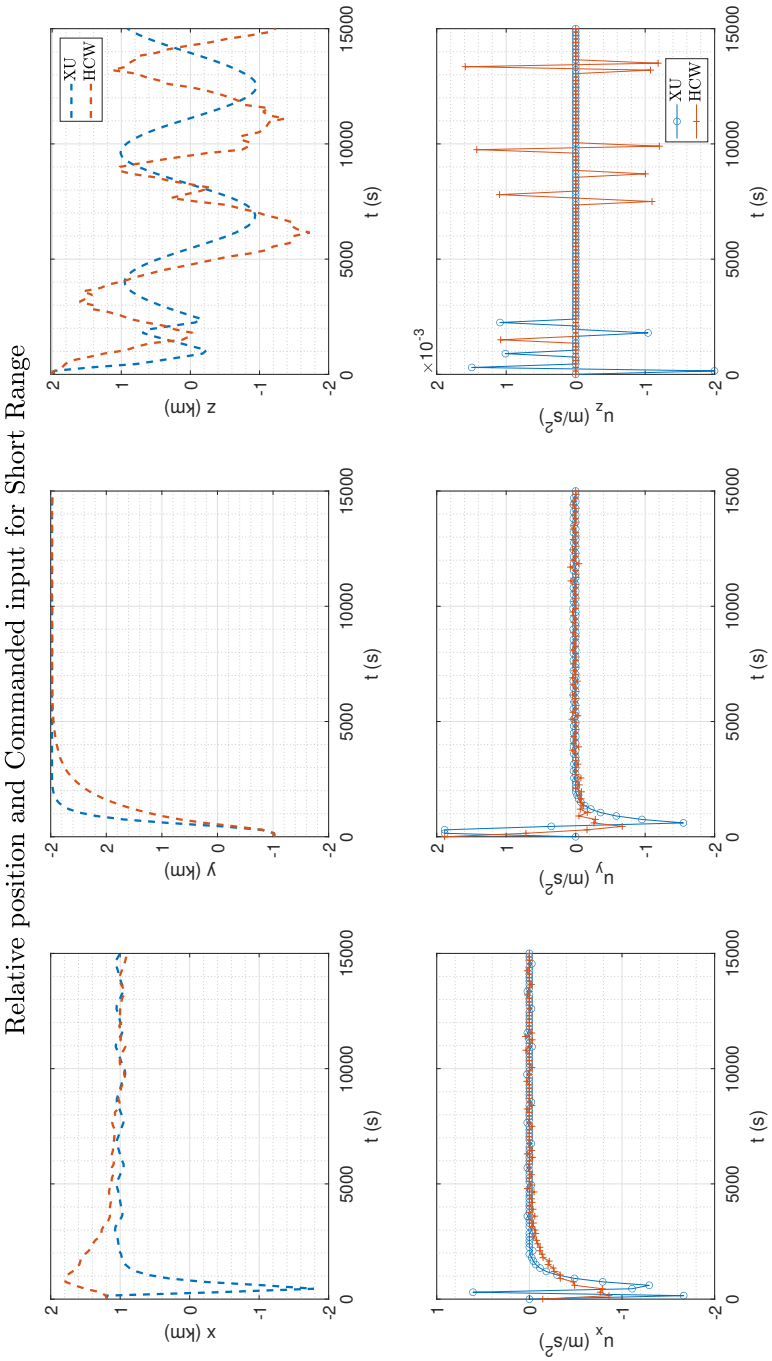

Figure 6-48: Response of best performing Short Range HCW and Xu-Wang controllers

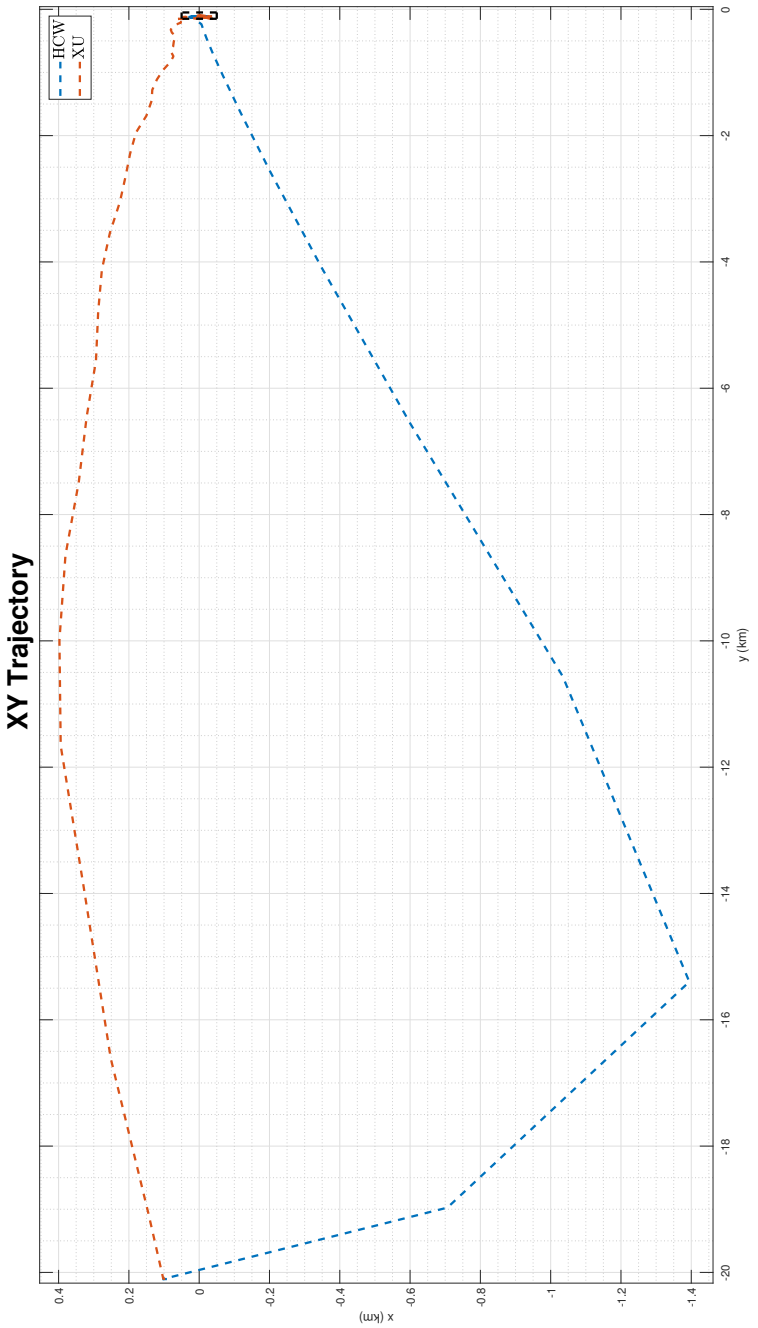

Figure 6-49: Orbital Plane trajectory best performing Short Range HCW and Xu-Wang controllers

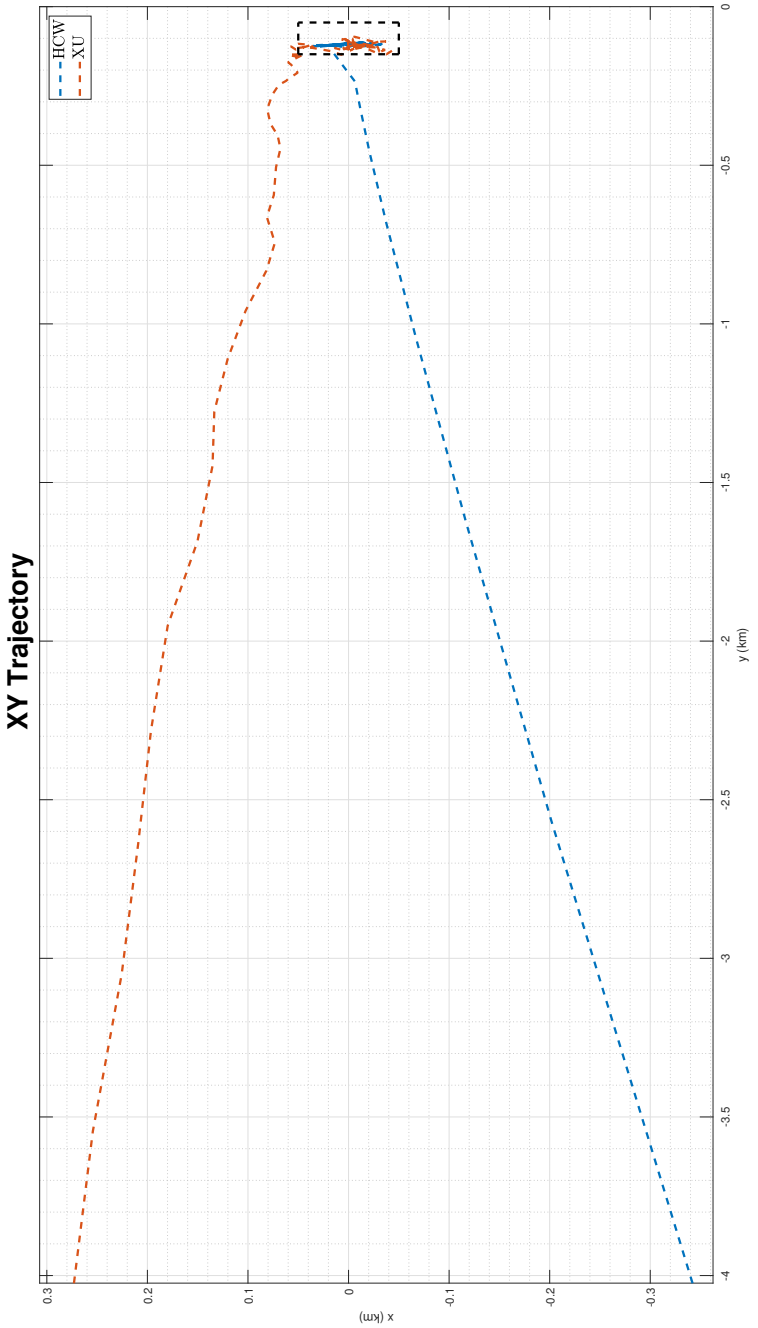

Figure 6-50: Magnified Orbital Plane trajectory best performing Short Range HCW and Xu-Wang controllers

6-4 Terminal to Capture Phase

In this Section the results of the controllers for the Short range phase presented in Section 5-3 will be presented.

The initial conditions for this phase are presented below, with a slight offset in each axis to represent the RMS error of the controllers in the first phase.

$$x(0) = \begin{bmatrix} 15 & -115 & 20 & 0 & 0 & 0 \end{bmatrix}^\mathsf{T} \tag{6-12}$$

Due to the shorter nature of this mission phase, sampling time and prediction horizon were chosen to account for the satellite to reach the target. This resulted in a sampling time of 3 seconds and a prediction horizon of, N_p, 25 steps. The simulation shown is for a target satellite rotating at 1 deg/s around the Z axis of the LVLH frame.

The state vector is enlarged for this mission phase to include the docking port location and the relative distance to the docking port, as explained in Section 5-3. The resulting state vector is:

$$\vec{x}(k) = \begin{bmatrix} x(k) & y(k) & z(k) & v_x(k) & v_y(k) & v_z(k) & r_x(k) & r_y(k) & r_z(k) & \dots \\ \sigma_x(k) & \sigma_y(k) & \sigma_z(k) & & & & & & & \end{bmatrix}^\mathsf{T} \tag{6-13}$$

6-4-1 HCW LMPC controllers

In this subsection, the results of the HCW based LMPC formulations will be presented. The cost matrices Q and R used for the simulations are presented in Table 6-14

Table 6-14: Cost matrices for HCW Terminal to Capture Controllers

Controller	Q_x	$Q_{\dot{x}}$	Q_r	Q_σ	R_u or $R_{\Delta u}$
LMPC	0	1×10^2	0	1×10^1	500
delayed LMPC	0	1×10^2	0	1×10^1	500
delayed LMPC + δ est	0	1×10^0	0	1×10^0	500
delayed LMPC + W δ est	0	1×10^2	0	1×10^1	500
Δu delayed LMPC	0	1×10^1	0	1×10^0	500
Δu delayed LMPC + δ est	0	1×10^1	0	1×10^0	500
Δu delayed LMPC + W δ est	0	1×10^1	0	1×10^0	500

Normal vs Delayed LMPC

Firstly, the trajectory and commanded input of the normal LMPC vs the delayed LMPC are presented in Figure 6-51. The trajectory in the orbital plane is presented in 6-52 and 6-53.

It can be seen from the figures that the delayed controller is slightly slower. Furthermore, it is clear that the delayed controller requires longer to accomplish docking. Although it follows a similar trajectory to the normal controller, the delayed controller follows the docking port for a few samples before making contact. From the approach, it is also visible how the chaser makes sure to stay within the LOS constraints.

Delayed LMPC with disturbance estimators

Next, in Figure 6-54 the trajectory and commanded input of the delayed LMPC vs the delayed LMPC with the two disturbance estimators presented in Subsection 5-3-3 are presented. Their trajectory in the orbital plane is shown in Figure 6-55 and 6-56.

The W of the disturbance estimator presented in (5-5) was set to:

$$W = 1 \times 10^{-5} * \mathrm{I}_{nx} \tag{6-14}$$

From the figures, it becomes evident that the classical disturbance estimator presented in (5-4) results in a more damped approach and directly approaches the docking port without any loop. The W matrix disturbance estimator on the other hand maintains a similar approach, but creates slightly more overshoot. Both disturbance estimators increase the completion time of the docking manoeuvre.

Incremental Input Delayed LMPC with disturbance estimators

Finally, in Figure 6-57 the trajectory and commanded input of the incremental input delayed LMPC vs incremental input delayed LMPC with the two disturbance estimators presented in Subsection 5-3-3 are presented. The same W matrix was used as for the delayed controllers. In Figure 6-28 and 6-59 the orbital plane trajectory of the controllers is presented. The disturbance estimators can be seen to have the same effect as for the normal delayed case in terms of trajectory and completion time. The ΔV performance will be evaluated in the next subsection.

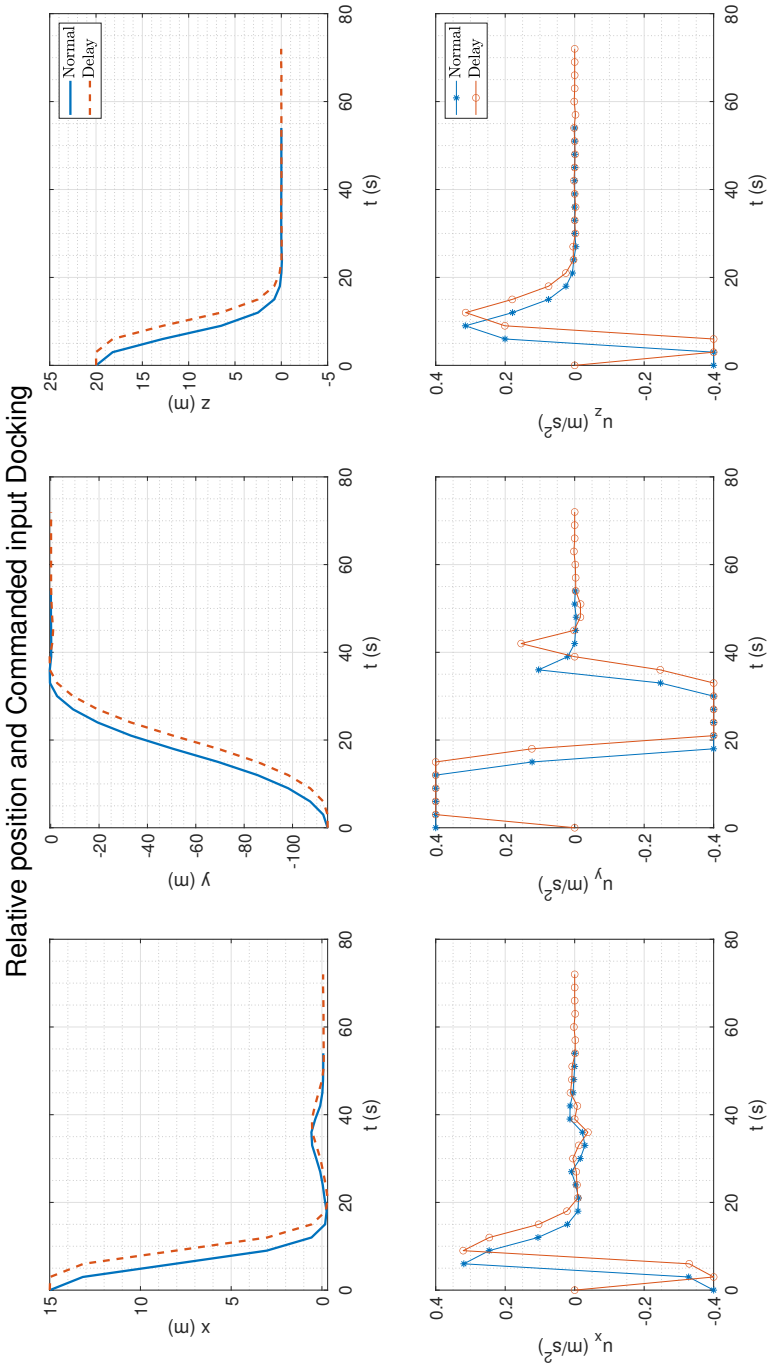

Figure 6-51: Response of HCW LMPC and delayed HCW LMPC for Docking phase

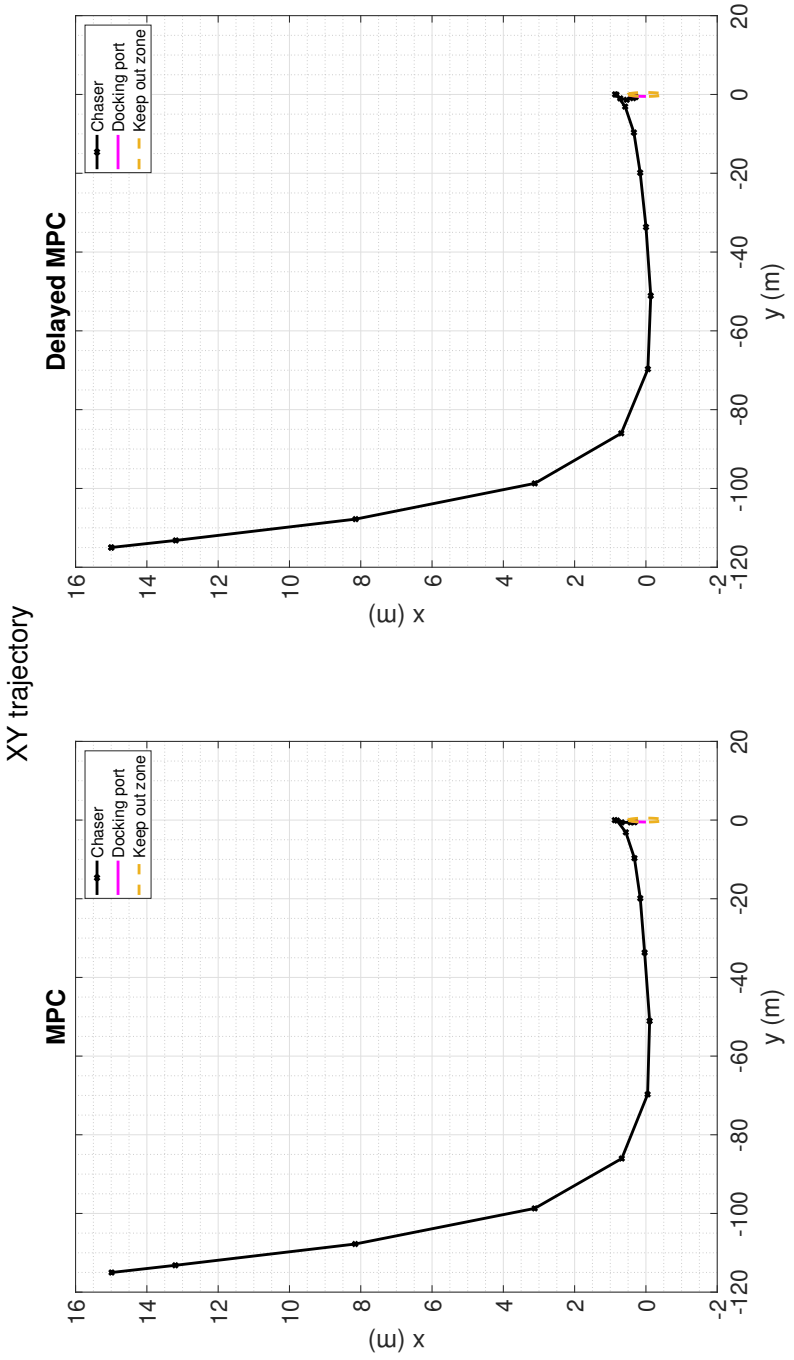

Figure 6-52: Orbital Plane trajectory of HCW LMPC and delayed HCW LMPC for Docking phase

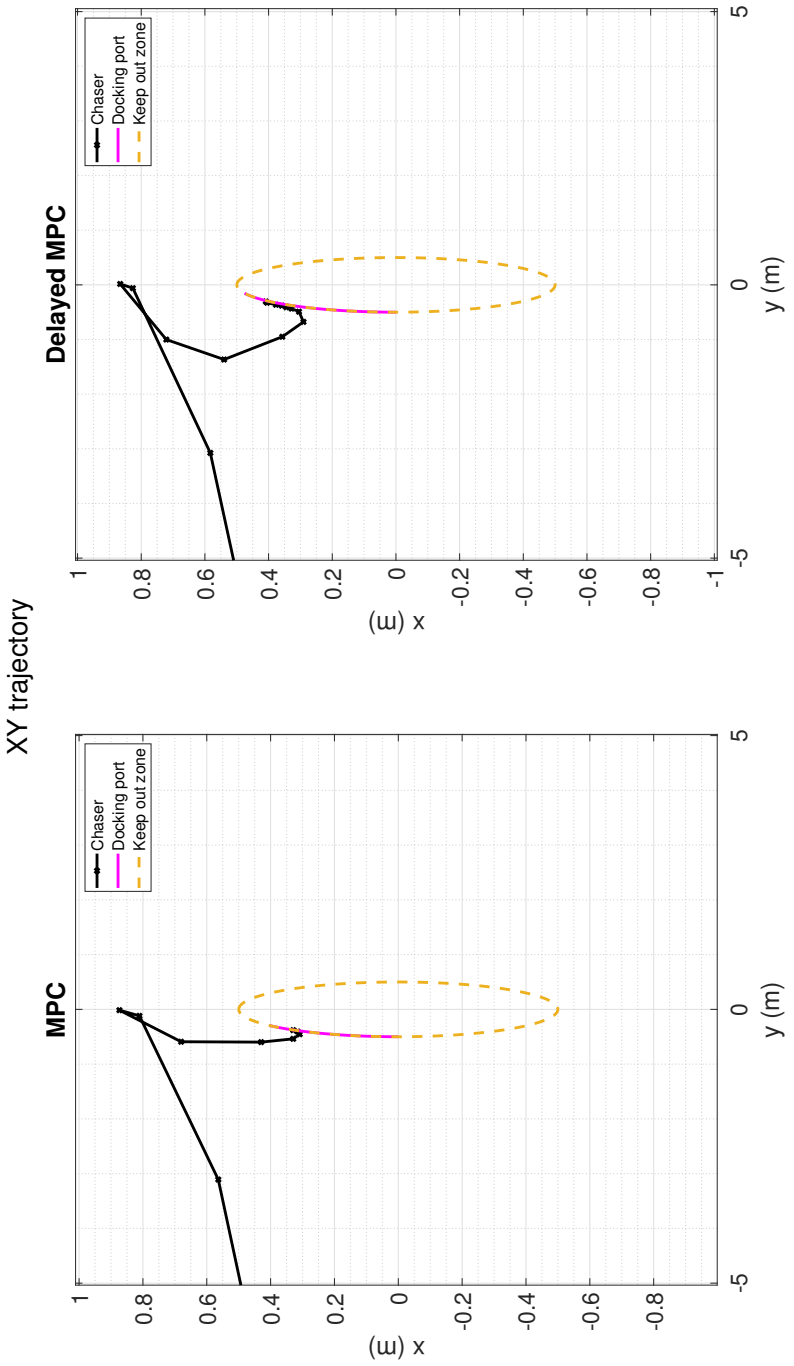

Figure 6-53: Magnified Orbital Plane trajectory of HCW LMPC and delayed HCW LMPC for Docking phase

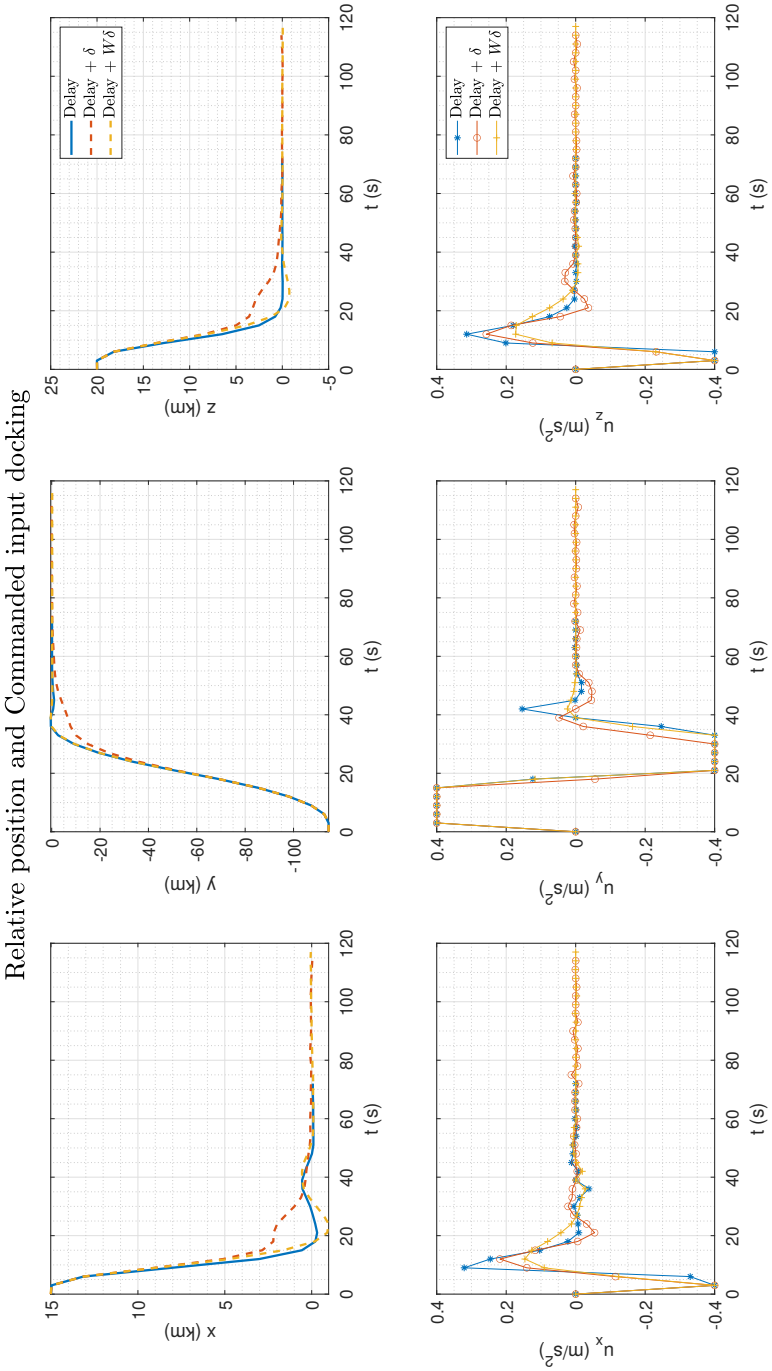

Figure 6-54: Response of delayed HCW LMPC vs delayed HCW LMPC with disturbance estimators for Docking phase

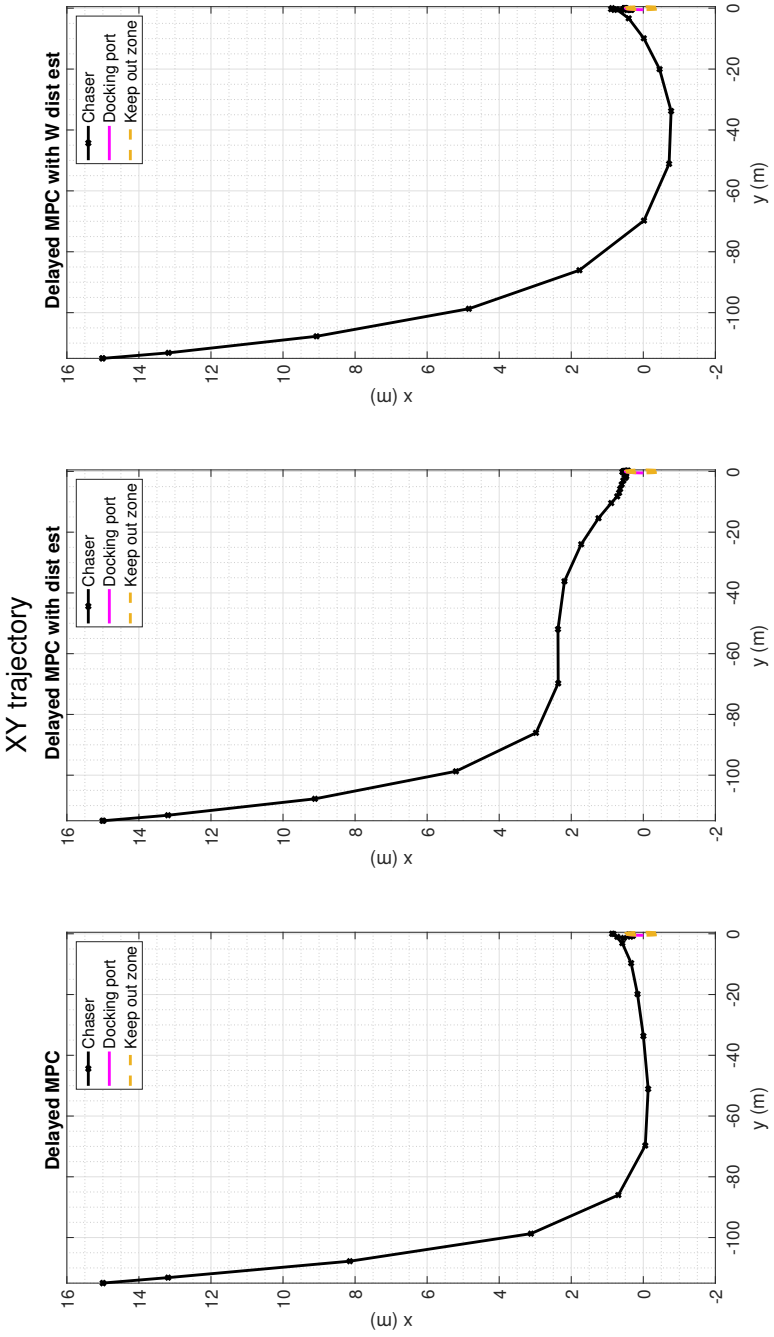

Figure 6-55: Orbital Plane trajectory of delayed HCW LMPC vs delayed HCW LMPC with disturbance estimators for Short range

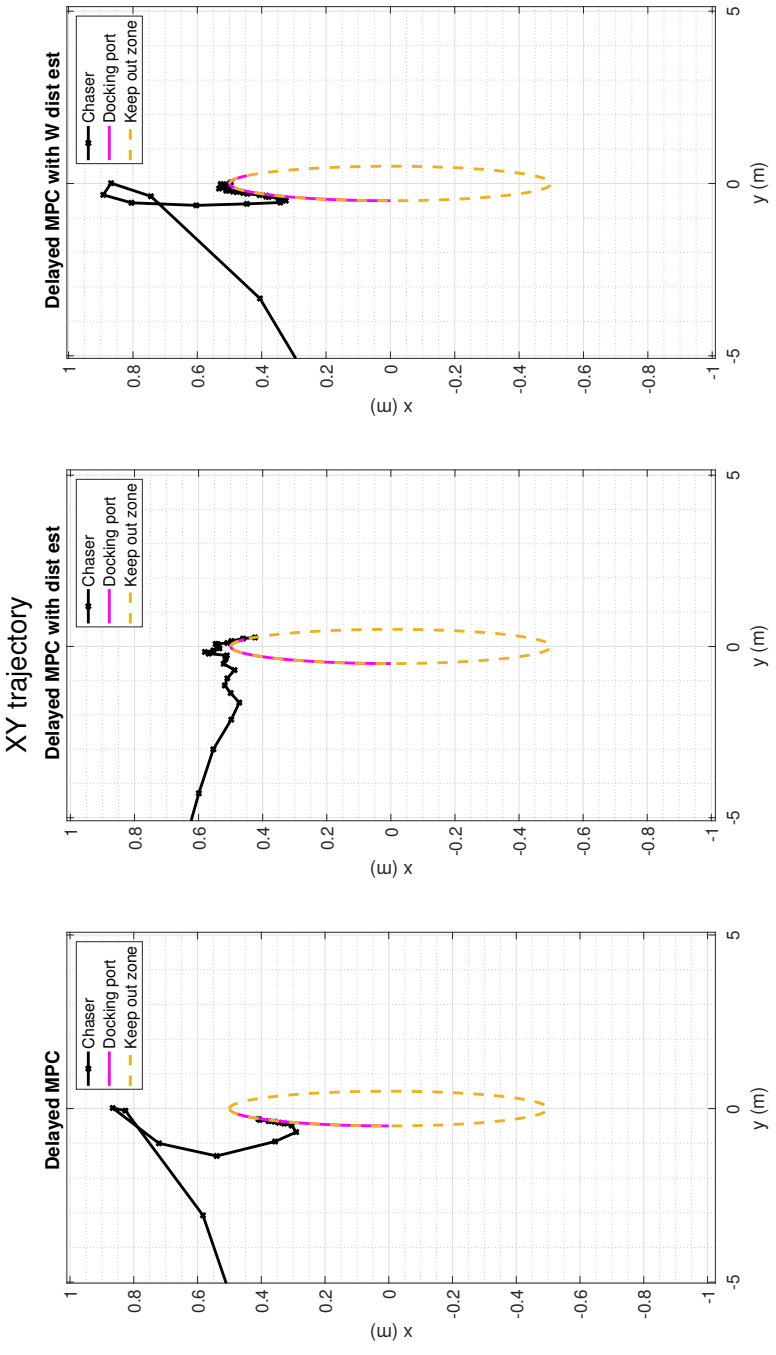

Figure 6-56: Magnified Orbital Plane trajectory of delayed HCW LMPC vs delayed HCW LMPC with disturbance estimators for Docking phase

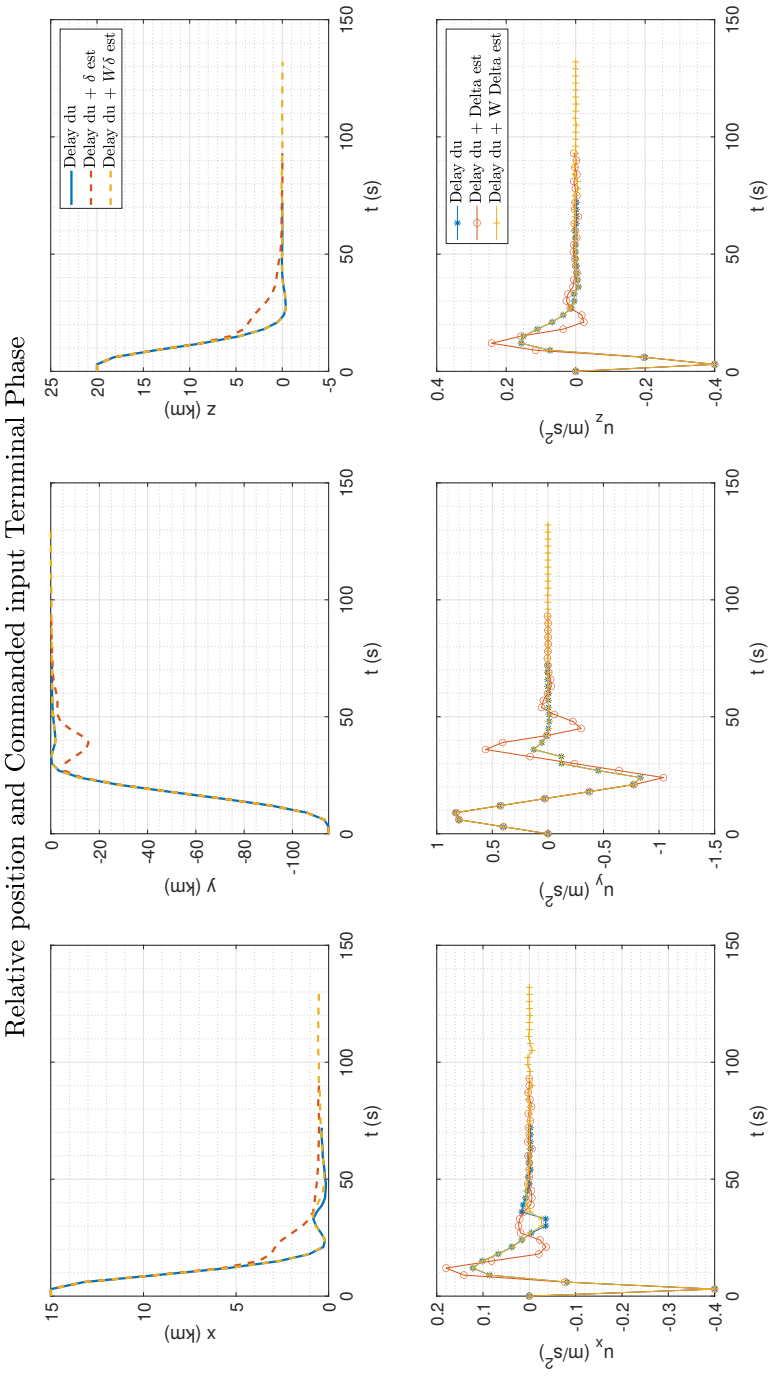

Figure 6-57: Orbital Plane trajectory of Δu delayed HCW LMPC vs Δu delayed HCW LMPC with disturbance estimators for Docking phase

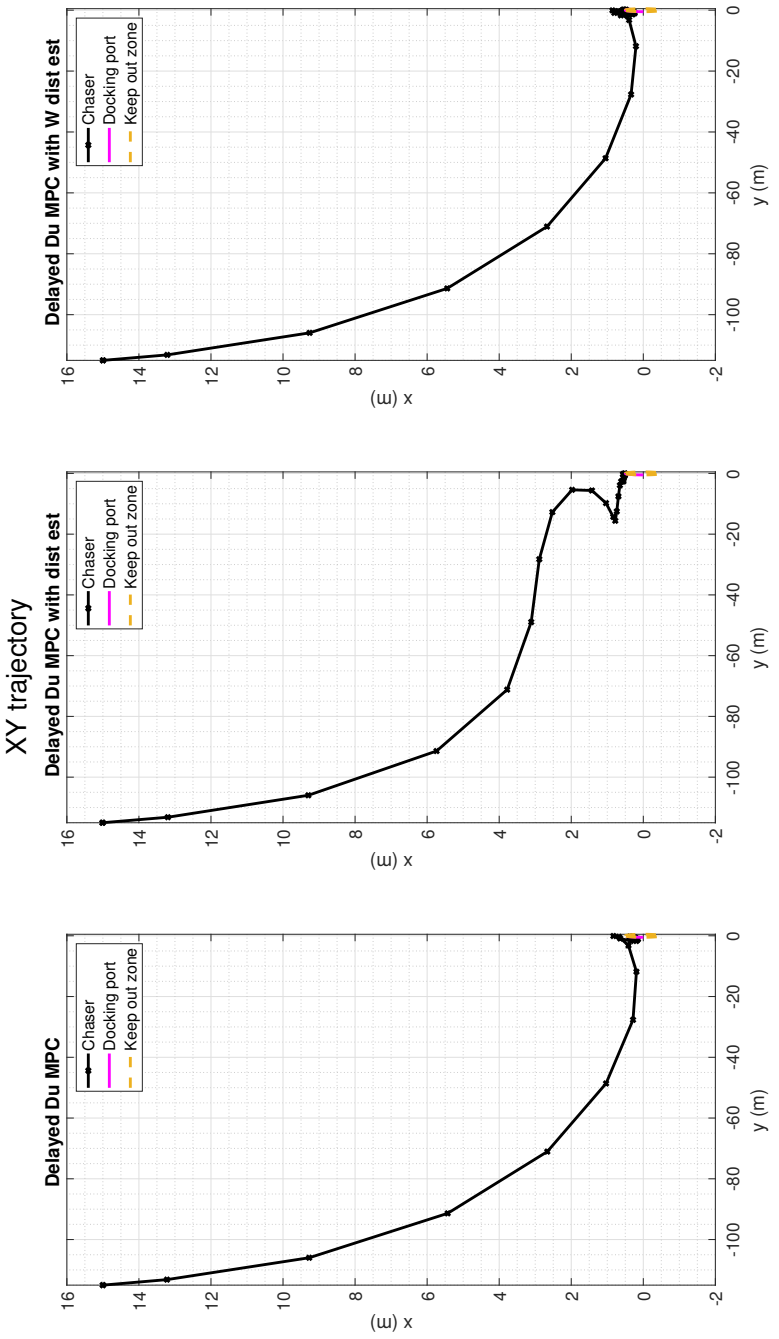

Figure 6-58: Orbital Plane trajectory of Δu HCW controllers, for Docking pahse

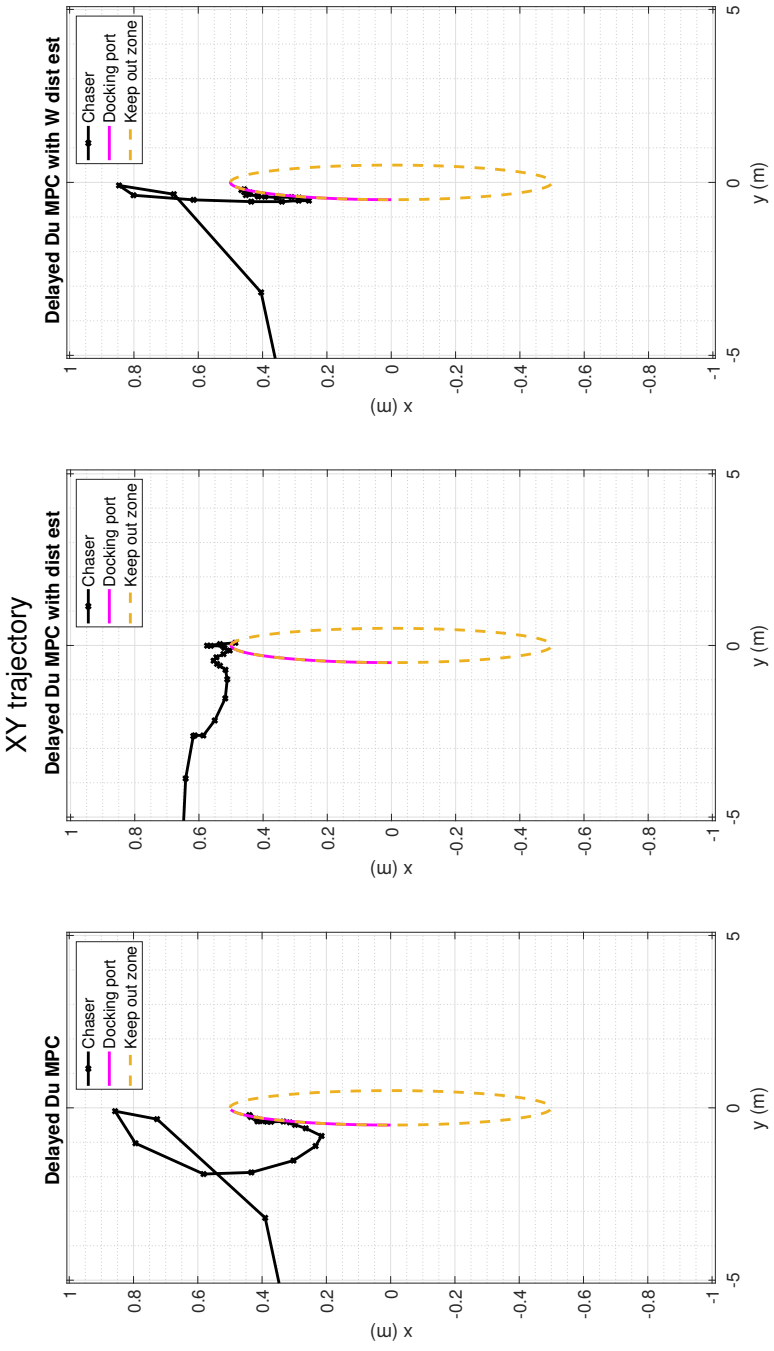

Figure 6-59: Magnified Orbital Plane trajectory of Δu HCW controllers, for Docking phase

ΔV and Steady state error

As the simulation did not include a time varying mass and modelled thrusters, it is best suited to compare required ΔV in order to not introduce more assumptions. Due to the nature of the terminal to capture phase, there is no steady state offset to evaluate. The distance from the centre of the docking port and the point of contact will be evaluated instead.

The required ΔV and docking errors for each controller are presented in Table 6-15. It is clear from the table that the delayed LMPC reduces performance in terms of error and slightly in terms of ΔV. Regardless of the greater error, the delayed controller is able to dock within the 20 by 20 cm docking port. The inclusion of a disturbance estimator to the delayed MPC was able to improve the required ΔV. However, only the classic disturbance estimator seems to improve the docking error, resulting in a smaller docking error than the non-delayed MPC. The W matrix disturbance estimator presented in [22] doesn't offer any benefit compared to the delayed LMPC in terms of docking error and actually increases the docking error. Lastly, it is to be noted that the incremental input cost function is able to decreases the docking error but marginally and it does not provide any benefits in terms of ΔV. Adding disturbance estimators to the incremental input cost function controllers results in worse performance than the delayed controller with disturbance estimators

Table 6-15: Results for HCW Terminal to capture controllers

Controller	ΔV $[m/s]$	Docking error x $[cm]$	Docking error y $[cm]$	Docking error
LMPC	23.01	8.26	7.39	0.55
delayed LMPC	23.14	8.24	16.26	0.40
delayed LMPC + δ est	20.19	0.82	1.44	2.80
delayed LMPC + W δ est	20.40	13.56	13.96	0.35
Δu delayed LMPC	23.05	5.76	15.66	0.66
Δu delayed LMPC + δ est	29.55	0.33	5.16	1.06
Δu delayed LMPC + W δ est	21.99	4.21	22.60	1.63

6-4-2 Yamanaka-Ankersen LMPC controllers

In this subsection, the results of the YA based LMPC formulations will be presented. It is to be noted that with the use of the YA prediction model, using a sampling time of 3 seconds was not possible for the YA controllers due to their larger error, a smaller sampling period of 2 seconds combined with a prediction horizon of $N_p = 38$ was used to still have the same prediction horizon as for the HCW terminal to capture phase controllers. The cost matrices Q and R used for the simulations are presented in Table 6-16.

Normal vs Delayed LMPC

Firstly, the trajectory and commanded input of the normal LMPC vs the delayed LMPC are presented in Figure 6-60. The trajectory in the orbital plane is presented in 6-61 and 6-62.

It can be seen from the figures that the delayed controller is slower, but unlike for the HCW there is no increase in overshoot. Even though the delayed controller has a slightly slower response, it is able to dock more precisely, as seen in Figure 6-62.

Table 6-16: Cost matrices for YA Terminal to Capture Controllers

Controller	Q_x	$Q_{\dot{x}}$	Q_r	Q_σ	R_u or $R_{\Delta u}$
LMPC	0	2×10^1	0	1×10^{-1}	500
delayed LMPC	0	2×10^1	0	1×10^{-1}	500
delayed LMPC + δ est	0	2×10^1	0	1×10^{-1}	500
delayed LMPC + W δ est	0	2×10^1	0	2×10^{-1}	500
Δu delayed LMPC	0	2×10^1	0	1×10^{-1}	500
Δu delayed LMPC + δ est	0	2×10^1	0	1×10^0	500
Δu delayed LMPC + W δ est	0	2×10^1	0	1×10^{-1}	500

Delayed LMPC with disturbance estimators

Next, in Figure 6-63 the trajectory and commanded input of the delayed LMPC vs the delayed LMPC with the two disturbance estimators presented in Subsection 5-3-3 are presented. Their trajectory in the orbital plane is shown in Figure 6-64 and 6-65. The W of the disturbance estimator presented in (5-5) was set to:

$$W = 1 \times 10^{-3} * \mathrm{I}_{nx} \tag{6-15}$$

From the figures, it is unclear clear whether the estimators help improve the performance of the delayed LMPC. The responses are very similar, so the ΔV and docking error will be compared later in this section.

Incremental Input Delayed LMPC with disturbance estimators

Finally, in Figure 6-66 the trajectory and commanded input of the incremental input delayed LMPC vs incremental input delayed LMPC with the W matrix disturbance estimator presented in Subsection 5-3-3 are presented. The same W matrix was used as for the delayed controllers. In Figures 6-67 and 6-68 the orbital plane trajectory of the controllers is presented. From the figures, it can be seen that the disturbance estimators do not provide an improvement to the delayed controller with incremental input cost function. The classical disturbance estimator is able to dock with more delicacy, but at the cost of a significantly longer time to docking.

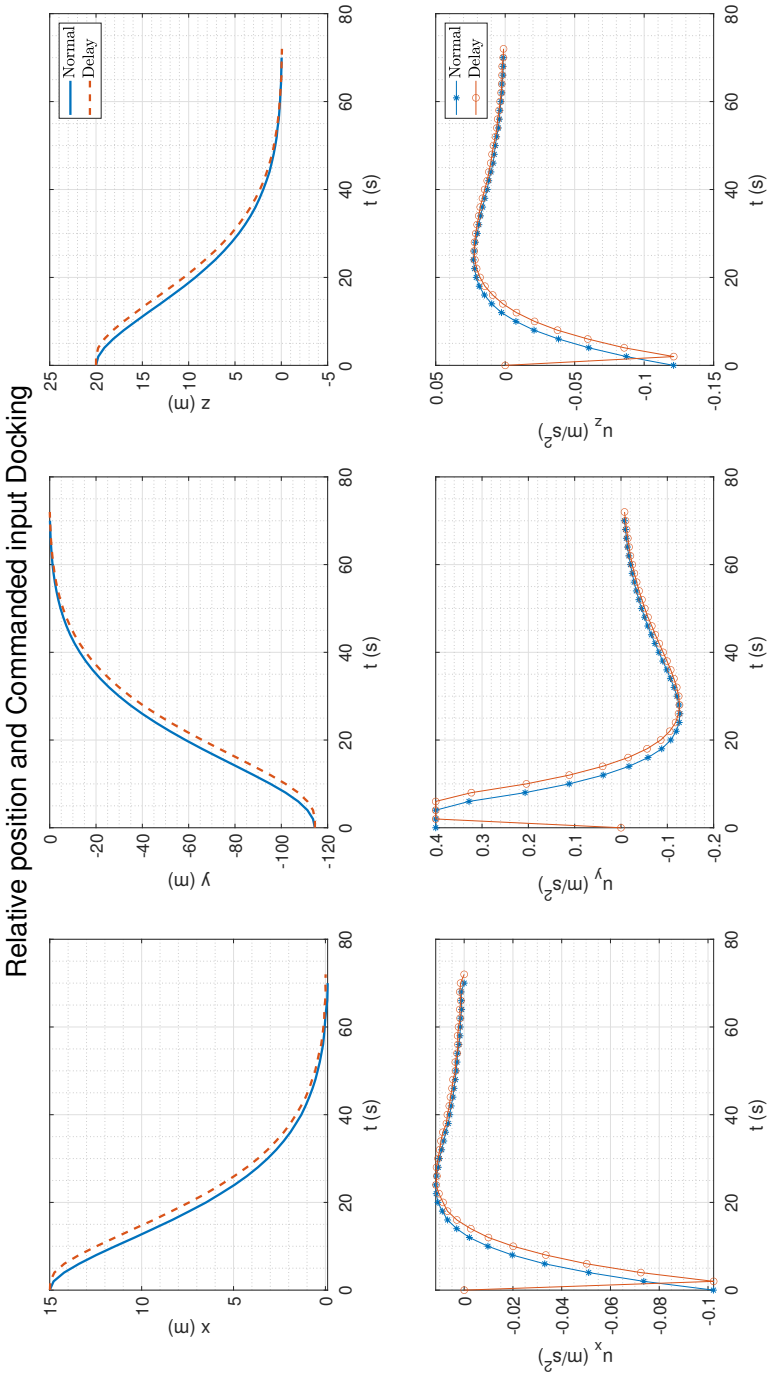

Figure 6-60: Response of YA LMPC and delayed HCW LMPC for Docking

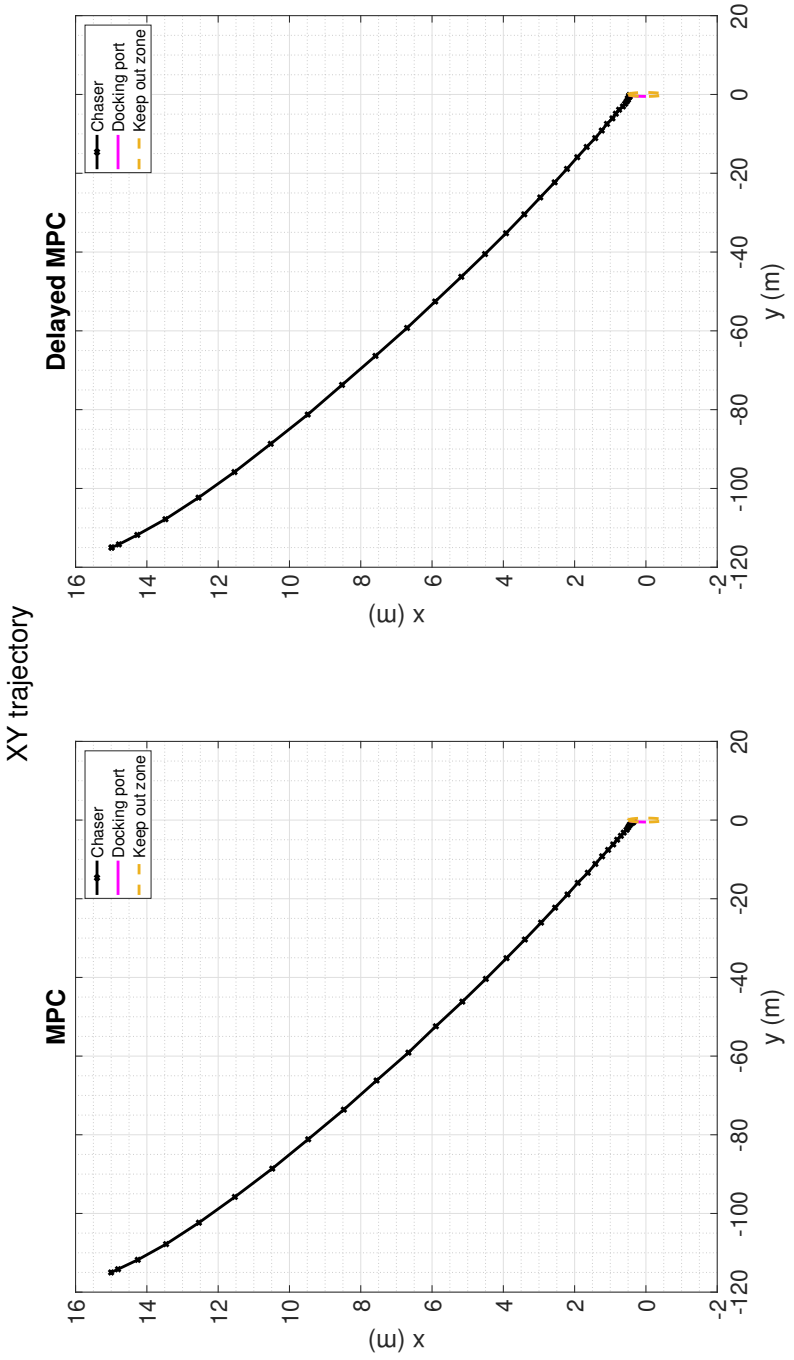

Figure 6-61: Orbital Plane trajectory of YA LMPC and delayed YA LMPC for Docking

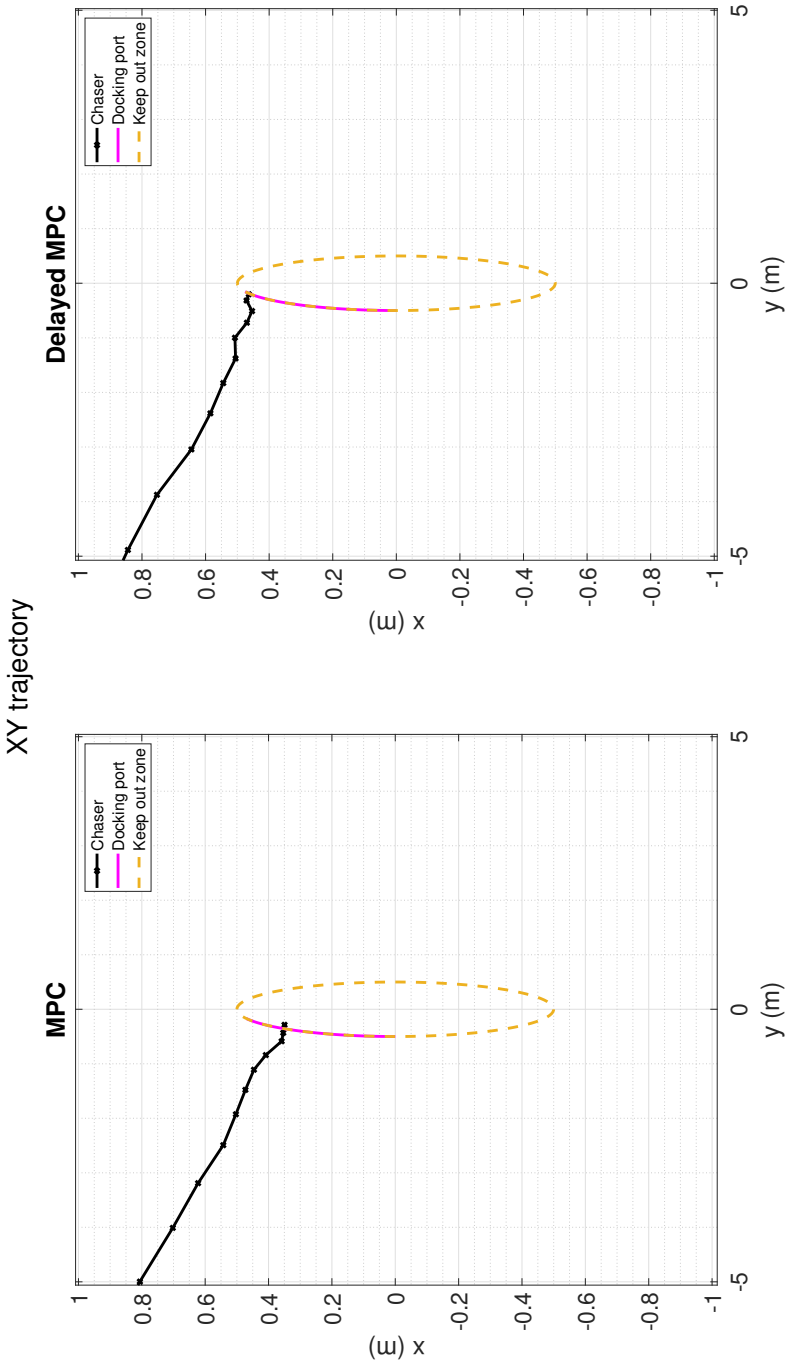

Figure 6-62: Magnified Orbital Plane trajectory of YA LMPC and delayed YA LMPC for Docking

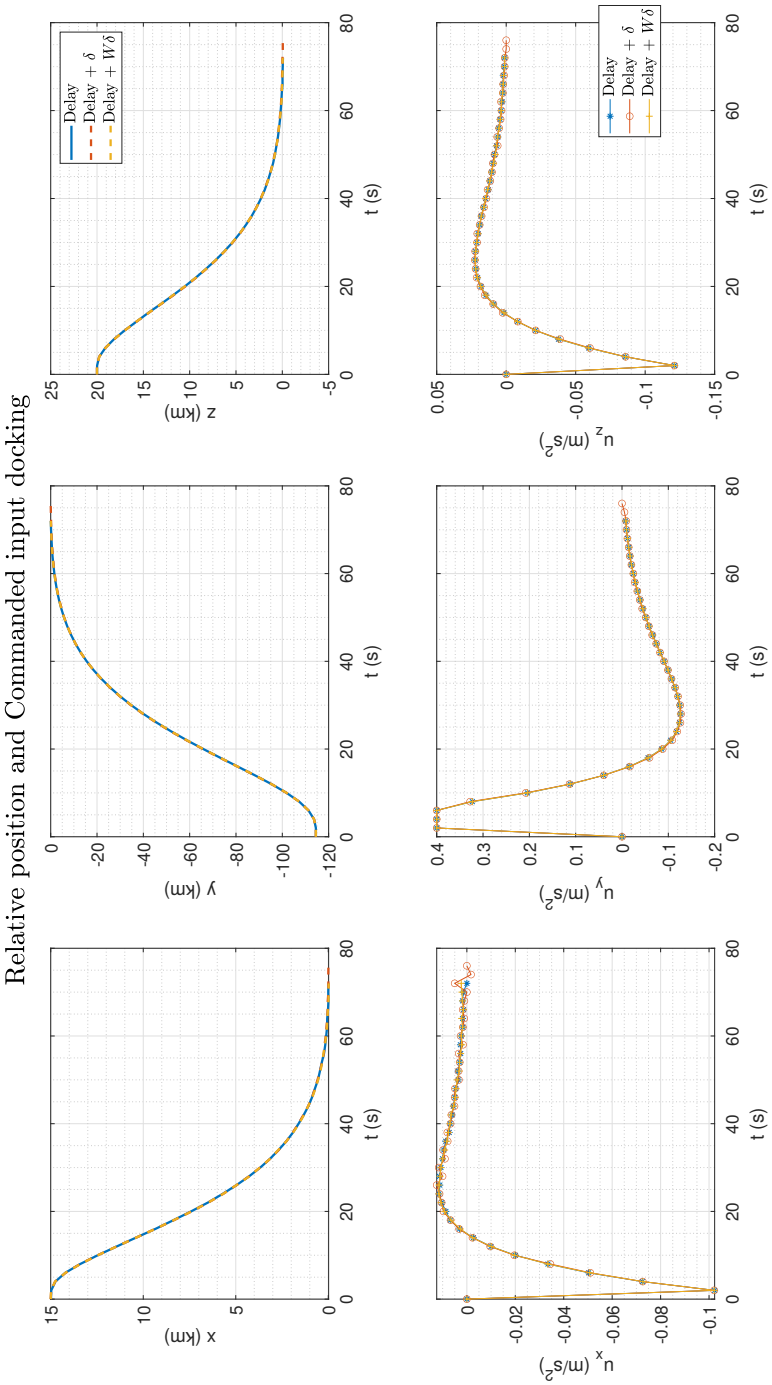

Figure 6-63: Response of delayed YA LMPC vs delayed YA LMPC with disturbance estimators for Docking

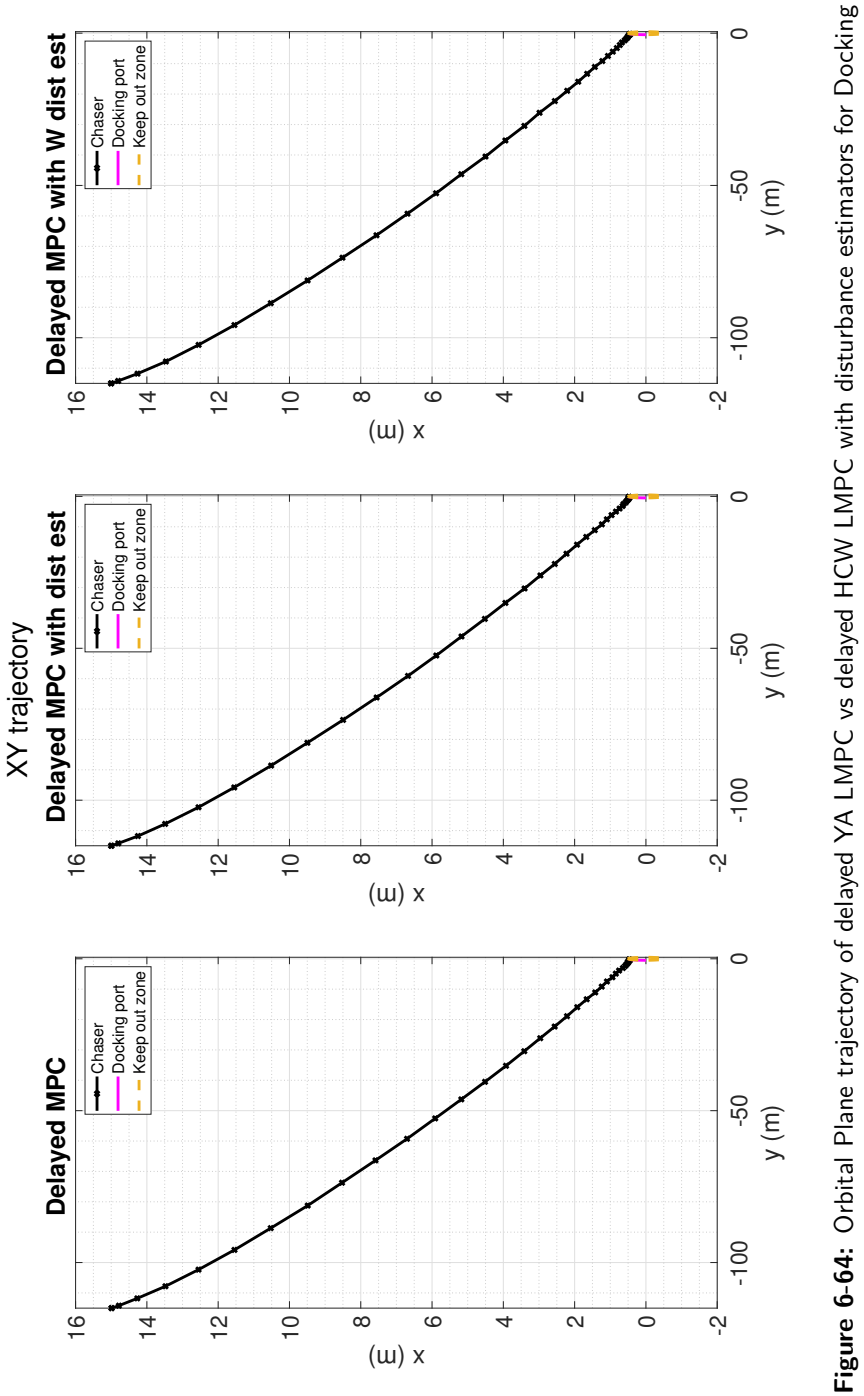

Figure 6-64: Orbital Plane trajectory of delayed YA LMPC vs delayed HCW LMPC with disturbance estimators for Docking

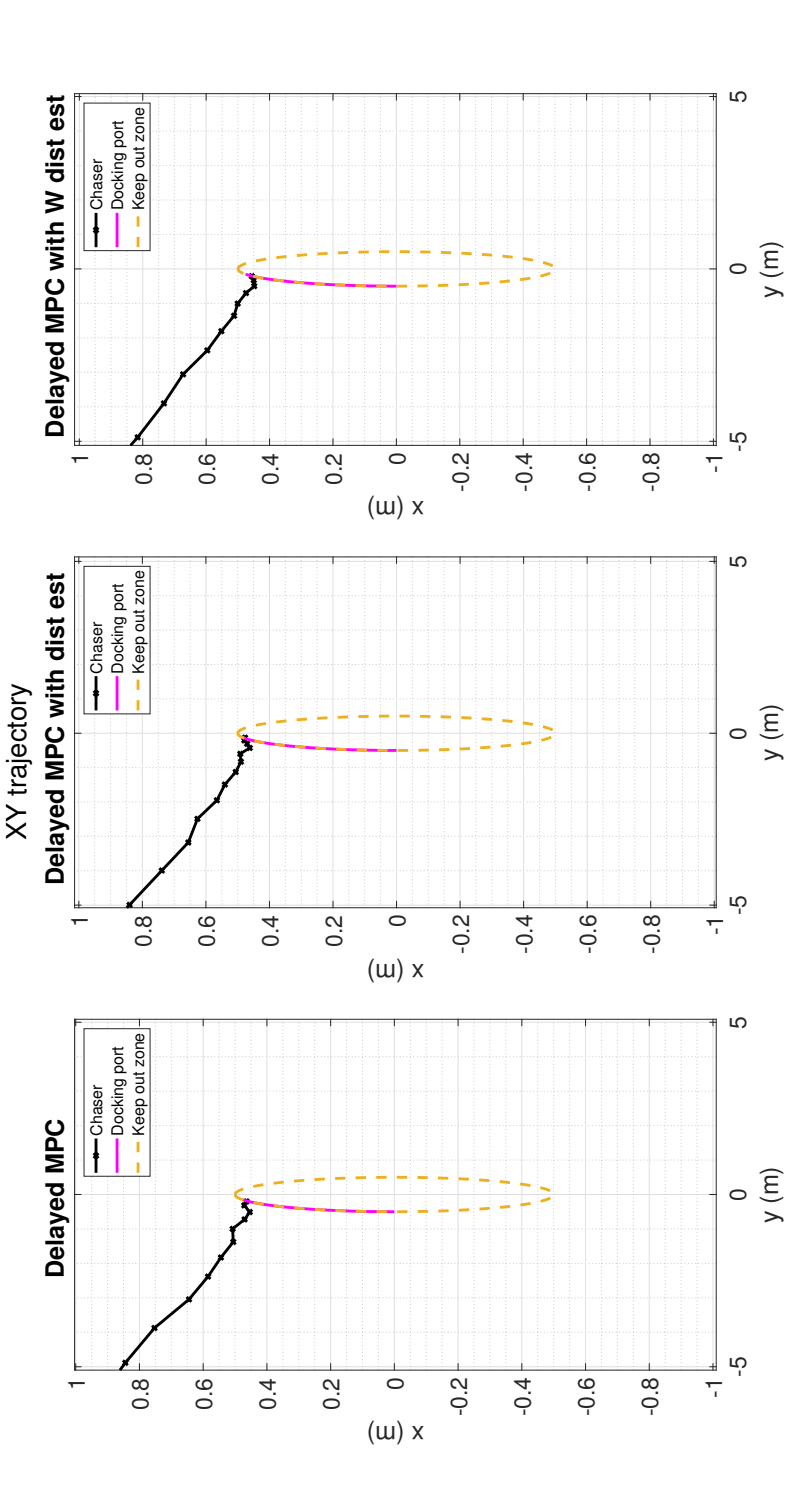

Figure 6-65: Magnified Orbital Plane trajectory of delayed YA LMPC vs delayed HCW LMPC with disturbance estimators for Docking

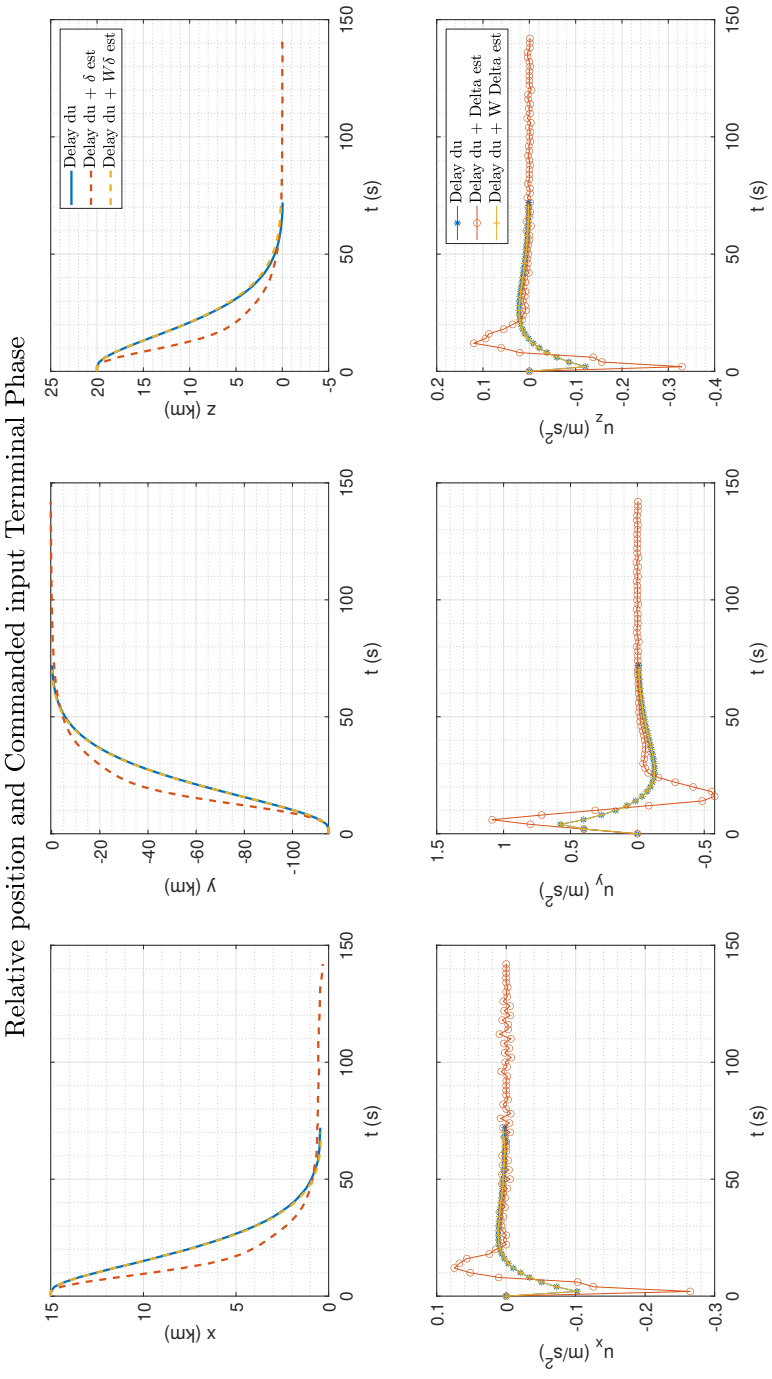

Figure 6-66: Orbital Plane trajectory of Δu delayed YA LMPC vs Δu delayed YA LMPC with disturbance estimators for Docking

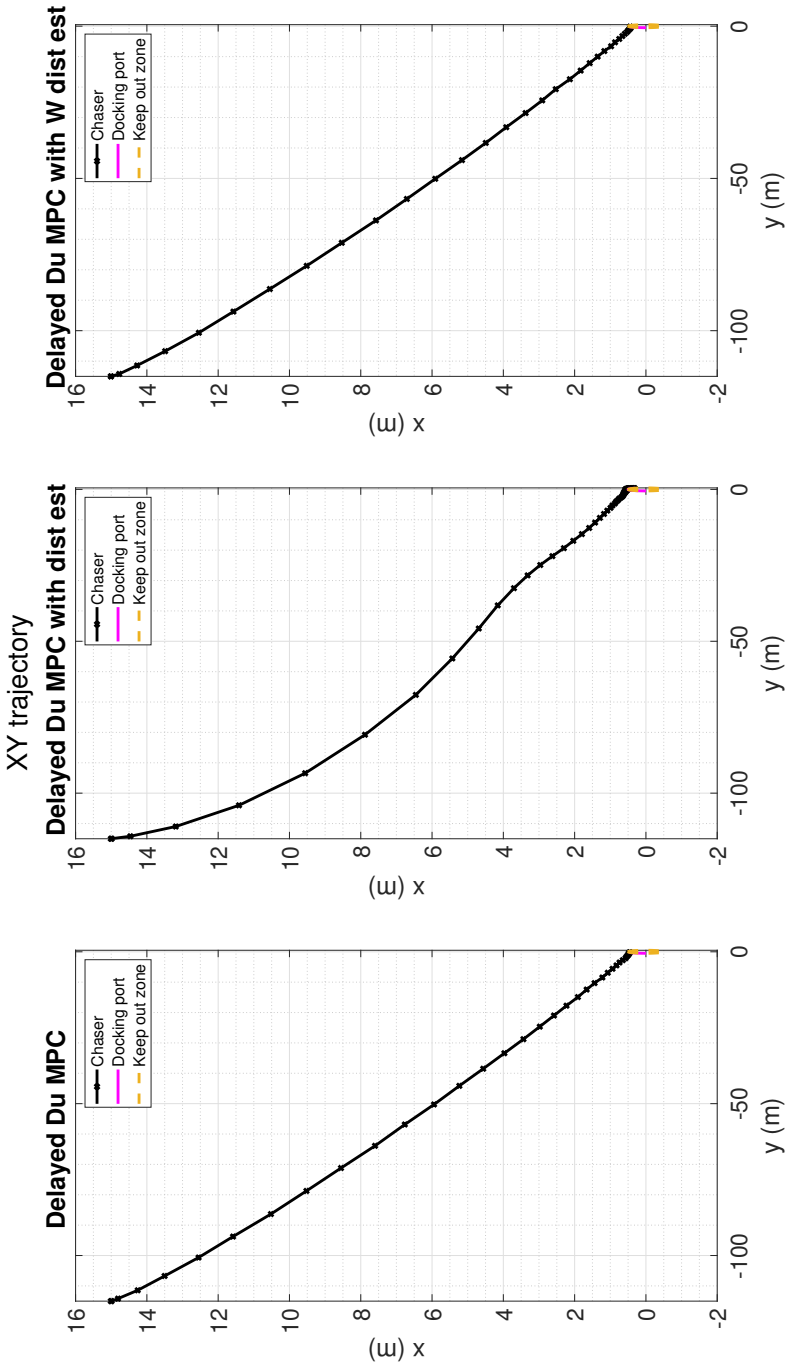

Figure 6-67: Orbital Plane trajectory of Δu YA controllers for Docking

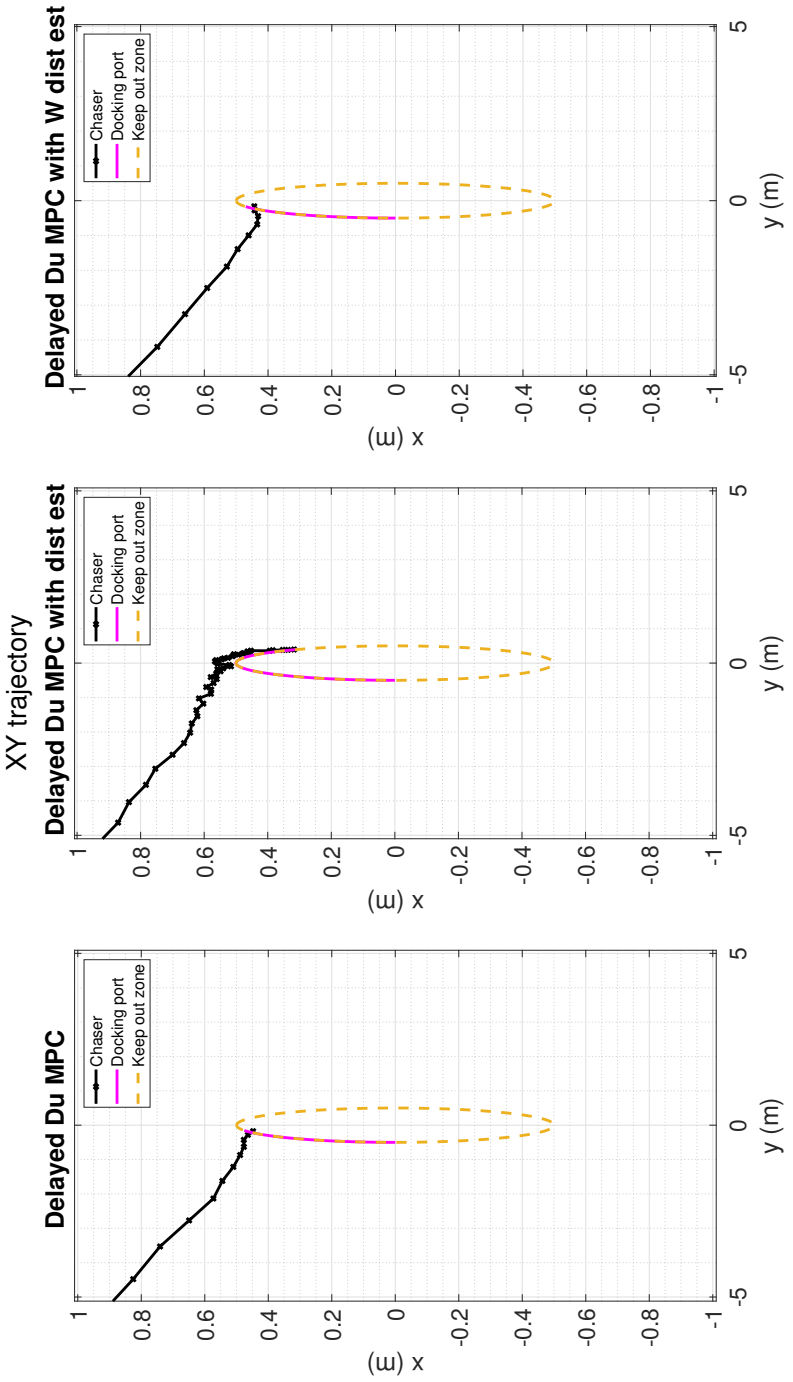

Figure 6-68: Magnified Orbital Plane trajectory of Δu YA controllers for Docking

ΔV and Steady state error

As the simulation did not include a time varying mass and modelled thrusters, it is best suited to compare required ΔV in order to not introduce more assumptions. Due to the nature of the terminal to capture phase, there is no steady state offset to evaluate. The distance from the centre of the docking port and the point of contact will be evaluated instead, as was done for the HCW controllers.

The required ΔV and RMS errors for each controller are presented in Table 6-17. Firstly, it can be seen that the delayed controller has a significantly lower docking error than the normal case. This is likely due to tuning, as they ΔV are very similar, and the normal controller should be more accurate. ext, it is clear that the use of a classic disturbance estimator improves docking accuracy, while the W matrix disturbance estimator presented in [22] does not. The use of an incremental input cost function also improves the docking accuracy with respect to the normal delayed case, but the addition of a disturbance estimator to it does not improve docking accuracy. It is interesting to see how in this case with the smaller relative distances the YA model is able to fulfil the constraints and dock with great accuracy. This is likely due to propagation error decreasing with the shorter relative distances between, but this is also a result of the smaller sampling time.

Table 6-17: Results for YA Terminal to capture phase controllers

Controller	ΔV $[m/s]$	Docking error x $[cm]$	Docking error y $[cm]$	Docking error
LMPC	9.76	12.03	11.43	3.64
delayed LMPC	9.74	1.16	4.73	6.90
delayed LMPC + δ est	9.81	0.82	0.70	4.85
delayed LMPC + W δ est	9.75	1.95	5.70	4.37
Δu delayed LMPC	9.85	0.00	1.50	4.50
Δu delayed LMPC + δ est	17.84	0.75	5.32	3.91
Δu delayed LMPC + W δ est	9.84	4.35	8.90	17.76

6-4-3 Xu-Wang LMPC controllers

In this subsection, the results of the Xu-Wang based LMPC formulations will be presented for the Terminal to Capture phase. The same sampling time of 3 seconds and prediction horizon, N_p, of 25 steps was used just as for the HCW terminal to capture phase controllers. The cost matrices Q and R used for the simulations are presented in Table 6-18.

Normal vs Delayed LMPC

Firstly, the trajectory and commanded input of the normal LMPC vs the delayed LMPC are presented in Figure 6-69. The trajectory in the orbital plane is presented in Figures 6-70 and 6-71.

It can be seen from the figures that the delayed controller is only slightly slower, and the delayed controller is still able to dock while satisfying the constraints. It can however be seen that the docking takes longer time to complete in the delayed case.

Table 6-18: Cost matrices for Xu-Wang Terminal to Capture Controllers

Controller	Q_x	$Q_{\dot{x}}$	Q_r	Q_σ	R_u or $R_{\Delta u}$
LMPC	0	1×10^1	0	5×10^0	500
delayed LMPC	0	1×10^1	0	4×10^0	500
delayed LMPC + δ est	0	1×10^1	0	2×10^0	500
delayed LMPC + W δ est	0	1×10^1	0	5×10^0	500
Δu delayed LMPC	0	1×10^2	0	2×10^0	500
Δu delayed LMPC + δ est	0	2×10^1	0	8×10^{-1}	500
Δu delayed LMPC + W δ est	0	1×10^1	0	3×10^0	500

Delayed LMPC with disturbance estimators

Next, in Figure 6-69 the trajectory and commanded input of the delayed LMPC vs the delayed LMPC with the two disturbance estimators presented in Subsection 5-1-3 are presented. Their trajectory in the orbital plane is shown in Figures 6-43 and 6-74.

The W of the disturbance estimator presented in (5-5) was set to:

$$W = 1 \times 10^{-5 * \mathrm{I}_{nx}} \text{(6-16)}$$

From the figures, it is clear that the classical disturbance estimator presented in (5-4) is able to decrease the required time for docking. The W matrix disturbance estimator also does the same, but not to the same extent.

Incremental Input Delayed LMPC with disturbance estimators

Finally, in Figure 6-75 the trajectory and commanded input of the incremental input delayed LMPC vs incremental input delayed LMPC with the two disturbance estimators presented in Subsection 5-1-3 are presented. The same W matrix was used as for the delayed controllers. In Figures 6-46 and 6-47 the orbital plane trajectory of the controllers is presented. Firstly, it is clear from the figures that the use of an incremental input cost function results in a smoother trajectory. The chaser directly approaches the target without any loop as the seen for the other cases. Adding the classical disturbance estimator is able to improve the trajectory and have a more direct approach. The W matrix disturbance estimator has the opposite effect and again results in a trajectory with a small loop before docking. Both disturbance estimators increase the time for docking, but for a more accurate docking.

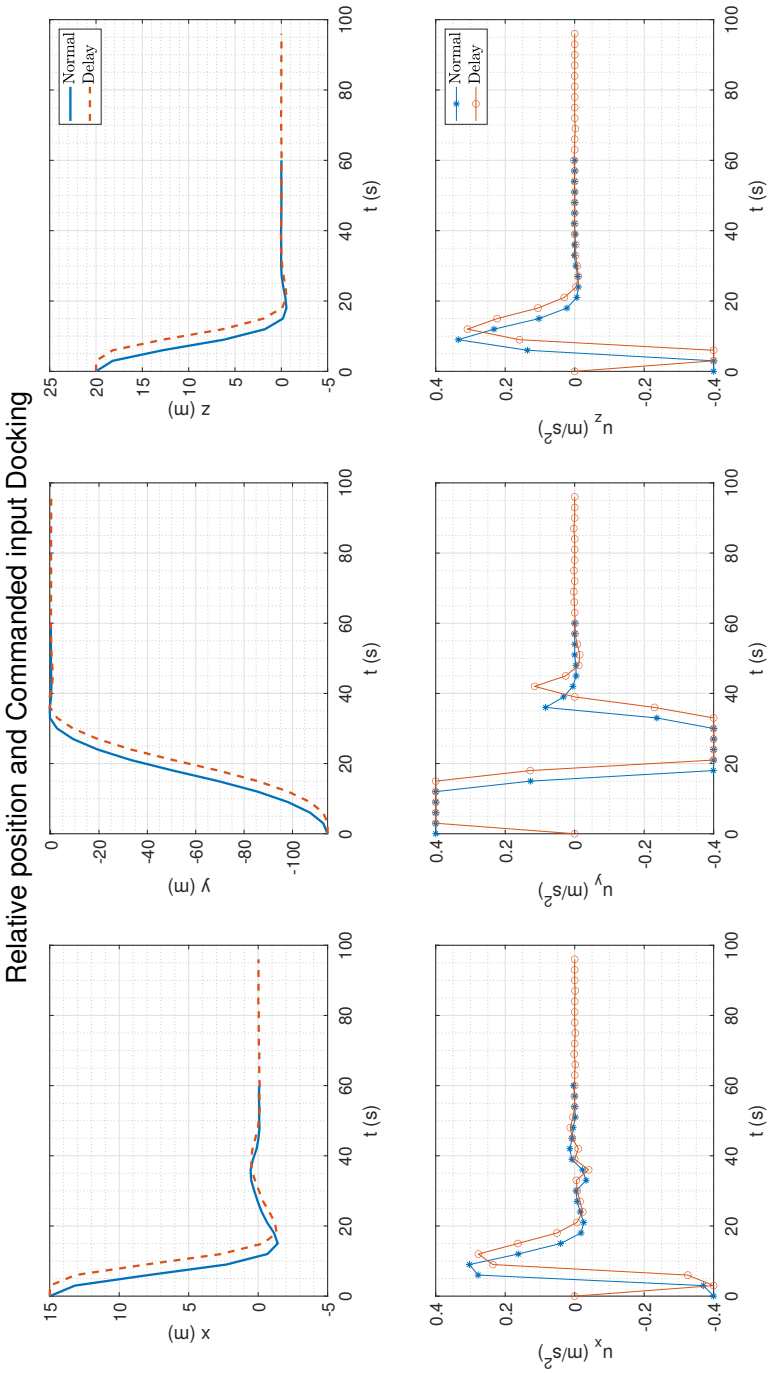

Figure 6-69: Response of Xu-Wang LMPC and delayed Xu-Wang LMPC for Short range

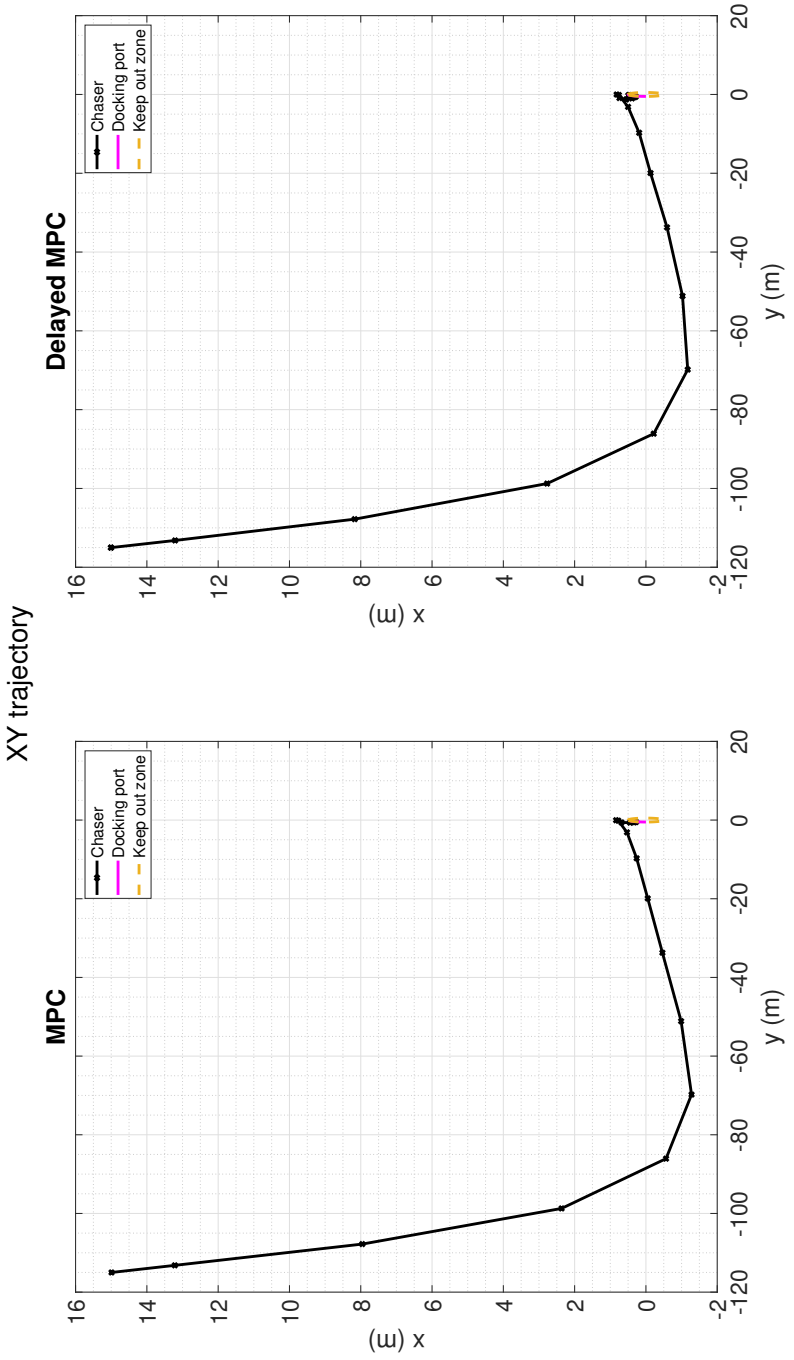

Figure 6-70: Orbital Plane trajectory of Xu-Wang LMPC and delayed HCW LMPC for Short range

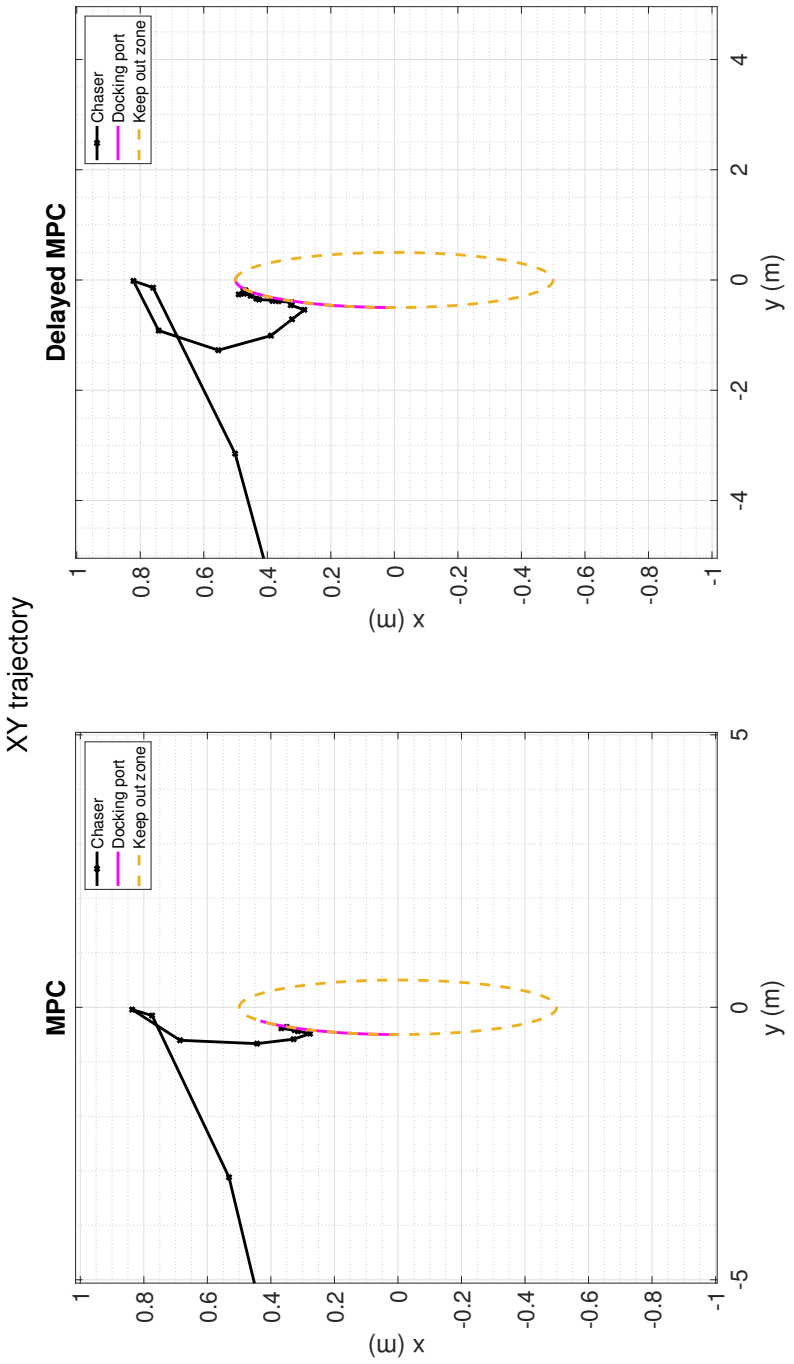

Figure 6-71: Magnified Orbital Plane trajectory of Xu-Wang LMPC and delayed HCW LMPC for Short range

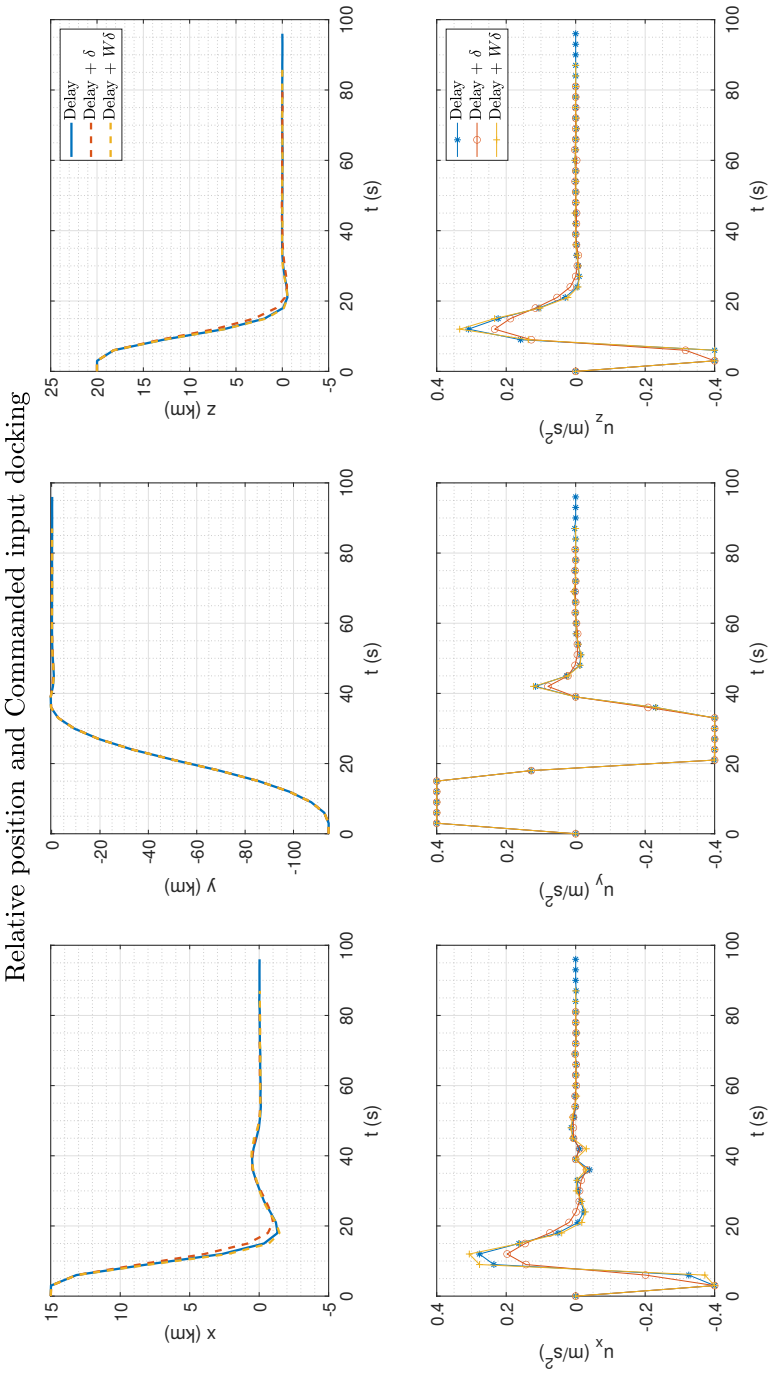

Figure 6-72: Response of delayed Xu-Wang LMPC vs delayed HCW LMPC with disturbance estimators for Short range

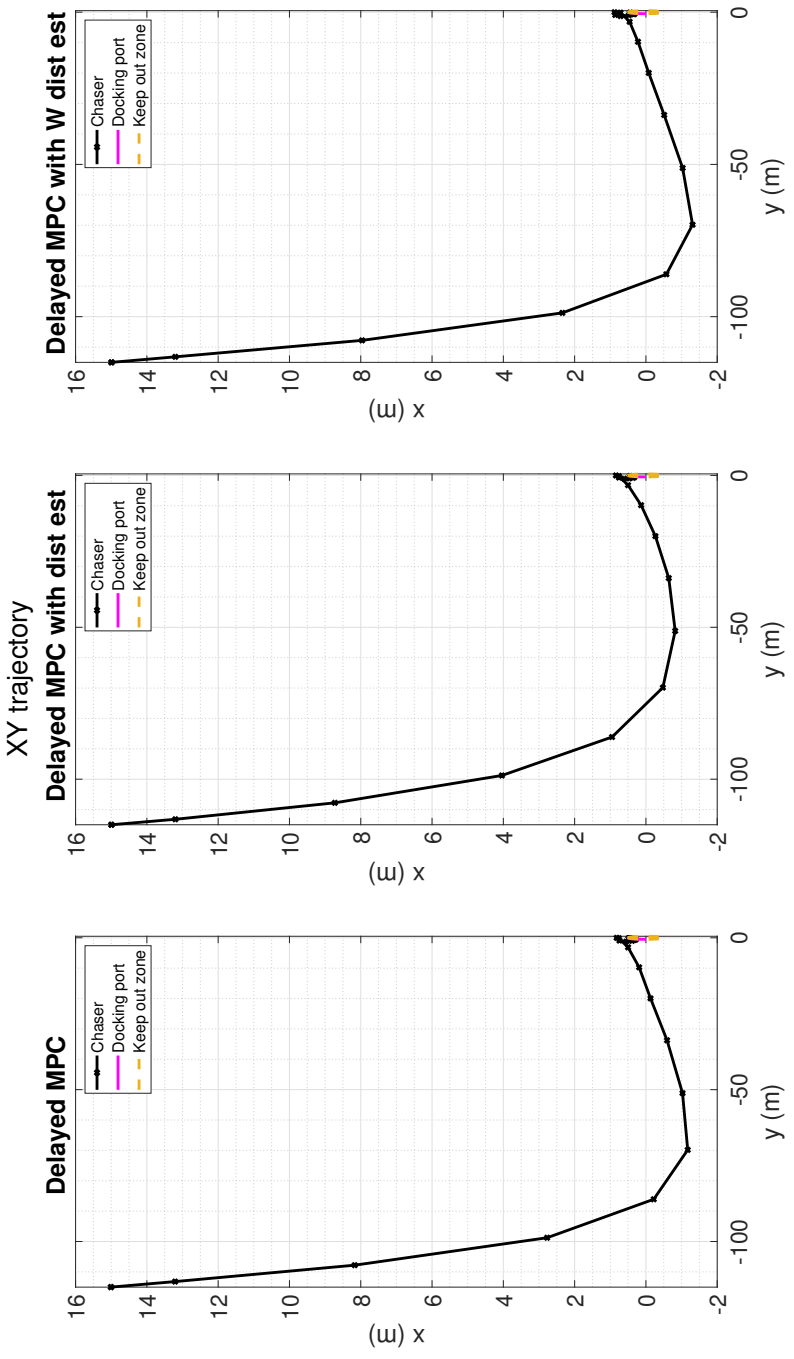

Figure 6-73: Orbital Plane trajectory of delayed Xu-Wang LMPC vs delayed HCW LMPC with disturbance estimators for Short range

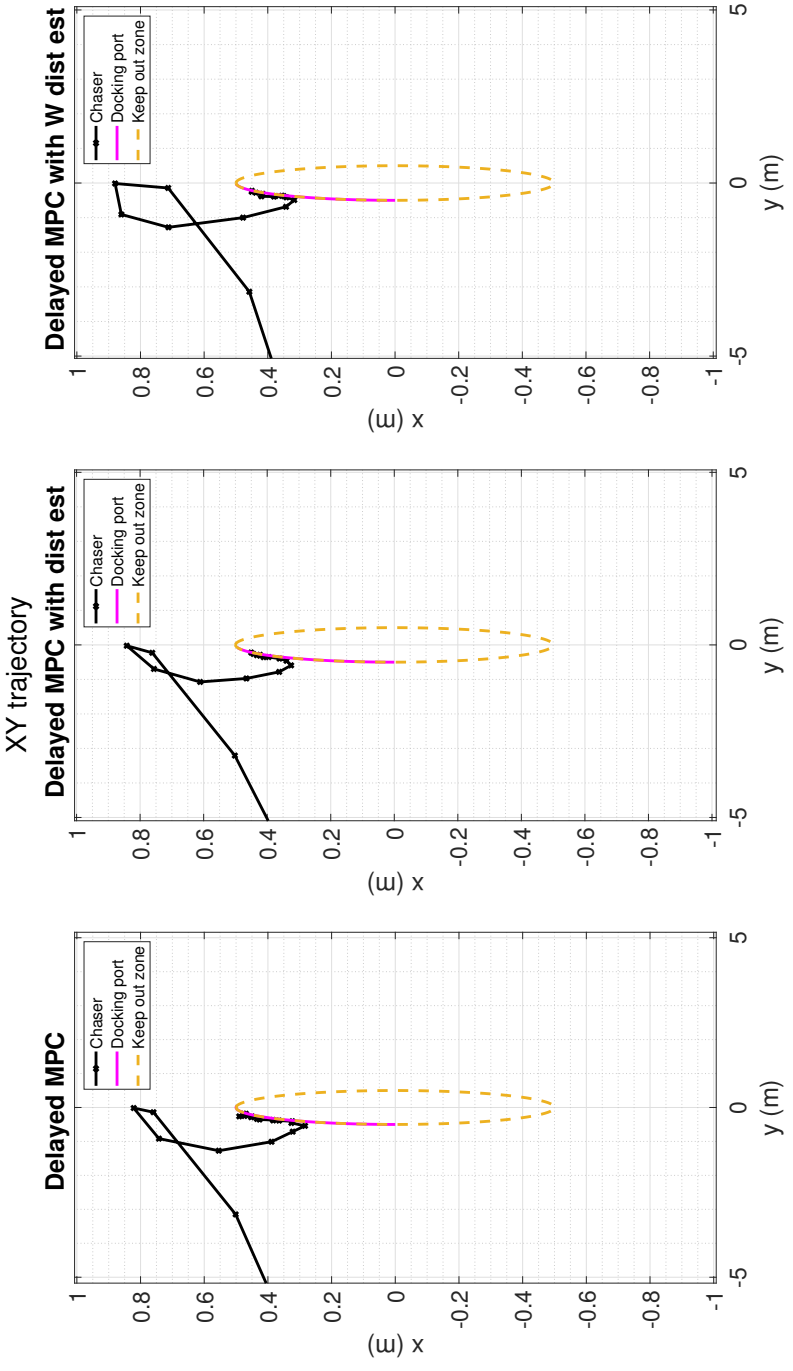

Figure 6-74: Magnified Orbital Plane trajectory of delayed Xu-Wang LMPC vs delayed HCW LMPC with disturbance estimators for Short range

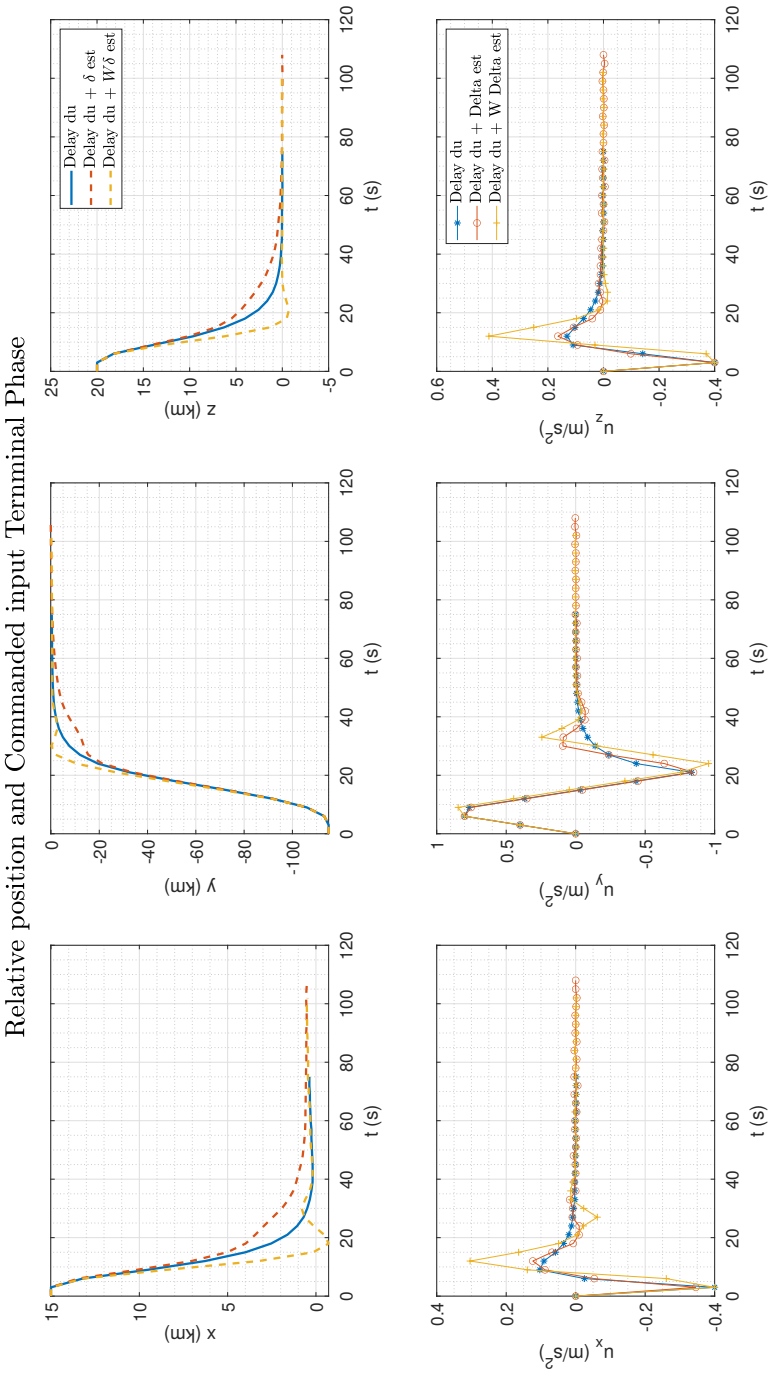

Figure 6-75: Response of delayed of Δu delayed Xu-Wang LMPC vs Δu delayed Xu-Wang LMPC with disturbance estimators for Short range

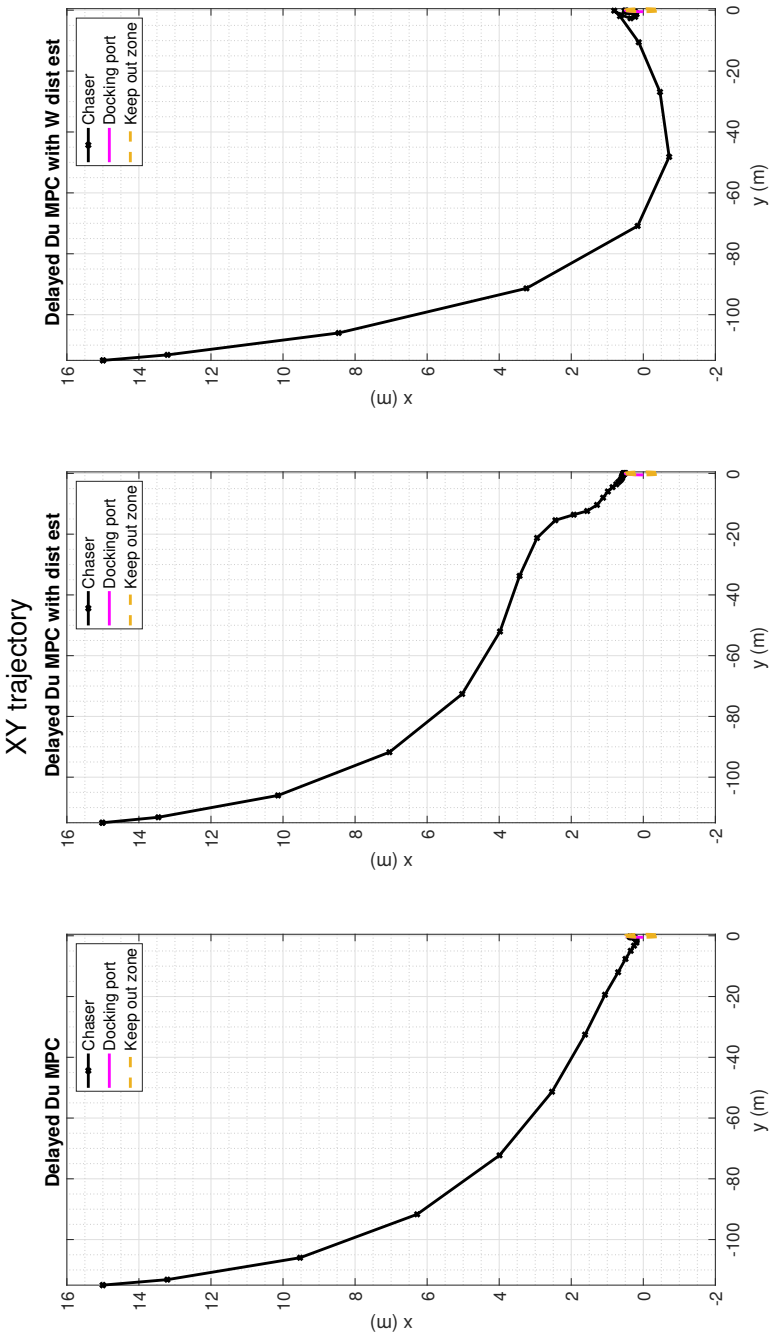

Figure 6-76: Orbital Plane trajectory of Δu XU LMPC and Δu delayed XU LMPC for Short range

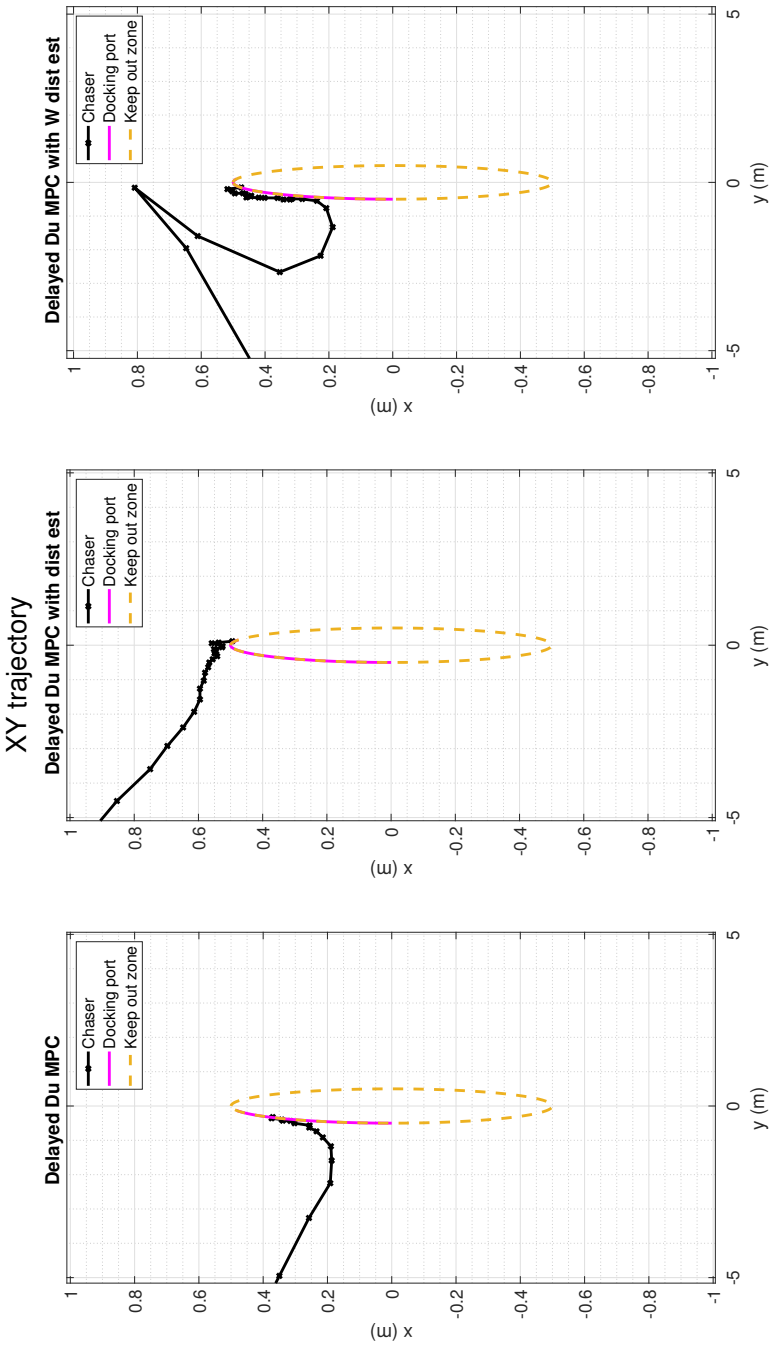

Figure 6-77: Magnified Orbital Plane trajectory of Δu XU LMPC and Δu delayed XU LMPC for Short range

ΔV and Steady state error

As for the YA and HCW controllers, the performance was evaluated based on required ΔV and docking error. The results of the various controllers are presented in 6-19. From the table, it can be seen how the delayed controller is not able to provide the same docking accuracy as the nominal case as expected. The inclusion of a disturbance estimator is however able to improve the docking accuracy, but there is no significant improvement in required ΔV.

The use of an incremental input cost function is able to provide an improvement in required ΔV but with no improvement in docking accuracy. The combination of incremental input cost function and the classical disturbance estimator is able to provide an improvement in both required ΔV and docking error. The combination of incremental input cost function and W matrix disturbance estimator does not provide any benefits, but actually decreases the performance of the controller.

Table 6-19: Results for XU Terminal to capture phase controllers

Controller	ΔV $[m/s]$	Docking error x $[cm]$	Docking error y $[cm]$	Docking error
LMPC	23.68	4.83	13.12	0.68
delayed LMPC	23.76	6.95	18.58	1.35
delayed LMPC + δ est	21.61	8.35	12.15	0.70
delayed LMPC + W δ est	23.74	13.47	14.44	0.09
Δu delayed LMPC	19.61	11.27	19.37	0.17
Δu delayed LMPC + δ est	20.44	1.88	3.76	1.33
Δu delayed LMPC + W δ est	26.72	1.44	25.3	5.25

6-4-4 Conclusion

In this section, we will compare the best controllers for each of the three prediction models. The best performing controllers are presented in Table 6-20. It is to be noted that for the docking phase, the YA controllers were able to satisfy the constraints and dock safely. Regardless of the fact that the YA STM being computed based on the assumption that the chaser satellite is flying in free motion, and that the external forces on chaser and target satellite are identical, which is not so under control. This is likely due to the smaller relative distance between chaser and target combined with the smaller sampling time, decreasing the effects of model error.

It is clear from the table that the inclusion of a disturbance estimator has clear benefits in terms of ΔV and docking error for the terminal to capture phase too, again proving that the use of robust methods has clear benefits. The usage of a more accurate prediction model does also not guarantee a decrease in ΔV or docking error. The YA controller provided the best performance in terms ΔV and docking error. The HCW controller provided similar performance in terms of docking error but requiring double the ΔV compared to the YA controller. The Xu-Wang model provided similar performance to the HCW controller, but marginally worse. This is surprising considering that the simulation makes used of the non-linear version of the Xu-Wang model. This is likely due to the controller compensating for disturbances included in the model to achieve this better steady state error, which can be seen

in Figures 6-79 and 6-80 with the trajectory of the Xu-Wang controller being more direct. Overall, the HCW controllers provide the best compromise in performance between ΔV and steady state error. Considering that the Xu-Wang model requires the integration of the RSV's at every computation being LTV systems, the HCW model provides better performance for no computational expense.

Table 6-20: Results for the Intermediate Range controllers

Controller	ΔV $[m/s]$	RMS error x $[m]$	RMS error y $[m]$	RMS error z $[m]$
HCW delayed LMPC + δ est	20.19	0.82	1.44	2.80
YA delayed LMPC + δ est	9.81	0.82	0.70	4.85
XU Δu delayed LMPC + δ est	20.44	1.88	3.76	1.33

The compared responses and trajectories of the three controllers are presented in Figures 6-78, 6-79 and 6-80

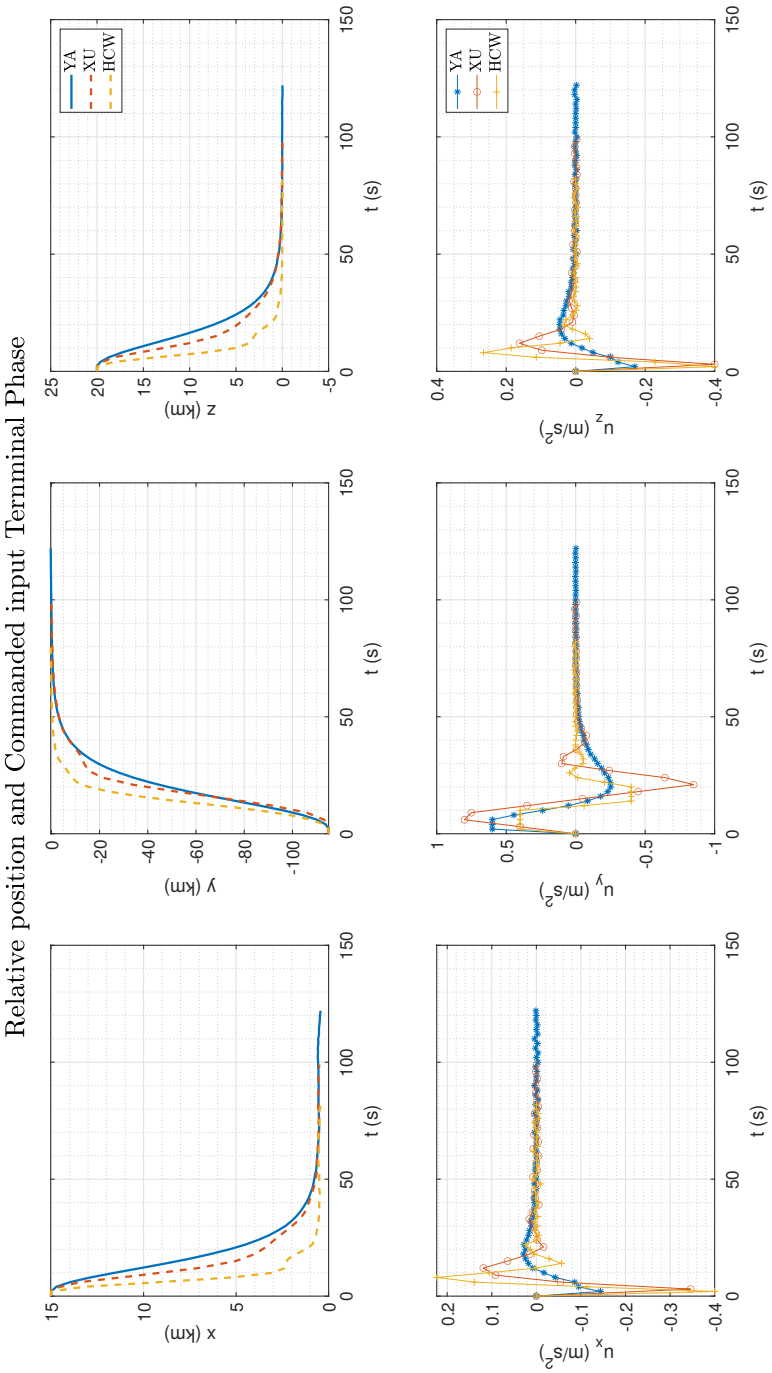

Figure 6-78: Response of best performing Short Range HCW and Xu-Wang controllers

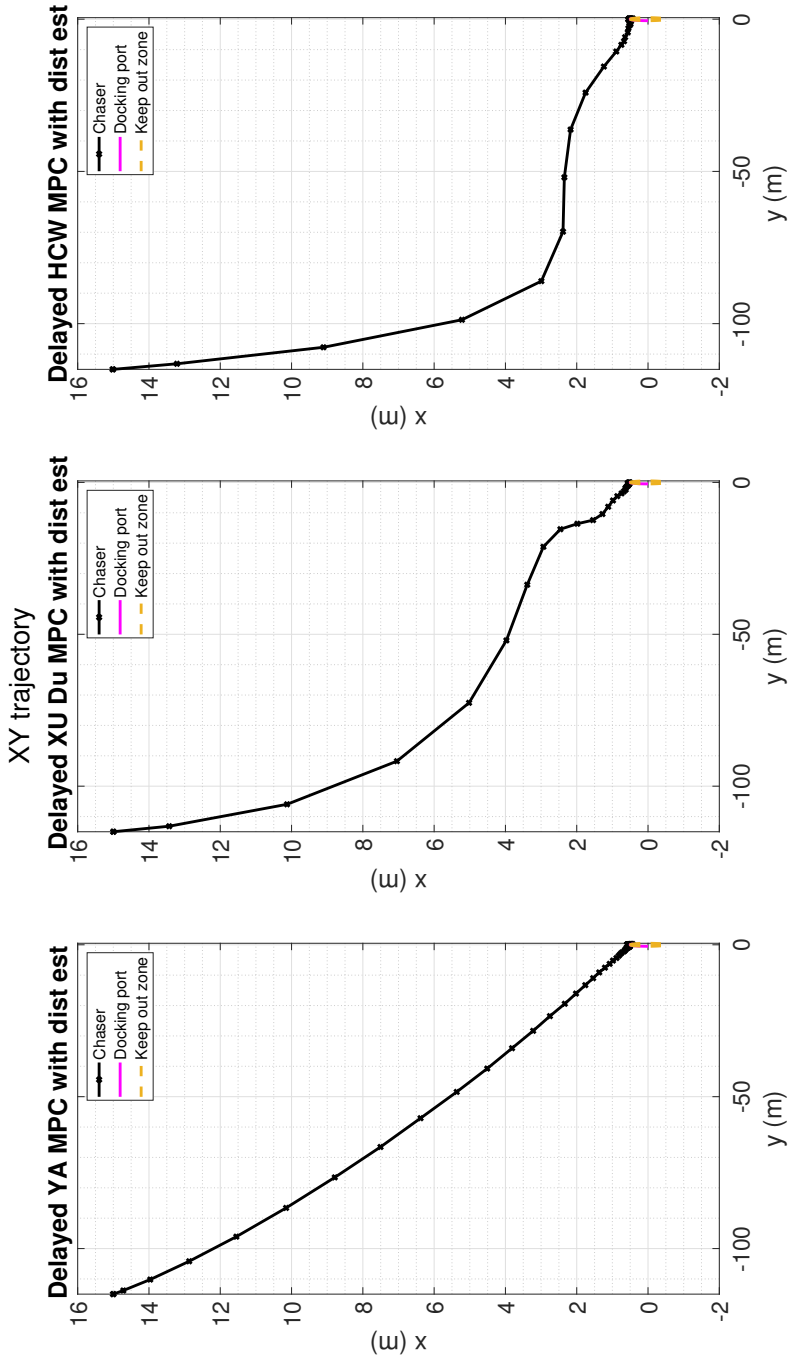

Figure 6-79: Orbital Plane trajectory best performing Short Range HCW and Xu-Wang controllers

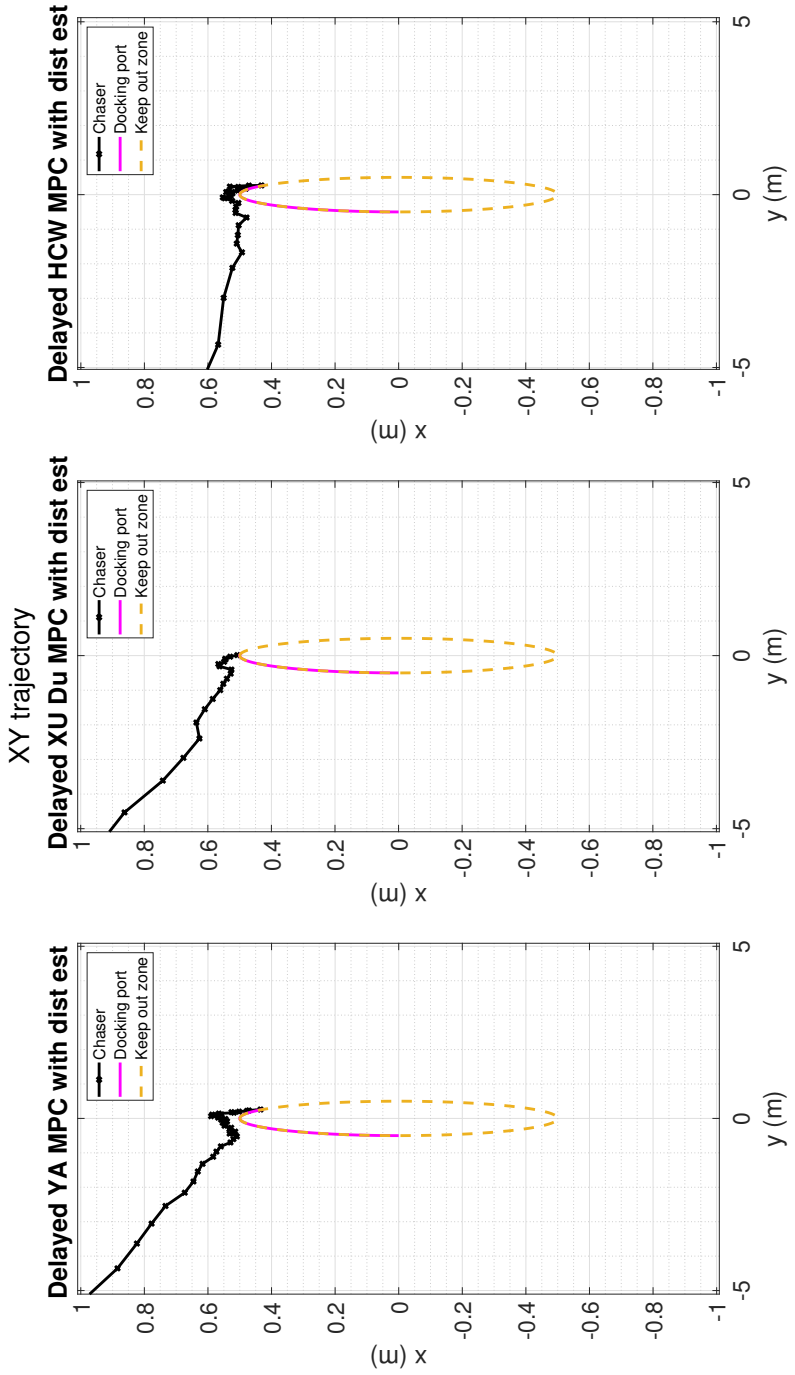

Figure 6-80: Magnified Orbital Plane trajectory best performing Short Range HCW and Xu-Wang controllers

Chapter 7

Conclusion, Discussion, and Recommendations

Having presented the methodological approach and the obtained results, conclusions can be drawn and evaluated to determined the validity of this research. In this Chapter the work reported and presented in this thesis will be reviewed. Firstly, the conclusion to the research question will be presented, followed by a discussion on the validity and representations of the results. Finally. recommendations for future research will be discussed at the end of the chapter.

7-1 Conclusion

The main objective of this research was to determine the most suitable Model Predictive Control (MPC) strategy for Rendezvous and Docking (RVD) of a chaser spacecraft to an uncooperative target spacecraft from various proven strategies. This objective was split into several sub-objectives, from which research questions were formulated. By answering these research questions, the primary objective can then be fulfilled. From the objectives explained above, it became possible to elaborate research questions that provide the scope of this thesis.

Main Research Question

What type of model predictive control strategy is best suited for real-time application in the complete rendezvous and docking problem, to minimize propellant use while maintaining adequate completion time?

The sub-research questions and their respective answers are presented below:

1. *What type of relative orbital dynamics model allows for the best description of the target and chaser spacecraft in orbit as to minimize propellant consumption and completion time?*

Extensive research hjas been done in the development of relative orbital dynamics models of satellites. There are too many to compare them all within the constraints of this thesis, but three models with flight heritage and of large interests in the future have been examined. The Clohessy Wiltshire (HCW), Yamanaka-Ankersen (YA) and Xu-Wang (XU) models were presented in Section 3-1-3. The HCW and YA model are described by a six-state differential equation representing the relative position and velocity, while the XU is described by a 11 state differential equation as it includes the five Reference Satellite Variables (RSV). Besides the choice of relative orbital dynamics, two disturbance estimators were evaluated for all three mission phases.

For the Intermediate Range phase, the HCW model proved to provide the best combination of Root Mean Squared (RMS) error, required ΔV and completion time. The YA model was able to provide the lowest propellant consumption but at the cost of significantly larger errors, so it was not deemed a feasible option. The XU controller provided similar performance in terms of RMS error to the HCW model, but at the cost of increased required ΔV. For all three models, the inclusion of a classical disturbance estimator provided significant improvement in required ΔV and RMS error. The W matrix disturbance estimator only provided benefit for the YA model but still not to the same extent as the classical disturbance estimator, The use of a more complete and accurate model did not provide any significant benefits compared to the standard HCW model, but the inclusion of disturbances in the model improved required ΔV and RMS error.

For the close range phase, the same trend was seen. The XU model provided the best performance in terms of error but at the cost of an increased required ΔV, The YA model error while in closed loop control was too high to fulfil the mission phase constraints and objectives, resulting in it not being a viable option. The HCW model required the least ΔV but had a slightly higher RMS error than the XU model, while satisfying the mission phase constraints and objectives. The inclusion of disturbance in the prediction model had the same effect as for the intermediate range. Consequently, even for the intermediate range phase, the use of a more complete and accurate model did not provide any significant benefits compared to the standard HCW model, but the inclusion of disturbances in the model improved required ΔV and RMS error.

For the terminal to capture phase, the relative distance to the docking port is of importance, and thus the three relative dynamics models are expanded by six states to include the target satellite docking port position and relative position to the chasers docking port. The findings for the terminal capture phase were quite different. The YA model required the least amount of ΔV for docking while providing similar docking error of the HCW and XU model. As for the first two mission phases, the inclusion of the classical disturbance estimator improved required ΔV and docking error, but this did not count for the W matrix disturbance estimator as it only provided benefit for the YA model. The use of a more accurate model was thus able to provide significant benefits, half the required ΔV to be compared to the HCW model, and the inclusion of disturbances in the model improved required ΔV and RMS error.

Overall, the use of a more accurate and complete model does not appear to provide significant benefits in terms of propellant consumption and completion time, with respect to the HCW model. This contradicts the findings presented in [53], as the chosen

reference orbit was nearly circular as meaning the benefits of modelling eccentricity are diminished. Even though the YA model required half the ΔV for the terminal to capture phase, the terminal to capture phase accounts for less than 2% of the total mission ΔV. Even if the chaser is inserted relatively close to the target and the intermediate range phase is not needed, the difference would be 10% between HCW and YA model, while the XU model always requires more ΔV. The models do not differ significantly in completion times either, thus the added benefit of a more complete model is minimal or actually negative in terms of the XU model. The inclusion of disturbances in the model improved the required ΔV, RMS error and docking error for all three phases when using the classical disturbance estimator.

2. *How can (LP, Time-Varying, Non-Linear, Stochastic and Robust) an MPC algorithm be constructed to carry out rendezvous and docking mission with an uncooperative (still, rotating or tumbling) target?*

   The MPC relies on a predictor model, which will be a model to predict the relative dynamics up to a certain defined horizon. The relative dynamics models which are used in discretized version for predictors are the HCW, YA and XU model. The predictors are augmented for the terminal to capture phase to include the target's docking port position and the relative position between the two docking ports. The prediction horizon is equal to the required time to complete each mission phase objectives. The predictor is then able to capture the future behaviour of chaser, target, and docking port based on the dynamics by also including the future control inputs. The number of control inputs for this problem is small and constant, thus the increased computational effort of including the inputs in the full prediction horizon is small.

   The simulation models the thruster input to be continuous, thus there is no need for a Hybrid formulation. Hard constraints are set on the maximum and minimum acceleration or ΔV depending on the model. This is because a satellite will be thrust limited and consequently acceleration or ΔV limited. However, the constraints are formulated as such, including a duty cycle in the limit as to represent the thrusters only being able to be used $1/\sqrt{2}$ per sample period for the first two mission phases due to their large sampling periods.

   The cost functions are the standard quadratic cost function with terminal cost and the same but for incremental input penalty instead of the input. These have been tested and proven to be effective in previous literature. The 1 norm cost function is not suitable as it is very sensitive to noise and state error and has been shown to result in higher required ΔV. The penalties are applied to the relative position, velocity, and input. For the terminal stage, the penalty is on the relative docking port position instead of the relative position. A squared sum penalty will thus incur for any required acceleration or ΔV and if the relative position and velocity deviate from the reference.

   The intermediate range, imposes terminal linear hard constraints on the position of the satellite to be within a certain range of the target. The short range phase similarly imposes a linear hard constraint on the position of the chaser satellite in order for it to remain within a holding point until the go ahead is given for the next mission phase. Finally, the terminal to capture phase imposes running linear hard constraints on the position of the chaser for it to remain within the Line-of-Sight (LOS) of the target and outside a keep out zone as to prevent a collision. All three prediction models are linear

and linear constraints are present for all three mission phases. The optimization problem within the optimizer of the MPC algorithm is classified as a Quadratic Programming (QP) problem. The Appropriate formulations are LMPC, delayed LMPC and Robust LMPC.

From the simulations, it becomes evident that the majority of the MPC formulations are able to control the chaser satellite to fulfil the various objectives of each mission phase. The first mission phase was controlled using a sampling period of 200 s and prediction horizon of $N_p = 43$ steps to have a prediction horizon of 1.5 orbits. The second using, 150 s and a prediction horizon of $N_p = 38$ steps to have a prediction horizon of 1 orbit. Finally, the final phase with 3 s and a prediction horizon $N_p = 25$ to have a prediction horizon large enough to include the whole docking manoeuvre. The YA MPC formulations failed to complete the mission objectives for the short range phase. The Robust formulations including a disturbance in their predictor provided the best performance for all prediction models and mission phases.

7-2 Discussion and recommendations

The work presented in this thesis and the conclusions drawn are all related to the methodology and assumptions made throughout. The interpretation and relevance of this work has to be discussed, which will be done in this section, including recommendations for future work to achieve a better understanding for future research.

7-2-1 Relative Orbital Dynamics, Simulation and Satellite Models

The relative orbital dynamics models presented and evaluated in this paper are well documented, and previous research has been undertaken to compare their relative performance. Three models were chosen to compare under closed loop form use for Model Predictive Control (MPC), from the simplest to an example of a more advanced relative dynamics model, but many more are present which have not been compared for this use. The input to these models is either acceleration or ΔV and not the actual thrust required by the thrusters on the chaser. From a practical point of view, thrust results in acceleration, but thrusters usually are not throttleable and if so usually not from 0% to 100%. For the purpose of comparing multiple models, it was not deemed necessary to model binary thrusters and a continuous input was used, which could be achieved through differential thrust.

Next, the models used and evaluated only represent translational dynamics. The assumption is made that the attitude of the satellite will be controlled through the ADCS system of the satellite, as the scope of this research was to compare relative dynamics models. This is possible, but in reality, reaction wheels and magnetometers are slow actuators and are not optimal for the terminal and docking stage. Missions often use multiple thrusters in a certain orientation, in order to control the translational and kinematic dynamics together, but the design of an optimal configuration for this theoretical mission was deemed unnecessary and outside the scope of this thesis.

Based on the limitations mentioned above, a recommendation would be to expand the comparison to more relative dynamics models at least for the firs two mission phases as to have more

data points to make a stronger conclusion. Furthermore, the modelling of binary thrusters should be evaluated in order to verify that the same tendencies determined by this research hold. Next to the thrusters, a recommendation would be to augment the models to also include the kinematics of the chaser, in order to allow the thrusters to control the translation and kinematic dynamics of the chaser satellite. Then one could also evaluate the effect of a more precise kinematic prediction model compared to a simpler one and if the results from this research change at all.

7-2-2 Simulation and Model based-predictive control Strategy

This research combined the models and simulation into a framework to evaluate different model-based predictive control strategies for optimizing propellant consumption during Rendezvous and Docking (RVD). However, certain assumptions limit the application of the framework for certain situations. The models used, as well as the control strategy, relied on variables which were assumed to be measured as mentioned above. The simulation used for this research also did not include the kinematics of the chaser and target satellite, as it was assumed that the target would be rotating with a constant velocity and as the controller did not control the attitude of the chaser there was no need for it. Furthermore, the simulation used for the research comprised of the Non-Linear (NL) Xu-Wang (XU) relative dynamics model. This model is exact for eccentric orbits under J_2 perturbation, however does not include other perturbations such as drag or the other J terms. In practice, however, the target and chaser will be undergoing different forces of drag, solar radiation and other disturbances which have now been added as random disturbances to the simulation. The simulation also does not take into account eclipses, as it was deemed that the docking could be carried out fast enough for the lack of light not to be a problem. Rendezvous and Docking (RVD) satellites make use of cameras, radar, and GPS to determine its position and attitude with respect to the target. These aspects were not included in the simulation as such a simulation was not readily available and the scope of this research was not for application but theoretical comparison. This was replaced by navigation uncertainties being added to the measured variables so as not to have a perfect simulation, however an inaccurate estimation of these values could severely affect the control performance.

Based on the limitations of the simulation mentioned above, a recommendation would be to expand the simulation in order to have more accurate results and provide a platform to evaluate RVD strategies for real time application. Ideally, one would simulate two independent satellites in orbit and their kinematics, including all relevant disturbances. The simulation should then also simulate varying mass, attitude sensors, camera, radar, and GPS signals from which the chaser can estimate its relative position and attitude. This would constitute almost a complete mission simulation, from which more accurate comparisons can be carried out to develop the optimal control solution for RVD, and not just translational dynamics control. This would allow one to simulate a whole mission as well as evaluate failure scenarios such as contact with the target altering its state or a failed docking resulting in having to wait through an eclipse till the next opportunity.

Bibliography

[1] DAWN Aerospace. Green propellants Superior reliability High performance Modular and scalable.

[2] Jean Sébastien Ardaens, Simone D'Amico, and Alexander Cropp. GPS-based relative navigation for the Proba-3 formation flying mission. *Acta Astronautica*, 91:341–355, 2013.

[3] Heike Benninghoff, Toralf Boge, and Tristan Tzschichholz. Hardware-in-the-loop rendezvous simulation involving an autonomous guidance, navigation and control system. *Advances in the Astronautical Sciences*, 145(April 2014):953–972, 2012.

[4] M Bhagat. Convex Guidance for Envisat Rendezvous. Technical report, Delft University of Technology, 2016.

[5] Chris Blackerby, Akira Okamoto, Kohei Fujimoto, Nobu Okada, Jason L Forshaw, and John Auburn. Elsa-D: an in-Orbit End-of-Life Demonstration Mission. 6:43644, 2018.

[6] Louis Breger and Jonathan P How. J 2 -Modified GVE-Based MPC for Formation Flying Spacecraft. pages 1–12, 2005.

[7] Floris Van Dam. *Literature Survey: Fuel-efficient control of a swarm of picosatellites.* Literature review, Delft University of Technology, 2019.

[8] DARPA. Orbital Express Fact Sheet. Technical report, Defense Advanced Research Projects Agency, 2007.

[9] T. M. Davis and D. Melanson. XSS-10 micro-satellite flight demonstration program results. *SPIE Defence and Security Symposium*, 5419:16–25, 2004.

[10] N. Demirer. *Density Control of Multi-Agent Systems with Safety Constraints: A Markov Chain Approach.* PhD thesis, Univeristy of Washington, 2017.

[11] Di Cairano, S., Park, H., and I. Kolmanovsky. Model Predictive Control approach for guidance of spacecraft rendezvous and proximity maneuvering. *International Journal of Robust and Nonlinear Control*, 22(May):1398–1427, 2012.

[12] ESA. Esa commissions world's first space debris removal. https://www.esa.int/Safety_Security/Clean_Space/ESA_commissions_world_s_first_space_debris_removal, 2019 accessed on 01.03.2021.

[13] ESA. Satellites vs debris. https://www.esa.int/ESA_Multimedia/Images/2021/02/Satellites_vs_Debris, 2021 accessed on 01.03.2021.

[14] ESA. We're launching more than ever. https://www.esa.int/ESA_Multimedia/Images/2021/03/We_re_launching_more_than_ever, 2021 accessed on 03.03.2021.

[15] W. Fehse. Automated Rendezvous and Docking of Spacecraft. *Proceedings of the Institution of Mechanical Engineers, Part G: Journal of Aerospace Engineering*, 2003.

[16] Gene Franklin, J. David Powell, and Abbas Emami-Naeini. *Feedback control of dynamic systems, 3e*, volume 55-2. 1994.

[17] Jorge L. Garriga and Masoud Soroush. Model predictive control tuning methods: A review. *Industrial and Engineering Chemistry Research*, 49(8):3505–3515, 2010.

[18] Francisco Gavilan, Rafael Vazquez, and Eduardo F. Camacho. Chance-constrained model predictive control for spacecraft rendezvous with disturbance estimation. *Control Engineering Practice*, 20(2):111–122, 2012.

[19] John L. Goodman. History of space shuttle rendezvous and proximity operations. *Journal of Spacecraft and Rockets*, 43(5):944–959, 2006.

[20] John L. Goodman. History of Space Shuttle Rendezvous. Technical Report October, National Aeronautics and Space Administration, Johnson Space Center, 2011.

[21] Pini Gurfil. Relative motion between elliptic orbits: Generalized boundedness conditions and optimal formationkeeping. *Journal of Guidance, Control, and Dynamics*, 28(4):761–767, 2005.

[22] Edward N. Hartley, Paul A. Trodden, Arthur G. Richards, and Jan M. Maciejowski. Model predictive control system design and implementation for spacecraft rendezvous. *Control Engineering Practice*, 20(7):695–713, 2012.

[23] IADC. Inter-Agency Space Debris Coordination Committee, Space Debris Mitigation Guidelines. (22):1–10, 2007.

[24] Gökhan Inalhan, Michael Tillerson, and Jonathan P. How. Relative dynamics and control of spacecraft formations in eccentric orbits. *Journal of Guidance, Control, and Dynamics*, 25(1):48–59, 2002.

[25] E. Kaiser, J. N. Kutz, and Steven L. Brunton. Sparse identification ofnonlinear dynamics for modelpredictive control in thelow-data limit. *arXiv*, 2018.

[26] Eric C. Kerrigan and Jan M. Maciejowski. Soft Constraints And Exact Penalty Functions In Model Predictive Control. *UKACC International Conference*, 2000.

[27] Elsa-d Launch Press Kit. ELSA-d Launch Press Kit 2021. 2021.

[28] Adam W. Koenig and Simone D'Amico. Safe spacecraft swarm deployment and acquisition in perturbed near-circular orbits subject to operational constraints. *Acta Astronautica*, 153(August 2017):297–310, 2018.

[29] P. Labourdetter, E. Julien, F. Chemama, and D. Carbonne. ATV Jules Verne mission maneuver plan. *International Symposiumon Space Flight Dynamics*, 2009.

[30] J.-C. Liou. Engineering and technology challenges for active debris removal. Technical report, NASA, Houston, 2013.

[31] J. C. Liou, N. L. Johnson, and N. M. Hill. Controlling the growth of future LEO debris populations with active debris removal. *Acta Astronautica*, 66(5-6):648–653, 2010.

[32] Glynn S. Lunney. Summary of Gemini Rendezvous Experience. In *Flight Test, Simulation and Support Conference*. American Institute of Aeronautics and Astronautics, 1967.

[33] Jianjun Luo, Liang Zhou, and Bo Zhang. Consensus of satellite cluster flight using an energy-matching optimal control method. *Advances in Space Research*, 60(9):2047–2059, 2017.

[34] Yazhong Luo, Jin Zhang, and Guojin Tang. Survey of orbital dynamics and control of space rendezvous. *Chinese Journal of Aeronautics*, 27(1):1–11, 2014.

[35] David Q. Mayne. Model predictive control: Recent developments and future promise. *Automatica*, 50(12):2967–2986, 2014.

[36] O. Montenbruck and E. Gill. *Satellite Orbits - Models, methods and Applications*. Springer Verlag, 2000.

[37] Daniel Morgan, Soon Jo Chung, Lars Blackmore, Behcet Acikmese, David Bayard, and Fred Y. Hadaegh. Swarm-keeping strategies for spacecraft under J2 and atmospheric drag perturbations. *Journal of Guidance, Control, and Dynamics*, 35(5):1492–1506, 2012.

[38] NASA. Demonstration of Autonomous Rendezvous Technology. Technical report, National Aeronautics and Space Administration, 2005.

[39] NRC. *NASA space technology roadmaps and priorities*. National Research Council, Washington D.C., USA, 2012.

[40] Yoshiaki Ohkami and Isao Kawano. Autonomous rendezvous and docking by engineering test satellite VII: A challenge of Japan in guidance, navigation and control - Breakwell memorial lecture. *Acta Astronautica*, 53(1):1–8, 2003.

[41] Hyeongjun Park, Richard Zappulla, Costantinos Zagaris, Josep Virgili-Llop, and Marcello Romano. Nonlinear model predictive control for spacecraft rendezvous and docking with a rotating target. *Advances in the Astronautical Sciences*, 160(February):1135–1148, 2017.

[42] Michael E. Polites. Technology of automated rendezvous and capture in space. *Journal of Spacecraft and Rockets*, 36(2):280–291, 1999.

[43] S. Joe Qin and Thomas A. Badgwell. A survey of industrial model predictive control technology. *Control Engineering Practice*, 11(7):733–764, 2003.

[44] L. Ravikumar, Radhakanth Padhi, and N.K. Philip. Trajectory optimization for Rendezvous and Docking using Nonlinear Model Predictive Control. *IFAC-PapersOnLine*, 53(1):518–523, 2020.

[45] James B. Rawlings and David Q. Mayne. *Model Predictive Control: Theory and Design*. Nob Hill Publishing, Madison, Wisconsin, 2nd edition, 2016.

[46] Jose P. Ruiz and Jeremy Hart. A comparison between Orion automated and Space Shuttle rendezvous techniques. *AIAA Guidance, Navigation, and Control Conference*, (August):1–10, 2010.

[47] Samuel A. Schweighart and Raymond J. Sedwick. High-fidelity linearized J2 model for satellite formation flight. *Journal of Guidance, Control, and Dynamics*, 25(6):1073–1080, 2002.

[48] SpaceWorks. 2020 Nano/Microsatellite Market Forecast. Technical report, SpaceWorks Enterprises, Inc., Atlanta, U.S.A., 2020.

[49] Space Station, Reference Coordinate, International Space, and Station Program. Space Station Reference Coordinate Systems International Space Station Program, 2001.

[50] Kamesh Subbarao and Sam Welsh. Nonlinear control of motion synchronization for satellite proximity operations. *Journal of Guidance, Control, and Dynamics*, 31(5):1284–1294, 2008.

[51] Joshua Sullivan, Sebastian Grimberg, and Simone D'Amico. Comprehensive survey and assessment of spacecraft relative motion dynamics models. *Journal of Guidance, Control, and Dynamics*, 40(8):1837–1859, 2017.

[52] A Tan, T X Zhang, and M Dokhanian. Analysis of the Iridium 33 and Cosmos 2251 Collision Using Velocity Perturbations of the Fragments. *Advances in Aerospace Science and Applications*, 3(1):13–25, 2013.

[53] Michael Tillerson, Gokhan Inalhan, and Jonathan P. How. Co-ordination and control of distributed spacecraft systems using convex optimization techniques. *International Journal of Robust and Nonlinear Control*, 12(2-3):207–242, 2002.

[54] J Tschauner and T Hempel. Rendezvous with a target in an elliptical orbits. *Astronautica Acta*, 11(2), 1965.

[55] David A Vallado and Wayne D Mcclain. *Fundamentals of Astrodynamics and Applications Fourth Edition with technical contributions by*. Microcosm Press and Springer, Hawthorne, CA, 2013.

[56] Andrea Valmorbida. Development and Testing of Model Predictive Control Strategies for Spacecraft Formation Flying. Technical Report January, Universit'a degli Studi di Padova Centro, 2014.

[57] Karel F. Wakker. *Fundamentals of Astrodynamics*. Delft University of Technology, Delft, 2015.

[58] Danwei Wang, Baolin Wu, and Eng Kee Poh. *Satellite Formation Flying: Relative Dynamics, Formation Design, Fuel Optimal Maneuvers and Formation Maintenance*, volume 48. Springer, 2016.

[59] David C. Woffinden and David K. Geller. Navigating the road to autonomous orbital rendezvous. *Journal of Spacecraft and Rockets*, 44(4):898–909, 2007.

[60] Guangyan Xu and Danwei Wang. Nonlinear dynamic equations of satellite relative motion around an oblate earth. *Journal of Guidance, Control, and Dynamics*, 31(5):1521–1524, 2008.

[61] Koji Yamanaka and Finn Ankersen. New State Transition Matrix for Relative Motion on an Arbitrary Elliptical Orbit. *Journal of Guidance, Control and Dynamics*, 25(1), 2002.

[62] Kenneth A. Young and James D. Alexander. Apollo Lunar Rendezvoous. *Journalofspacecraftandrockets*, 7:1083–1086, 1970.

[63] Douglas Zimpfer, Peter Kachmar, and Seamus Tuohy. Autonomous rendezvous, capture and in-space assembly: Past, present and future. *A Collection of Technical Papers - 1st Space Exploration Conference: Continuing the Voyage of Discovery*, 1(February):234–245, 2005.

Glossary

List of Acronyms

MPC	Model Predictive Control
ISS	International Space Station
HCW	Clohessy Wiltshire
LTV	Linear Time Variant
LTI	Linear Time Invariant
NL	Non-Linear
ECI	Earth-centred Inertial
LVLH	Local-Vertical, Local-Horizontal
RAAN	Right Ascension of the Ascending Node
EOM	Equations of Motion
LEO	Low Earth Orbit
RSV	Reference Satellite Variables
STM	State Transition Matrix
ROE	Relative Orbital Elements
GVE	Gauss's Variational Equations
ESA	European Space Agency
PID	Proportional Integral Derivative
DP	Dynamic Programming
CT	Continuous-Time
QP	Quadratic Programming
LMPC	Linear MPC
LIDAR	Light Detection and Ranging
GPS	Global Positioning System

ORCSAT	On-line Reconfiguration Control System and Avionics Techniques
LOS	Line-of-Sight
MIB	Minimum Impulse Bit
QP	Quadratic Programming
RVD	Rendezvous and Docking
NASA	National Aeronautics and Space Administration
DEOS	Deutsche Orbitale Servicing
LM	Lunar Module
YA	Yamanaka-Ankersen
CSM	Command Service Module
IMU	Internal Measurement Unit
ATV	Automated Transfer Vehicle
EOL	End-of-Life
LEO	Low Earth Orbit
GEO	Geosynchronous Earth Orbit
IADC	Inter-Agency Space Debris Coordination Committee
PMD	Post Mission Disposal
ADR	Active Debris Removal
VESPA	Vega Secondary Payload Adapter
LCvx	Lossless convexification
ORCSAT	On-line Reconfiguration Control System and Avionics Techniques
RMS	Root Mean Squared
XU	Xu-Wang

List of Symbols

n	Mean Motion
$\mathcal{B}$	Body-centered Rotating Frame
$\mathcal{B}$	Body-fixed Frame
$\mathcal{I}$	Earth-Centered Inertial
$\mathcal{R}$	Earth-Centered Rotating
$_{chs}$	Chaser Satellite
$_{tgt}$	Target Satellite
$\mathcal{F}$	Frame of reference

n